~~CONFIDENTIAL~~

NASA-CR-72031

AEC RESEARCH and DEVELOPMENT REPORT

TUNGSTEN WATER MODERATED REACTOR FUEL SUPPORT DESIGN ANALYSIS [U]

D. T. AASE
F. J. KEMPF
D. P. O'KEEFE
W. C. TOWNSEND

(NASA-CR-72031) TUNGSTEN WATER MODERATED REACTOR FUEL SUPPORT DESIGN ANALYSIS (Battelle-Northwest) 247 p

N73-70995

Unclas
00/99 53532

FACILITY FORM

251 (PAGES)
CR 72031 (NASA CR OR TMX OR AD NUMBER)
21 (CODE)
22 (CATEGORY)

AUGUST, 1966

RESTRICTED DATA

THIS DOCUMENT CONTAINS RESTRICTED DATA AS DEFINED IN THE ATOMIC ENERGY ACT OF 1954. ITS TRANSMITTAL OR THE DISCLOSURE OF ITS CONTENTS IN ANY MANNER TO AN UNAUTHORIZED PERSON IS PROHIBITED.

CLASSIFICATION CHANGE

TO = UNCLASSIFIED ~~CONFIDENTIAL~~

By authority of T.D. No. 73-221

Changed by [illegible] Date 1-30-73

BATTELLE-NORTHWEST
BATTELLE MEMORIAL INSTITUTE / PACIFIC NORTHWEST LABORATORY

U. S. Government Agencies and Contractors Only

~~CONFIDENTIAL~~

LEGAL NOTICE

This report was prepared as an account of Government sponsored work. Neither the United States, nor the Commission, nor any person acting on behalf of the Commission:

A. Makes any warranty or representation, expressed or implied, with respect to the accuracy, completeness, or usefulness of the information contained in this report, or that the use of any information, apparatus, method, or process disclosed in this report may not infringe privately owned rights; or

B. Assumes any liabilities with respect to the use of, or for damages resulting from the use of any information, apparatus, method, or process disclosed in this report.

As used in the above, "person acting on behalf of the Commission" includes any employee or contractor of the Commission, or employee of such contractor, to the extent that such employee or contractor of the Commission, or employee of such contractor prepares, disseminates, or provides access to, any information pursuant to his employment or contract with the Commission, or his employment with such contractor.

PACIFIC NORTHWEST LABORATORY
RICHLAND, WASHINGTON
operated by
BATTELLE MEMORIAL INSTITUTE
for the
UNITED STATES ATOMIC ENERGY COMMISSION UNDER CONTRACT AT(45-1)-1830

PRINTED BY/FOR THE U. S. ATOMIC ENERGY COMMISSION

AEC-RLOO RICHLAND, WASH.

C66-8623

~~CONFIDENTIAL~~

NASA-CR-72031

C-91, Nuclear Reactors
for Rocket Propulsion
(M-3679, 45th Ed)

TUNGSTEN WATER MODERATED REACTOR FUEL SUPPORT DESIGN ANALYSIS [U]

D T Aase
F J Kempf
D P O'Keefe
W C Townsend
D S Trent

NOTE This document contains information affecting the national defense of the United States within the meaning of the Espionage Laws, Title 18, USC, Sections 793 and 794 The transmission or the revelation of its contents in any manner to an unauthorized person is prohibited by law

Engineering Analysis Section
Engineering Development Department

Sponsored by

The National Aeronautics and Space Administration

Technical Management
NASA Lewis Research Center
Cleveland, Ohio

Armin F Lietzke Nuclear Reactor Division

August, 1966

RESTRICTED DATA

This document contains Restricted Data as defined in the Atomic Energy Act of 1954 Its transmittal or disclosure of its contents in any manner to an unauthorized person is prohibited

~~Group I~~

~~Excluded from Automatic Downgrading and Declassification~~

U. S. Government Agencies and Contractors Only

PACIFIC NORTHWEST LABORATORY
RICHLAND, WASHINGTON

~~CONFIDENTIAL~~

TABLE OF CONTENTS

		Page
1 0	INTRODUCTION	1 1
1 1	Axial Fuel Column Support Concepts .	1 1
1 2	Lateral Support Concepts . . .	1 2
1 3	Analytical Procedure . .	1 5
1 4	Flat Plate W-UO_2 Fuel Design .	1.6
2 0	SUMMARY AND CONCLUSIONS . . .	2 1
2 1	Cold End Support Designs	2 1
2 1.1	General Results .	2 1
2 1.2	Specific Results . . .	2 4
2 2	Possible Modifications to Cold End Support Design. .	2 8
2 2 1	Changing the Natural Frequency	2 8
2 2 2	Increased System Damping . .	2 9
2 3	Alternate Support Designs	2 10
2 3 1	Hot End Support Design . . .	2 10
2 3 2	Reentrant Flow-Cooled Design. .	2 11
3.0	EFFECT OF LATERAL SUPPORTS ON ADJACENT TUBES . .	3 1
3 1	Introduction . .	3 1
3.2	Method of Analysis	3 1
3 2.1	Heat Transfer Analysis . .	3.1
3 2 2	Stress Analysis .	3.7
3 3	Preliminary heat Transfer Models. . . .	3 16
3 4	Corrugated Strip Support Concepts	3 20
3 5	Summary of Corrugated Strip Heat Transfer Results	3 26
3.6	Tube Stresses . . .	3.39
3 7	Tungsten Support Tube Creep	3 48
3 8	References	3 52

		Page
4.0	STRESS ANALYSIS OF CORRUGATED STRIP LATERAL SUPPORT	4 1
	4.1 Models and Assumptions	4 1
	4 2 Method of Analysis	4 3
	4 3 Results	4 6
	4 4 Model Verification and Alternate Models	4 10
	4 5 Reference	4.11
5 0	DYNAMIC ANALYSIS	5 1
	5 1 Unsupported Tube Model	5.1
	5 1 1 Model Description	5 1
	5 1.2 Method of Analysis	5.3
	5 1.3 Results.	5 7
	5.2 Cold End Support Concept	5.14
	5 2 1 Assumptions and Model Description	5 14
	5.2.2 Method of Analysis	5 15
	5 2 3 Results	5.21
	5 3 References	5 43
6 0	HOT END SUPPORT DESIGN	6.1
	6 1 Method of Thermal Analysis.	6 1
	6 2 Preliminary Support Models	6 2
	6.2.1 Hanger Support	6 3
	6.2.2 Bracket Support	6 6
	6 3 Model Comparisons	6 9
	6.4 Tungsten Support Leg Stresses	6 12
7 0	REENTRANT-FLOW-COOLED LATERAL SUPPORT DESIGN	7 1
	7 1 Introduction	7 1
	7 2 Thermal Hydraulic Analysis.	7 2
	7 3 Parameter Studies.	7 15

		Page
7 4	Conclusions and Recommendations .	7 21
7 5	References	7 24
8.0	FLAT PLATE STOCK W-UO_2 TWMR FUEL DESIGN . .	8 1
8 1	References . .	8 12
9 0	APPENDICES	
A	Tungsten Support Tube and Aluminum Pressure Tube Stress Component Curves for Study Cases 4 Through 10	A 1
B.	Derivation of Lateral Support Stress Equations	B 1
C	Solution of A Homogeneous Clamped-Pinned Tube With End Restraint Excitation .	C 1
D	Analog Circuit for Cold End Support	D 1
E.	Approximate Pressure Losses for Heated Compressible Fluid . . .	E 1

LIST OF FIGURES

Figure	Title	Page
3 1	Gamma Heat of Aluminum Versus Distance from Inlet End of First Fuel Stage	3 6
3 2	Bulk Coolant and Bulk Moderator Temperature Versus Axial Position	3 8
3 3	TUNGSTEN, Static Young's Modulus Versus Temperature	3 15
3 4	Preliminary Heat Transfer Models	3 17
3 5	Typical Circumferential and Radial Temperature Distributions for Preliminary Heat Transfer Models (Reference Figure 3 3)	3 17
3 6	Typical Circumferential and Radial Temperature Distributions for Preliminary Heat Transfer Models (Reference Figure 3 4)	3 18
3 7	Heat Transfer Model for Corrugated Strip Support	3 21
3 8	Heat Transfer Model for Corrugated Strip and Porous Media	3 25
3 9	Radial and Circumferential Temperature Distributions at the Inside Surface of Aluminum Pressure Tube	3 27
3 10	Aluminum Tube Inside Diameter Surface Temperature Versus Distance from Core Inlet	3 28
3 11	Typical Circumferential and Radial Temperature Distributions for the Aluminum Pressure Tube Near the Reactor Exit for Various Support Concepts	3 29
3 12	Tungsten Tube Outside Diameter Surface Temperature Versus Distance from Core Inlet	3 30
3 13	Typical Circumferential and Radial Temperature Gradients for the Tungsten Support or Sheath Tube Near the Reactor Exit for Various Lateral Support Concepts	3 31

Figure	Title	Page
3 14	Aluminum Tube Inside Diameter Surface Temperature Versus Distance from Core Inlet	3 32
3 15	Typical Circumferential and Radial Temperature Distributions for the Aluminum Pressure Tube Near the Reactor Exit for Various Support Concepts	3 33
3 16	Tungsten Tube Outside Diameter Surface Temperature Versus Distance from Core Inlet	3 34
3 17	Typical Circumferential and Radial Temperature Gradients for the Tungsten Support or Sheath Tube Near the Reactor Exit for Various Lateral Support Concepts	3 35
3 18	Tungsten Tube Primary Membrane Stress Components and Allowable Stress Versus Axial Position	3 41
3 19	Aluminum Tube Primary Membrane Stress Components and Allowable Stress Based on Case 8 Tube Temperature	3 42
3 20	Tungsten Tube, Primary Membrane Plus Maximum Thermal Stress at Outside Tube Radius and Point of Support Contact Versus Axial Position	3 43
3.21	Aluminum Tube, Primary Membrane Plus Maximum Thermal Stress at Tube Inner Surface Versus Axial Position	3 44
3 22	Hot End Support, Maximum Tungsten Support Tube Axial Stress at Outer Tube Radius, Case 10	3 46
3 23	Cold End Support, Tungsten Support Tube Thermal Stress Due to Circumferential Temperature Gradient Versus Distance from Lateral Support Contact Location, Case 10	3 47
3 24	Tungsten Creep Constant "B" Versus Temperature	3 49
3 25	Tungsten Support Tube Strain after 10 hr of Operation Versus Axial Position	3 50
3 26	Tungsten Support Tube Increase in Tube Diameter (Due to Creep) After 10 hr of Operation	3 50
3 27	X/L Transfer, Vibration and Thermal NASA Nuclear Rocket Reactor Length	3 51

Figure	Title	Page
4 1	Eight Segment Corrugated Strip Model	4 1
4 2	Case 4 Typical Model	4 3
4 3	Case 10 Typical Model	4 3
4 4	Eight Support Segment Load Versus Lateral Deflection (Hot Condition)	4 7
4 5	Twelve Support Segment Load Versus Lateral Deflection (Hot Condition)	4 7
4 6	Sixteen Support Segment Load Versus Lateral Deflection (Hot Condition)	4 8
4 7	Eight Support Segment Load Versus Lateral Deflection (Cold Condition)	4 8
4 8	Twelve Support Segment Load Versus Lateral Deflection (Cold Condition)	4 9
4 9	Sixteen Support Segment Load Versus Lateral Deflection (Cold Condition)	4 9
4 10	Decrease in Gap Dimension Versus Axial Position	4 11
5 1	Unsupported Tube Model	5 2
5 2	Unsupported Tube Concept Launch Conditions	5.9
5 3	Bending Stress Versus Excitation Frequency, Tungsten Support Tube Without Lateral Supports	5 10
5 4	Bending Stress Versus Excitation Frequency Tungsten, Support Tube Without Lateral Supports	5.11
5 5	Unsupported Tube Model - Analog	5 16
5 6	NASA Tungsten Fueled Reactor Unsupported Tube Model Analog-Digital Comparison	5 18
5 7	Cold End Support Case Concept and Analog Model	5 19
5 8	Support Tube Bending Stress Versus Frequency	5 24
5.9	Pressure Tube Bending Stress Versus Frequency	5 25

Figure	Title	Page
5 10	Lateral Support Deflection	5.26
5 11	Tie-Rod Case, Concept and Analog Model	5.28
5.12	Bending Stress Versus Frequency	5 29
5 13	Bending Stress Versus Frequency	5 30
5 14	Lateral Support Deflection Versus Frequency	5 31
5 15	Lateral Support Deflection Versus Frequency	5 32
5 16	Effect of Lateral Support Damping (Inlet End Support Model with Clamped-Pinned Boundary Conditions)	5 34
5 17	Effect of Lateral Support Damping (Cold End Support Model with Clamped-Pinned Boundary Conditions)	
5 18	Support Tube Bending Stress Comparison of Hot and Cold Operation	5 37
5 19	Support Tube Bending Stress	5 39
5 20	Lateral Support Deflection	5 40
5 21	Lateral Support Deflection	5 41
6.1	Heat Transfer Model for Hot End Support Analysis	6 2
6 2	Hot End Support Model	6 4
6 3	Heat Transfer Model for Exit End Support	6 5
6 4	Bottom Support Heat Transfer Model	6 7
6 5	Temperature Distributions (Hot End Support Components) Versus Distance from Last Fuel Stage	6 10
6 6	Temperature Distributions (Hot End Support Components) Versus Distance from Last Fuel Stage	6 10
6 7	Temperature Distributions (Hot End Support Components) Versus Distance from Last Fuel Stage	6 11

Figure	Title	Page
6 8	Temperature Distributions (Hot End Support Components) Versus Distance from Last Fuel Stage	6 11
6 9	Design Concepts Showing Insulating Material Enclosed in Thin Metallic Membrane	6 13
6 10	Hot End Support Tungsten Support Leg Critical Buckling Pressure and Primary Membrane Stress	6 14
7 1	Model for Evaluation of Reentrant Bleed Flow Cooling of Lateral Supports	7 3
7 2	Schematic Diagram of Reentrant Flow--Main Program	7 11
7 3	Bulk Bleed Flow Outlet Temperature Versus Insulation Thickness	7 17
7 4	Maximum Support Tube Temperature Versus Axial Position for Various Insulation Thicknesses	7 17
7 5	Comparison of Support Tube Temperatures for Stainless Steel and Tungsten Support Tube Materials	7 18
7 6	Deviation of Maximum Support Tube Temperature Versus Fluctuation of Main Coolant Pressure	7 20
7 7	Bleed Flow Temperature Rise	7 22
7 8	Maximum Stainless Steel Support Tube Temperature Versus Axial Location	7.22
7 9	Maximum Aluminum Pressure Tube Temperature Versus Axial Location	7 23
8 1	Geometries Considered in Grid Design Studies	8 3
8 2	Geometries Considered in Grid Design Studies	8 4
8 3	Geometries Considered in Grid Design Studies	8 5
8 4	Typical Detail - Slotted Strips	8 7
8 5	Transverse Section Through the Grid Coated by the Hydrogen-Tungsten Hexafluoride Decomposition Process	8.8

Figure	Title	Page
8 6	Model Number One of the Plate Stock Fuel Grid Assembly	8 9
8 7	Model Number Two of the Plate Stock Fuel Grid Built with 0 020 in Unfueled Tungsten Sheets	8 9
8 8	Detail of Tungsten Sheath Tube Spun from 0 060 in Gage Sheet	8 11
A.1	Cold End Support, Maximum Tungsten Support Stress at Outer Tube Radius - Case 4	A 2
A 2	Cold End Support, Maximum Aluminum Tube Stress at Inside Tube Radius - Case 4	A.3
A 3	Hot End Support, Tungsten Sheath Tube Axial Stress at Outside Tube Radius - Case 7	A 4
A 4	Hot End Support, Maximum Tungsten Sheath Tube Tangential Stress Versus Axial Position - Case 7	A 5
A 5	Hot End Support, Maximum Aluminum Tube, Stress at Tube Inner Radius and Support Contact Case 7	A 6
A.6	Cold End Support, Maximum Tungsten Support Tube Stress at Outer Tube Radius - Case 8	A 7
A 7	Cold End Support, Maximum Aluminum Tube Stress at Inside Tube Radius - Case 8	A 8
A 8	Hot End Support, Tungsten Sheath Tube, Maximum Stress at Inside Tube Radius - Case 9	A 9
A.9	Hot End Support, Maximum Aluminum Tube Stress at Tube Inner Radius and Support Contact, Case 9	A 10
B 1	Lateral Support Segment Load Function Model	B 3
B 2	Lateral Support Segment Elastic Constants Model	B 6
B 3	Reaction Moments on Symmetrical Portion of Eight Segment Lateral Support	B 10
B 4	Moment/Load Ratio Versus Number of Spring Segments	B 11

Figure	Title	Page
B 5	Maximum Strip Temperature and Allowable Bending Stress Versus Axial Position	B 13
B 6	Lateral Support Frame Geometry	B 17
B 7	Circumferential Translation Δ_n Versus Support Lateral Deflection	B 18
D 1	NASA Fuel Support, Tungsten-Water Moderated Reactor (Cold End Support Model Pressure Tube Simulation)	D 2
D 2	NASA Fuel Support, Tungsten-Water Moderated Reactor (Cold End Support Model Fuel and Fuel Support Simulation)	D 3
D 3	NASA Fuel Support, Tungsten-Water Moderated Reactor (Excitation Oscillator and Lateral Support Coupling)	D 4
D 4	NASA Fuel Support, Tungsten-Water Moderated Reactor (Lateral Support Coupling and Moderator Damping)	D 5
D 5	NASA Fuel Support, Tungsten-Water Moderated Reactor (Moderator and Lateral Support Damping)	D 6

LIST OF TABLES

Table	Title	Page
2 1	Vibration Data Summary	2 2
2 2	Cold End Support Design - Case 10	2 5
3 1	Material Thermal Properties and Parameters for Stagnant Hydrogen Annulus Heat Transfer Models	3 3
3 2	Values Used in the Computer Calculations for Gamma Heating, Propellant Temperature and Moderator Temperature as a Function of X/L	3 7
3 3	Summary of Corrugated Strip Cases for h_2 = 5,000 and 35,000 Btu/hr-ft^2°F	3 22
3 4	Summary of Cases, 0 0625 in Annulus h_2 = 5000 and 35,000 Btu/(hr)(ft^2)(°F)	3 23
3 5	Summary of Cold End Support Cases, 0 125 in Annulus, h_2 = 5000 and 35,000 Btu/(hr)(ft^2)(°F)	3 24
5 1	Natural Frequencies for Unsupported Tube Model	5 7
5 2	Comparison of Analytical and Experimental Unsupported Tube Model Studies	5 12
5 3	Input Data Summary, Runs Be (Cold) and BF (Hot)	5 23
5 4	Analog Simulation Parameters	5 42
6 1	Summary of Hot End Support Heat Transfer Calculations--Hanger Support	6 6
6 2	Summary of Hot End Support Heat Transfer Computation (Bracket Support)	6 8
7 1	Flow Channel Sizing Parameters	7 15
7 2	Reentrant Bleed Flow Reference Parameters	7 21

Table	Title	Page
B 1	Lateral Support Segment Dimensions	B 9
B 2	Load Functions and Elastic Constants	B 9
B 3	Lateral Support Bending Moments at Tungsten Tube Contact Locations	B 11
B 4	Allowable Lateral Support Segment Loads for 0 003, 0 006 and 0 010 in Thick Segments (8 Segment Model)	B 14
B 5	Circumferential Displacements of Lateral Support Segment	B 15
B 6	Average Segment Temperature, Static Young's Modulus and Total Segment Load Versus Axial Position Along Fuel Column (Case 10, with 8 Segment Support Model)	B 16
B 7	Segment Load as a Function of Axial Position, Segment Thickness and Circumferential Displacement	B 16

TUNGSTEN WATER MODERATED REACTOR FUEL SUPPORT DESIGN ANALYSIS

1 0 INTRODUCTION

1 1 AXIAL FUEL COLUMN SUPPORT CONCEPTS

The fuel subassembly for the reference design of the Tungsten Water Moderated Reactor (TWMR) contains 26 fueled pieces, called stages, stacked in a column Each fuel stage is contained within an outer unfueled tungsten tube called the sheath tube In this study, two basic methods of supporting the axial loads on the fuel stages were considered These methods were designated as cold-end support and hot-end support designs

The basic difference in method of fuel support is the location at which the loads are finally transmitted to the reactor structure

In the cold-end support design the sheath tube transmits the axial forces on each fuel stage, via pinned connections or a support ledge, to a surrounding support tube The support tube then transmits the axial loads to the cold-inlet end of the reactor where it is built into the inlet plenum structure The cold end of the support tube can be considered a fixed end, and the hot end is simply supported to allow for axial thermal expansion

In the hot-end support design, the axial fuel column load is transmitted by the sheath tube to a support built into the moderator outlet plenum structure A support tube is not required, if adequate provision is made for flow channel alignment and shrouding of the junctions, the fuel stages may be simply stacked on each other In this case, the hot end is considered a fixed connection while the cold end of the sheath tube is simply supported

In both the hot- and cold-end support designs, the sheath or support tube is surrounded by a hydrogen annulus to separate the hot support structure from the aluminum pressure tube The pressure tube serves to contain the moderator water between the subassemblies, and is fixed in tube sheets at each end

Operating temperatures in the cold-end support design require a support tube made of tungsten During the initial phase of this study it was not apparent that a tungsten tube of the necessary length, diameter, and thickness could be successfully fabricated A design involving bleed-flow cooling in the annulus between the support and pressure tubes was therefore studied to determine the feasibility of lowering support tube temperatures an amount sufficient to allow use of a stainless steel support tube

1 2 LATERAL SUPPORT CONCEPTS

Since the TWMR is assumed to be launched by chemically propelled lower stages, there are known dynamic loads imposed on it during launch During hot operation of the reactor the dynamic loading is not well known, but some maximums can be estimated The fuel subassembly, if unsupported laterally, is susceptible to damage by a lateral vibration This is indicated by a high length-to-diameter ratio (~20 1) The fact that during hot operation the support structures are at relatively high temperature, with correspondingly weak mechanical properties, also indicates there could be a vibration problem during operation as well as during launch, even though vibration loads are expected to be lower

There are two components of the fuel subassembly that are susceptible to vibration damage Large dynamic deflections would cause large bending stresses in both the support tube and pressure tube Since the fuel stages are not rigidly coupled, it was assumed the support tube would be damaged before the fuel

In addition to large bending stresses, damage could also result from large relative deflections between the fuel column and the pressure tube This would result in slapping which could damage part of the subassembly

The dynamic response of the fueled subassembly was estimated for both a laterally unsupported case and several designs of lateral supports The bending stresses and relative deflections were of particular concern

If a rigid lateral support could be used, the design problem would be relatively simple However, the lateral support must allow the inner structure to expand during heat-up, while still maintaining good coupling during vibration The amount of structural material spanning the gap is critical because it determines the heat lost from the subassembly to the moderator This not only affects the moderator flow and temperature conditions, but even more critically it reflects back into large radial and circumferential thermal gradients in the support and pressure tubes

Several lateral support concepts were investigated in varying degrees of detail The corrugated strip support was the most thoroughly investigated design This design was selected for detailed study primarily because it appeared to require the least development to incorporate it with the TWMR design Some of the other designs considered were

- Particulate Ceramic This design consists of simply filling the gap between the support and pressure tube with large grain ceramic sand The principle advantage of the design is in elimination of large circumferential thermal gradients in both the support tube and pressure tube The main disadvantages arise from difficulty in containing the sand and insuring that reliable lateral support is not lost, due to densification, during thermal cycling

- Fibrous Ceramic This lateral support concept envisions placement of ceramic fibers, in the form of a mat, in the gap between support and pressure tubes Here again the idea is to lower the thermal gradients in the support members The problems envisioned are maintaining the resiliency of the mat and finding a ceramic fiber, which in mat form, would withstand the necessary temperatures
- Combination Particulate Ceramic and Corrugated Strip This design has the hydrogen gas annulus partially filled with ceramic sand and the remainder spanned by a corrugated strip The advantages include reduced thermal gradients while maintaining insured flexibility for radial thermal expansion In general, the strip is at lower temperatures and therefore has better physical properties The main disadvantage with this design is the problem of containing the sand

Several variations of the above lateral support designs could also be postulated, such as

- Multiple wraps of either corrugated or dimpled strips, thereby increasing the frictional damping in the lateral support system
- Ceramic "rope" wrapped spirally around the assembly
- Axially continuous corrugated sleeve This would increase the rigidity of the subassembly somewhat since it could transmit a bending moment
- Axially corrugated ring around each segment This has the advantage of moving the point of critical bending moment in the corrugation to the cold side of the gap

The design variations which were considered, other than adding lateral supports, were

- Replace the support tube with a tie-rod down the center of the fuel segments
- Add a tube sheet at the center plane of the core

1 3 ANALYTICAL PROCEDURE

A brief outline of the analytical procedure used for the corrugated strip type of lateral support will indicate how the material in each section of this report is related

(1) The corrugated strip thickness, hydrogen gas annulus width, insulating strip material, and thickness at lateral support contact locations are selected

(2) A thermal analysis is performed to define, as a function of axial position along the fuel column, the temperatures and gradients in all of the support members

(3) The type of fuel column support, either cold-end or hot-end support, is selected, and primary stresses in the support and pressure tubes are evaluated Thermal stresses at lateral support contact locations along the support and pressure tubes are calculated and added to the primary stresses

(4) Local allowable primary stresses are established based on material temperatures of the support and pressure tubes The primary plus thermal stress levels serve as a basis for comparison of alternate lateral support concept and are also compared with twice the material yield strength

(5) Lateral support load-deflection characteristics are calculated and spring constants and allowable lateral deflections of the corrugated strip are established Allowable loads are based on material properties with corrugated strip temperatures at the support tube contact locations Allowable deflections are based on average strip temperatures and take into account relative thermal expansion of the support and pressure tubes

(6) Corrugated strips, with spring constants which may vary along the fuel column, are selected and used to determine dynamic bending stresses in the support and pressure tubes and their relative deflections

Only the corrugated strip design was carried through all these steps Most of the other designs were carried only through Step 4

In presenting the results of this study, the axial position along the subassembly is indicated by two different distance-to-length ratios The length ratio $(X/L)_v$ pertains to the vibration analysis referenced to the clamp support at the reactor inlet reflector, whereas $(X/L)_t$ is used in discussing the thermal and stress analysis with X = 0 at the inlet end of the first fuel stage Figure 3 27 in Section 3 of this report shows the relationship between the vibration and thermal X/L values

1 4 FLAT PLATE W-UO_2 FUEL DESIGN

Although not closely related to the analysis of lateral fuel support concepts it has been convenient to include, as Section 8 of this report, the results of plate-type fuel element design studies conducted at Battelle-Northwest

2 0 SUMMARY AND CONCLUSIONS

High temperatures and dynamic loads associated with reactor operation are significant problems in design of an acceptable fuel column support In general, the study results indicate that a number of technically feasible options can be used to reduce the undesirable effects of reactor operating temperatures on lateral support devices Some of these options, although feasible, increase the complexity of the lateral support device Since vibration was found to be the major design problem, the results of the dynamic analyses are emphasized in this section These results apply to hot or reactor operating conditions, assuming 1 g lateral end support acceleration, except where otherwise noted

2 1 Cold End Support Designs

2 1 1 General Results

Initial vibration analyses of the clamped-pinned laterally unsupported fuel support tube, with material damping only, indicated that the first resonance would occur at a relatively low frequency of approximately 42 cycles/sec, or well within the specified 5 to 2000 cycles/sec bandwidth Calculated support tube bending stresses at the clamped end of the support tube, during the first mode of vibration, indicated values in excess of the tensile strength of the material (Table 2 1, Case 1) Parametric studies showed that a sufficient stress reduction by increasing the stiffness of the support tube was impractical Further, since the resonant frequency varies as the square root of tube stiffness, the first mode could not be effectively reduced by decreasing the stiffness

Energy dissipation from the fuel support tube to the moderator could be realized by laterally coupling the pressure tube to the support tube The moderator, being in contact with the pressure

CONFIDENTIAL

TABLE 2 1 VIBRATION DATA SUMMARY

Case	Lateral Spring Rate, lb/in		Frequency cycles/sec	Bending Stress, psi				Lateral Support Deflection, mils	
				Fuel Support			Pressure Tube		
	X/L ≤ 0 5	X/L ≥ 0 5		X/L = 0	X/L = 0 50	X/L = 0 75	X/L = 0	X/L = 0 75	X/L = 0 875
Laterally Unsupported Tube Concept Room Temperature Operation	NA	NA	42 2	482,370	282,330	250,340	NA	NA	NA
Basic Cold End Support (BC 18) C/C_c = 0 (Lateral Supports) Moderator Damped	15 690	14 300 to 366	55	135 000	67,000	62,300	23,500	84	88
Tie Rod Cold End Support (C 1) Tube Sheet at X/L = 0 50	7,500	500	30	465	25 000	26,780	1,850	325	350(a)
C/C_c/L S = 0		to 215	95	4 900	9,630	120	11,300	15	64 5
Tie Rod Cold End Support (C 2) Tube Sheet at X/L = 0 5,	7,500	5,000	80	5 150	9,250	12,710	10,300	192	101
C/C_c/L S = 0			95	2 750	4 630	10 030	6,500	64	96
Basic Cold End Support (BD 1) C/C_c/L S = 0 50 Moderator Damped	15 690	14,300 to 366	55	5,920	2 685	2,430		5 25	4
Basic Cold End Support (BF) Hot Operation C/C_c = 0 10	50,000 to 42,319	8,766 to 1 016	55	134 000	56,000	70 800	23,850	105	100
Basic Cold End Support (BE) Initial Launch C/C_c = 0 10	50,000	14 290 to 1 923	57	45,000	25 000	25,000	10,500	24	26

(a) Data Point at 20 cycles/sec

CONFIDENTIAL

tube, would serve as a damping medium for the system This concept was termed the basic cold end support case Analog solution of the lumped node mathematical model, with materials properties corresponding to calculated reactor operating conditions, indicated excessive support tube bending stress and excessive deflection (Table 2 1, Case 2) Parametric studies, investigating lateral support spring rate and damping, indicated that a significantly over-damped lateral support is required to reduce the bending stresses and lateral support deflections to acceptable levels

A conceptual design modification simulating a solid tungsten axial fuel support rod through the fuel column resulted in significant reduction in bending stress levels, but increased lateral support deflections The first resonant mode frequency, although decreased because of the decreased stiffness, still occurred in the operating bandwidth Two summary cases for this design are shown in Table 2 1, these use different spring configurations in the hottest half of the assembly $(X/L)_V > 0\ 5$ These cases also used a tube sheet at the midplane of the core in an attempt to reduce the absolute deflections of the support and pressure tubes and the corresponding maximum bending stresses It does not appear that one additional tube sheet would suffice, and, since, more than one tube sheet would introduce excessive fabrication problems, this approach was not pursued Further studies of the tie-rod model were not conducted because of the deviation from the original tungsten water-moderated reactor concept

The design case summary data and operating conditions compiled above indicate acceptable bending stresses and lateral support deflections for the initial cold launch conditions However, the cases studied, show excessive stresses and deflections for a 1 0 g excitation at hot operating conditions Failure analyses of the

system were not conducted since failure data for tungsten at any operating temperature were not available, and in all hot models, the stress at some location greatly exceeded the tensile strength of the material

2 1 2 Specific Results

An expanded summary of information on a selected design case is shown in Table 2 2 This case is similar to the basic cold end support case of Table 2 1, but with higher spring constants in the lateral supports This table presents spring characteristics along the fuel column length, system dynamic response data, and also shows the effect of the corrugated lateral supports on the combined stresses in the support and pressure tubes The axial position along the subassembly is indicated by the distance to length ratio $(X/L)_V$ used in the vibration analysis The subassembly consists of a 20 mil tungsten support tube surrounding the fuel stages and sheath tube, and a 60 mil aluminum pressure tube enclosing a 1/8 in stagnant gas annulus between the support and pressure tubes The corrugated strip lateral supports span the gas annulus between the support tube and the pressure tube

The first column under "Corrugated Strip Lateral Support Characteristics" shows the thickness of the corrugated strips The second column indicates individual segment spring constants and the third column shows the effective spring constant for the lumped nodes of the dynamic system model The varying spring constants are the result of changing material temperatures and lateral support thickness along the fuel column The fourth column is the average temperature of the corrugated strip which determines its load deflection characteristics and spring constant The total allowable corrugated strip deflection is shown in Column 5, this must provide for any initial preset in the corrugated strips, the thermal expansion during heatup and the dynamic deflection during operation Column 6 shows typical thermal expansion

TABLE 2 2 COLD END SUPPORT DESIGN - CASE 10

Axial Position	Corrugated Strip Lateral Support Characteristics						Dynamic Response Data (a,b,c)				Support Tube Stresses				Pressure Tube Stresses		
$(X/L)_V$	Thickness, t, mils	Spring Constants K_l lb/in	K_T, lb/in	Temperature, °F	Deflection Allowable mils	Thermal mils	Support Tube Stress σ_{ST} max, ksi	Pressure Tube Stress σ_{PT} max, ksi	Lateral Support Deflection δ_{LS} max, mils	Pressure Tube Deflection δ_{PT} max, mils	Primary σ_p, ksi	Allowable Primary σ_p allowable, ksi (d)	Primary+ Thermal $\sigma_p + \sigma_t$, ksi (e) (f)	Allowable Primary+ Thermal $\lvert\sigma_p + \sigma_t\rvert$ allowable ksi (g)	Primary σ_p, ksi	Allowable Primary σ_p allowable, ksi	Primary+ Thermal $\lvert\sigma_p + \sigma_t\rvert$ ksi
0																	
0 250	10	1819	50,000	925	~12		134 0	23 9			4 95	>100			0 57	25 5	-6 5
0 325	↓			1525				3 12	1 15	14 0	4 45		2 3	2 3	0 51	20 0	6 7
0 400				1900	~10						3 93	>75	0 1	0 1	0 45	17 0	-7 0
0 475				2175		2 5					3 43	>60	+2 0	+2 0	0 40	15 5	7 4
0 500		1540	42,319														
0 555				2375	~7 5	4	56 1	21 26	12 0	28 0	2 93	4 0	+3 4	+4 3	9 0	0 34	15 0	7 9
0 625	6	319	8,766														
0 630				2530							2 41	2 95	+3 9	+6 0	7 6	-0 30	14 7	8 2
0 710				2675	~4 0	7					1 90	↓	+3 9	+7 0	↓	0 22	14 5	8 5
0 750	3	38 5	1,058														↓
0 785	↓			2775			70 8	3 99	100 0	17 0	1 40		+3 8	+7 8		0 16	8 7
0 860				2850	~2 5	8					0 90		+3 6	+8 4		0 10	8 7
0 875		37 0	1,016														
0 940									100 0		0 40	↓	+3 7	+8 7	↓	0 05	↓ 8 6

(a) End restraint input acceleration 1 0 g sinusoidal

(b) With 10% damping $C_c^2 = 4k\,\Sigma(1/m_1)/\Sigma(1/m_1)^2$

(c) Resonance at 55 cycles/sec

(d) $(\sigma_p)_{allowable}$ at 0 8 tensile yield strength

(e) Young's Modulus from ASD TDR 63 383

(f) Young's Modulus from DMIC 191

(g) $(\sigma_p + \sigma_t)_{allowable}$ taken at two times tensile yield strength

CONFIDENTIAL

deflections which are greater than the allowable corrugated strip deflection at the hotter axial locations, and on this basis the corrugated strip with the indicated characteristics is unacceptable

The "Dynamic Response Data" show bending stresses in both the support and pressure tubes which are similar to the values obtained for the basic cold end support case (Table 2 1) Lateral support deflections of 100 mils, are in part, attributed to the small degree of coupling or low spring constant between the support and pressure tubes in the hotter sections of the subassembly Also, the support tube pinned end condition gives the hottest part of the subassembly relatively little rigidity and allows large support tube deflections The pressure tube, being relatively rigid, has fairly small lateral displacements The lateral support deflection is simply the difference between the support tube and pressure tube absolute deflections Another factor which contributes to the lateral support deflection, is the difference in mode shape of the support tube and fuel column and the pressure tube Since the pressure tube is clamped at both ends and the fuel support tube is clamped at the cold end and pinned at the hot end, maximum deflection occurs near the subassembly midpoint but displaced slightly toward the hot end In this region the pressure tube deflections are reduced

Under "Support Tube Stresses" are shown the primary stress and primary plus thermal stresses compared with allowable values Since the gas annulus is vented at the hot end of the reactor, in the cold end support design, the pressure in the annulus is lower than that in the fuel section The primary stresses in the support tube are therefore highest near the cold end of the reactor, where the allowable stresses are also the highest. At axial positions greater than $(X/L)_V \cong 0.5$, the tungsten tube is operating above recrystallization temperature Columns 3 and 4 in this

section show two different values of the primary plus thermal stresses based on two different sources for the value of Young's Modulus It is seen that the calculated stress levels may exceed the estimated allowable stress, depending on the value used for Young's Modulus This emphasizes the importance of establishing accurate material properties in designing the TWMR It should be noted that the results presented in Table 2 2 are for the study case representing the lowest tungsten tube thermal stress levels of any cold end support case with corrugated strip lateral support

The "Pressure Tube Stresses" section of Table 2 2 indicates the primary stress in the aluminum tube to be rather low and compressive This, of course, can be varied by changing the moderator pressure outside of the tube The combined primary and thermal stresses for the aluminum pressure tube appear to be reasonable along the length of the subassembly The primary plus thermal stresses shown in Column 3 are, in all cases, less than the allowable primary The thermal stress in both the support tube and pressure tube is a highly localized stress, occurring only in the region of contact of the lateral support piece

The support tube primary and thermal stresses for the study case presented in Table 2 2 appear to be in a reasonable range Allowable lateral support deflections are insufficient to accommodate thermal expansion in the hotter axial locations The dynamic response yields tube bending stresses which are excessive and also lateral support deflections which cannot be tolerated It is concluded that this design is not acceptable during reactor operation with any dynamic input

The above design was also analyzed using material properties expected during the initial cold launch with 10% of critical damping

in the lateral supports and a 1 0 g input acceleration Maximum dynamic support tube bending stress and lateral support deflection were reduced, because of increased support tube stiffness, to values of 45,000 psi and 26 mils These bending stresses and lateral support deflections are within allowable cold material limits and the design is acceptable for cold launch condition with 1 0 g transverse input acceleration

2 2 Possible Modifications to Cold End Support Design

In the cold end support design, the resonant dynamic response is excessive during reactor operation Since damping controls system response at resonance, any proposed design modification must provide increased energy dissipation from the support tube and/or change the resonance location within the frequency spectrum

2 2 1 Changing the Natural Frequency

Shifting the resonant frequency out of the expected operating bandwidth is not feasible with the clamped-pinned model since this implies increasing the fuel column and support tube stiffness by a factor of 1600 However, a theoretically feasible method of reducing resonant system response, based upon the dependence of tube deflections on boundary conditions, was suggested by comparison of NASA-Lewis cold vibration test results of this study

During large lateral deflections of the fuel column and support tube, the pinned connection at the hot end tends to bind This introduces an axial force component into the restraining forces which, effectively, changes the response of the system to the resonant frequency of the clamped-pinned column Specific hardware to provide the altered boundary

condition at resonance was not defined in this study but the potential for reduced resonant response throughout the operating spectrum is apparent

Attempts to force the pressure tube and the support tube to respond in phase and with similar mode shapes were unsuccessful because of structural limitations at the hot end and because the system is significantly controlled by the inertia of the fuel and support tube

Increased system stiffness, accomplished with an alternate tungsten corrugated strip design, would attenuate the response characteristics of the support tube The lateral support would consist of an axially corrugated annular ring around each fuel segment with the portion of the ring which is subjected to maximum moment placed against the aluminum pressure tube The better physical properties of tungsten at lower temperatures would allow a more rigid lateral support, particularly if the temperature can be maintained below the tungsten recrystallization temperature

2 2 2 Increased System Damping

Increased support tube energy dissipation could be accomlished by using laminated corrugated strip lateral supports, however, the allowable deflection of these springs at the hot end of the subassembly would probably remain insufficient to accommodate the thermal deflections during reactor operation

A laminated support tube would increase energy dissipation if such a tube can be fabricated

A lateral support consisting of particulate ceramic material combined with a corrugated strip would introduce additional system damping, reduce corrugated strip temperatures and thereby increase

allowable stresses and deflections A large degree of damping, dependent upon the relative velocity between the support and pressure tubes, would be caused by motion of the particulate material Design tests would be required to determine concept feasibility

2 3 Alternate Support Designs

Feasibility studies were performed on two alternate fuel support design concepts Both of these concepts were predicated on eliminating the tungsten support tube to determine the relative advantages from the standpoint of support or ease of fabrication

2 3 1 Hot End Support Design

In this design, the fuel stages are stacked one on top of each other The aerodynamic loading and weight of the fuel stages are transported to a support piece located at the hot end of the reactor The support piece is coupled to the aluminum pressure tube which supports the fuel column To establish feasibility of this concept, three factors were considered The size of the support piece required for the loads imposed, the effect on aluminum pressure tube temperatures, resulting from the heat flow through a relatively massive support, and the dynamic response of the fuel column

The hot end support concept consisted of a tungsten cone, on which the fuel stages bear, separated from a stainless steel sleeve inside the aluminum pressure tube by a ceramic liner

Since the hot end support design must have the gas annulus vented at the cold end of the reactor to prevent hot gas leakage outward between stages, the external pressure which must be sustained across the tungsten cone is approximately 100 psi The primary factor in establishing the thickness of this support cone is the pressure load and the materials temperatures expected during operation A preliminary buckling analysis and evaluation of

primary membrane stresses indicated a 40 mil cone would be adequate The heat flow from the hot fuel stages through a cone of this size would cause very high aluminum pressure tube temperatures if the cone were not separated from the pressure tube by a ceramic liner However, a 30 mil ceramic liner allows the aluminum pressure tube temperatures to be maintained at approximately 360 ^{o}F maximum, which is low enough to obtain reasonable stresses The question that arises when considering this design is the integrity of the ceramic liner during vibration and thermal cycling A proposed solution to this problem is a thin metallic coating over the entire liner Thus, if it does tend to crack and breakup, it will be contained within the metallic film, which still maintains the desired thermal properties Fiber reinforced ceramics are also candidate materials for this application

The dynamic response of the fuel subassembly utilizing a hot end support design was qualitatively surmised from the results of the cold end support study It appears that the hot end support design could have greater lateral deflection because the stacked fuel column is less rigid in the lateral direction than the cold end support design The lateral support design problem would therefore be somewhat greater than in the cold-end support case Since the hot-end support offers no advantage in dynamic response characteristics, it is not recommended unless it is found impractical to fabricate the tungsten support tube

2 3 2 Reentrant Flow-Cooled Design

This design eliminates the tungsten support tube by introducing a bleed flow of hydrogen in the gas annulus to cool a stainless steel support tube Coolant flows along the pressure

tube from the cold end to the hot end and then returns along the outer surface of the support tube to the cold end of the reactor where it is discharged into the main coolant stream The purpose of this design is to cool the support tube enough so it can be fabricated of stainless steel To sustain the bulk of the temperature gradient between the hot fuel stages and the reentrant flow coolant, a 20 mil layer of ceramic insulation was introduced between the sheath tube and support tube A bleed flow rate of 0 25 lb/sec yields a maximum support tube temperature of about 1200 ^{o}F or slightly over 600 ^{o}C

The effect of pressure fluctuations at the inlet of the reactor appears to be quite small on the maximum support tube temperatures A pressure fluctuation of +5 psi at the inlet to the inlet to the reactor causes only 100 ^{o}F rise in the maximum support tube temperature Therefore, it appears it would not be necessary to orifice the entrance to the bleed-flow circuit

Primary and thermal stresses in the sheath, support and pressure tubes were not calculated for this design However, it is expected that the primary stresses would not deviate much from other cold end support designs for which the stress calculations have been performed With the 20 mils of insulation between the sheath and support tube the thermal gradients in the support tube and aluminum pressure tube indicate there would be no problem with thermal stresses

Aside from eliminating tungsten as a support tube material, the reentrant flow cooled design could possible show some advantages in the dynamic response of the subassembly Although a vibration analysis was not performed on the reentrant flow cooled design, some qualitative conclusions can be drawn Bleed flow causes low material temperatures, in the gas gap, over the full length of the subassembly This would allow very rigid coupling

between the support tube and the aluminum pressure tube, particularly near the hot end of the reactor, where the stainless steel support tube temperature and the lateral support temperature are modest

The detailed design of a reentrant flow-cooled fuel support system would have to address itself to three problems The first would be maintaining the thermal integrity of the insulating layer between the sheath and support tubes, while supporting the fuel stages adequately in a fixed position The second would be to insure adequate after-cooling of the stainless support tube during shutdown of the TWMR The rigid lateral supports would provide a very good cooling path from the support tube through the aluminum pressure tube to the moderator circuit The third problem would be designing the entrance to the bleed-flow passage, that is, from the inlet plenum, through the beryllium reflector at the cold end of the reactor, and into the annulus separating the support and pressure tubes Also of concern would be an adequate flow divider design that insures downflow and upflow passages with relatively little intermixing

3 0 EFFECT OF LATERAL SUPPORTS ON ADJACENT TUBES

3 1 Introduction

The placement of lateral supports in the static gas gap can cause high localized tube temperatures at support contact points on the adjacent pressure and support tubes These high localized temperatures are accompanied by increased average tube temperatures, reduced allowable tube stresses and large temperature gradients To determine the effect of various fuel column lateral support configurations on the adjacent aluminum pressure tube and tungsten support or sheath tubes, the temperature gradients near lateral support contact points were defined in detail and the resulting thermal stresses were estimated

Several different support concepts and configurations were analyzed The evolution of these lateral support designs was directly influenced by measures taken to reduce either corrugated strip temperatures, thereby increasing allowable stresses, or to reduce tube temperature gradients and the associated thermal stress levels

3 2 Method of Analysis

3 2 1 Heat Transfer Analysis

In most of the lateral support concepts investigated, an exact or analytic solution was inappropriate because the required model would have been a gross simplification of the actual geometry and would have yielded questionable results Thus, the finite difference method was used This approach requires a minimum amount of model simplification since the nodes can be taken sufficiently small and of different shapes so that any of geometric complexities can be closely approximated However, the

finite difference solution requires an enormous amount of numerical calculation for even a small number of nodes For this reason, the numerical procedures were carried out using an IBM 7090 computer code called "STHTP" (1) This program will handle simultaneous steady state heat transport by radiation and conduction with a total capacity of 500 radiation and conduction nodes

The heat transfer region involves the tungsten support tube and/or sheath tube, the aluminum pressure tube, and the enclosed static gas annulus which includes a support device Although this region is cylindrical, the thickness of the annulus is small compared to the mean radius, therefore, a flat plate model is adequate and more simple This approximation leads to slightly conservative temperature estimates in the aluminum pressure tube A unit depth heat transfer model was also assumed, thereby neglecting the effect of axial heat conduction During actual operation of the reactor there will be a flow of heat from the hot end, near the reactor exit, toward the reactor flow entrance The net result of the flat plate and unit depth model assumptions is that the model will predict temperatures too high near the reactor exit and temperatures too low near the core entrance

In all of the models analyzed, heat transfer across the stagnant hydrogen annulus was allowed to take place by conduction and also, when applicable, by radiation The thermal conductivity and emissivity of all materials were assumed to be independent of temperature, except that the conductivity of the tungsten corrugated strip was taken at the average strip material temperature, and was therefore higher than that of the sheath tube Table 3 1 indicates the values of thermal conductivity and emissivity for the various materials used in this study These values are common to all cases investigated

TABLE 3 1 MATERIAL THERMAL PROPERTIES AND PARAMETERS FOR STAGNANT HYDROGEN ANNULUS HEAT TRANSFER MODELS

Moderator Film Coefficient	5600	Btu/hr-ft^2 ^{o}F
Propellant Film Coefficient	2200	Btu/hr-ft^2 ^{o}F
Thermal Conductivity		
Hydrogen, Stagnant annulus	0 28	Btu/hr-ft ^{o}F
Tungsten, Corrugated strip	67 0	Btu/hr-ft ^{o}F
Tungsten, Support and/or sheath	60 0	Btu/hr-ft ^{o}F
Aluminum, Pressure tube	100 0	Btu/hr-ft ^{o}F
Zirconia (ZrO_2), Insulation	1 2	Btu/hr-ft ^{o}F
Emissivity		
Tungsten, Support and/or sheath	0 25	
Aluminum, Pressure tube	0 10	

The values listed are estimates for average thermal conditions at the hot end of the reactor except for the moderator and propellant film coefficients Tungsten thermal conductivity will be somewhat higher at the core entrance, while the average hydrogen conductivity in the same core region will be much lower The thermal conductivity of aluminum over the core length will not vary significantly These thermal conductivities lead to lower than actual average aluminum tube temperatures in the colder region of the reactor because of the lower gap thermal conductivity but will give slightly higher temperature gradients in rib or corrugated strip models as a result of the higher support device conductivity

Typical values of the pressure tube-flow splitter film coefficient as a function of bulk moderator velocity are calculated by the equation

$$N_{Nu} = 0\ 023(N_{Re}{}^{8}N_{Pr}{}^{4})_b$$

The subscript b indicates that the Reynolds number and Prandtl number are evaluated at the moderator bulk temperature Using the average annulus flow rate given by [2]

$$W_{core} = 229\ W_{annulus}$$

where,

$$W_{core} = 1200\ lb/sec$$

yields a minimum velocity of approximately 15 4 ft/sec The minimum film coefficient occurs at the reactor inlet and is approximately 5600 Btu/hr-ft^{2}oF Under the same conditions, the film coefficient will be approximately 6200 Btu/hr-ft^{2}oF at the reactor exit

The propellant film coefficient was evaluated for conditions near the reactor entrance using the equation

$$N_{Nu} = 0\ 021(N_{Re}{}^{8}N_{Pr}{}^{4})_f\left(\frac{T_b}{T_f}\right)^8$$

where the subscript f indicates properties evaluation to be made at the film Results indicate that heat transfer is significant between the propellant and sheath tube only over approximately the entrance half of the core and here the heat is transferred to the propellant Therefore, using the lower coefficient yields higher temperatures in the tungsten tubes and thus more conservative results Near the reactor exit, however, the heat flow may be in the opposite direction (i e , heat may be transferred from the propellant to the sheath or support tube), thus, a smaller film coefficient would yield less conservative results at this

location A check case was run, however, which showed that under the most adverse condition an infinite film coefficient at the reactor exit will increase the aluminum tube temperatures less than 4 ^{o}F

Contact coefficients between metal bearing surfaces were calculated in terms of an equivalent stagnant hydrogen gap For instance, 0 001 in of stagnant hydrogen would yield an equivalent contact coefficient of

$$h = \frac{k_H}{\Delta X} = \frac{(0\ 28)(12)}{0\ 001} = 3360 \text{ Btu/hr-ft}^2{}^{o}F$$

In some cases application of a coating of ZrO_2 was incorporated in the model to obtain an equivalent contact coefficient For example, if

$$h = 5000 \text{ Btu/hr-ft}^2{}^{o}F$$

then

$$\Delta X_{ZrO_2} = \frac{(1\ 2)(12)}{5000} = 0\ 00288$$

$$\approx 0\ 003 \text{ in } ZrO_2$$

That is to say, if a contact coefficient of 5000 Btu/hr-ft$^2{}^{o}F$ is desired between two metallic surfaces, then a coat of about 3 mils of ZrO_2 will be required If this approximation is made, contact resistance, in the true sense, is neglected

The contact coefficient between the support tube and the sheath tube was taken to be 4000 Btu/hr-ft$^2{}^{o}F$ for all applicable cases This corresponds to something less than 1 mil of stagnant hydrogen between the tubes Contact coefficients at the lateral support contact surfaces for the corrugated strip models were taken to be either 5000 or 35,000 Btu/hr-ft$^2{}^{o}F$ As

seen above, a contact coefficient of 5000 Btu/hr-ft^{2}oF corresponds to approximately 3 mils of ZrO_2 The value 35,000 Btu/hr-ft^{2}oF corresponds to a moderate pressure contact in an H_2 atmosphere

The axial unit volumetric heat generation distribution for aluminum and tungsten is illustrated in Figure 3 1 Where solid ceramic or porous materials were used, the heat generation rates were calculated Table 3 2 shows the values for tungsten and aluminum used in the computer program

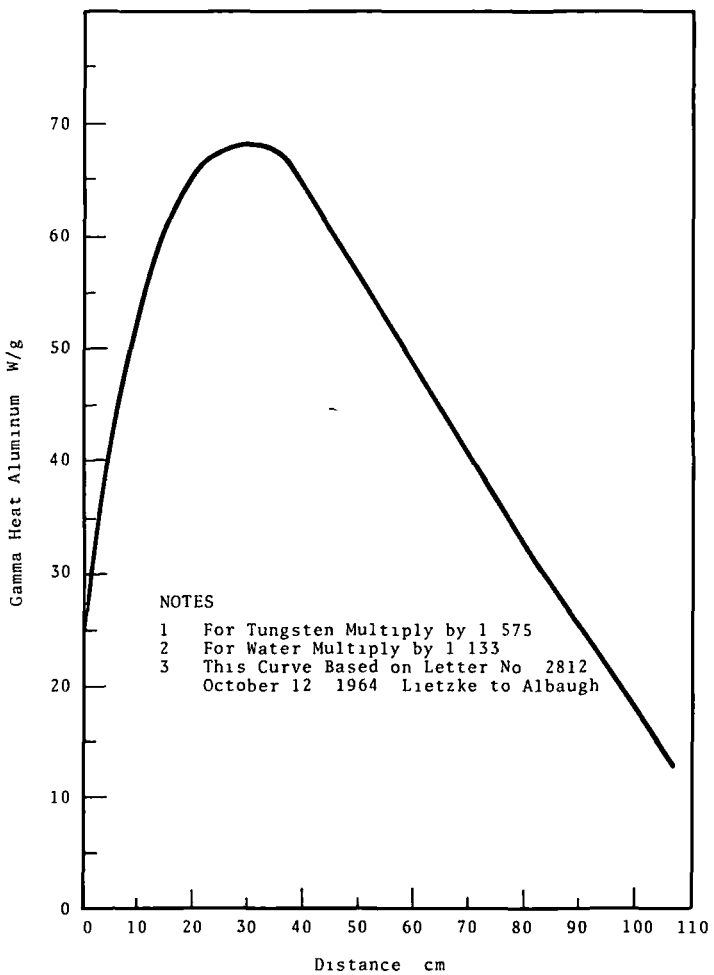

FIGURE 3 1 Gamma Heat of Aluminum Versus Distance from Inlet End of First Fuel Stage

TABLE 3 2 VALUES USED IN THE COMPUTER CALCULATIONS FOR GAMMA HEATING, PROPELLANT TEMPERATURE AND MODERATOR TEMPERATURE AS A FUNCTION OF X/L

Axial Location $(X/L)_t$	Peak Avg	$Q(W)10^4$ Btu/hr-in^3	$Q(Al)10^4$ Btu/hr-in^3	Moderator Temperature, ^oF	Propellant Temperature, ^oF
0 1	1 15	9 01	0 800	211	280
0 2	1 44	11 3	1 00	216	823
0 3	1 47	11 5	1 02	220	1387
0 4	1 36	10 6	0 945	224	1952
0 5	1 16	9 09	0 806	228	2472
0 6	0 97	7 60	0 675	233	2932
0 7	0 79	6 19	0 549	237	3312
0 8	0 62	4 85	0 431	241	3622
0 9	0 45	3 62	0 313	246	3872
1 0	0 285	2 23	0 198	250	4040

Table 3 2 also shows the values used for the moderator and propellant temperature at the various axial locations Figure 3 2 illustrates the axial bulk propellant and moderator temperature distribution The moderator inlet and outlet temperatures were obtained from the reference design and a linear distribution was assumed between these points according to

$$T_M = 207 + 43 \left(\frac{X}{L}\right)$$

3 2 2 Stress Analysis

Tungsten support tube and aluminum pressure tube stresses were calculated for a number of study cases at reactor operating conditions The study cases were identified as cold-end support or hot-end support depending upon the core location at which the fuel column was fixed Cold-end support cases utilized essentially the same arrangement of core components as the TWMR

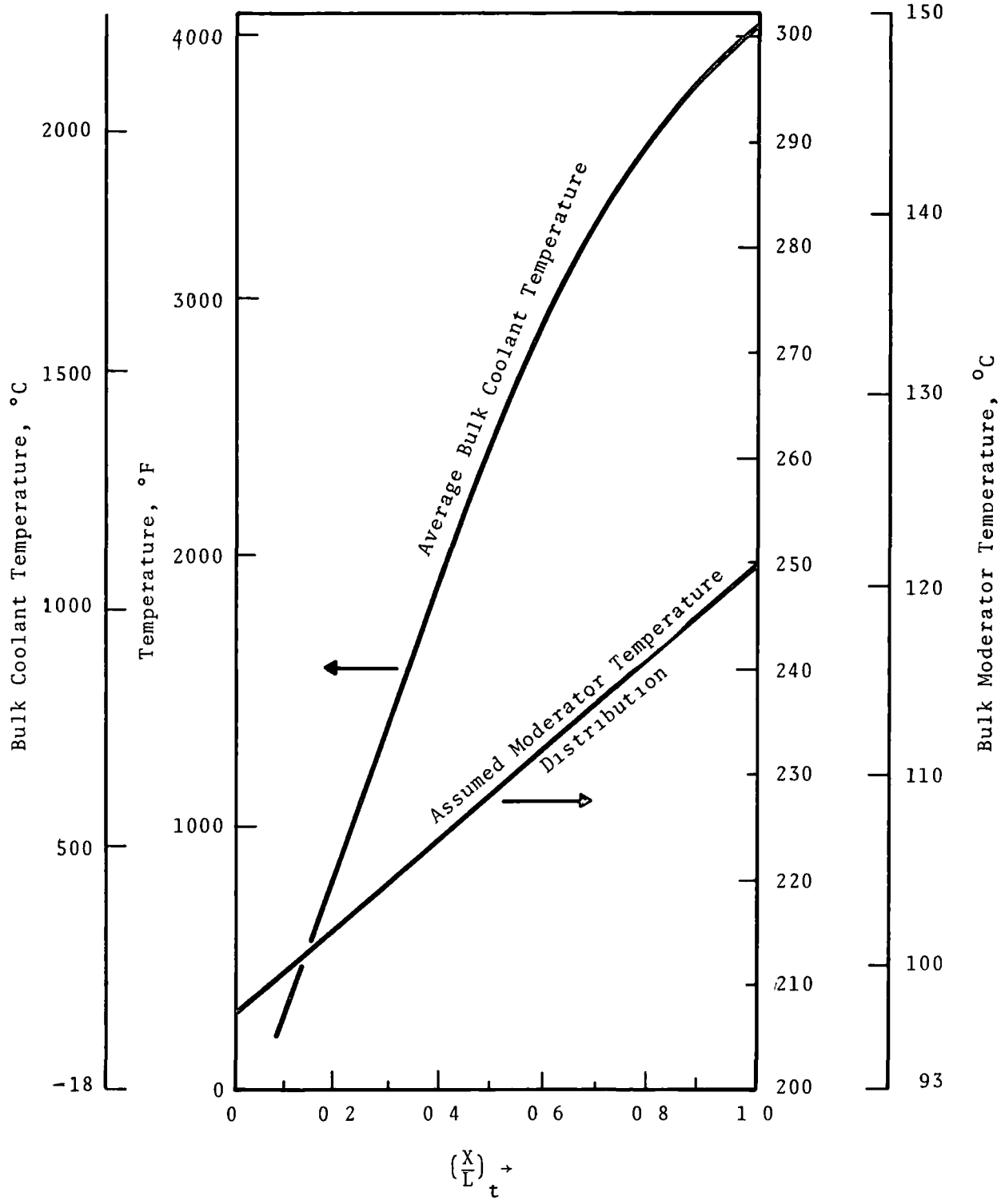

FIGURE 3 2 *Bulk Coolant and Bulk Moderator Temperature Versus Axial Position*

reference design concept [3] Two hot end support study cases, differing only in the type of lateral support, were evaluated with respect to aluminum pressure tube stresses and estimated fuel stage sheath stresses These study cases considered elimination of the tungsten fuel support tube and axial support of the fuel column by a structure located near the hot end of the fuel column At least a loose interlocking of fuel stages and provision of a lateral support device in the static gas annulus would be required in the hot end fuel support concept

For convenience in presenting the analysis results, the tube stresses for both cold end and hot end support cases are discussed in this section The thermal analysis of the hot end support structure is discussed in Section 6 of this report

Tube stress calculations were performed primarily over the axial length of the fuel column, i e , an axial position $(\frac{X}{L})_t = 0$ corresponds to the first fuel stage and $(\frac{X}{L})_t = 1$ corresponds to the last stage of the fuel column

3 2 2 1 Cold End Support

Tungsten fuel support tube stresses during reactor operation arise from several conditions

- Differential pressure between the static gas annulus and the interior of the fuel support tube The static gas annulus was assumed to be at reactor exit pressure of 600 psi In the absence of a preferred fuel design the preliminary stress calculations were based upon an assumed linear pressure gradient from 703 psi at the first stage to 608 psi at the last stage of the fuel column At axial positions $0.4 < (X/L)_t < 1.0$ the selected pressure

gradient closely approximates the pressure gradient calculated for the concentric fuel element design in Reference (3)

The differential pressure produces hoop stresses calculated from

$$\sigma = \frac{PR}{t}$$

where P is the differential pressure, R is the mean radius of the tube and t the tube thickness

- Support tube axial loads due to fuel weight were calculated assuming 1 g axial acceleration The weight of each fuel stage including the sheath tube was taken at 1 15 lb Lateral acceleration loads were not considered in this portion of the analysis

- Flowing hydrogen produces aerodynamic loads which are transmitted to the fuel support tube The accumulated aerodynamic loads, increasing in value from the hot end to the cold end of the fuel column, were estimated using the linear approximation of static pressures in the fuel column and the cross sectional area of the fuel stage The axial tensile stresses were calculated from

$$\sigma = \frac{P_a}{A_{st}}$$

where P_a is the accumulated axial load at the tube location of interest and A_{st} is the cross sectional area of the support tube wall

- Radial temperature gradients cause thermal stresses in the fuel support tube Axial and tangential thermal stresses, of equal magnitude at the tube surfaces, can be calculated from[4]

$$\sigma_{tangential} = -\frac{E\alpha}{1-\nu} \frac{1}{r^2} \left[Tr^2 - \int_a^r Trdr - \frac{r^2 + a^2}{b^2 - a^2} \int_a^b Trdr \right]$$

$$\sigma_{axial} = -\frac{E\alpha}{1-\nu} \left[T - \frac{2}{b^2 - a^2} \int_a^b Trdr \right]$$

where

E = Young's Modulus
α = coefficient of thermal expansion
ν = Poissons ratio = 0 3
a = inside radius of tube
b = outside radius of tube
T = radial temperature distribution
r = radius of tube

When the tube wall is thin compared with the mean radius, the above equations can be simplified, giving the approximate equation(5)

$$\sigma_{tangential} = \sigma_{axial} \cong \frac{-E\alpha}{1-\nu} \left[T - \frac{1}{t} \int_o^t Tdx \right]$$

where $t = b - a$

and $o \leq x \leq t$

- In study cases which consider lateral supports placed in the static gas annulus, circumferential temperature gradients cause thermal stresses near lateral support contact points The maximum axial tube stress at the centerline of the lateral support can be calculated from(6)

$$\sigma_{axial} \cong - E\alpha\Delta T_{max}$$

where

ΔT_{max} = the maximum tube surface circumferential temperature difference (ΔT_{max} is negative at the tungsten tube and positive at the aluminum pressure tube)

In cold-end support study cases the aluminum pressure tube stresses arise from differential pressure, radial temperature gradients across the tube wall and circumferential temperature gradients at lateral support contact locations Compressive hoop stresses in the aluminum pressure tube were calculated with 600 psi static gap pressure and moderator pressures varying linearly from 631 psi at $(\frac{X}{L})_t$ = 0 0 to 602 psi at $(\frac{X}{L})_t$ = 1 0 Axial fuel weight and aerodynamic loads do not cause aluminum tube stresses since these loads are transmitted to the beryllium reflector During a reactor startup the aluminum pressure shell and pressure tubes will increase in temperature together so that essentially no thermal stresses are imposed upon the pressure tubes due to relative displacement between these components

3 2 2 2 Hot End Support

Replacement of the tungsten fuel support tube with an axial support structure located near the hot end of the reactor core alters the pressure profile on both the aluminum pressure tube and the fuel element sheath tubes The 0 125 in static gas annulus was considered sealed at the hot end support location and vented at the core inlet Tube stresses were evaluated with 703 psi static gap pressures The sheath tube model did not assume any support from the fuel itself The calculated pressure stresses in the sheath tube were therefore much higher than would be

typical of some of the fuel designs being considered, e g , honeycomb or egg-crate fuel designs However, the buckling strength of the sheath tube is low, and reinforcement of the tube in this manner or reduction of the pressure differential would be essential

In the case of hot end support of the fuel column, the fuel weight and aerodynamic loads were assumed to be applied to the aluminum pressure tube at or below $(\frac{X}{L})_t = 1\ 0$

3 2 2 3 Tube Stress Limits

Two types of stress, classified as general and local, are recognized[7] when establishing allowable thermal stress limits General thermal stress is associated with distortion of the structure in which it occurs and local thermal stresses do not produce significant overall distortion General thermal stress is also classified as a secondary stress since local yielding and minor distortions can satisfy the conditions which cause the stress (for example, stresses produced by the temperature difference between a nozzle and the shell to which it is attached) General thermal stresses which exceed twice the yield strength of the material have a special significance Two times the yield strength determines the borderline between loads which, when repetitively applied, allow the structure to "shake down" to elastic action and loads which produce plastic action each time they are applied

The tube thermal stresses arising from both radial and circumferential temperature gradients are of a type associated with almost complete suppression of the differential thermal expansion and thus produce no significant distortion of the overall tube structure These stresses, classified as local thermal stresses, are objectionable as a possible source of a fatigue crack or brittle fracture In considering these local or peak

stresses from a fatigue standpoint, calculations normally proceed on the assumption of elastic material behavior When the elastic limit of the material is exceeded, the elastic calculation gives a stress value which, although fictitious, is proportional to strain The localized tube strain in turn can be used as a measure of damage if appropriate fatigue data are available

Fatigue curves of stress versus cycles to failure, which are obtained from tests in which strain rather than stress is the controlled variable, are not available at the tungsten temperatures of interest In the absence of these data a detailed fatigue analysis was not performed The effects of alternate lateral support configurations on tube stress levels were, however, estimated by comparison of combined primary and thermal stress components at the location of maximum localized stress in the tube

As a first estimate of lateral support acceptability it was judged that the combined primary and maximum thermal stress should be less than twice the yield strength of the material While this criterion is more appropriate as an allowable primary plus secondary stress intensity limit, there is some justification in the case of localized tube stresses which occur with corrugated strip lateral supports having 12 or more segments The localized stress region spacing in the tube meridional direction becomes less as the number of support segments increases, and the localized stresses have some of the characteristics of a secondary stress

The major difference between thermal and mechanical stresses is that the thermal stress pattern need satisfy only the requirement for equilibrium of internal forces, and of course strain compatibility, whereas the externally loaded structure must satisfy an equilibrium requirement which, in general, is not mitigated by yielding Allowable primary membrane stresses, that is, those due to pressure, aerodynamic and fuel weight loads, were taken at 80% of tube material tensile yield strength

3 2 2 4 Material Properties

The tungsten tube thermal stresses were calculated with values of static Young's Modulus obtained from Reference 8 and and coefficient of thermal expansion from Reference 9 Recent measurements of tungsten Young's Modulus at elevated temperatures[10] agree more closely with the Reference 9 values and suggest that these data should more appropriately be used Thermal stresses were recalculated, with corrected values of Young's Modulus, in one cold end fuel support study case Figure 3 3 indicates the magnitude of discrepancies in reported Young's Modulus data

The aluminum tube thermal stresses were calculated with coefficient of thermal expansion values for 6063 aluminum[11] and typical Young's modulus values for 6061-T6 alloy [12]

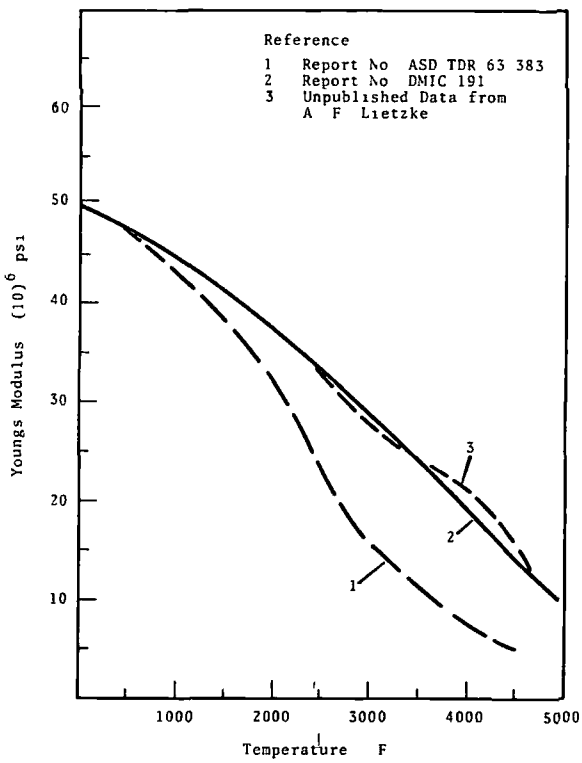

FIGURE 3 3 TUNGSTEN, Static Young's Modulus Versus Temperature

3 2 2 5 Computer Code Modifications

Modification of the STHTP computer code, to include the stress calculations, allowed the tube stress distribution to be defined in greater detail than otherwise possible Radial and circumferential thermal stresses and total axial and tangential stresses were calculated at locations corresponding to each thermal node used in calculating tube temperatures The material properties, Young's Modulus and coefficient of thermal expansion, were introduced into the calculations through interpolating polynomials imbedded in the computer program

3 3 Preliminary Heat Transfer Models

The initial thermal studies of a lateral fuel support were concerned mainly with gaining relative magnitude information regarding tube temperature, support device size, and heat transferred for a 0 062 in hydrogen annulus For these studies the rib support model shown in Figure 3 4-A was used This model is merely two flat plates separated by a hydrogen gas gap and connected by a thin rib which constitutes the support device The rib support is a first approximation of an actual support since it neglects radiation blockage and provides only a simple conductive path Since the heat transfer models are broken down into a number of nodes, any change of geometry changes the amount of the computer input data The rib model has great utility from the standpoint that dimensional changes do not greatly change the amount of computer input Thus, a large amount of information was obtained from this model with a minimum of time and effort The rib model was also useful in determining the relative size of the support device and the general range of tube temperatures The effect of contact resistances placed at either end of the support device was also determined Specifically, the rib model revealed that a support device such as the one shown in Figure 3.4-A

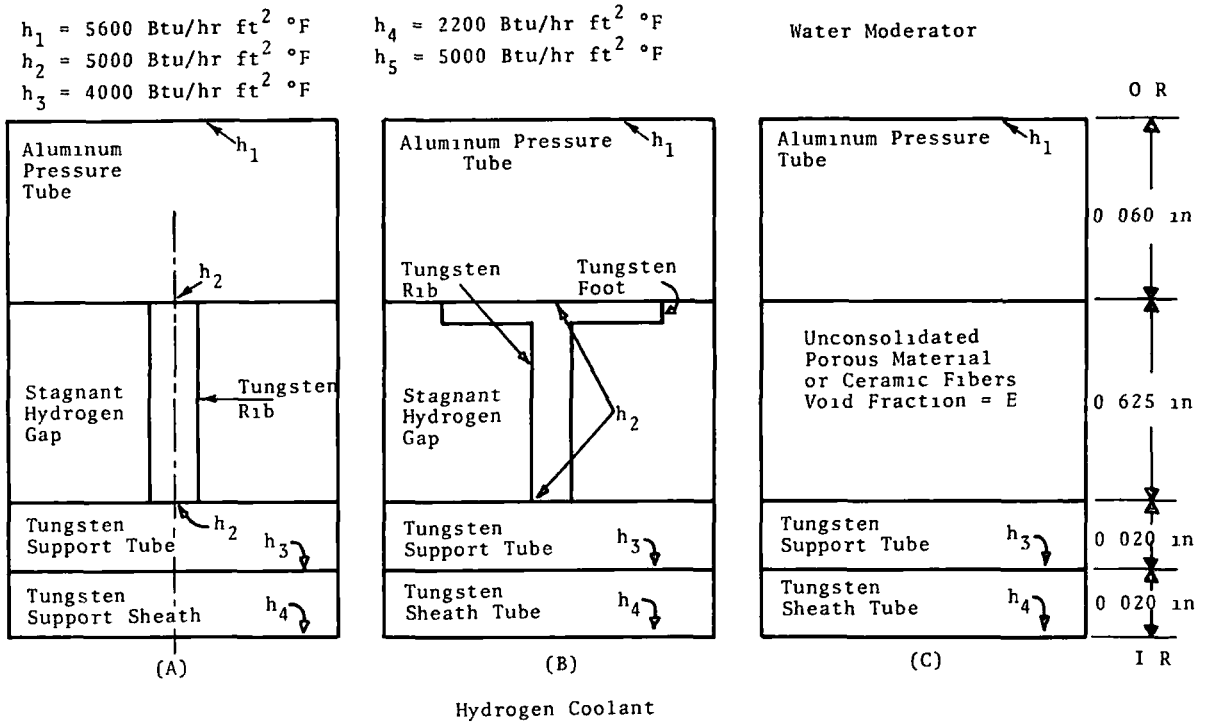

FIGURE 3 4 Preliminary Heat Transfer Models

would yield satisfactory tube temperatures away from the rib contact point, but that localized peak temperatures in the aluminum pressure tube at the support contact would be intolerably severe (see Figure 3 5) Contact of the rib support

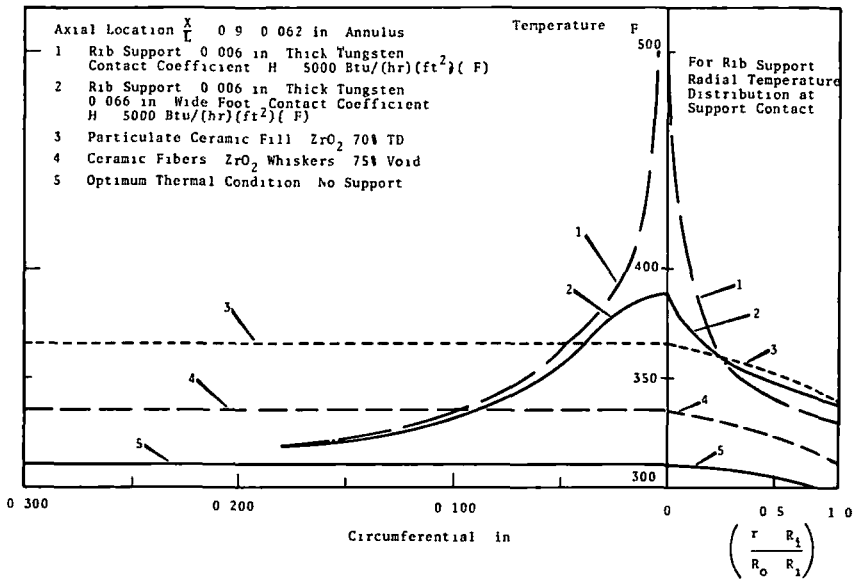
Axial Location X/L 0 9 0 062 in Annulus
1 Rib Support 0 006 in Thick Tungsten Contact Coefficient H 5000 Btu/(hr)(ft2)(F)
2 Rib Support 0 006 in Thick Tungsten 0 066 in Wide Foot Contact Coefficient H 5000 Btu/(hr)(ft2)(F)
3 Particulate Ceramic Fill ZrO2 70% TD
4 Ceramic Fibers ZrO2 Whiskers 75% Void
5 Optimum Thermal Condition No Support
Temperature F
500
400
350
300
For Rib Support Radial Temperature Distribution at Support Contact
0 300
0 200
0 100
0
0 5
1 0
Circumferential in
(r - Ri)/(Ro - Ri)

FIGURE 3 5 Typical Circumferential and Radial Temperature Distributions for Preliminary Heat Transfer Models (Reference Figure 3 3)

with the tungsten support tube also introduced large temperature gradients in the support tube (see Figure 3 6)

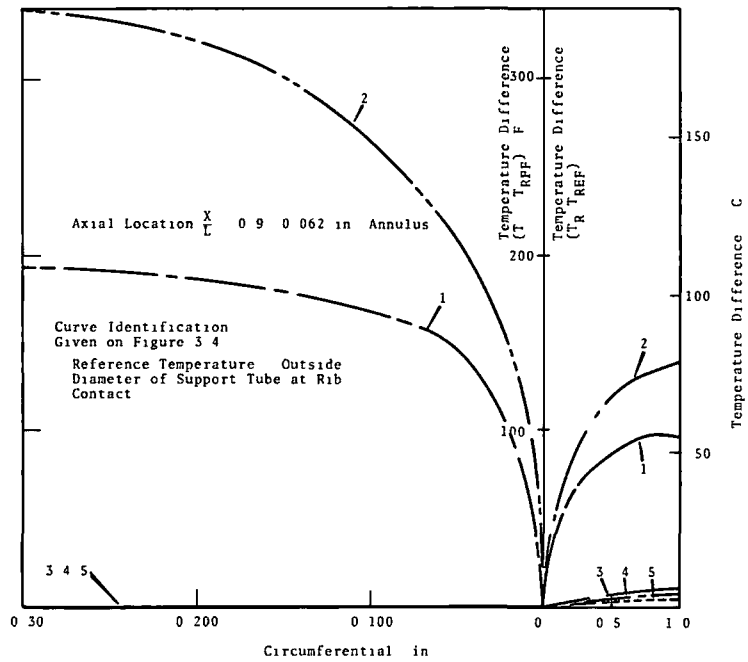

FIGURE 3 6 Typical Circumferential and Radial Temperature Distributions for Preliminary Heat Transfer Models (Reference Figure 3 4)

The large localized temperatures in the aluminum pressure tube prompted the first variation in the rib model A foot was added to the aluminum side of the rib The beneficial effect of the foot is in distributing the heat flow over a large contact area thereby causing the heat flux to occur at a much lower potential To be effective, an insulation strip must be placed between the foot and the pressure tube to effect a more even distribution of heat flux over the foot contact area Figure 3 4-B illustrates the heat transfer model used for the analysis Simplicity is again a pertinent feature of this model since dimensional changes can be accomplished without a great change in computer input The rib with foot configuration was effective in reducing the localized

temperature in the pressure tube (see Figure 3 5) A contact coefficient of about 5000 Btu/hr-ft^2°F provided sufficient thermal resistance between the foot and pressure tube Thermal gradients in the support tube were not mitigated, but actually become more severe (see Figure 3 6) The implication is that the increased contact area allowed a larger flow of heat to the pressure tube even with the much smaller potential between the foot and aluminum pressure tube

The addition of a foot, or extended contact area, on the aluminum tube side of the rib support alleviated concern over localized hot spots in the aluminum pressure tube However, the large temperature gradients in the support tube were undesirable For this reason an investigation of concepts, which might mitigate or eliminate circumferential thermal gradients in the support tube, was initiated

Two concepts which accomplish the desired reduction in thermal gradients are illustrated by the model of Figure 3 4-C The annular region between the tungsten support tube and aluminum pressure tube consists of ceramic fibers or is filled with unconsolidated particulate ZrO_2 The ceramic fibers could either be in mat form, having random orientation and length, or in the form of a large number of individual fibers, having predictable length and cross section, with one end bonded to the aluminum pressure tube The individual fibers would then act as small cantilevered supports This heat transfer model permits heat to be transferred across the annulus in an amount which depends on the radiation blockage A detailed discussion of the assumptions which went into the analysis along with detailed results are presented in NASA-CR-54409 (13)

The model having the annular region filled with particulate ZrO_2 requires definition of an effective thermal conductivity,

which includes the heat transfer by conduction and radiation through the annular region A detailed discussion of the assumptions used in defining the effective thermal conductivity and results obtained can be found in NASA-CR-54721 (14)

Figure 3 5 illustrates typical aluminum tube temperatures and temperature gradients for the four models considered at this point Gradients are depicted in Figure 3 6 for the tungsten support tube These curves are typical results for the indicated heat transfer models near the reactor exit

From a thermal viewpoint, the ceramic whiskers and porous models are far superior to either of the rib cases Nevertheless, several disadvantages or unresolved questions render both methods less attractive In the case of porous ZrO_2, the disadvantages include possible slumping or compaction during thermal cycling and vibration, obtaining an acceptable packing arrangement and density, and accommodating thermal expansion of the support tube and particle containment Problems in obtaining ceramic fibers that will withstand the temperature and are long enough to form a mat or act as cantilevers across the annulus, are the principal reasons for discounting the ceramic whisker concept

3 4 Corrugated Strip Support Concepts

As indicated in the previous section, the rib support did not account for radiation blockage across the annulus, nor did it yield a good approximation of the heat generated in an actual support An actual support would most likely be a slanted configuration or corrugated strip which would block radiation and also generate considerably more heat than the preliminary rib models Models used in the analysis of a corrugated strip support have the same general geometry for the lateral support member as shown in Figure 3 7 This support allows for radiation blockage

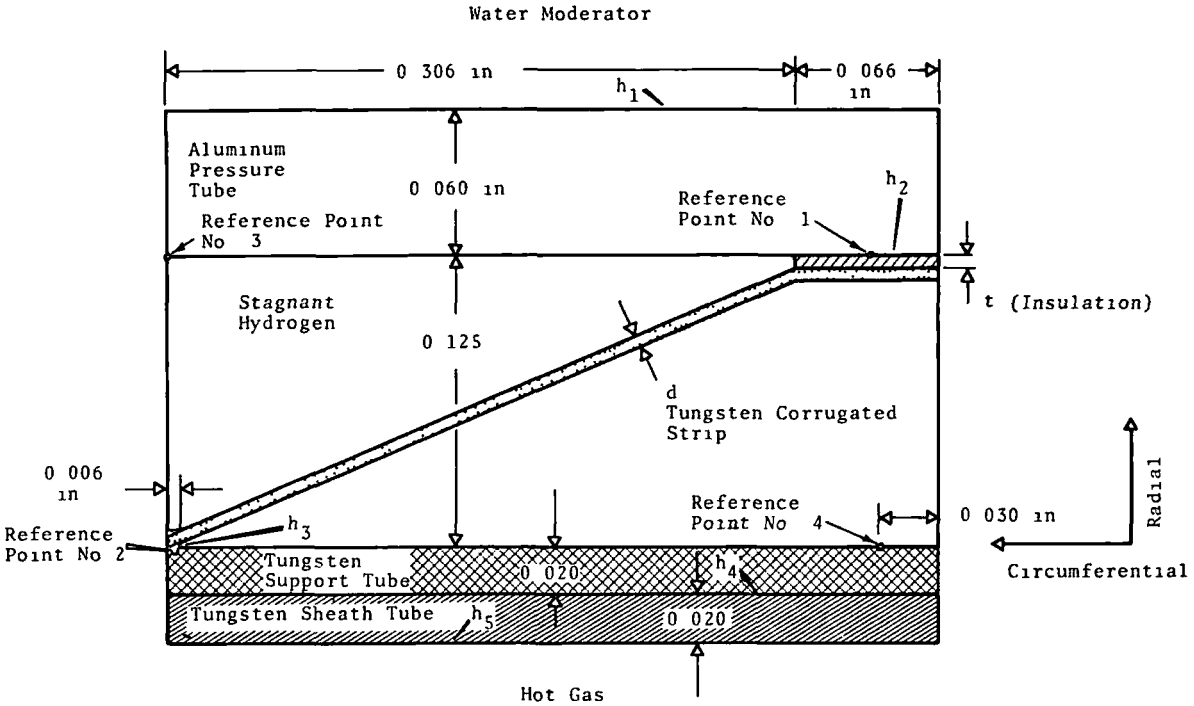

FIGURE 3 7 Heat Transfer Model for Corrugated Strip Support (Cold End Support - Cases 4,5,6, and 10, Hot End Support - Case 7)

and is also a good approximation to the actual conduction path and heat generation In discussion of the corrugated strip models, case numbers have been assigned to identify each variation in strip geometry, insulating material and end support location A summary of pertinent corrugated strip data with each selected study case identification number is presented in Table 3 3

3 4 1 Corrugated Strip - 0 0625 in Annulus

Initial investigations of the corrugated strip model assumed a 0 0625 in annulus and the dimensions L and W, of 0 300 and 0 066 in , respectively, as shown in Figure 3 7 The investigations conducted with this geometry include study of the effects of two different contact coefficients between the pressure tube and the corrugated strip (h_2 = 35,000 and 5,000 Btu/hr-ft^2°F), two different strip thicknesses (0 006 and 0 003 in), and either

TABLE 3 3 SUMMARY OF CORRUGATED STRIP CASES FOR h_2 = 5,000 and 35 000 Btu/hr ft^2 ^{o}F

Case Number	Corrugated Strip Thickness, in	Annulus Width, in	Insulating Strip	Fuel Column Axial Support	Remarks
1	0 006	0 0625	None	Cold End	
2	0 006	0 0625	0 010 in ZrO_2	Cold End	K_{ZrO_2} = 1 2 Btu/hr ft ^{o}F
3	0 003	0 0625	0 010 in ZrO_2	Cold End	
4	0 006	0 125	0 010 in ZrO_2	Cold End	
5	0 003	0 125	0 010 in ZrO_2	Cold End	
6	0 006	0 125	See remarks	Cold End	k = 0 20 Btu/hr ft ^{o}F ρ = 150 lb/ft^3, 0 010 in thick
7	0 006	0 125	0 010 in ZrO_2	Hot End	
8*	0 010	0 125	**	Cold End	Combination Support Porous Material K=0 75,E=0 30(Void Fraction)
9*	0 010	0 125	**	Hot End	Combination Support Porous Material K=0 75,E=0 30(Void Fraction)
10*	0 010	0 125	See remarks	Cold End	Insulating Strip both sides of Corrugated Strip 0 005 in thick at pressure tube 0 010 in thick at support tube

* Not analyzed for h_2 = 35,000 Btu/hr ft^2 ^{o}F

** Insulation strip replaced by contact coefficient equivalent to 0 010 in ZrO_2

CONFIDENTIAL

NASA-CR-72031

with or without insulation between the pressure tube and the support strip A thickness of insulation was used instead of an equivalent contact coefficient to account for heat generation in the insulation Table 3 4 lists the critical dimensions and contact coefficients used in the thermal analysis of the first three corrugated strip cases It will be noted that two different values of h_2, i e , 5,000 and 35,000 Btu/hr-ft^2-^{o}F were used

TABLE 3 4 SUMMARY OF CASES, 0 0625 in ANNULUS
h_2 = 5000 AND 35,000 Btu/(hr)(ft^2)($^\circ$F)

	Case 1	Case 2	Case 3
h_1 Btu/hr-ft^2-^{o}F	5,600	5,600	5,600
h_2 Btu/hr-ft^2-^{o}F	5,000	5,000	5,000
	35,000	35,000	35,000
h_3 Btu/hr-ft^2-^{o}F	0	0	0
h_4	35,000	35,000	35,000
h_5	4,000	4,000	4,000
h_6	2,200	2,200	2,200
Strip thickness, d, in	0 006	0 006	0 003
t, in	0	0 010	0 010

The model indicated by Figure 3 7 with a 0 0625 annulus applies to the first three cases presented in the summary of results, Section 3 5 1

3 4 2 Corrugated Strip - 0 125 in Annulus

Corrugated strip supports, in cases which consider a 0 125 in annulus, fall into two categories depending on the manner in which the fuel column is supported The model shown in Figure 3 7 applied to cold end fuel support cases Figure 3 7

also illustrates the model for the hot end fuel support case These two models are identical in every respect except the support tube is not present in Figure 3 7 The results for study Case 7 were derived from the model shown by Figure 3 7

Four cases numbered 4, 5, 6, and 10, were investigated with the cold end support model, and results were obtained in each case with two different values of h_2 A summary of these cases is listed in Table 3 5 Cases 4 and 5 assumed 0 010 in of ZrO_2 insulation between the pressure tube and support strip but differed in support strip thickness Case 6 was selected to determine the effect of using a less dense insulating material or one which generated less heat than ZrO_2

TABLE 3 5 SUMMARY OF COLD END SUPPORT CASES, 0 125 in ANNULUS, h_2 = 5000 AND 35,000 Btu/(hr)(ft^2)(°F)

	Case 4	Case 5	Case 6	Case 10*
h_1 Btu/hr-ft^2-°F	5,600	5,600	5,600	5,600
h_2 Btu/hr-ft^2-°F	5,000	5,000	5,000	5,000
	35,000	35,000	35,000	
h_3 Btu/hr-ft^2-°F	5,000	5,000	5,000	5,000
	35,000	35,000	35,000	
h_4 Btu/hr-ft^2-°F	4,000	4,000	4,000	4,000
h_5 Btu/hr-ft^2-°F	2,200	2,200	2,200	2,200
Strip thickness, d, in	0 006	0 003	0 006	0 010
t, in	0 010	0 010	0 010	0 005

* *Has 0 010 in of ZrO_2 between support strip and support tube at reference point # 2(Figure 3 7)*

Case 10 is different from the other cold end support models in that 0 010 in of ZrO_2 insulation was assumed between the corrugated strip and the support tube Also, the corrugated strip is 0 010 in thick, and the insulation thickness between the support strip and the pressure tube has been decreased from 10 to 5 mils This case was selected in an attempt to decrease the severity of the tungsten support tube thermal gradients indicated by Cases 4, 5, and 6 results

3 4 2 1 Combination Support - Corrugated Strip and Porous Material

Results obtained from the preliminary model which assumed porous material in the gas annulus were appealing from a thermal viewpoint since circumferential thermal gradients in the support tube were eliminated However, the possibility of structural failure from thermal expansion remained a problem area The combination support model shown in Figure 3 8 would allow space for the particulate material to expand yet maintain the required lateral support

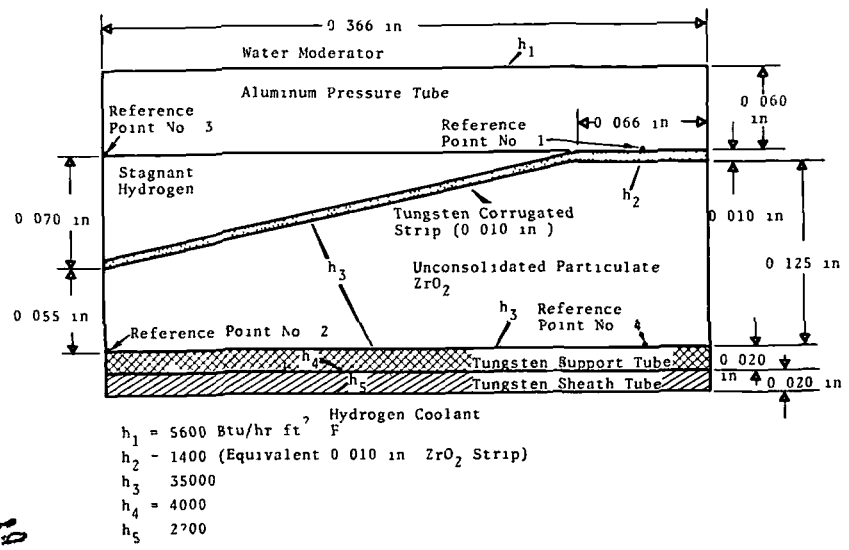

FIGURE 3 8 Heat Transfer Model for Corrugated Strip and Porous Media (Combination Support - Cases 8 and 9)

Two combination support models were analyzed, a cold end support model, Figure 3 8 and a hot end support model which omits the tungsten support tube as indicated by Figure 3 8 Both of these models consider the porous material to be unconsolidated particulate zirconia

Study Cases 8 and 9 were derived from the Figure 3 8 model In both of these cases, the contact coefficient, h_2, was selected at 5,000 Btu/hr-ft^2-^{o}F, which is equivalent to a 0 010 in thick insulating strip between the support strip and pressure tube

3 5 Summary of Corrugated Strip Heat Transfer Results

A minimum number of curves is shown which relate the more relevant temperatures and temperature gradients associated with the aluminum pressure tube and either the tungsten support tube or sheath tube These curves are sufficient to illustrate the effects of the different model configurations and variations More detailed information concerning the results of each particular model may be found in NASA-CR-54721, except for Cases 4,5,6, and 10 The detailed results for these cases have not previously been formally presented Figure 3 9 applies to the 0 0625 annulus and the model used in Cases 1, 2, and 3 Table 3 3 lists the various cases analyzed and indicates the differences between cases Figures 3 10 through 3 17 are summary curves of the thermal calculations for the indicated case numbers

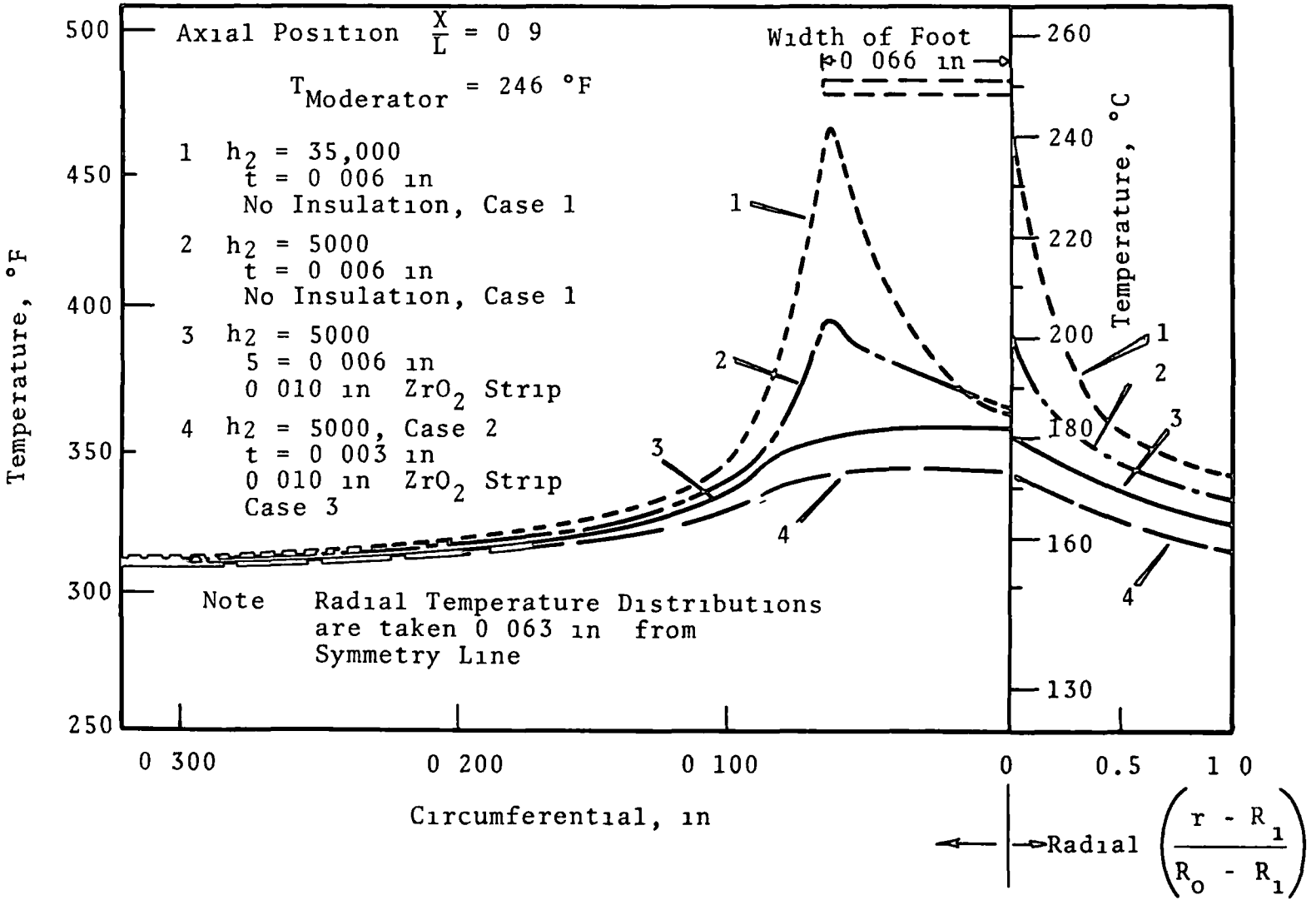

FIGURE 3 9 Radial and Circumferential Temperature Distributions at the Inside Surface of Aluminum Pressure Tube (Illustrates the effect of thermal resistance at the support strip-pressure tube contact surface Plot also illustrates the effect of reducing the corrugated strip thickness)

CONFIDENTIAL

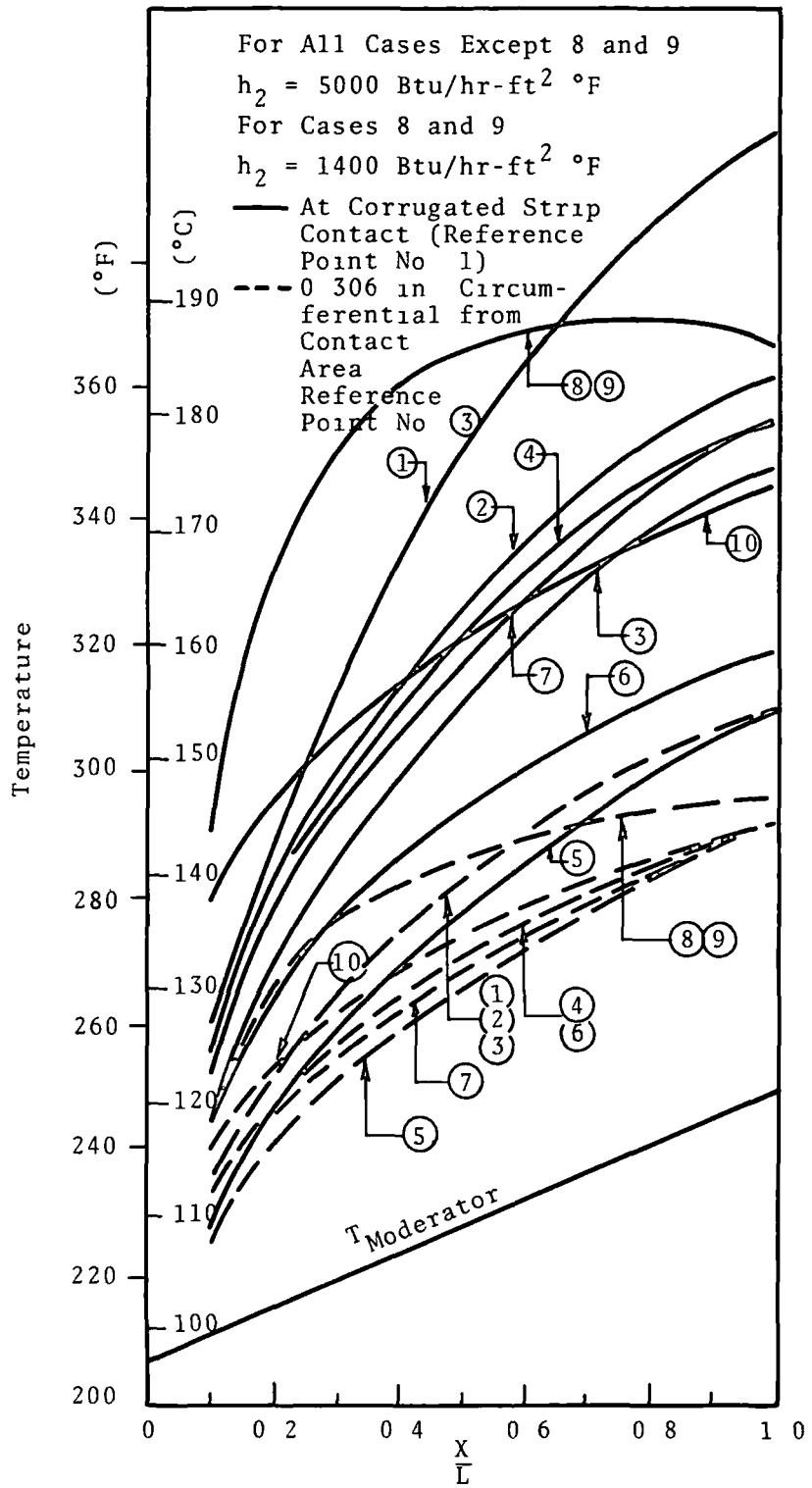

FIGURE 3 10 Aluminum Tube Inside Diameter Surface Temperature Versus Distance from Core Inlet

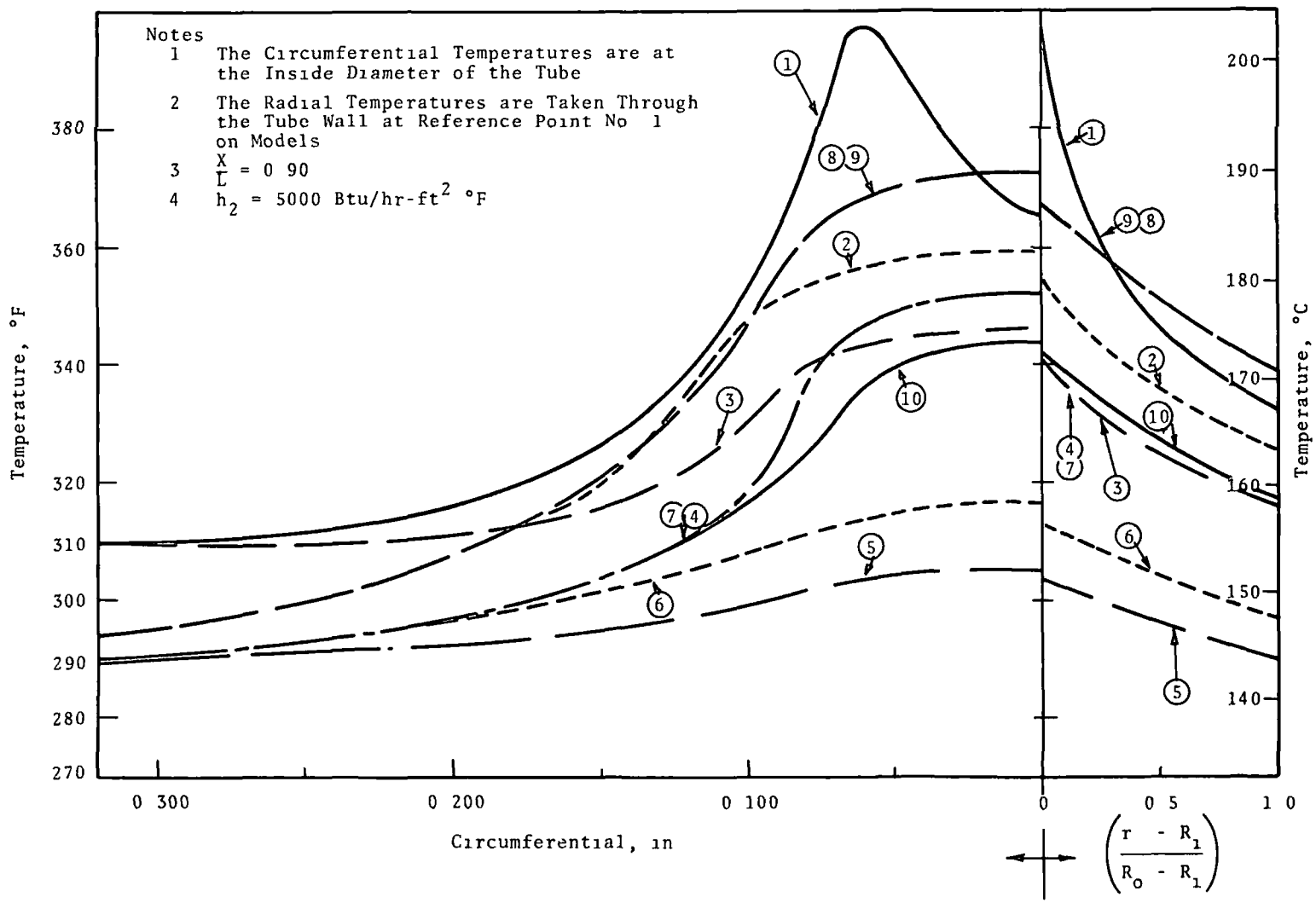

FIGURE 3 11 Typical Circumferential and Radial Temperature Distributions for the Aluminum Pressure Tube Near the Reactor Exit for Various Support Concepts

CONFIDENTIAL

NASA-CR-72031

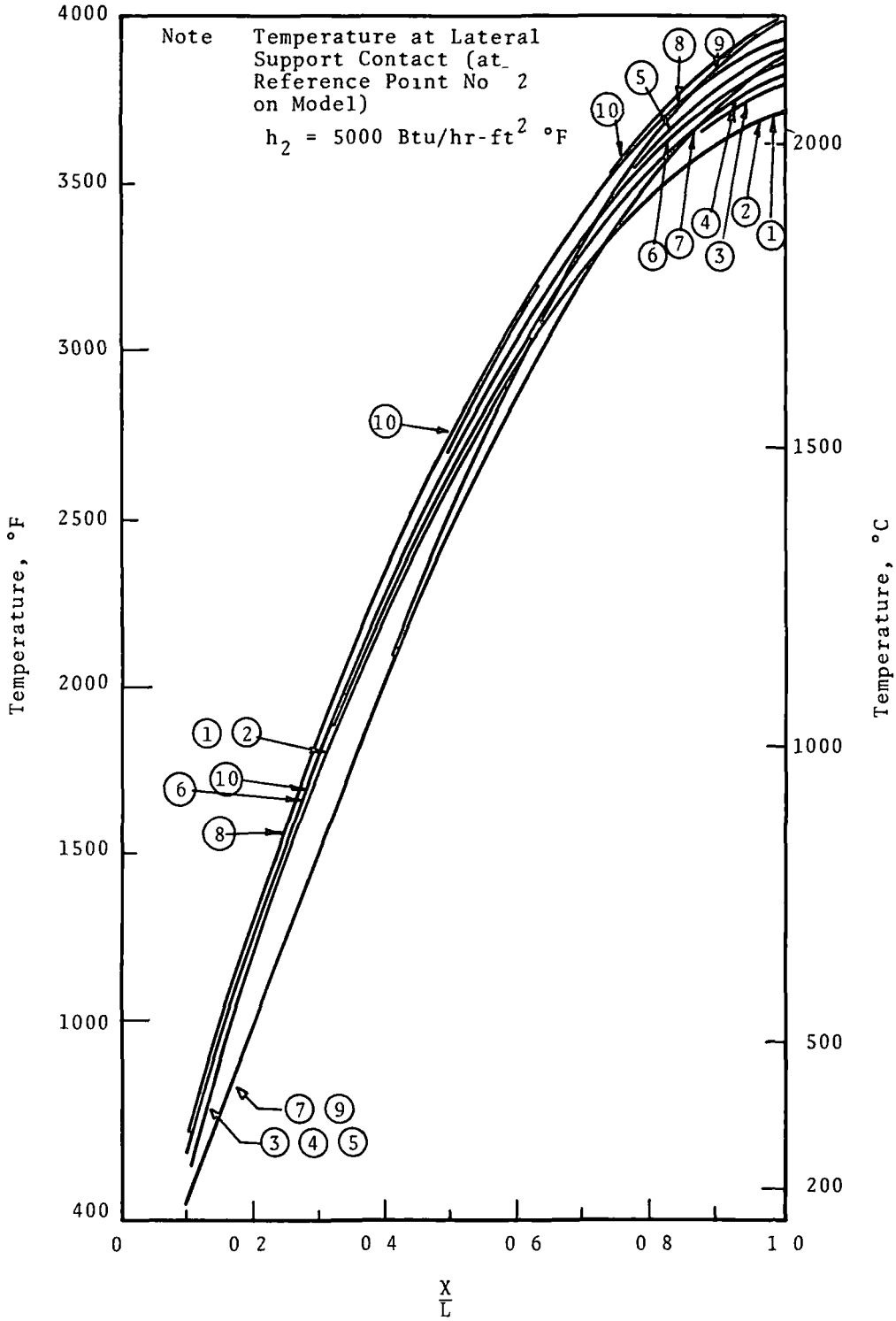

FIGURE 3 12 Tungsten Tube Outside Diameter Surface Temperature Versus Distance from Core Inlet

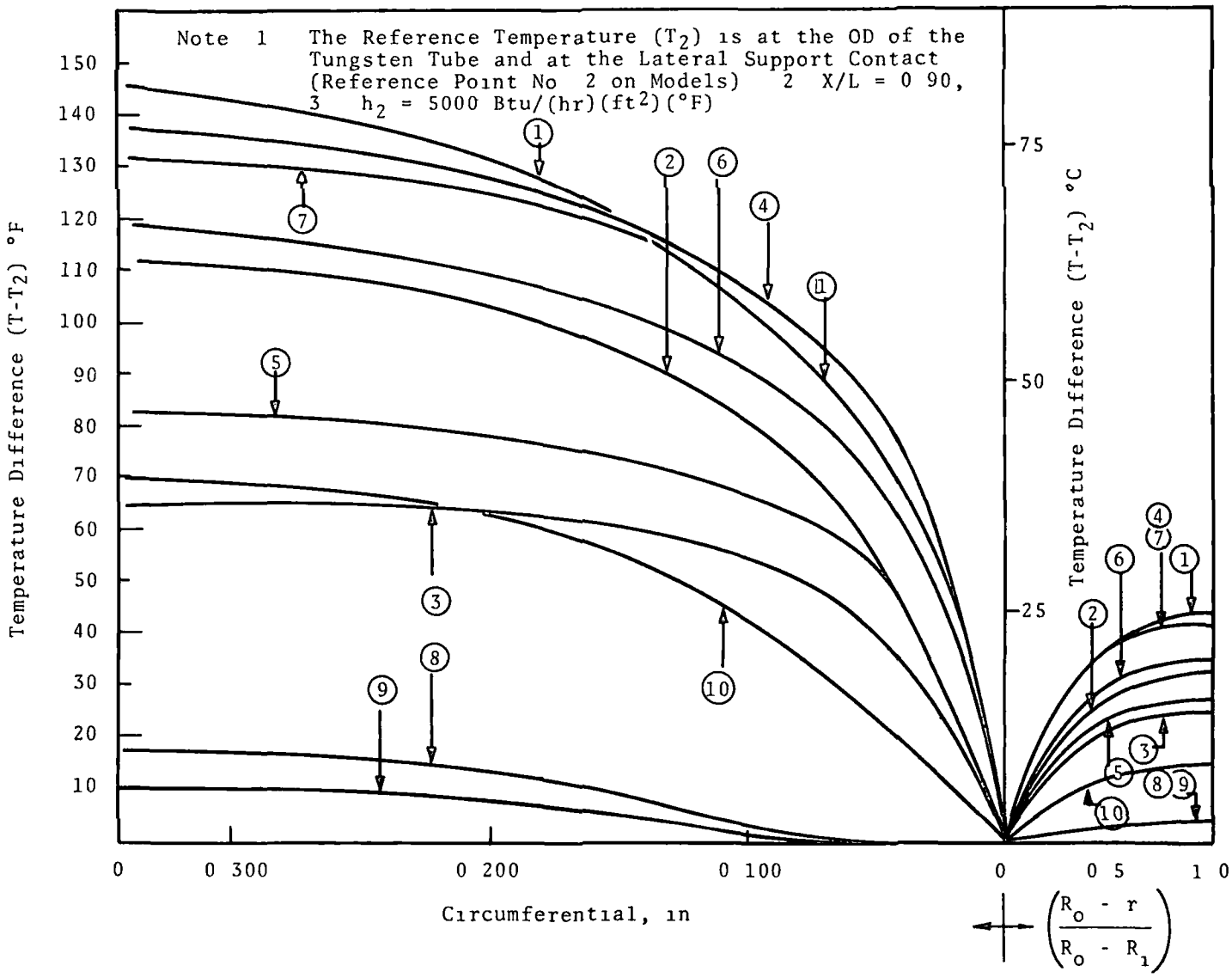

FIGURE 3 13 Typical Circumferential and Radial Temperature Gradients for the Tungsten Support or Sheath Tube Near the Reactor Exit for Various Lateral Support Concepts

CONFIDENTIAL

NASA-CR-72031

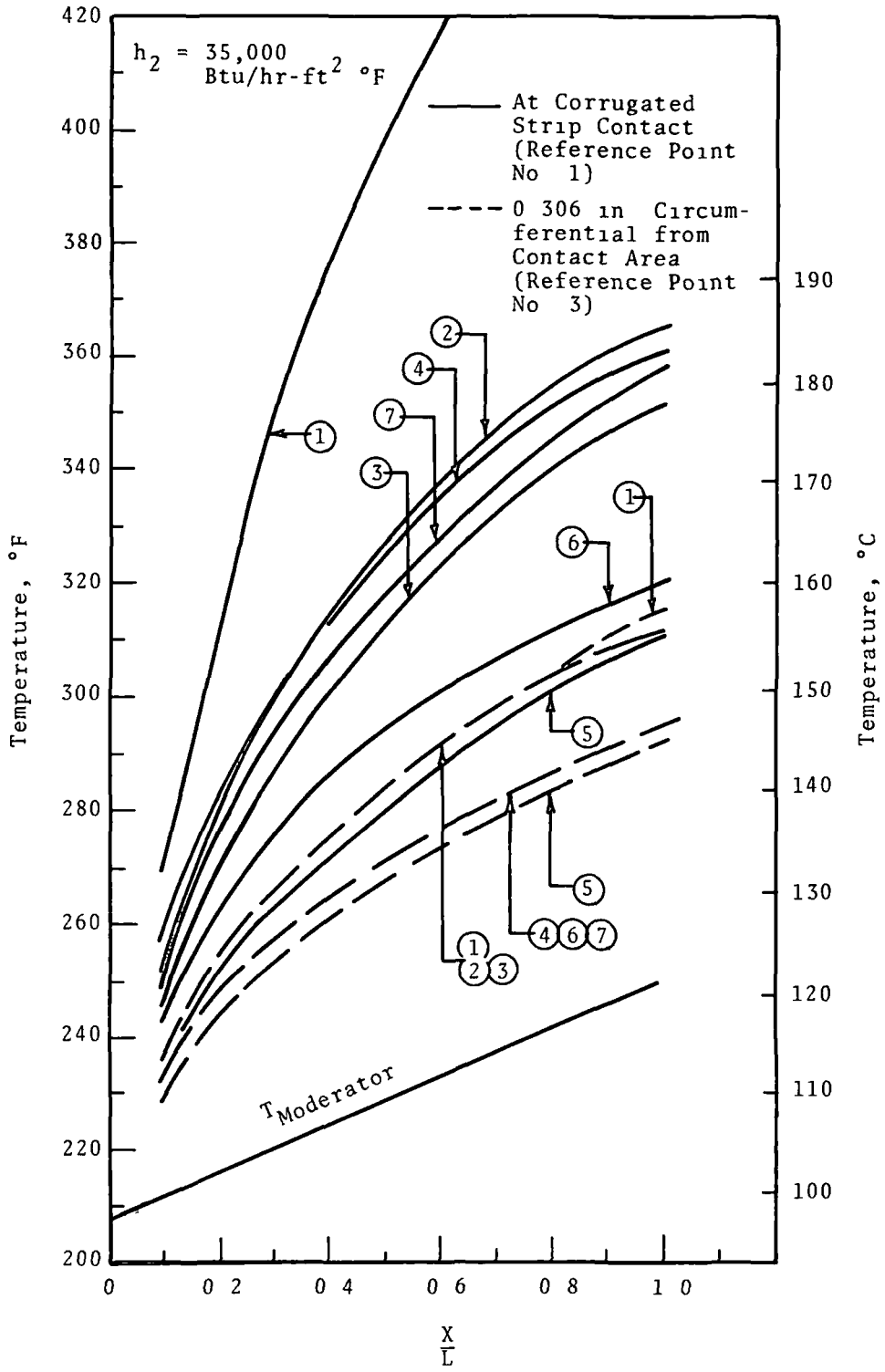

FIGURE 3 14 Aluminum Tube Inside Diameter Surface Temperature Versus Distance from Core Inlet

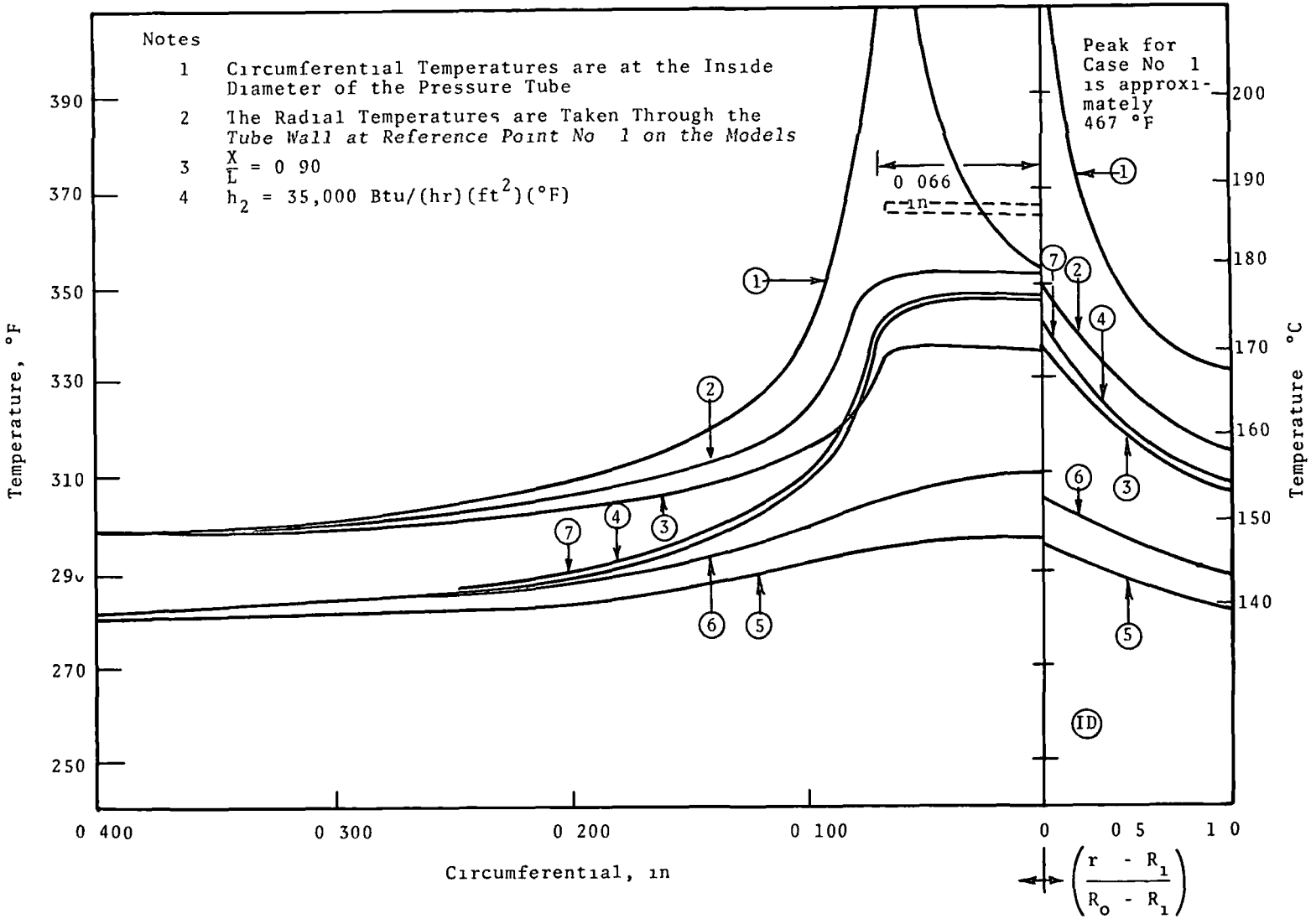

FIGURE 3 15 Typical Circumferential and Radial Temperature Distributions for the Aluminum Pressure Tube Near the Reactor Exit for Various Support Concepts

CONFIDENTIAL
CONFIDENTIAL
3 33
NASA-CR-72031

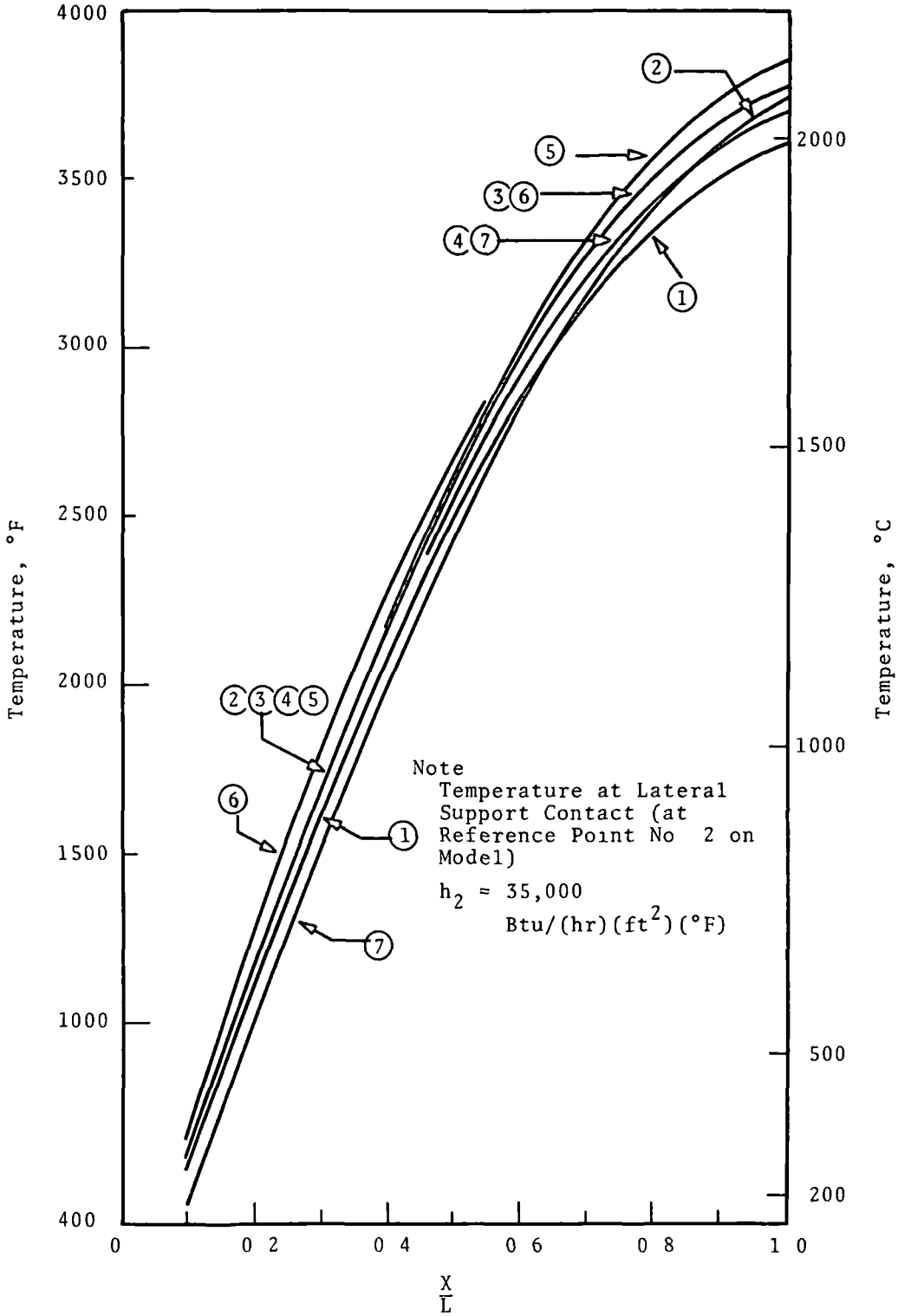

FIGURE 3 16 Tungsten Tube Outside Diameter Surface Temperature Versus Distance from Core Inlet

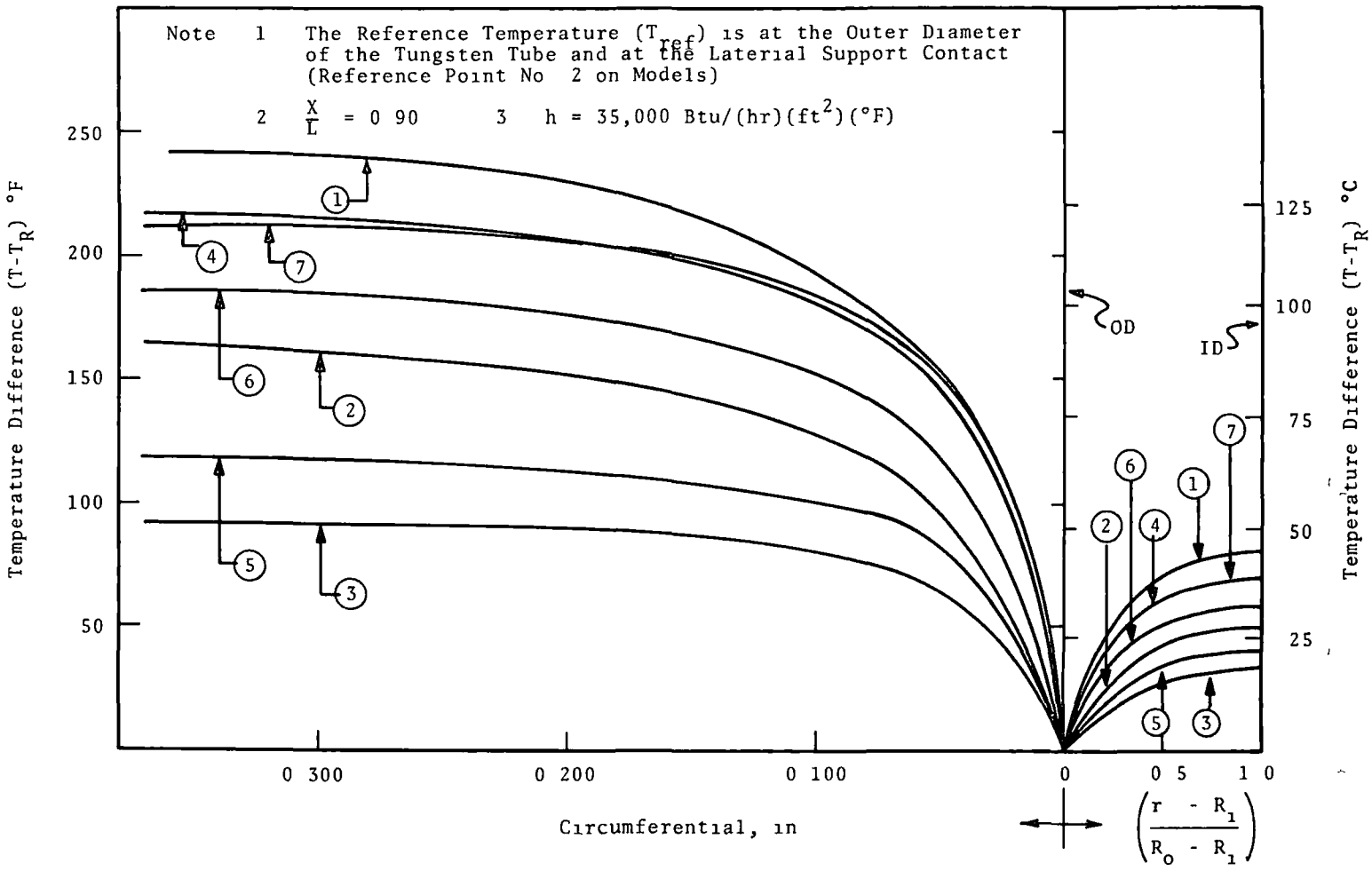

FIGURE 3 17 Typical Circumferential and Radial Temperature Gradients for the Tungsten Support or Sheath Tube Near the Reactor Exit for Various Lateral Support Concepts

CONFIDENTIAL
CONFIDENTIAL

NASA-GRC

3 5 1 Corrugated Strip - 0 0625 in Annulus

Figure 3 9 shows the circumferential temperature distribution at the inside diameter of the aluminum pressure tube and the radial distribution at the point of lateral support contact These curves are typical of conditions near the reactor exit and serve to illustrate the effect of insulation and contact resistance between the lateral support and pressure tube

Curve 1, Figure 3 9, shows the result of good thermal contact between the lateral support and the pressure tube In this case, the extended contact area is of little use in reducing the peak temperature A significant change results from increasing the contact resistance as illustrated by comparing curves 1 and 2 Curve 3 shows the results for a case identical to curve 1, except an insulating strip consisting of 10 mils of ZrO_2 has been placed between the two members The relative flatness of the curve over the contact area indicates that a nearly equipotential exists over the contact area, thus no more than 10 mils of ZrO_2 is required to eliminate the localized temperature peaks If the lateral support member is only 3 mils thick instead of 6 mils, the temperature distribution is given by curve 4 The maximum temperature is somewhat less in this case since the thinner lateral support does not provide as good a heat conduction path and generates less heat than the 6 mil support

The case numbers listed in Figure 3 9 correspond to those cases listed in Table 3 3, and the curves shown in the subsequent Figures 3 10 through 3 17

In general, the figures illustrate that increasing contact resistance or placing insulation on the contact area serves two purposes it reduces local peaks in the aluminum pressure tube and retards heat flow through the support device, thus reducing the

magnitude of thermal gradients in the tungsten support tube Additions of insulation on the support tube side of the lateral support would also retard heat flow through the support, but since the temperature near the reactor exit is nearly 4000 ^{o}F, it is not apparent that insulation can be applied or retain its mechanical integrity during normal operation

The curves shown in Figure 3 10 also indicate that the lowest temperature expected at the inner surface of the pressure tube without any lateral support is approximately 310 ^{o}F A more detailed discussion of the analysis and results of study cases associated with the corrugated strip support in a 0 0625 in annulus is given in NASA-CR-54721

3 5 2 Corrugated Strip and Combination Support 0 125 in Annulus

Of the cases listed in Table 3 3, cases 4 through 10 consider a 0 125 in annulus Cases 4, 5, 6, and 7 were analyzed twice The first analysis considered a contact coefficient h_2 = 5,000 Btu/hr-ft^2-^{o}F The second analysis assumed h_2 = 35,000 Btu/hr-ft^2-^{o}F In cases 8 and 9, the insulating strip at the support contact has been replaced by an equivalent contact coefficient Only the case h_2 = 1400 Btu/hr-ft^2-^{o}F ($\sim$ 0 010 in ZrO_2 insulation) was considered Case 10 was not considered with h_2 = 35,000 Btu/hr-ft^2-^{o}F since a contact coefficient of 5,000 or greater contributes only a small portion of the overall thermal resistance in the lateral support member

In case 10, insulation has been added to both lateral support-tube contact locations With contact coefficients of 5,000 Btu/hr-ft^2-^{o}F or more, the insulating strips on either end of the lateral support are responsible for nearly all of the thermal resistance, and there is not a significant difference between results whether h_2 = 5,000 or 35,000

Figure 3 10 shows the axial temperature distribution at the corrugated strip contact area and at a circumferential distance 0 306 in away from this contact location on the inside surface of the aluminum pressure tube Figure 3 11 illustrates the circumferential temperature distribution in the aluminum tube near the exit of the reactor Both figures show by comparison of Cases 4 and 5 that a decrease of the corrugated strip thickness decreases the temperature peaks and gradients in the aluminum tube Also, Figure 3 13 shows that thinner corrugated strips reduce gradients in the tungsten tube Comparison of Cases 4 and 6 on Figures 3 10 and 3 11 reveals that an increase of insulation thickness or a better insulating strip between the aluminum tube and the corrugated strip decreases the temperature peaks and gradients in the aluminum tube Figure 3 13 indicates that an increase of insulation decreases the temperature gradients in the tungsten tube Comparison of Cases 4, 5, and 6 on Figure 3 12 shows that any method of retarding the heat flow in the corrugated strip will reduce temperature gradients in both the pressure tube and support tube, cause lower localized temperature peaks in the pressure tube, and slightly increase the support tube temperature Case 8 of Figure 3 10 considers the combination support and shows that the temperature in the pressure tube is higher than cases without combination supports, especially between the reactor entrance and the central region of the reactor This increased temperature is explained by the increased gamma heating in the annulus material Although the thermal gradients in pressure tube are greater, as indicated by Figure 3 11, Figure 3 13 reveals that the gradients in the support tube are essentially negligible Figure 3 12 shows that the support tube is also hotter for this case

Case 10 reveals that placing insulation on both contact areas of the lateral support has a pronounced effect on the temperatures in the aluminum and tungsten tubes This case assumes a 10 mil thick corrugated strip, compared to 6 mils and 3 mils in the other cases Yet, the gradients in the aluminum tube compare with the 6 mil cases, and gradients in the tungsten tube compare with the 3 mil cases Figure 3 12 indicates that the support tube will run hotter - at least at the lateral support contact points, as a result of less heat conducted through the support device

Figures 3 14 through 3 17 present summary results for the cases described in Table 3 3, with the exception of Cases 8, 9, and 10 The results were derived using higher corrugated strip contact coefficients Generally speaking, the increased contact coefficient permits more heat to flow from the tungsten tube to the pressure tube, via the corrugated strip, thus, both localized temperature peaks and thermal gradients are higher in the pressure tube, temperatures are slightly cooler in the tungsten tube, but the thermal gradients (as revealed by Figure 3 17) are much more severe in the tungsten tube These figures emphasize the importance of retarding the heat flow through the corrugated strip

3 6 Tube Stresses

The initial tube stress analysis, reported in Reference 15, assumed cold end fuel support with a 1/16 in static gas annulus between the fuel support tube and the aluminum pressure tube Tungsten fuel support tube stresses without lateral support were compared with those calculated assuming an idealized metallic rib support in the static gas annulus

In the study case without lateral support, stress levels due to pressure, radial temperature gradients, fuel weight, and

aerodynamic loads were within the strength capability of the material In the absence of lateral supports, however, vibration-induced support tube stresses were excessive

The initial studies also showed that a full tube length metallic rib support caused high localized thermal stresses in the hottest half of the tungsten tube These stresses, attributed primarily to circumferential temperature gradients at support locations, were a factor of four greater than the tensile strength of the material at the hot end of the tube Stresses of this magnitude, when calculated on an elastic basis, give obviously incorrect estimates of strain

Since it was apparent that high aluminum tube stresses would also exist in the rib support case, attention was directed toward methods of reducing the temperature gradients A rib support, with an extended contact area or foot on the aluminum end of the tungsten support, was one of the early models evaluated Although extension of the contact area at the aluminum tube reduced the localized aluminum tube stresses, the tungsten tube stresses were increased because of greater heat flow through the lateral support

Other lateral support models considered (a) porous ceramic, (b) slanted lateral supports (or corrugated strip), and (c) combined corrugated strip with porous ceramic

The porous ceramic lateral support consisted of filling the annulus between the tungsten support tube and the aluminum pressure tube with ceramic filaments or unconsolidated ceramic particles The effect of support material density on tube stress levels, reported in Reference 14, was determined by considering support void fractions of 0 0, 0 5, and 1 0 Calculated aluminum tube stresses were well below an allowable stress taken at twice the yield strength of 6061-T6 aluminum alloy It was also found

that porous ceramic in the static gas gap would effectively eliminate the most significant thermal stresses in the tungsten support tube, however, the mechanical properties of the ceramic would have to be augmented to obtain a satisfactory lateral support A particular disadvantage was that ceramic supports could produce excessive tube stresses due to relative expansion of the tungsten and aluminum tubes Later study cases considered primarily corrugated strip lateral support models and their effect on tube stress levels

3 6 1 Primary Membrane Stresses

Figure 3 18 shows tungsten sheath and support tube primary membrane stresses in both hot and cold end support cases Allowable stresses, determined at typical tube temperatures, are also indicated In the cold end support cases, primary membrane stresses are within the strength capability of the material

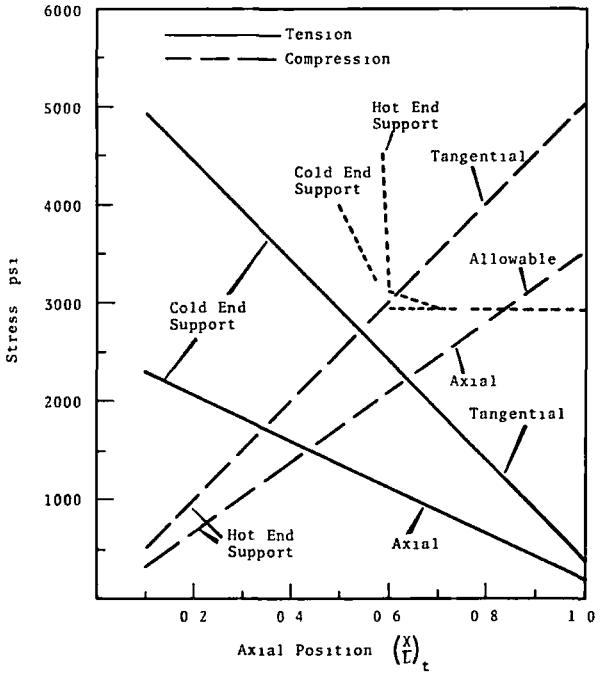

FIGURE 3 18 Tungsten Tube Primary Membrane Stress Components and Allowable Stress Versus Axial Position

Since the calculated pressure stresses in the sheath tube did not assume support from the fuel itself, the hot end support tangential stress is greater than would actually be the case for any of the contemplated fuel designs with the possible exception of concentric fueled cylinders

Primary membrane stress components in the aluminum tube are indicated on Figure 3 19 Both hot end and cold end support stresses are well within allowable material stresses taken at the highest temperatures of any study case with corrugated strip supports The aluminum tube temperatures associated with study Cases 8 and 9 were selected in establishing indicated allowable stress values The lower allowable stress curve, Figure 3 19, corresponds to the maximum tube temperature occurring at the

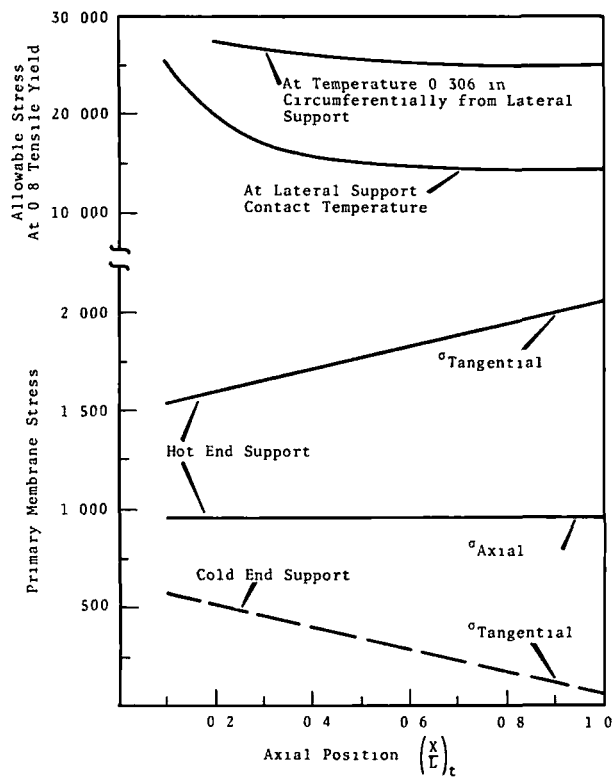

FIGURE 3 19 Aluminum Tube Primary Membrane Stress Components and Allowable Stress Based on Case 8 Tube Temperature

lateral support contact location while the other allowable stress curve is based on temperature 0 306 in circumferentially away from the corrugated strip contact The latter temperatures more closely approximate average tube temperatures

3 6 2 Primary Plus Thermal Stresses

Figure 3 20 indicates primary membrane plus maximum thermal stress at the outside radius of the tungsten tube for each of the selected study cases with corrugated strip lateral supports Figure 3 21 shows the corresponding aluminum tube stresses

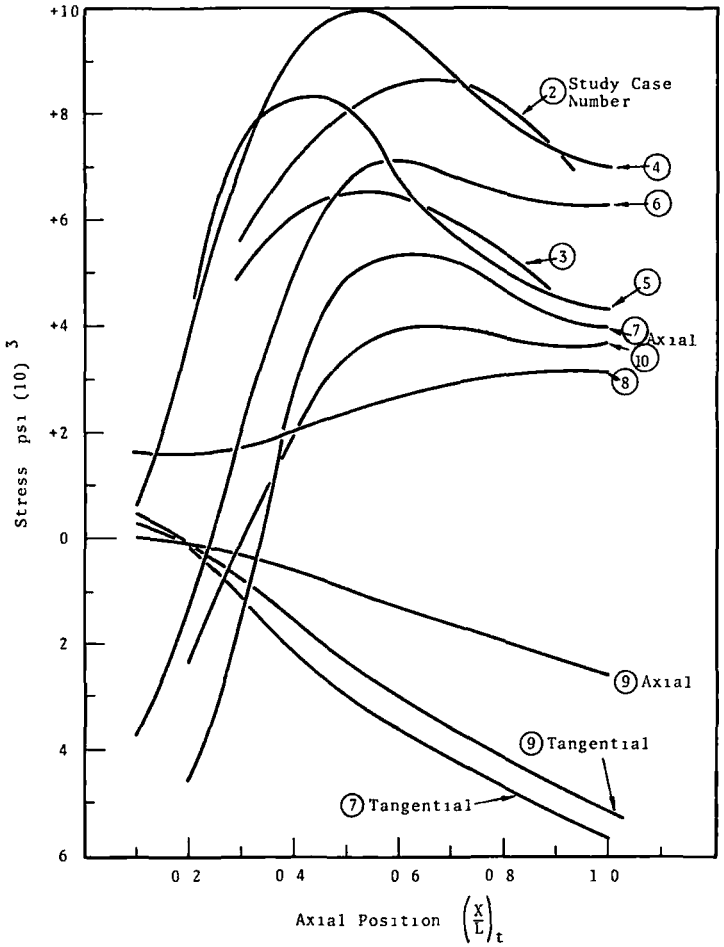

FIGURE 3 20 Tungsten Tube, Primary Membrane Plus Maximum Thermal Stress at Outside Tube Radius and Point of Support Contact Versus Axial Position

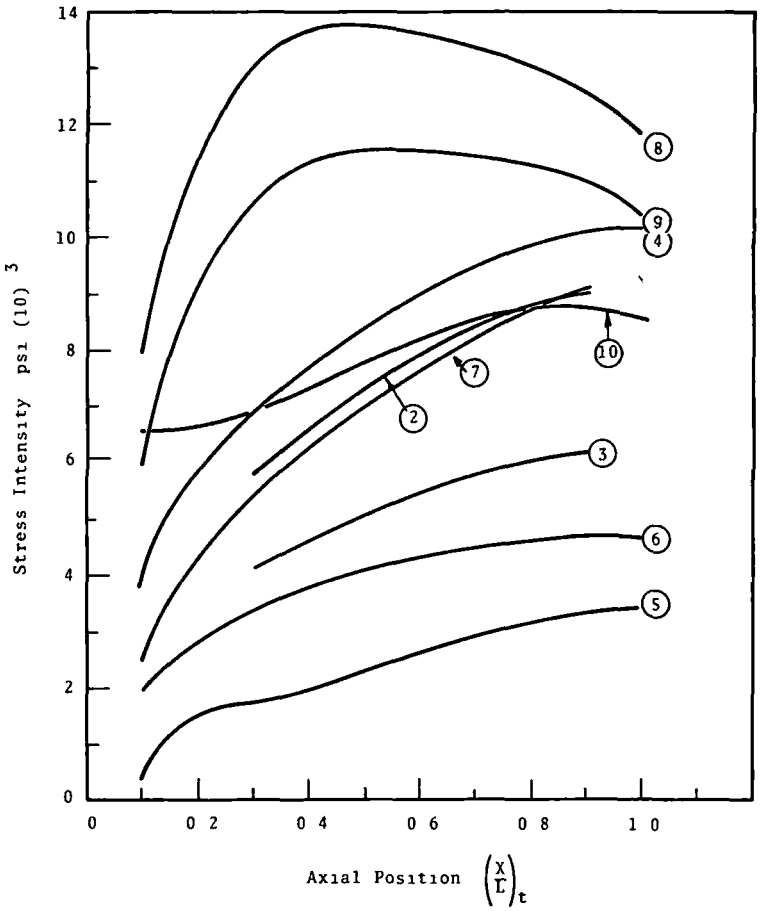

FIGURE 3 21 Aluminum Tube, Primary Membrane Plus Maximum Thermal Stress at Tube Inner Surface Versus Axial Position, h_2 = 5000 Btu/hr-ft^2-^{o}F

Selected tube stresses for 0 0625 in gap study cases, Table 3 3, Cases 2 and 3, and also one 0 125 in gap study case with combination porous ceramic and corrugated strip support, Case 9, are indicated on Figures 3 20 and 3 21 for comparison with the later study results

The tungsten and aluminum tube stresses presented on Figures 3 20 and 3 21 for the corrugated strip models are based on contact coefficients of 5000 Btu/hr-ft^2-^{o}F at the lateral support contact surfaces The thermal stresses using contact coefficients of 35,000 Btu/hr-ft^2-^{o}F are somewhat higher but vary similarly with axial position These stresses are not presented

Comparison of Curves 4 and 2 on Figures 3 20 and 3 21 indicate the effect of changing the static hydrogen gap from 1/16 in to 1/8 in when the corrugated strip thickness is 0 006 in Curves 3 and 5 show a similar comparison with 0 003 in thick corrugated strip support Curve 6 can be compared with Curve 4 to indicate the reduction in tube stresses when the insulation on lateral support-aluminum tube interface is changed from ZrO_2 to a material with density of 150 lb/ft^3 and thermal conductivity of 0 20 Btu/hr-ft-°F Curve 8 shows the reduction in support tube stresses when a combination corrugated strip and porous ceramic lateral support is considered The reduced stress levels result primarily from decreased circumferential temperature gradients at the support tube-corrugated strip contact It will also be noted that Cases 8 and 9, which consider combination lateral supports, produce higher aluminum tube stresses than the other cases This increased stress level is attributed to greater heat generation in the support materials and higher aluminum tube peak temperatures

Estimated sheath tube stresses with hot end fuel column support are indicated by Curves 7 and 9 on Figure 3 20 Maximum axial and tangential stresses are indicated in the hot end support cases

When ceramic insulation is placed on corrugated strip contact interfaces at both tungsten and aluminum tubes, the tube stresses are as indicated by Curve 10 on Figures 3 20 and 3 21

Of the corrugated strip lateral support study cases considered, Case 10 would appear to be the best choice of lateral fuel support since relatively low support tube stresses are obtained with reasonable aluminum tube stresses However, when considering the tungsten tube temperature, development of an

acceptable ceramic insulation and method of attachment to the hot end of the corrugated strip become significant problems

As indicated in Section 3 2 2 4, the study Case 10 thermal stresses were recalculated using the corrected higher values of Young's Modulus Figure 3 22 shows the Case 10 comparison of primary membrane plus maximum thermal stress in the tungsten support tube The difference in the two curves is due to the discrepancy in Young's Modulus data A recalculation of tungsten support tube thermal stresses in the other study cases would show similar differences Case 10 thermal stresses due to circumferential thermal gradients at lateral support contact locations on the tungsten tube vary with circumferential distance from the contact point as indicated on Figure 3 23 Other corrugated strip type lateral support study cases produce similar thermal stresses near the tungsten tube contact points

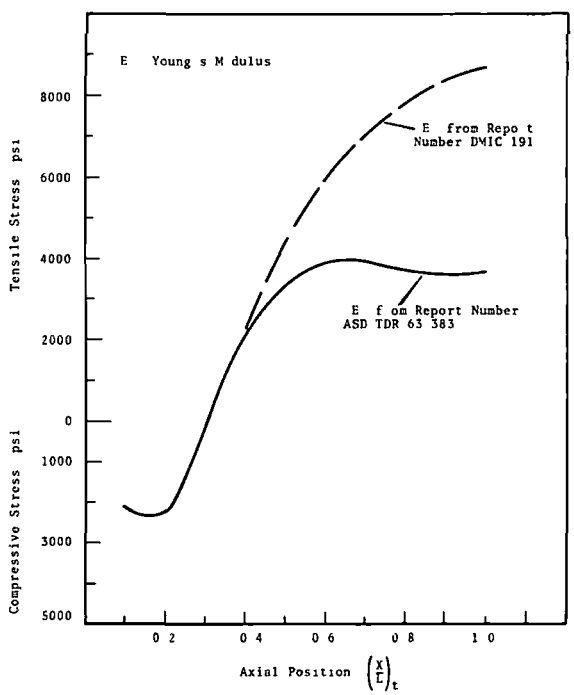

Figure 3 22 Hot End Support, Maximum Tungsten Support Tube Axial Stress at Outer Tube Radius, Case 10

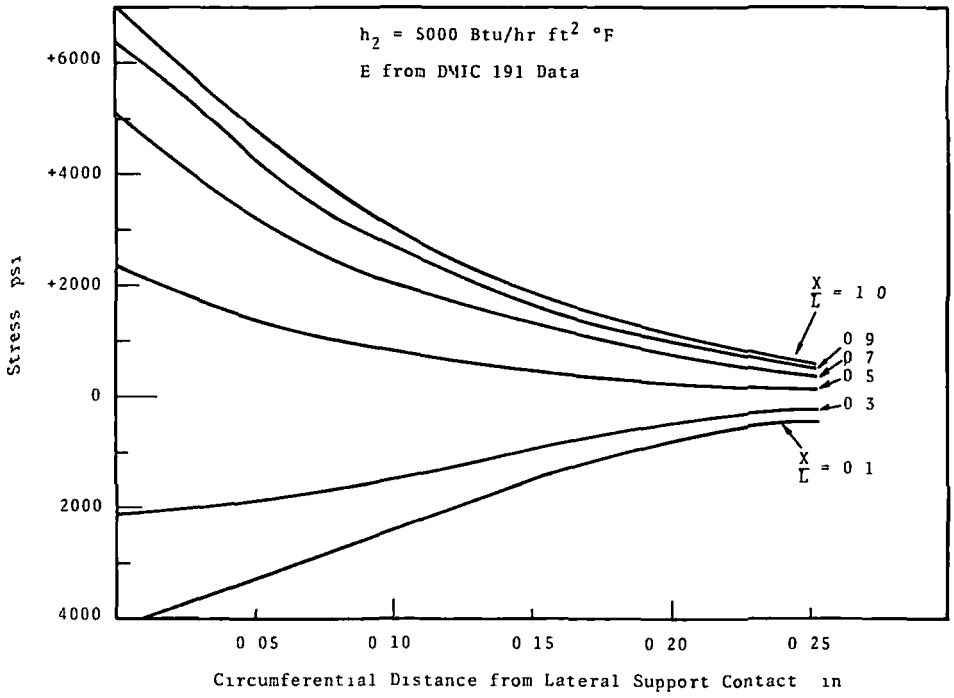

FIGURE 3 23 Cold End Support, Tungsten Support Tube Thermal Stress Due to Circumferential Temperature Gradient Versus Distance from Lateral Support Contact Location, Case 10

A corrugated strip model which would reduce circumferential temperature gradients at the tungsten support tube without addition of ceramic particles or other schemes which increase the complexity of assembly, can be envisioned This lateral support consists of a modified corrugated strip or corrugated concentric reducer Essentially continuous lateral support contact at the tungsten support tube would all but eliminate the most troublesome thermal stresses due to circumferential temperature gradients Ceramic insulation on the aluminum tube-lateral support interface would still be necessary to reduce high localized aluminum tube stresses Considering the lower material temperatures, selection of an appropriate insulation should not be difficult Other advantages of this lateral support model are discussed in Section 4 4 of this report

The stress component curves for study Cases 4, 5, 6, 7, 8, 9, and 10 are included as Appendix A

3 7 Tungsten Support Tube Creep

A preliminary analysis of thermal creep in the tungsten support tube was performed Creep loads due to internal pressure, axial loading due to fuel weight assuming 1 g acceleration, and aerodynamic loads were considered Tube temperatures associated with a 1/16 in static gap study case without lateral support were selected for the creep analysis since these temperatures were slightly higher than in lateral support cases The tungsten tube was considerd fixed at the core inlet and creep strains were calculated assuming 10 hr of steady-state operation In the creep calculations, values of Young's Modulus[8] were taken at the average tube temperature of each axial position between $\frac{X}{L}$ = 0 5 and $\frac{X}{L}$ = 1 0 Tungsten tube strains were calculated from the following equations which are derived in Reference 15

$$\epsilon_Z = \frac{1}{E}(\sigma_2 - \nu\sigma_1) + \frac{B\sigma_1^n}{2}\left[1 - \alpha + \alpha^2\right]^{\frac{n-1}{2}}\left[2\alpha - 1\right] T$$

$$\epsilon_\tau = \frac{1}{E}(\sigma_1 - \nu\sigma_2) + \frac{B\sigma_1^n}{2}\left[1 - \alpha + \alpha^2\right]^{\frac{n-1}{2}}\left[2 - \alpha\right] T$$

ϵ_Z = Axial strain

ϵ_τ = Tangential strain

E = Young's Modulus

σ_1 = Tangential stress

σ_2 = Axial stress

ν = Poisson's ration = 0 3

α = Stress ratio $\frac{\sigma_2}{\sigma_1}$

T = Time in minutes

n and B = Creep constants depending on material and temperature

The creep constants n and B were determined from second stage linear creep data [16] For creep following a simple power function of stress, $\varepsilon = B\sigma^n$, where ε is the creep rate, the constant n can be determined at each temperature for which data are available by the inverse slope of the second stage creep versus stress plot The constant B is determined by the stress intercept at unit creep rate

The constant $n \approx 9$, determined from data at temperatures of 2912 ^{o}F and 5072 ^{o}F, was assumed to apply also at intermediate temperatures The constant B, varying with temperature as indicated on Figure 3 24, was used in the calculations The calculated tungsten support tube strain and increase in tube diameter after 10 hr of operation are shown on Figures 3 25 and 3 26

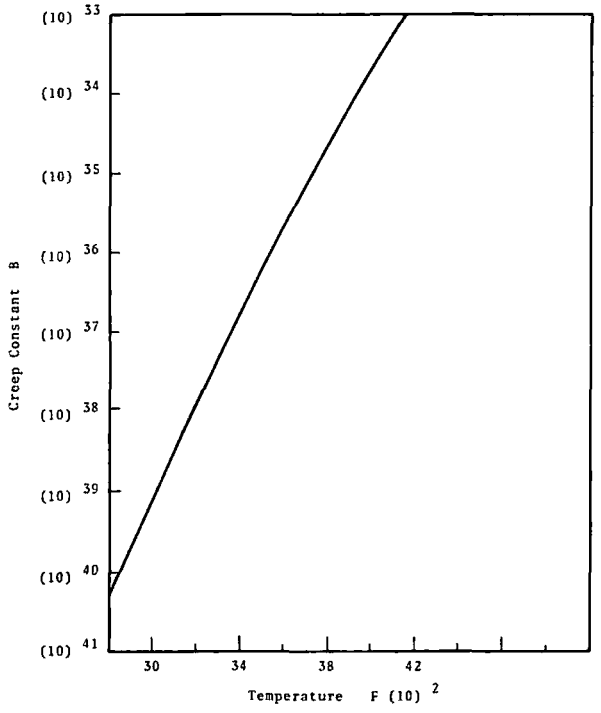

FIGURE 3 24 Tungsten Creep Constant "B" Versus Temperature

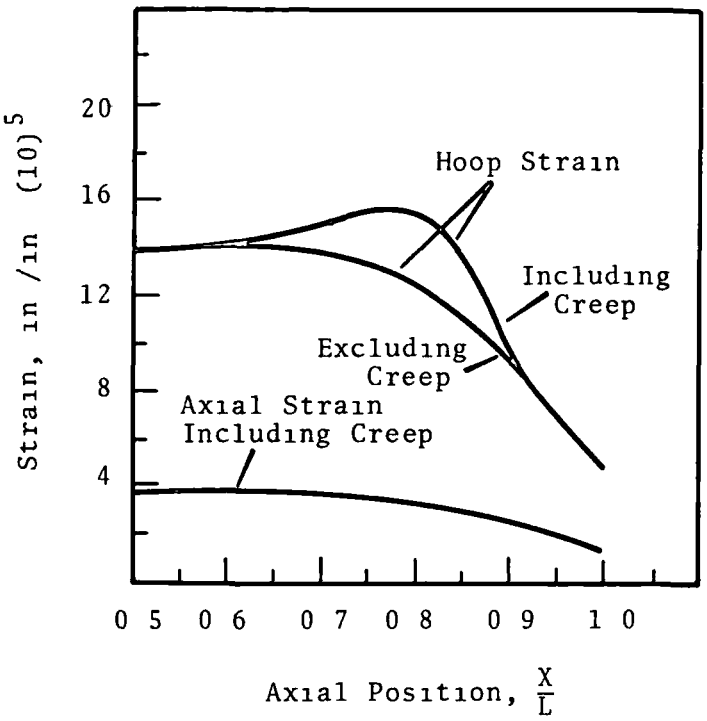

FIGURE 3 25 Tungsten Support Tube Strain after 10 hr of Operation Versus Axial Position

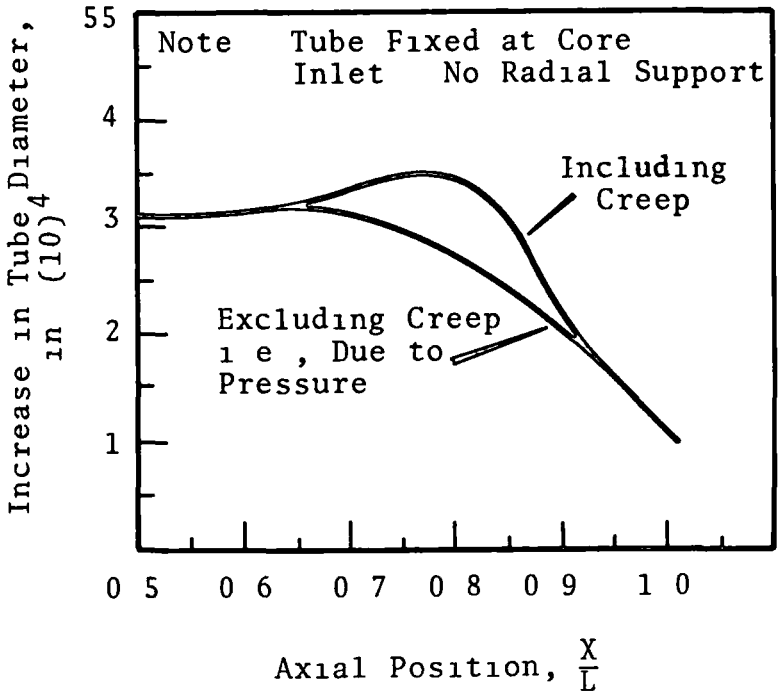
Increase in Tube Diameter, in (10)^4
55
4
3
2
1
Note Tube Fixed at Core Inlet No Radial Support
Including Creep
Excluding Creep i e , Due to Pressure
0 5 0 6 0 7 0 8 0 9 1 0
Axial Position, $\frac{X}{L}$

Figure 3 26 Tungsten Support Tube Increase in Tube Diameter (Due to Creep) after 10 hr of Operation

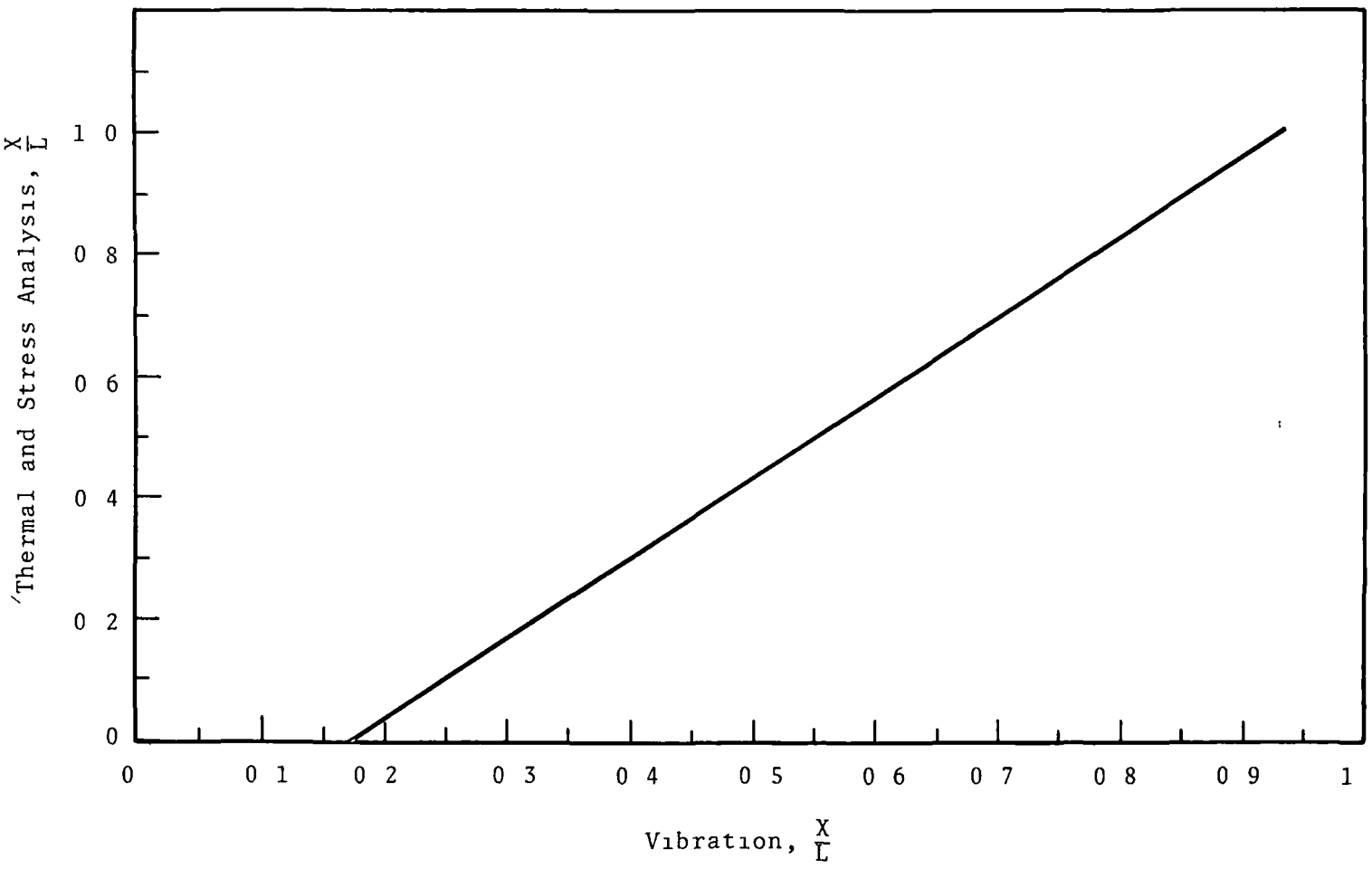

FIGURE 3 27 *X/L Transfer, Vibration and Thermal NASA Nuclear Rocket Reactor*

Length

Thermal *42 125 in*

Vibration *55 0 in*

NASA CR-72037

3 8 REFERENCES

1 F J Mollerus, Jr *User's Manual for STHTP-A Steady State Heat Transfer Program for the IBM 7090 Computer*, HW-73668 May 21, 1962

2 NASA Lewis Research Center *Tungsten-Water Moderated Nuclear Rocket Program*, vol 2, Status Report February, 1964

3 NASA Lewis Research Center *Tungsten-Water Moderated Nuclear Rocket Program*, vol 1, Status Report February, 1964

4 Timoshenko and Goodier *Theory of Elasticity* - Second Edition, pp 404-412 1951

5 Pfenningweth *Stress Analysis with Applications to Pressurized Water Reactors*, WAPD-TM-300 January, 1963

6 J P Den Hertog "Temperature Stresses in Flat Rectangular Plates and in Thin Cylindrical Shells," *J Franklin Institute*, vol 222, p 149 2936

7 "Nuclear Vessels," Section III, *ASME Boiler and Pressure Vessel Code*, p 14 1963

8 Doury, Kay, Bennett, and Albom *Mechanical Properties of Wrought Tungsten*, vol 2, Technical Documentary Report ASD-TDR-63-383 Marquardt Corporation, August, 1963

9 F F Schmidt and H R Ogden *The Engineering Properties of Tungsten and Tungsten Alloys*, DMIC-191, p A-5 Battelle Memorial Institute, September 27, 1963

10 A F Lietzke and M Krasner NASA-Lewis Research Center Unpublished Data (Personal Communications) September 16, 1965

11 Reactor Handbook, vol 1, *Materials*, p 485

12 Aluminum Company of America Unpublished Data

13 Reactor and Materials Technology Department *Quarterly Report on Tungsten-Uranium Dioxide Cermet Research and Development Activities, January, February, March, 1965*, NASA-CR-54409

14 Reactor and Materials Technology Department *Quarterly Report on Tungsten-Uranium Dioxide Cermet Research and Development Activities, April, May, June, 1965*, NASA-CR-54721

15 *Goldenblat and Nikolaenka "Calculation of Thermal Stresses in Nuclear Reactors," pp 19-21 Consultants Bureau, New York*

16 *General Electric Company, Cincinnati* *High Temperature Materials Progress Report No 23, Part A p 14 May 31, 1963*

4 0 STRESS ANALYSIS OF CORRUGATED STRIP LATERAL SUPPORT

4 1 MODEL AND ASSUMPTIONS

A preliminary estimate of lateral support load-deflection characteristics was obtained by treating a corrugated strip as a continuous frame, subjected to radially symmetric loads The continuous frame closely approximates the simplified model used in the heat transfer analysis The lateral support was considered pinned to the fuel element support tube at one contact point, uniformly loaded at contact locations around the inner circumference of the aluminum tube, and free to slide circumferentially in the static gas gap (Figure 4 1) Resistance to circumferential sliding due to gap curvature was neglected Bending stresses at lateral support contact locations along the tungsten tube were considered to be the most significant stress condition

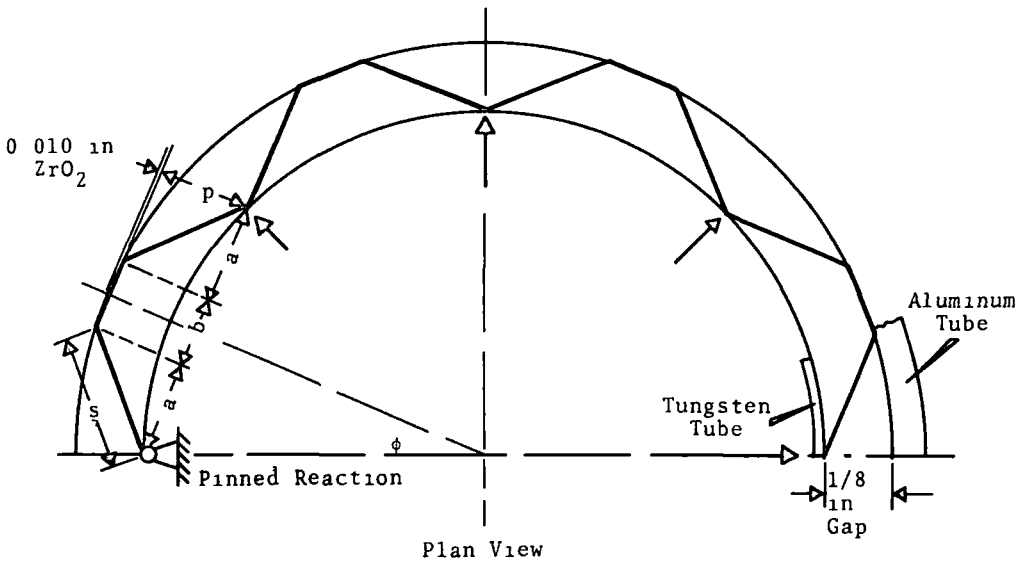

FIGURE 4 1 Eight Segment Corrugated Strip Model

Linear load-deflection characteristics of lateral supports having 8, 12, and 16 segments were determined in both the cold- and hot-reactor operating conditions The product of Young's Modulus and lateral support Moment of Inertia, EI, was assumed constant to obtain linear spring rates in both hot- and cold-reactor conditions

The preliminary assumption of constant EI in both the hot and cold operating conditions is somewhat misleading If EI is constant during reactor operation when Young's Modulus varies significantly along the inclined portion of the spring segment, the moment of inertia must also be a function of the inclined length of spring The same spring in the cold condition will therefore not have a constant EI

A constant thickness but variable depth spring segment could be designed to produce a lateral support with constant EI during reactor operation This modification to the model does not, however, solve the problem of insufficient deflection to accommodate thermal and dynamic loads

The lateral support stress analysis considered a study case with the tungsten fuel support tube fixed at the reactor core inlet The corrugated strips were located in a 0 125 in static gas annulus between the tungsten and aluminum tube A 0 010 in thick layer of ceramic insulation, located at each lateral support segment-aluminum tube interface, was assumed (Figure 4 2) Analysis of bending stresses indicated the need for low spring rates in lateral supports located in the hottest half of the fuel column This analysis also showed that allowable segment loads were low in the hot half of the column because of lateral support temperatures at tungsten tube contact points

To reduce corrugated strip temperatures, a similar study case having insulation on both aluminum and tungsten tube contact

locations was considered (Figure 4 3) Temperature gradients and tube stresses were improved by the addition of insulation between the lateral support and the tungsten support tube Maximum temperatures at the hot end of the corrugated strip segment were also reduced but remained above a tungsten recrystallization temperature of 2700 °F at axial positions below $(X/L)_t = 0\ 7$

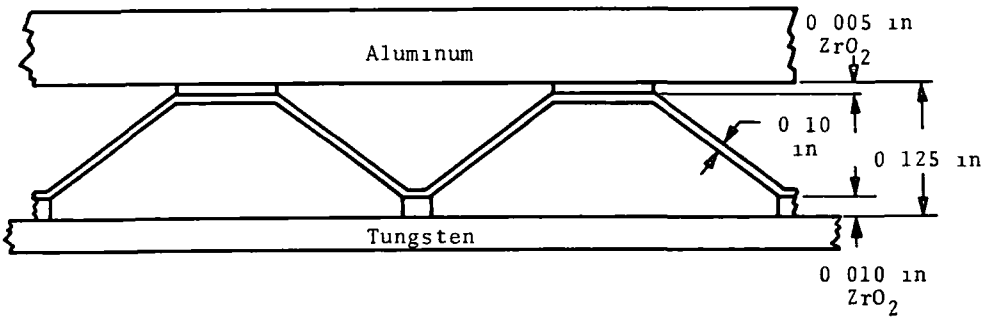

FIGURE 4 2 Case 4 Typical Model

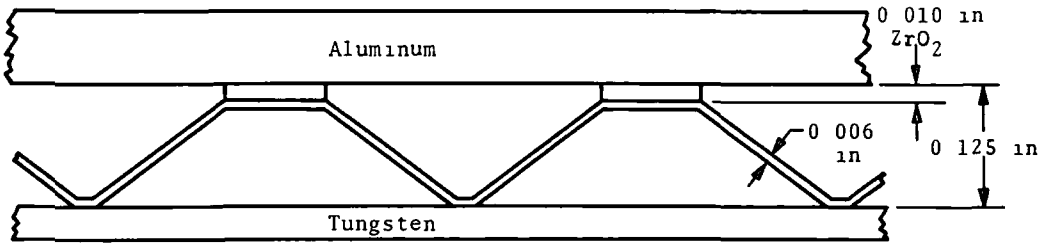

FIGURE 4 3 Case 10 Typical Model

4 2 METHOD OF ANALYSIS

A deformation method was used in the lateral support deflection and stress analysis Angular deformations and linear displacements at the tungsten tube reaction points were determined in terms of the applied load and the lateral support segment dimensions The statically indeterminate lateral support

bending moments at the tungsten tube reaction points were also found in terms of the applied segment loads by writing equations of equilibrium of angular deformations at these reaction points Allowable segment loads were determined as a function of lateral support axial position along the fuel column Appendix B contains the derivation of lateral support segment load functions and elastic constants, and also a sample calculation of load-deflection characteristics for an eight-segment model Load functions, consisting of an angular deformation θ and a linear deformation Δ_o may be calculated from the following equations

$$EI\theta = \frac{wabs}{4} + \frac{w}{2}\left(\frac{L^3}{12} - a^2L + \frac{4a^3}{3}\right) \quad (1)$$

$$EI\Delta_o = \frac{wabps}{3} + wp\left(\frac{L^3}{12} - a^2L + \frac{4a^3}{3}\right) \quad (2)$$

where
- E = Young's Modulus
- I = lateral support segment Moment of Inertia
- θ = angular deformation of the lateral support at the tungsten tube reaction point due to applied uniform load
- Δ_o = linear deformation of the lateral support at the tungsten tube reaction point
- w = uniform load applied to the lateral support
- a,b,p,s,L = spring segment dimensions defined by Figure B-1

The elastic constants, or angular and linear deformations, due to unit moment application at one end of the lateral support segment depend on the geometrical shape of the frame and may be determined from Equations (3), (4), and (5)

$$EI\alpha = \left(s + \frac{b}{2}\right)\frac{Z}{L} \quad (3)$$

$$EI\beta = \left(s + \frac{b}{2}\right)\frac{\bar{X}}{L} \tag{4}$$

$$EI\Delta^{m} = \frac{p}{2}(s + b) \tag{5}$$

In these equations α and β are the angular deformations of the lateral support segment due to unit bending moment at the point of its application and at the far end of the segment respectively (Figure B-2) $\bar{X}$ and $\bar{Z}$ define the centroid of the M/EI diagram

In calculating the statically indeterminate lateral support bending moments at the tungsten tube reaction points, the selected sign convention considered angular deformations as positive when the bending moment or applied load produced clockwise segment rotation Application of the moment Equation (6) at each reaction produced a set of equations

$$\beta M_{J-1} + 2\alpha M_{J} + \beta M_{J+1} = \theta(w_{J-1,J} + w_{J,J+1}) \tag{6}$$

from which the unknown bending moments could be determined The location of the maximum bending moment at points of lateral support contact with the tungsten tube were also determined and used in the flexure formula to define allowable segments loads Allowable bending stress was established by 80% of tungsten tensile yield strength at the segment temperature near the tungsten tube contact point At temperatures less than 2700 °F tensile strength data for stress relieved tungsten sheet were used [1] Recrystallized tungsten tensile strength data were used in determining allowable stresses at temperatures greater than 2700 °F

Lateral support segment displacements due to circumferential sliding in the gas gap were determined in terms of the applied segment load The corresponding lateral displacement of the support segment was then established by the lateral support geometry In determining the load-displacement characteristics of the

corrugated strip support average segment temperatures were used to estimate material properties Values of Young's Modulus at elevated temperatures from Reference 1 were used in the deflection calculations

4 3 RESULTS

Figures 4 4 through 4 6 indicate the calculated load-deflection characteristics of 8, 12, and 16 segment corrugated strips during reactor operation The lateral support temperatures obtained for the study case with ceramic insulation at both tungsten and aluminum tube contact locations (Figure 4 3) were used to estimate the deflection characteristics of 0 003, 0 006, and 0 010 in thick corrugated strips Allowable loads based on 80% of tungsten tensile yield strength at maximum lateral support temperature are also indicated as a function of axial position along the fuel column

Figures 4 7 through 4 9 show both static and dynamic load-deflection characteristics and allowable spring segment loads during cold reactor conditions

A number of conclusions can be derived from analysis of the lateral support during reactor operation

- In the hottest half of the fuel column soft springs or corrugated strips with low spring constants are required However, soft springs can contribute to excessive dynamic deflections
- The allowable spring segment loads in the hottest half of the fuel column, and the corresponding allowable deflections are extremely low because the temperatures at the hot end of the segment are above tungsten recrystallization temperature The bending moment at the hot end of the segment determines the maximum allowable segment load

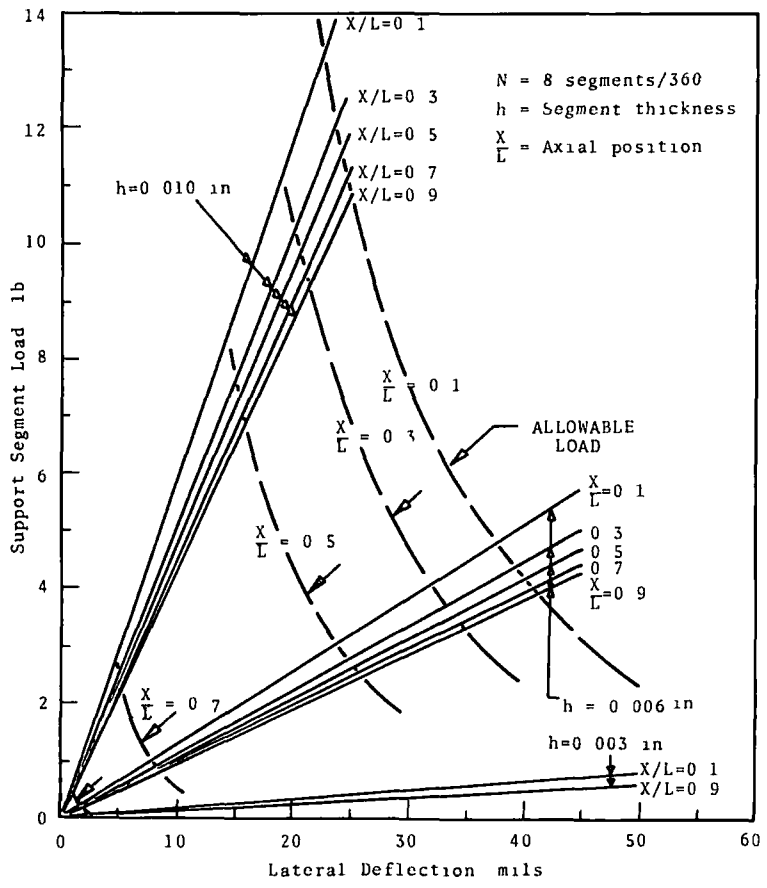

FIGURE 4 4 Eight Support Segment Load Versus Lateral Deflection (Hot Condition)

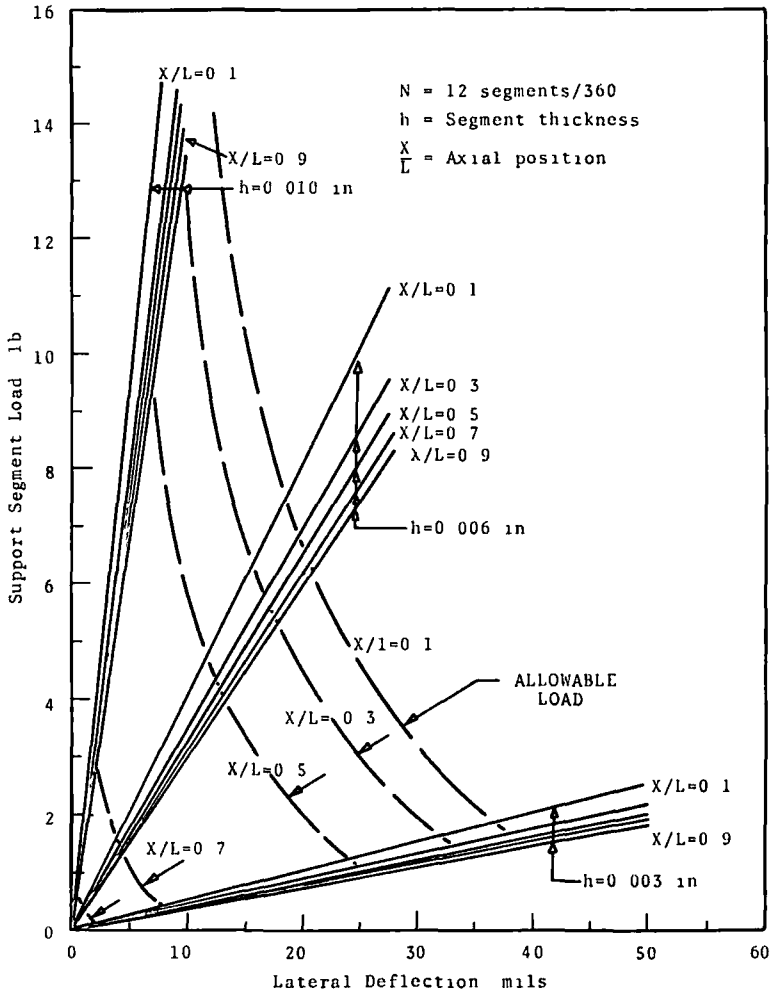

FIGURE 4 5 Twelve Support Segment Load Versus Lateral Deflection (Hot Condition)

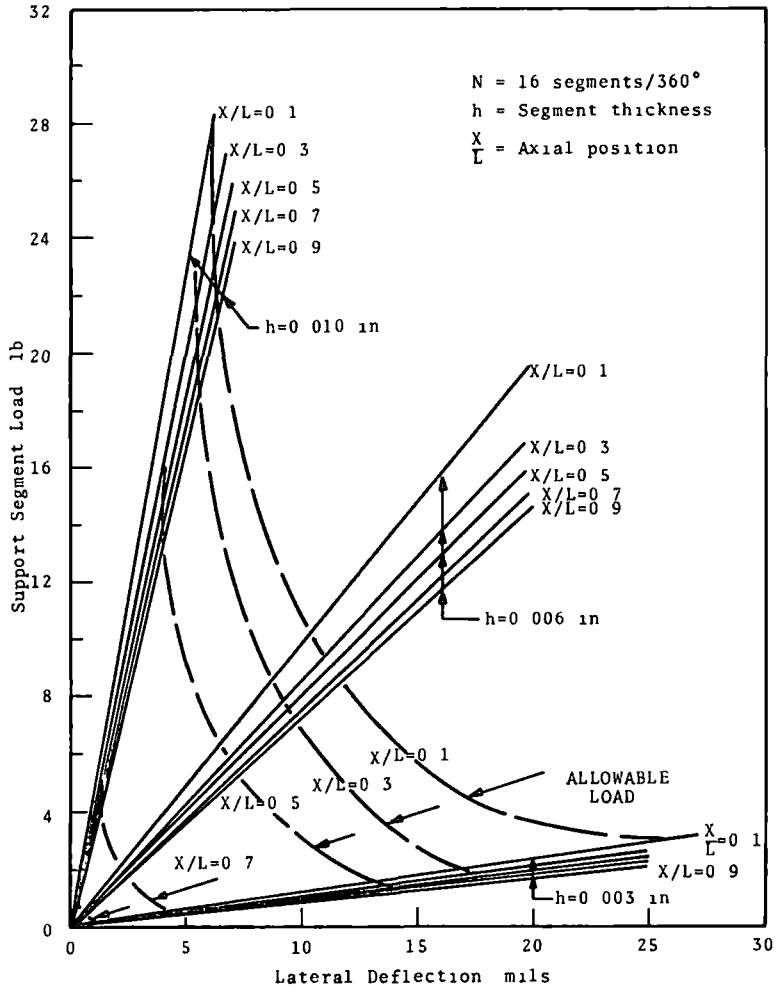

FIGURE 4 6 Sixteen Support Segment Load Versus Lateral Deflection (Hot Condition)

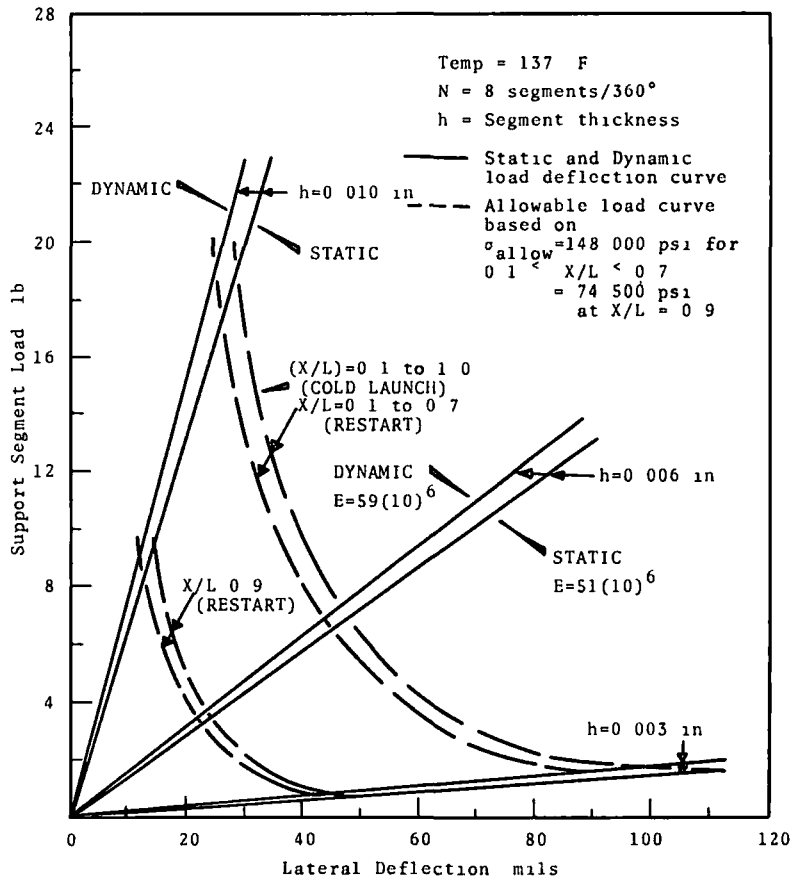

FIGURE 4 7 Eight Support Segment Load Versus Lateral Deflection (Cold Condition)

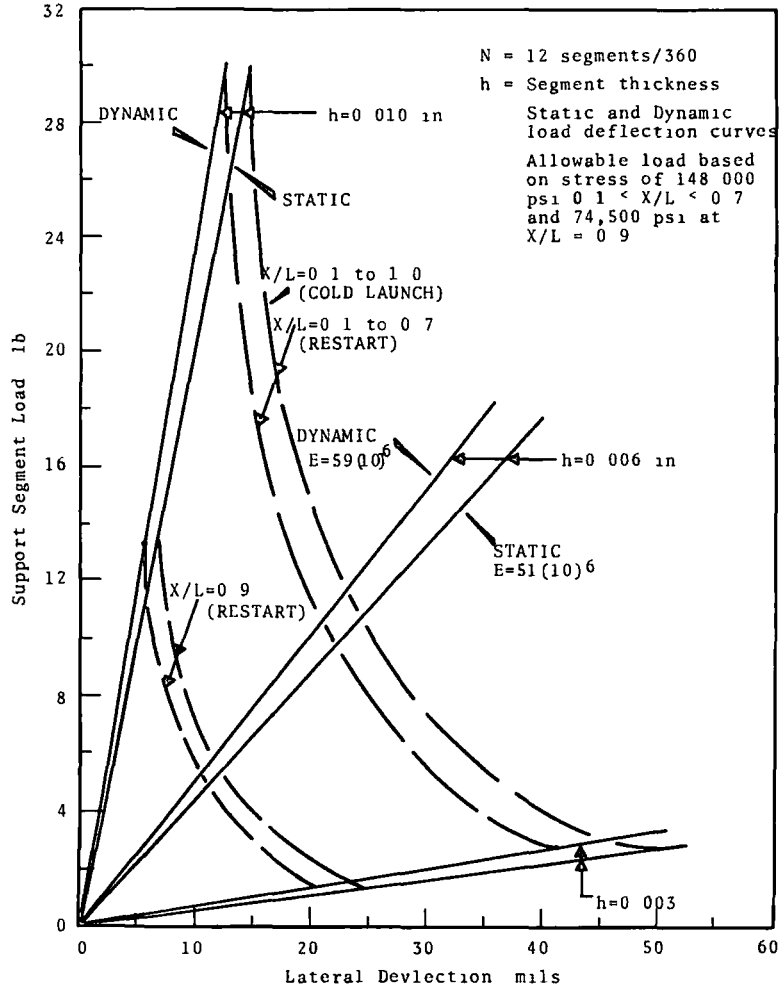

FIGURE 4 8 Twelve Support Segment Load Versus Lateral Deflection (Cold Condition)

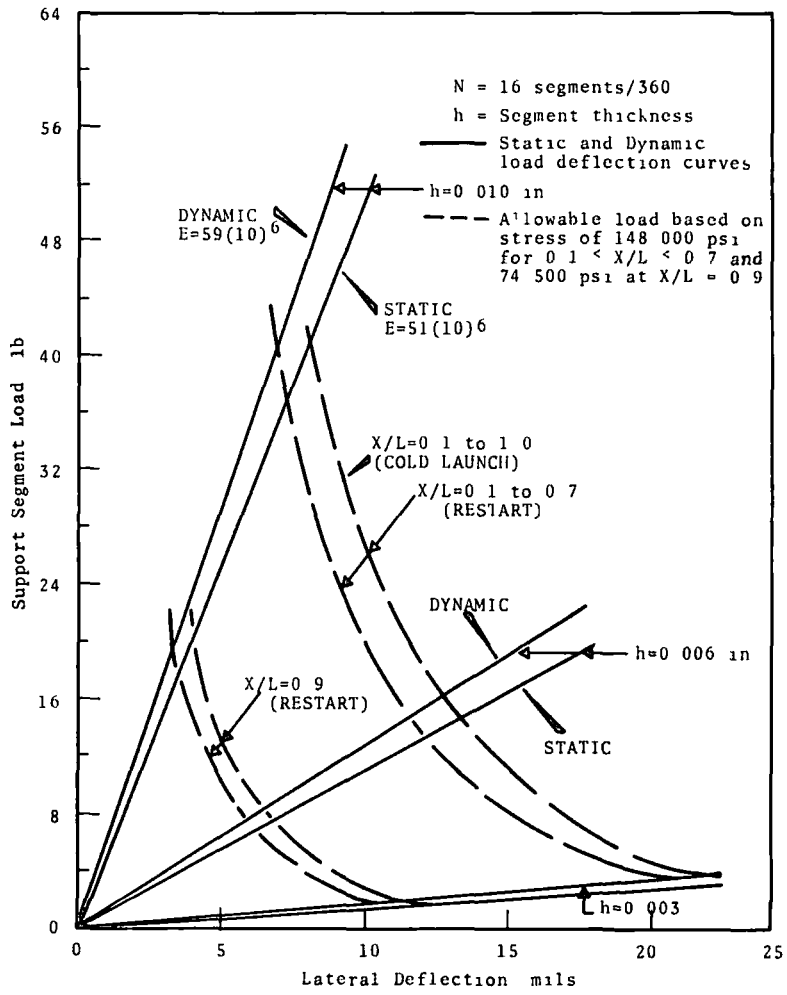

FIGURE 4 9. Sixteen Support Segment Load Versus Lateral Deflection (Cold Condition)

- Unless the temperatures at the hot end of the spring segment are reduced to values below tungsten recrystallization temperature, the allowable deflections at axial positions below $(X/L)_t = 0.7$ are insufficient to accommodate either the hot deflection or the dynamic deflections This conclusion applies to the softest spring (i e , eight 0 003 in thick segments per 360°) evaluated with this spring segment model

In the colder half of the fuel column, $0.1 < (X/L)_t < 0.5$, there appears to be a reasonably wide range of spring constants from which acceptable lateral supports might be selected Spring segment deflections due to thermal expansion, Figure 4 10, are considerably less than in the hot half of the column, and selection of a spring with appropriate stiffness should help reduce dynamic deflections When considering the lateral support load deflection characteristics under cold conditions, the problem of insufficient allowable deflections at $0.5 < (X/L)_t < 1.0$ is not as severe as in the operating reactor case Higher loads and larger deflections can be accommodated without exceeding the allowable stresses in the spring segment

4 4 MODEL VERIFICATION AND ALTERNATE MODELS

Tests conducted by NASA-Lewis personnel indicate that a 12 segment, 0 005 in thick tungsten corrugated strip has a measured static spring constant of approximately 1900 lb/in This corrugated strip was 1 5 in long and had diametral dimensions corresponding to the 1/8 in static gap study cases A calculated spring constant of 2280 lb/in , assuming similar dimensions and room temperature material properties, indicated agreement, within 20%, between the analytical and test models

Continuation of the TWMR analysis could consider alternate lateral support models A lateral support with adequate load-deflection characteristics at the hot end of the fuel column might

be attainable with other types of support structures One model consists of discrete pairs of corrugated segments which are pinned at one end and free to slide axially in the static gas gap The maximum corrugated strip bending moments will occur at the aluminum tube contact locations, where the operating temperature will be lower, and should yield significantly higher allowable loads and deflections than obtained with the previous model

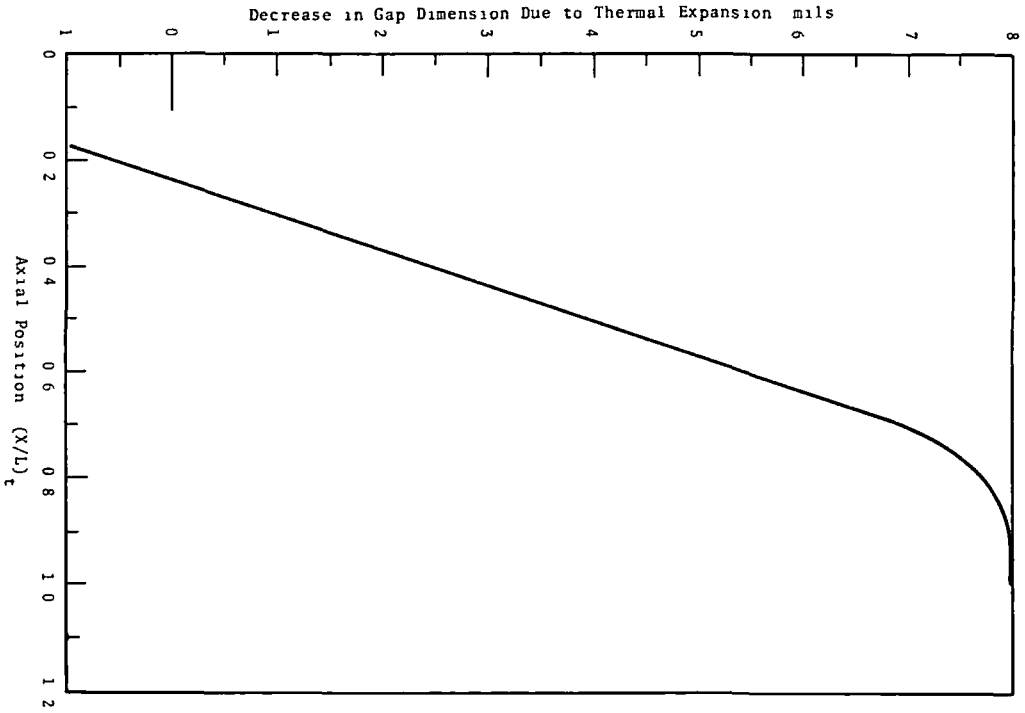

FIGURE 4 10 Decrease in Gap Dimension Versus Axial Position

4 5 REFERENCES

1 *F F Schmidt and H. R Ogden The Engineering Properties of Tungsten and Tungsten Alloys, DMIC-191, Table A-7 Battelle Memorial Institute, September 27, 1963*

5 0 DYNAMIC ANALYSIS

Structural integrity of the reactor fuel column, pressure tube and support tube must be maintained during launch and reactor operation Dynamic response analyses defining the bending stresses and deflections of the unsupported tube concept and subsequent design modifications were conducted, primarily for the hot operating condition, since this was regarded as the more difficult one to satisfy

5 1 Unsupported Tube Model

The unsupported tube model[1] was understood to consist, in part, of the fuel column and reflector, the sheath tube immediately surrounding the fuel, the clamped-pinned tungsten support tube in which the fuel column and reflector were rigidly attached, and the clamped-clamped aluminum pressure tube End restraint conditions are understood to refer to the inlet and outlet ends, respectively This configuration was considered to be the basic model, that of supporting the fuel column within the support tube which was enclosed by the pressure tube

Model Excitation

Specification of system vibratory excitation as defined in WANL-TNR-027 (NERVA environmental characteristics) were initially considered Discussion concerning the proposed excitation with NASA-Lewis personnel concluded that the NERVA specifications were excessive for this system, therefore, a constant 1 0 g sinusoidal end restraint excitation was maintained for all analyses

5 1 1 Model Description

The analysis of the unsupported tube concept assumed a homogeneous one dimensional clamped-pinned (inlet-outlet) tungsten support tube with material damping as shown in Figure 5 1.

Since the analysis was based on a one dimensional tube in the transverse plane, axial force components induced at the end restraints are neglected The fuel column was considered to provide negligible lateral stiffness and was further assumed to be rigidly coupled to the support tube Fuel column mass was assumed to be uniformly distributed over the length of the tube Axial temperature distribution of the homogeneous tube was assumed to be constant Therefore, the structural rigidity of the tube was independent of axial location

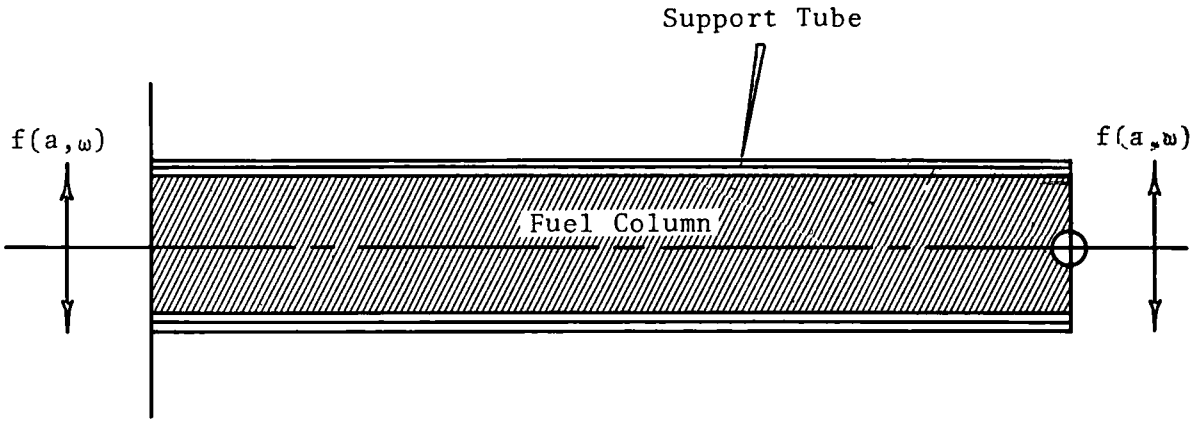

FIGURE 5 1 Unsupported Tube Model

Structural damping was considered and was based on a constant Q hypothesis [2] The "Q" of a mechanical system is defined as being proportional to the ratio of the peak energy stored per cycle to the energy dissipated per cycle This representation of material damping in an analysis of a cantilever beam closely resembles the actual transient response The concept was then adopted to the mathematical model of the unsupported tube case One value of the log decrement for swaged tunsten was found [3] and used in the analysis This value (δ = 0 0615, c/c_c = 0 0026) was obtained by revolving deflected rods, a method that does not duplicate the subject application but should give reliable damping

CONFIDENTIAL

data The log decrement of other materials were examined by this method and the data were noted to agree with other published data of the same material It is worth noting that the energy dissipation of tungsten is greater than that for most other metallic materials

Parametric studies investigating the effect of material damping indicated that the degree or amount of damping is very critical as deviations from a conservative system are made This, of course, is in agreement with basic vibration theory which predicts a decreasing exponential relationship when steady state amplitude, at a single excitation frequency, is plotted versus fraction of critical damping

5 1 2 Method of Analysis

The support tube and fuel element were treated as a one dimensional, continuous, damped, homogeneous structure with the clamped-pinned end restraints forced sinusoidally For small deformation of a conservative system, the flexural equation states

$$M = - EI \frac{\partial^2 y}{\partial x^2} \tag{1}$$

In the absence of externally applied forces and moments the inertial loading force, F_I, is defined by

$$F_I = \frac{\partial V}{\partial x} \tag{2}$$

and the vertical shear, V, being classically defined by

$$V = \frac{\partial M}{\partial x} \tag{3}$$

permits combining Equations (1), (2), and (3)

Performing this operation and employing Newton's second law results in

$$\frac{\partial^2}{\partial x^2} EI\left[\frac{\partial^2 y}{\partial x^2}\right] + m\frac{\partial^2 y}{\partial t^2} = 0 \qquad (4)$$

which defines the dynamic response of a conservative system Equation (4) must be modified to account for structural energy dissipation

Sewaza[4] proposed that material damping could be represented by a Stokes viscosity coefficient This approach assumes that the damping is dependent upon the excitation frequency More recent investigations[2] have shown that material damping is independent of frequency Therefore, the constant Q damping concept was considered applicable and was modeled in the analysis by replacing Young's modulus, E, in Equation (4) by the term

$$E = E + \frac{E}{Q\omega}\frac{\partial}{\partial t}$$

where

ω = circular frequency, rad/sec

Q = Q (from electrical analog)

$\frac{\partial}{\partial t}$ = operator

making this substitution into Equation (4) results in

$$\frac{\partial^2}{\partial x^2}\left[EI\frac{\partial^2 y}{\partial x^2} + \frac{EI}{Q}\frac{\partial^3 y}{\partial x^3 \partial t}\right] + m\frac{\partial^2 y}{\partial t^2} = 0 \qquad (5)$$

which defines the dynamic response of a continuous, damped, homogeneous structure Limiting analysis to steady state response and substitution of applicable boundary conditions into and solving Equation (5) results in

$$y(x,t) = [C_1 \sin\phi x + C_2\cos\phi x + C_3\sinh\phi x + C_4\cosh\phi x]\ \sin zt \qquad (6)$$

where

Y = deflection of support tube x inches from clamp (X/L = 0) and time t, in

a = input acceleration, in /sec^2

ω = circular frequency, rad/sec

$U = C_1 \sin \phi + C_2 \cos \phi$

$V = C_3 \sinh \phi + C_4 \cosh \phi$

$\phi = 2m\omega^2 / \left[EI\left(1 + \sqrt{1-4\beta^2}\right)\right]$

x = axial distance from clamp, in

M = mass per unit length, lb-sec^2/in

E = dynamic Young's modulus, lb/in^2

I = moment of inertia, in^4

β = fraction of critical damping

$$C_1 = (\gamma_3 C_4 - \gamma_2 C_2)/\gamma_1$$

$$C_2 = \frac{1 - \gamma_3(1 + \gamma_4/\gamma_1)}{\gamma_2(1 - \gamma_4/\gamma_1) - \gamma_3(1 + \gamma_4/\gamma_1)}$$

$$C_3 = -C_1$$

$$C_4 = 1 - C_2$$

$$C_5 = 2\beta\omega / \left[1 + \sqrt{1 - 4\beta^2}\right]$$

$$\gamma_1 = \sin\phi\ell + \sinh\phi\ell$$

$$\gamma_2 = \cos\phi\ell$$

$$\gamma_3 = \cosh\phi\ell$$

$$\gamma_4 = \sin\phi\ell + \cosh\phi\ell$$

$$Z = \frac{\omega\{2[(1 + \sqrt{1-4\beta^2}) - 2\beta^2]\}^{1/2}}{1 + \sqrt{1-4\beta^2}}$$

t = time, sec

Detailed derivation of Equation (6) is provided in Appendix III The maximum or peak steady state amplitude, Y_{SS}, is defined as

$$Y_{SS}(x) = [C_1\sin\phi x + C_2\cos\phi x + C_3\sinh\phi x + C_4\cosh\phi x] \quad (7)$$

where the independent variables are defined above

Steady state bending stress, σ_{SS}, was calculated from Equations (1) and (6) which results in

$$\sigma_{SS}(x) = Ec\frac{\partial^2 X}{\partial x^2} \quad (8)$$

where

X = U + V

c = distance from neutral to outermost fibre

σ = bending stress, lb/in ^{2}

Preliminary natural frequency calculations were conducted by using published eigenvalues[5] evaluated from the transcendental relationship given by Equation (7) with the applicable boundary conditions

Detailed frequency response data were generated by the IBM 7090 computer operating on Equations (7) and (8) These calculations were made at a single frequency, the calculated data readout, the frequency incremented and the computation cycle repeated

5 1 3 Results

Natural frequency calculations of the continuous, homogeneous clamped-pinned tube, assumed to represent the unsupported tube concept, resulted in the data presented in Table 5 1

TABLE 5 1 NATURAL FREQUENCIES FOR UNSUPPORTED TUBE MODEL

		Resonance Frequency, cycles/sec	
Mode	ϕ	$E = 59(10^6)$ psi	$E = 50(10^6)$ psi
1st	0 0715	45 8	42 2
2nd	0 1283	93 4	136 0
3rd	0 1859	196 6	286 0
4th	0 2425	334 0	486 0

A support tube length of 55 in and a weight per unit length of 0 6455 lb/in was used for the above calculations Support tube moment of inertia was calculated to be 0 0902 in ^{4} The eigenvalues, ϕ, to be used in

$$\omega_N = \phi^2 \sqrt{\frac{EIg}{\gamma S}}$$

for the natural modes are presented in Table 5 1 Approximation of resonant modes at reactor thermal operating conditions was afforded by decreasing the Young's modulus, E, to a value of 50×10^6 corresponding with material properties at an estimated average support tube temperature of 2400 °F

These data, being well within the specified excitation of 5 to 2000 cycles/sec indicated that the system would probably require some form of energy dissipation in order to obtain reasonable bending stresses

Preliminary resonant frequency response calculations were conducted by hand to investigate the effects of damping and stiffness on the system These calculations considered room temperature

operation and were based at the antinode of the first mode $(X/L)_V = 0.58$. Deviations in the characteristic frequency from variations in structural damping were neglected, however, the deviation attributed to changes in support tube stiffness was considered. The data are presented in Figure 5.2 and indicate that a significant increase in the damping capacity and/or tube stiffness is required to yield acceptable bending stresses in the support tube.

The fraction of critical damping values used are of parametric interest only as that for the actual structure was realized to be quite low. Lower values of the fraction of critical damping were not considered as the accuracy of the solution would be subject to considerable round-off error and hence the data would be questionable.

Detailed frequency response data were generated with the IBM 7090 digital computer. These data are presented in Figures 5.3 and 5.4 for the clamp $(X/L)_V = 0$ and the antinode of the first mode $(X/L)_V = 0.58$, respectively. Bending stresses greatly in excess of the cold tensile strength are observed at both locations at resonant modes. The fraction of critical damping used ($\beta = 0.0025$) was the only value found[3] of material damping in tungsten.

Additional energy dissipation of the system is required as indicated from the response data. The alternate solution of reducing the bending stress by decreasing the mass to stiffness ratio is impracticable as it implies increasing the thickness of the support tube. The dimensions of the support tube are such that the major modifications required in this case would not be possible. Therefore, it was clear that a lateral support was required which would permit the transfer of energy from the

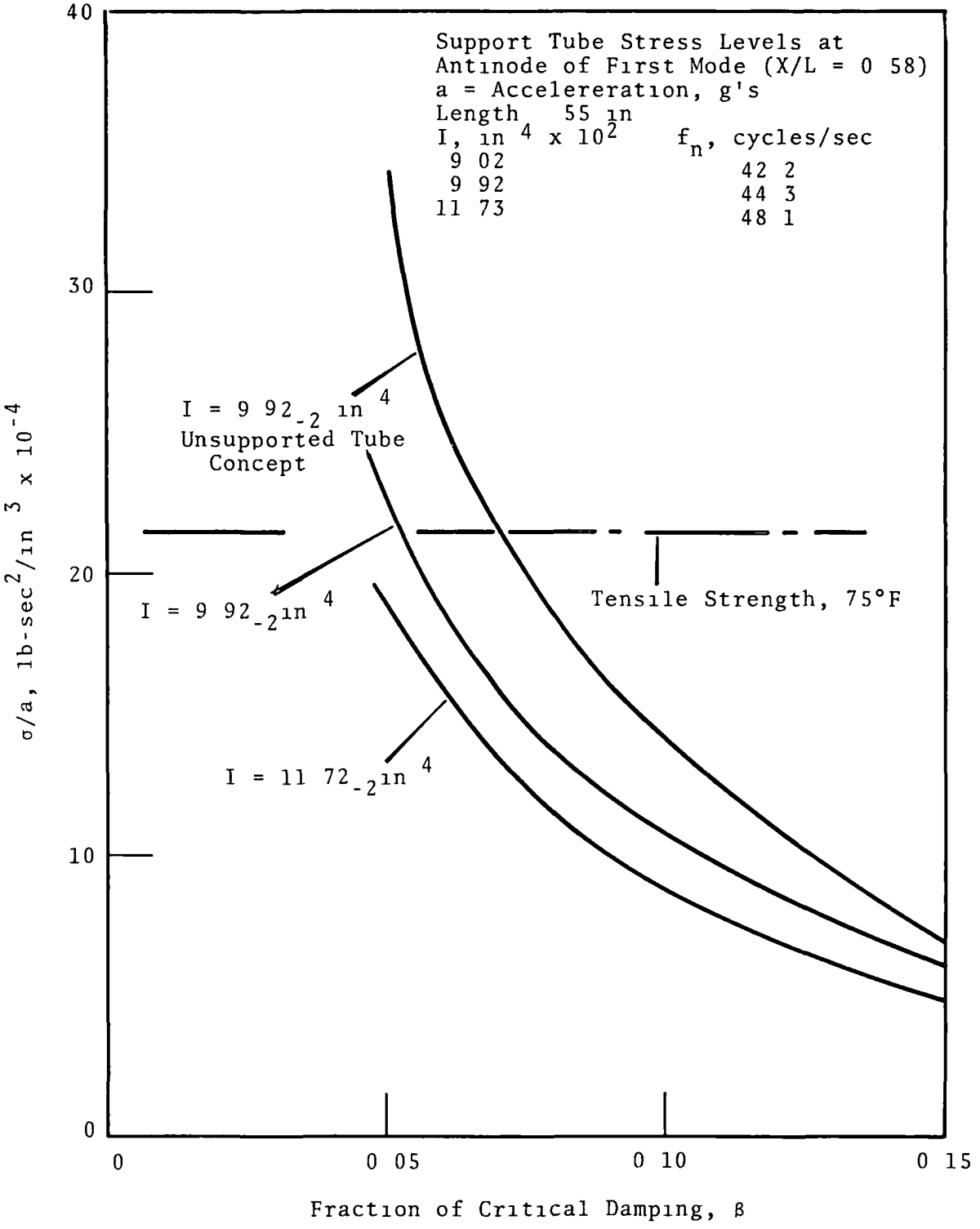

FIGURE 5 2 Unsupported Tube Concept Launch Conditions

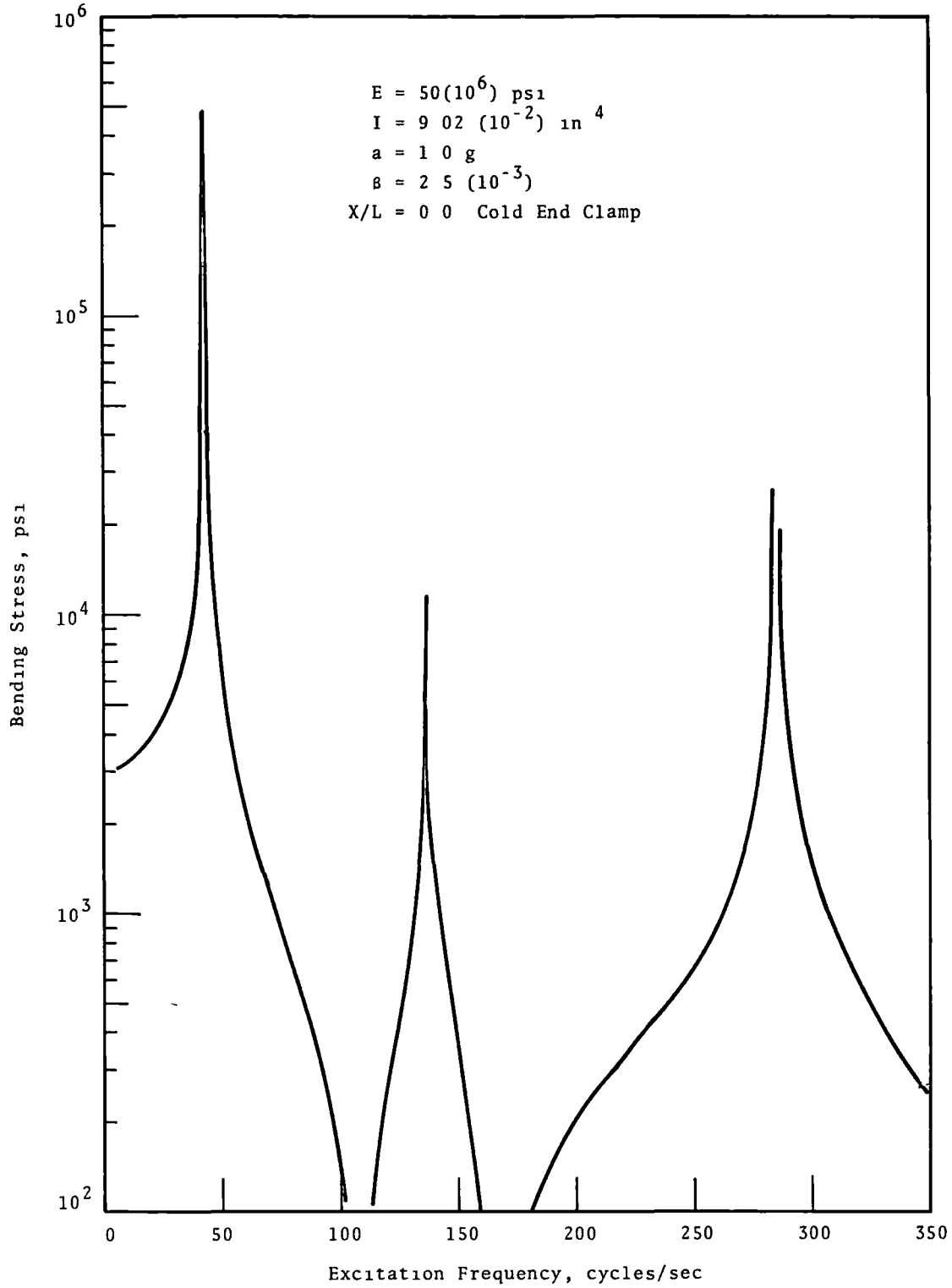

FIGURE 5 3 Bending Stress Versus Excitation Frequency, Tungsten Support Tube Without Lateral Supports

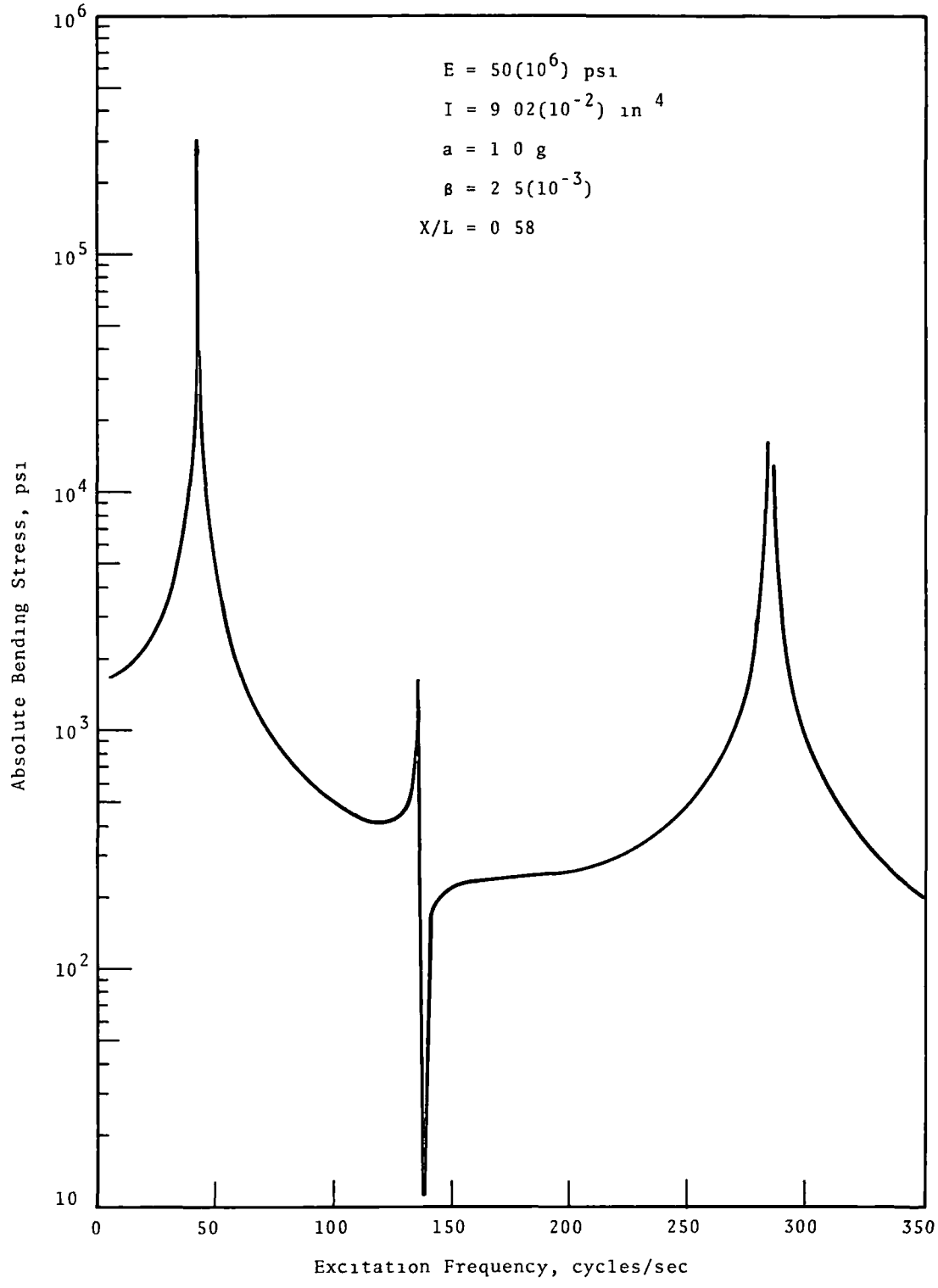

FIGURE 5 4 Bending Stress Versus Excitation Frequency Tungsten, Support Tube Without Lateral Supports

support tube through the aluminum pressure tube and into the moderator This configuration would then reduce the energy content of the support tube, thereby yielding lower bending stresses and deflections

Comparison of analytical data of the unsupported tube model with those obtained experimentally on a composite material model by NASA-Lewis indicate dissagreement in the bending stress values and displacement, although resonant frequencies are predicted quite closely as noted in the summary data presented in Table 5 2

TABLE 5 2 COMPARISON OF ANALYTICAL AND EXPERIMENTAL UNSUPPORTED TUBE MODEL STUDIES

Frequency Cycles/sec	$(X/L)_V$	Bending Stress, psi	
		Test Model	Analytical Model
40	0 019	5,000	
	0 585	36,400	
	0 981	4,320	
42 2	0		482,370
	0 580		316,660
	1 000		0
230	0 019	600	
	0		412 9
	0 585	3,940	
	0 580		328
	0 981	1,000	
	1 000		0
662	0 019	500	
	0 585	1,000	
	0 981	1,000	
660	0		158
	0 58		77 5
	1 00		1 8

Basic experimental data indicate that the composite test system significantly differed from the analytical model The low

"Q" or relatively flat response is normally indicative of a heavily damped system, however, axial force components caused by the knife-edge used at the pinned end may also be significant Bending stresses of the experimental model at the antinode of the first mode are observed in Table 5 2, to be lower than those predicted analytically at the first resonance, while at higher frequencies the opposite case is noted The stress distribution, of the data received, is typical of a pinned-pinned beam The moment near the knife edge, however, appears to be increasing (relative to the clamped end) as the frequency is increased Damping in the analytical model assumed that the fraction of critical damping was independent of frequency Further, energy dissipation in the end restraints was not condisered Published information[6] indicates that the energy dissipation at a clamped boundary is normally 10 to 20 times that in metallic components at low stress magnitudes This mechanism is not well-defined, however, it is undoubtedly referred to the physical and metallurgical properties at the interface of the clamp and the clamping pressure These observations and the assumptions modeled in the analysis imply that the material damping of the experimental composite tube was high and was decreasing with frequency, a trend differing from normal behavior, and/or the axial force component was increasing at resonance

The apparent pinned-pinned boundary condition at the fundamental resonance indicates that this frequency should have been approximately 18 cycles/sec Yet, the resonance occurred at 40 cycles/sec It is then postulated that the experimental model simulated a clamped-pinned beam (based on the resonance frequency agreement) which was changed to a pinned-pinned beam at resonance because of a significant axial force component and possible rotation of the cold end clamp This would tend to reduce the dynamic

response of the tube at the clamped-pinned resonance since at this frequency the boundary conditions are indicated to be pinned-pinned

5 2 Cold End Support Concept

Vibratory energy may be extracted from the support tube-fuel combination by transferring energy through the pressure tube and into the moderator The energy transfer would be through nonrigid, nonconservative lateral supports which couple the support tube to the pressure tube Vibratory energy dissipation would be in the form of viscous drag forces from the moderator acting on the pressure tube and opposing pressure tube velocity variations Additional energy dissipation would be realized at the lateral supports in the form of coulomb damping resulting from slippage of the coupling support and the tubes

5 2 1 Assumptions and Model Description

The basic model was conceived as being the clamped-pinned (inlet-outlet) support tube in which the fuel and reflector columns were rigidly attached The tungsten support tube would be laterally supported by the clamped-clamped pressure tube at several axial locations with flexible supports These supports, described in Section 4 of this report, would afford the coupling between the two tubes

Sinusoidal end restraint excitation was defined as 1 0 g peak and being in-phase at all boundaries

Energy dissipation of the model was assumed to result from pressure tube motion in the moderator and from slippage of the lateral supports Damping present in the structural components was assumed negligible in comparison with that above The method

of analysis and available computation equipment required simulating the coulomb damping in the lateral supports with viscous damping This deviation from the basic model was believed minor, particularly in the low frequency range

5 2 2 Method of Analysis

Coupling the pressure tube to the support tube-fuel combination with the lateral supports would significantly complicate the boundary conditions and definition of a continuous, homogeneous model of the inlet end support case The homogeneous model would be further complicated as the effect of reactor thermal operating conditions were required which implies variations of system stiffness (EI) along the longitudinal axis These considerations suggested that the inlet end support case should be simulated on the analog computer in a lumped node analysis

Initial simulation of the system was directed toward determining the number of nodes required to yield acceptable accuracy The magnitude of the anticipated model and the computation equipment available indicated that a maximum of six nodes should be initially considered The criterion used was based on an acceptable comparison of the reference design frequency response data from the exact homogeneous digital solution and a simulated finite difference analog solution Structural damping was assumed negligible for the analog simulation

The analysis of a nine node analog model shown in Figure 5 5, was based on the finite difference representation of the classical beam equations

$$V = \frac{\partial M}{\partial x} \tag{11}$$

and

$$M = - EI \frac{\partial^2 y}{\partial x^2} \tag{12}$$

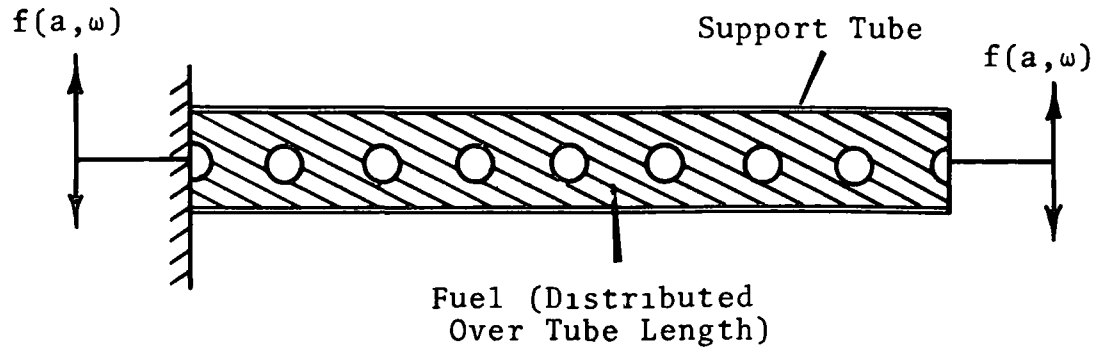

FIGURE 5 5 Unsupported Tube Model - Analog

coupled with Newton's second law and double integration of the nodal acceleration to yield the velocity and deflection of the node being considered The generalized finite difference equations are presented below

$$m_1 y_1 = V_{1+1/2} - V_{1-1/2} - F_1$$

$$F_1 = K_1 \left[y_1 - y_{1 \pm J} \right] + F_{D_1}$$

$$F_{D_1} = \rho S C_D y_1^{\,2}/2 + C \left[y_1 - y_{1 \pm J} \right]$$

$$V_1 = \frac{1}{\Delta x} \left[M_{1+1/2} - M_{1-1/2} \right]$$

$$\frac{M_1}{\Delta x} = \frac{-EI}{(\Delta x)^3} \left[\Delta^2 y_1 \right]$$

$$\Delta^2 y_1 = \Delta y_{1+1/2} - \Delta y_{1-1/2}$$

$$\Delta y_1 = y_{1+1/2} - y_{1-1/2}$$

$$y_1 = \frac{1}{m_1} \int m_1 y_1$$

$$y_1 = \int \dot{y}_1$$

where

i = node being considered

j = number of nodes in each structure

y_i = deflection of node, in

$\dot{y}_i$ = velocity of node, in /sec

$\ddot{y}_i$ = acceleration of node, in /sec^2

m_i = lumped node mass, lb-sec^2/in

V_i = transverse shear, lb

F_i = external forces applied on node, lb

F_{D_i} = damping forces applied on node, lb

K_i = lateral spring rate, lb/in

ρ = moderator density, lb-sec^2/in ^{4}

S = effective projected area of pressure tube, in ^{2}

Δx = nodal spacing, in

M = bending moment, lb-in

E = dynamic Young's modulus, lb/in ^{2}

I = moment of inertia, in ^{4}

c = viscous damping coefficient of lateral support, lb-sec/in

Externally applied forces, F_i, are, by definition, zero for the unsupported tube model used for the comparison of the analog and digital solutions

Unsupported tube frequency response data of the six-node analog model, nine-node analog model and digital model are shown in Figure 5 6 The accuracy of the six node model was not

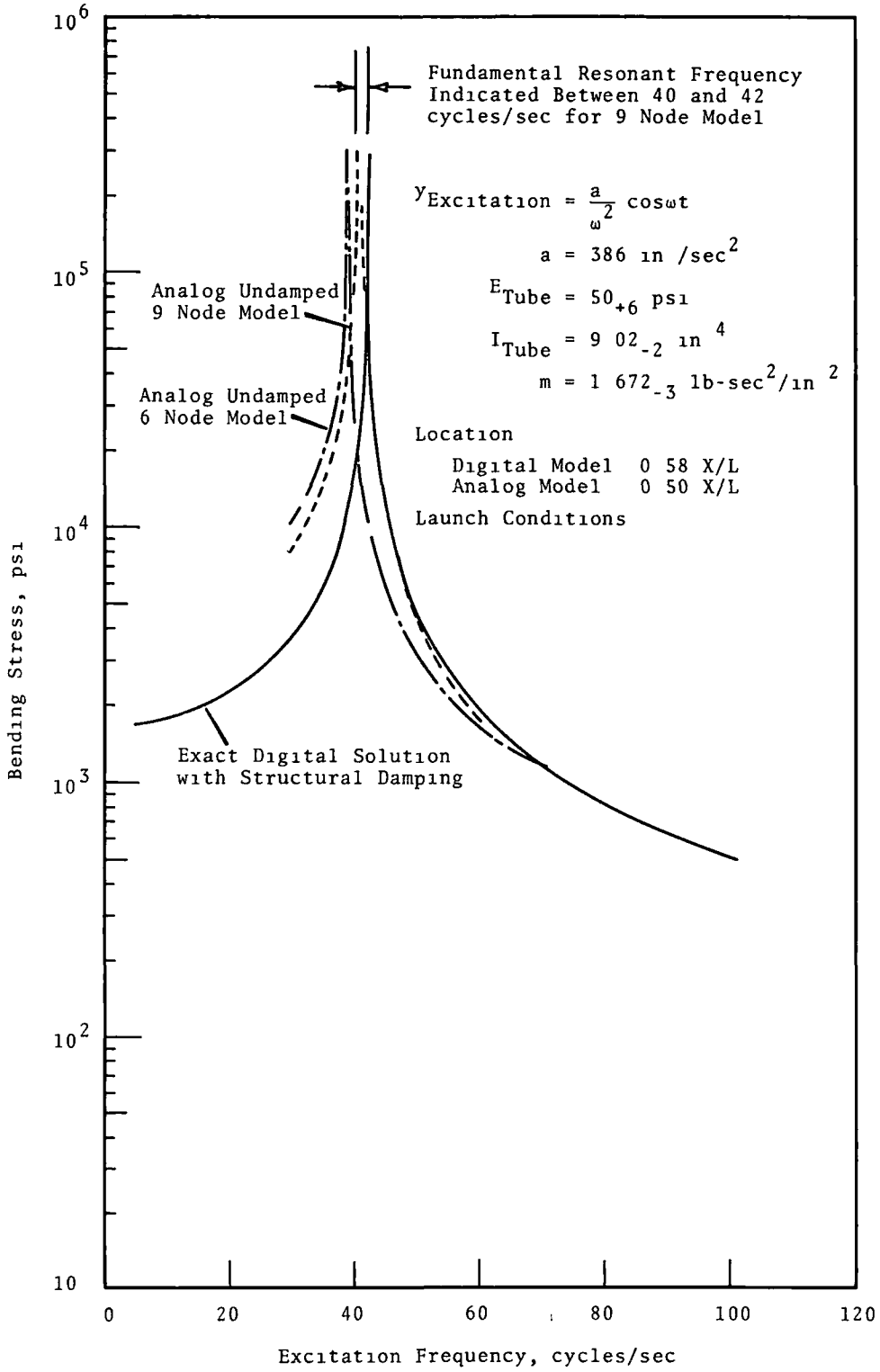

FIGURE 5 6 NASA Tungsten Fueled Reactor Unsupported Tube Model Analog-Digital Comparison

acceptable, therefore, the model was enlarged to represent the tube by nine nodes The results of the nine node analog simulation are considered acceptable when compared with the exact solution The nine node model was therefore used for simulation of the cold end support case shown in Figure 5 7

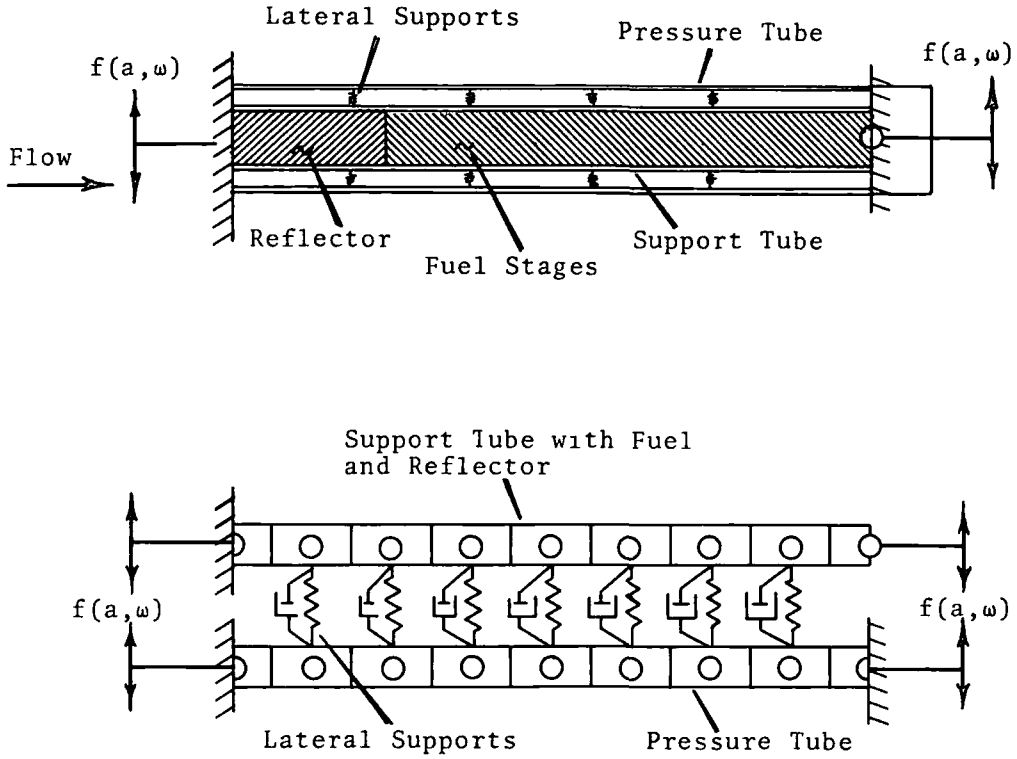

FIGURE 5 7 Cold End Support Case Concept and Analog Model

The analog computer program for the cold end support simulation is included in Appendix D and requires the following components

Integrators	34	Potentiometers	74
Summing Amplifiers	71	Multipliers	7
Inverters	35		

This complement was available on the BNW EASE 2133 analog computer without using the EASE 1132 computer, however, function generator components were utilized

Bending stresses were calculated from the recorded term

$$\phi \Delta^2 Y_1$$

by employing the definition of bending moment

$$M_1 = - E_1 I_1 \frac{\partial^2 y_1}{\partial x^2} \tag{13}$$

and

$$\sigma = \frac{MC}{I} \tag{14}$$

Combining Equations (13) and (14) results in

$$\sigma = \frac{EC}{\phi(\Delta x)^2}\left[\phi \Delta^2 y_1\right] \tag{15}$$

where

ϕ = analog amplitude scale factor

Evaluation of the equivalent lateral support spring rate to be used on each lumped analog node considered the planar transverse displacement of an inner ring with respect to an outer ring These rings simulated the support tube and pressure tube, respectively The total load, P_{V_T}, required to deflect the inner ring δ_V inches is

$$P_{V_T} = \sum_{1=0}^{180} 2K\delta_y \cos^2\theta_1 \tag{17}$$

where

θ_1 = angle between an arbitrary reference plane and the lateral support load point, degree

K = individual node spring rate, lb/in

δ_V = maximum transverse displacement, in

and defining an equivalent spring rate as

$$\overline{Ke} = \frac{P_{V_T}}{\delta_V} \tag{18}$$

the relationship between the individual lobe spring rate, K, and the equivalent single lateral support spring rate, $\overline{Ke}$ is defined as

$$\overline{Ke} = 2K \sum_{i=0}^{180} \cos^2\theta_i \tag{19}$$

The nine node analog model then implies that each node was equivalent to 4 58 fuel stages, each of which has a lateral support Therefore, the equivalent spring rate, K_e, of each analog node will be

$$K_e = 9\ 16\ K \sum_{i=0}^{180} \cos^2\theta_i \tag{20}$$

5 2 3 Results

Initial analyses of the cold end support case considered the lateral supports described in Section 4 The assumption was made that the principle form of energy dissipation in the lateral supports would be due to structural damping This component, as that in the support and pressure tubes, was assumed negligible in comparison with the damping afforded by the moderator

The lateral support spring rate was specified with axial temperature distribution considered This work is reported

in Section 4 and defines the spring rate as varying inversely as temperature The magnitude of the support tube bending stress was found to be relatively insensitive to variations of lateral support spring rate above a value of approximately 1000 lb/in The resonance shift is considered minor for reasonable variations of the spring rate Detailed frequency response studies concerning the effect of lateral support spring rate are invalid because of a loose patchcord in the analog patchboard The data are however, believed technically applicable and are indicative of the generalized trends noted above

Frequency response characteristics of the conservative cold end support case simulating thermal operating conditions were conducted with spring rates prescribed in this report Input data defining the mass, spring rate, dynamic Young's modulus and stiffness are presented in Table 5 3

Support tube bending stresses at the clamp $(X/L)_V = 0$), $(X/L)_V = 0\ 50$, and $(X/L)_V = 0\ 75$ are shown in Figure 5 8 These data are presented to 100 cycles/sec which is beyond the first resonance Pressure tube bending stresses at the cold clamp, $(X/L)_V = 0\ 50$, and $(X/L)_V = 0\ 75$ are shown in Figure 5 9 Lateral support deflection at $(X/L)_V = 0\ 375$, and $(X/L)_V = 0\ 500$ and for $(X/L)_V = 0\ 75$ and $(X/L)_V = 0\ 875$ are shown on Figure 5 10 These data indicate that the conservative system produces excessive bending stresses in the thermally hot section of the support tube Lateral support deflections are also excessive The fundamental of the system is observed to be caused by the support tube and fuel column Resonance resistance, observed from the sharpness of the resonant peak, is not sufficient to reduce the bending stresses to acceptable levels

TABLE 5 3 INPUT DATA SUMMARY RUNS BC (COLD) AND BF (HOT)

X/L_{vib}	Mass lb sec^2/in		I in ^{4}		Dynamic Young s Modulus lb/in ^{2}			Lateral Supports			
								Hot		Cold	
	P T	S T	P T	S T	P T	S T (Hot)	S T (Cold)	K, lb/in	C_C $\frac{lb\ sec}{in}$	K lb/in	C_C $\frac{lb\ sec}{in}$
	8 0773(10 ^{4})	2 402(10 ^{3})	3 488(10 ^{1})	0 0902	10 0(10^6)	58 7(10^6)	58 7(10^6)	N A	N A	N A	N A
0 125		3 048(10 ^{3})				56 1(10^6)		5 0(10^4)	1 38(10)	5 0(10^4)	1 27(10)
0 250		1 443(10 ^{3})				53 7(10^6)		5 0(10^4)	1 27(10)		1 27(10)
0 375						51 4(10^6)		4 48(10^4)	1 205(10)		1 27(10)
0 500						48 6(10^6)		4 23(10^4)	1 168(10)	5 0(10^4)	1 27(10)
0 625						45 6(10^6)		8 77(10^3)	5 32	1 429(10^4)	6 79
0 750						42 1(10^6)		1 06(10^3)	1 85	1 923(10^3)	2 49
0 875						38 7(10^6)		1 016(10^3)	1 81	1 923(10^3	2 49
1 00	8 0773(10 ^{4})	1 443(10 ^{3})	3 488(10 ^{1})	0 902	10 0(10^6)	36 8(10^6)	58 7(10^6)	N A	N A	N A	N A

NOTE

Lateral support configuration same for both runs

C/C_C = 0 10 for both runs

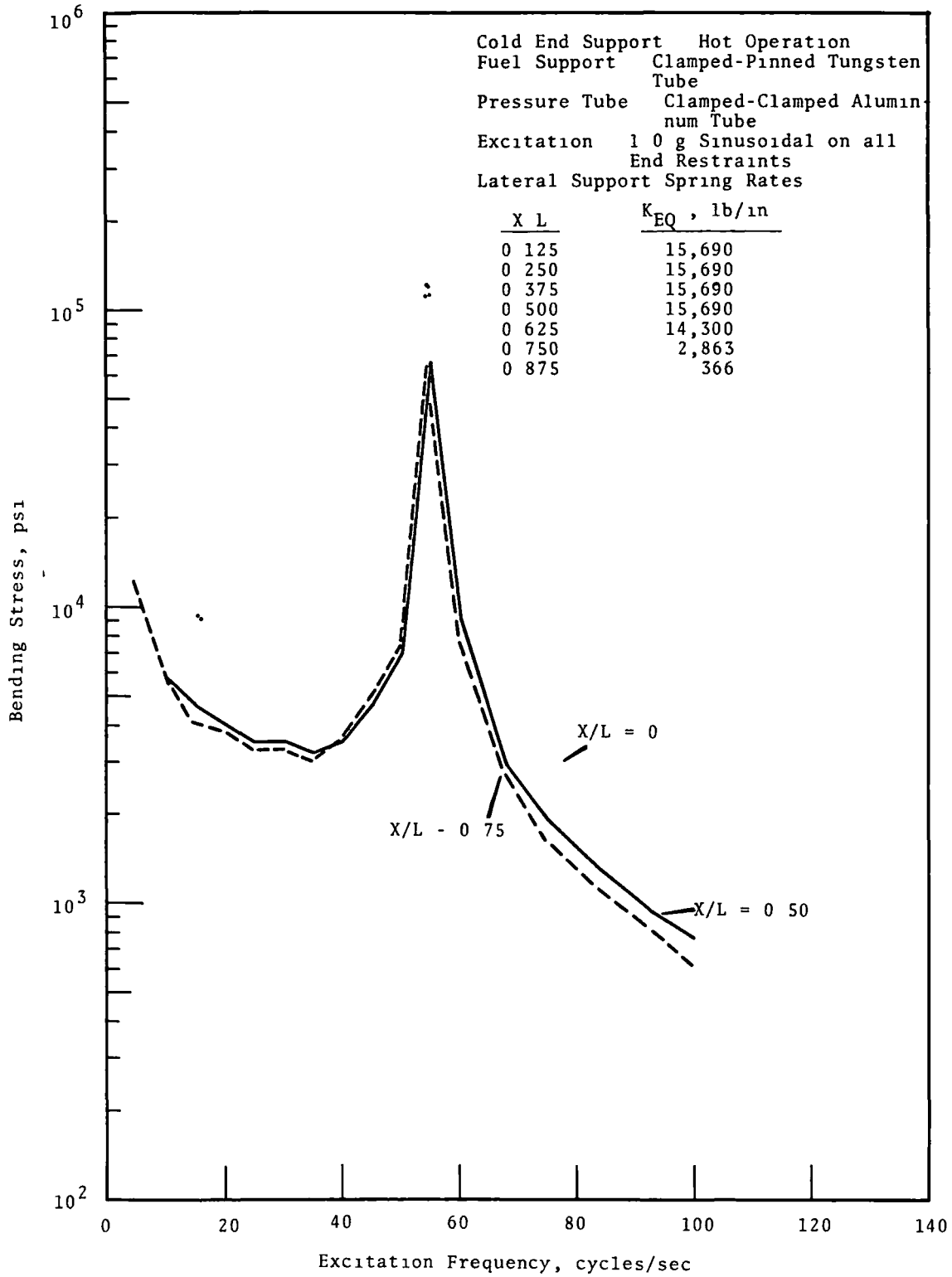

FIGURE 5 8 Support Tube Bending Stress Versus Frequency

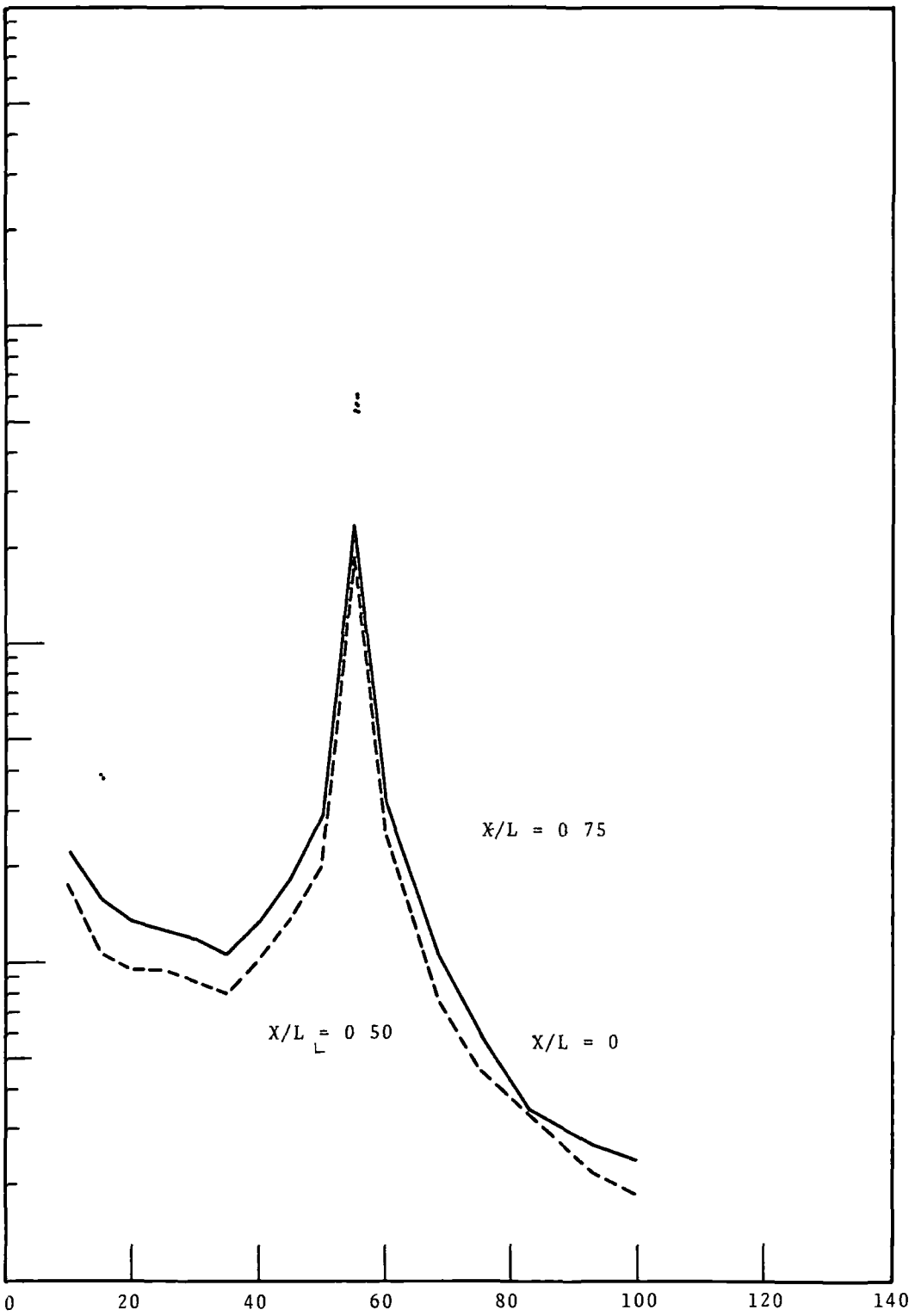

FIGURE 5 9 Pressure Tube Bending Stress Versus Frequency

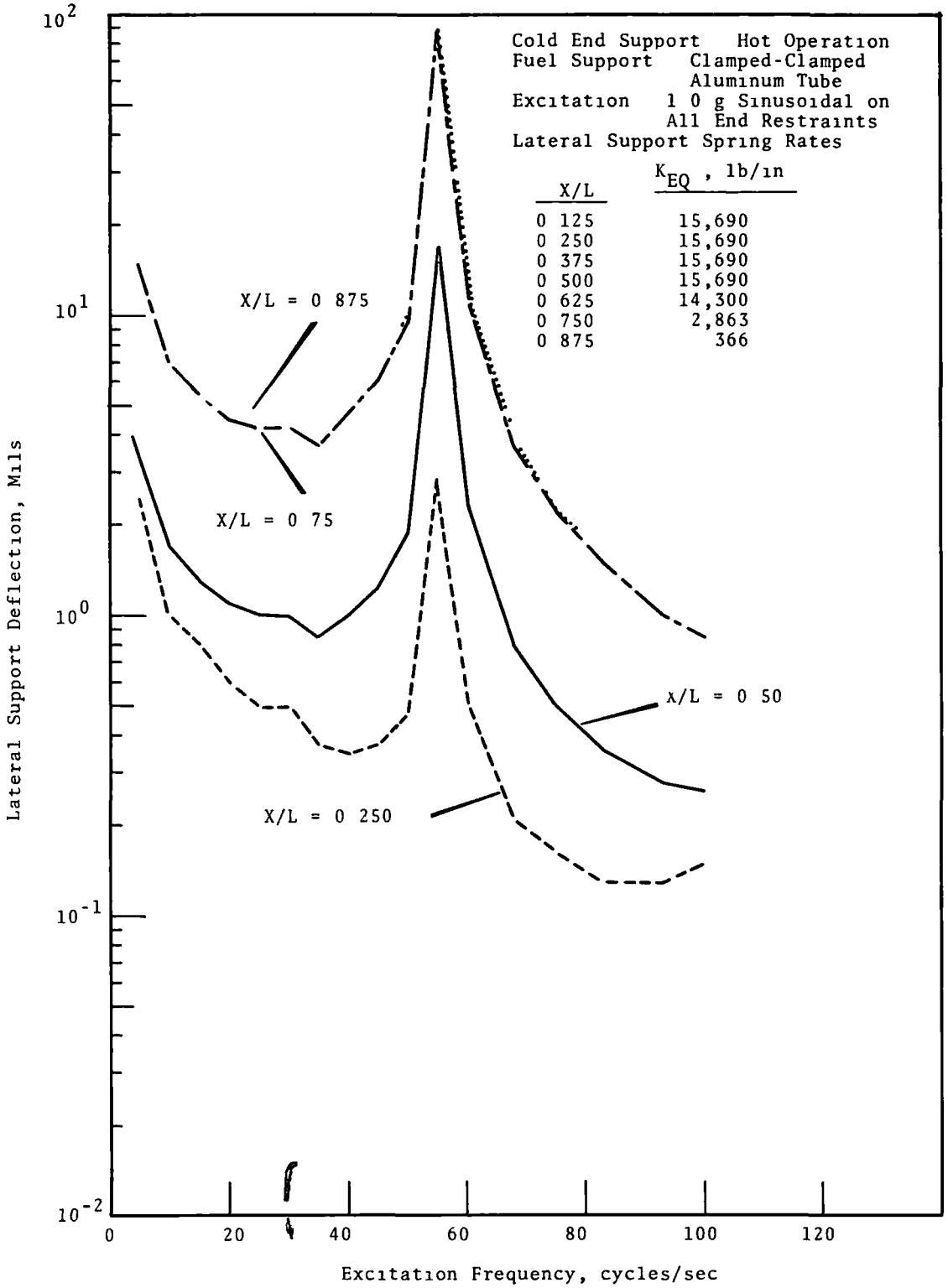

FIGURE 5 10 Lateral Support Deflection

Reduction of fuel support member bending stresses may be realized by replacing the support tube with a cylindrical rod projected through the axial centerline of the fuel column This would reduce the distance from the neutral to the outermost fiber Deflections were expected to increase, however, the subsequent reduction of the fuel support fundamental and its high inertia would decrease the fundamental of the system, possibly below the lower excitation frequency expected This concept, termed the tie-rod configuration and shown in Figure 5 11 was briefly studied One additional tube sheet at X/L = 0 50 was provided and was intended to effectively reduce the length of the dynamic model

Frequency response characteristics of the tie-rod configuration were evaluated between 5 and 120 cycles/sec which is beyond the first major resonance Two different values of equivalent lateral support spring rate were specified and are denoted by run numbers C-1 and C-2 on the applicable figures Lateral support spring rates used for run C-1 were specified from the lateral support study The spring rates used on the hot end of the system for run C-2 are believed excessive, the data are thus of parametric interest only

Fuel support bending stress for runs C-1 and C-2 at the clamp and at X/L = 0 50 are presented in Figures 5 12 and 5 13, respectively Lateral support deflection for the same runs and at X/L of 0 75 and X/L of 0 875 are presented in Figures 5 14 and 5 15, respectively These data indicate that the bending stresses are significantly reduced by the slender rod and additional tube sheet, however, the stress at the hot end is still considered to be excessive The frequency of maximum stress has decreased from 55 to 30 cycles/sec The apparent resonance at 30 cycles/sec was

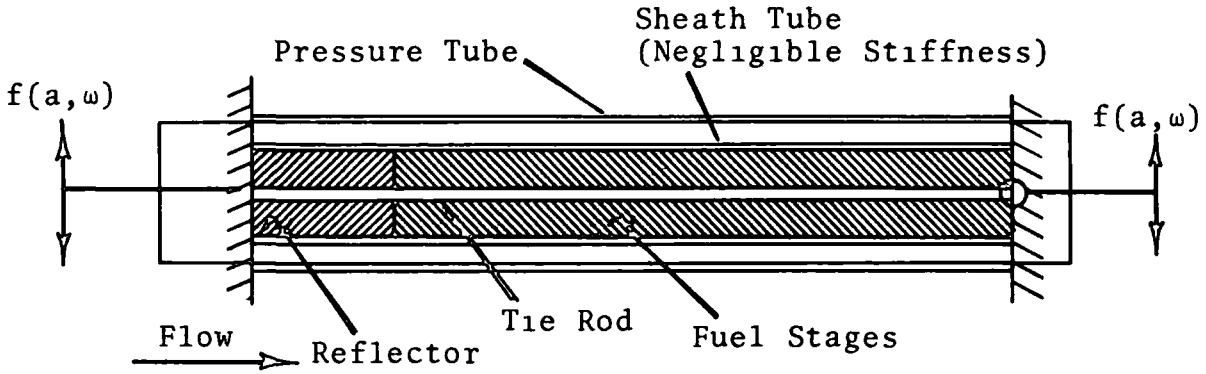

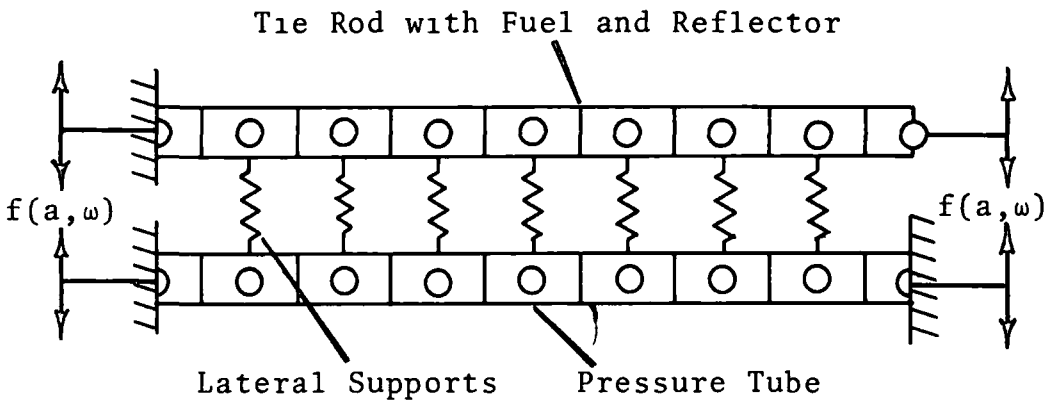

FIGURE 5 11 *Tie-Rod Case, Concept and Analog Model*

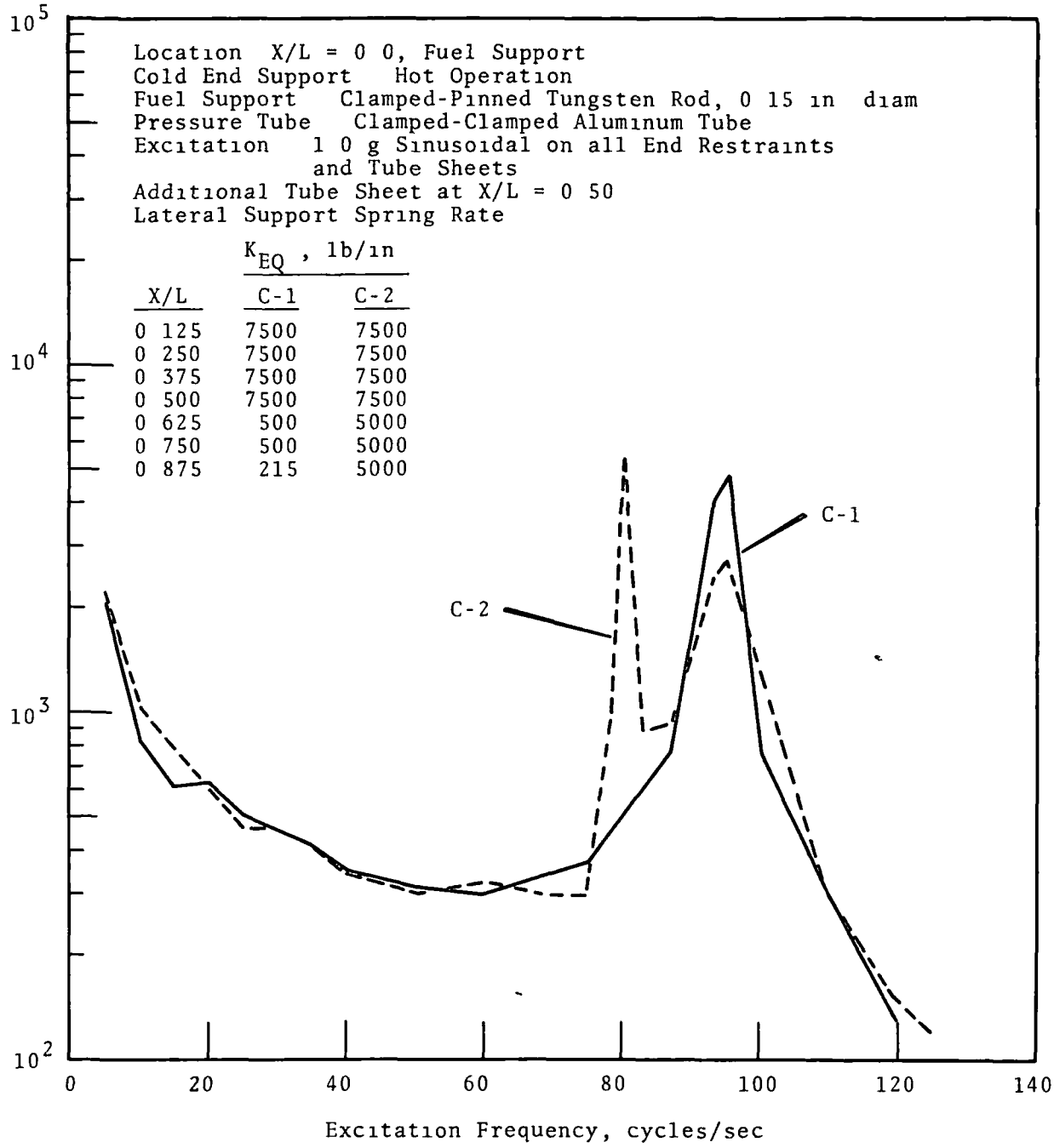

FIGURE 5 12 Bending Stress Versus Frequency

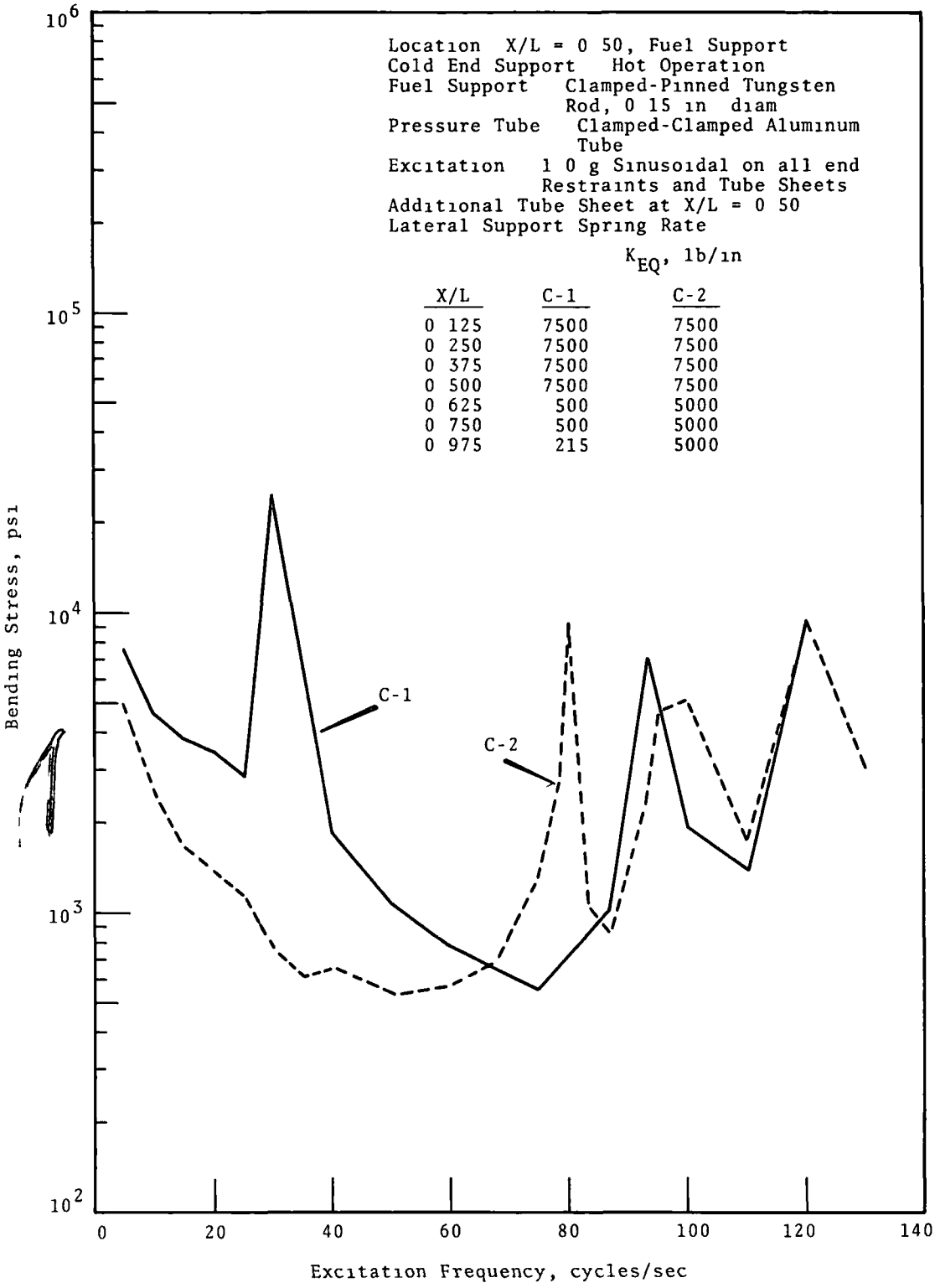
Location X/L = 0 50, Fuel Support
Cold End Support Hot Operation
Fuel Support Clamped-Pinned Tungsten Rod, 0 15 in diam
Pressure Tube Clamped-Clamped Aluminum Tube
Excitation 1 0 g Sinusoidal on all end Restraints and Tube Sheets
Additional Tube Sheet at X/L = 0 50
Lateral Support Spring Rate
K_{EQ}, lb/in
X/L C-1 C-2
0 125 7500 7500
0 250 7500 7500
0 375 7500 7500
0 500 7500 7500
0 625 500 5000
0 750 500 5000
0 975 215 5000
Bending Stress, psi
10^6
10^5
10^4
10^3
10^2
C-1
C-2
0 20 40 60 80 100 120 140
Excitation Frequency, cycles/sec

FIGURE 5 13 Bending Stress Versus Frequency

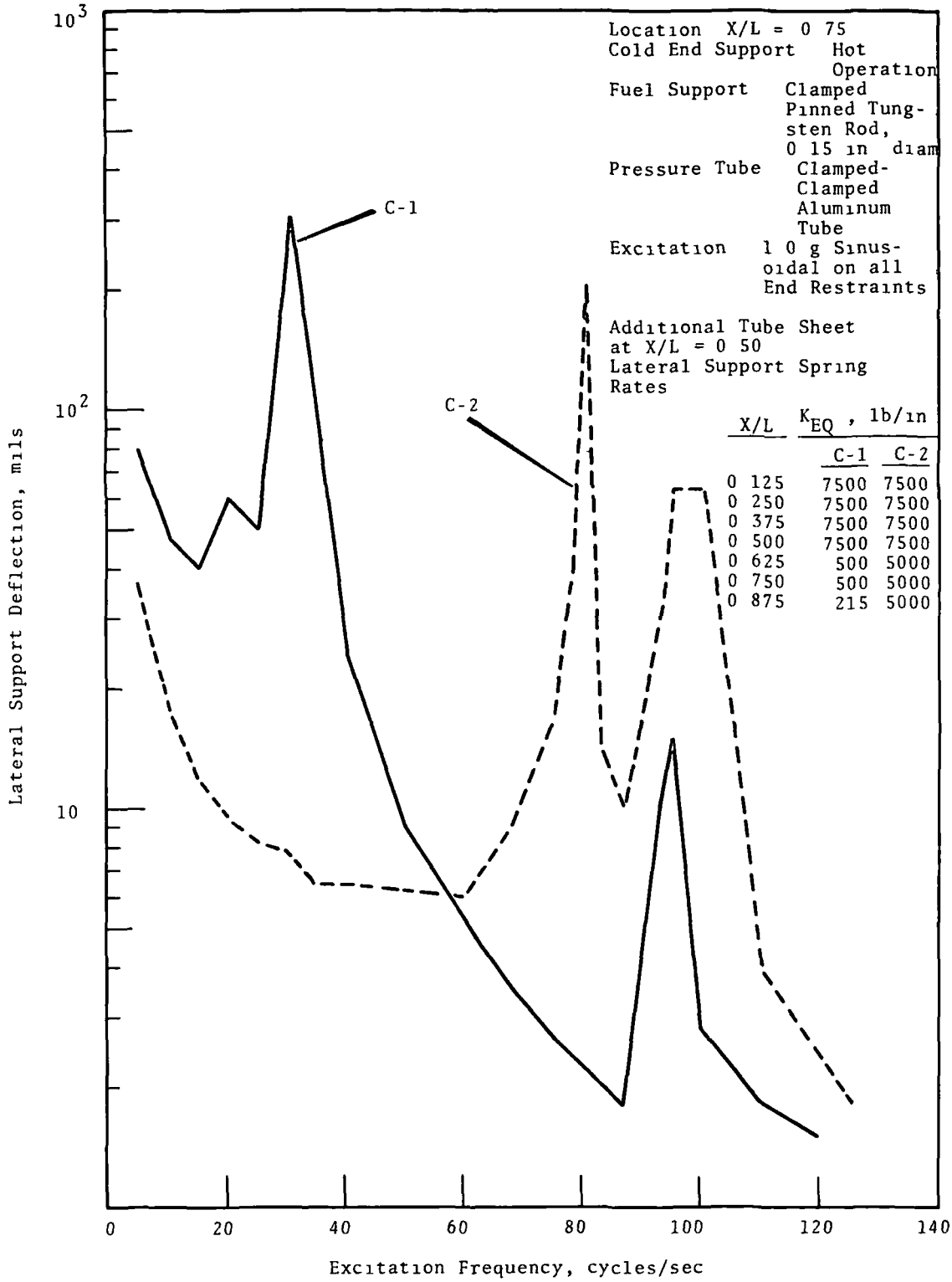
Location X/L = 0 75
Cold End Support Hot Operation
Fuel Support Clamped Pinned Tungsten Rod, 0 15 in diam
Pressure Tube Clamped-Clamped Aluminum Tube
Excitation 1 0 g Sinusoidal on all End Restraints
Additional Tube Sheet at X/L = 0 50
Lateral Support Spring Rates
X/L
K_EQ , lb/in
C-1 C-2
0 125 7500 7500
0 250 7500 7500
0 375 7500 7500
0 500 7500 7500
0 625 500 5000
0 750 500 5000
0 875 215 5000
C-1
C-2
10^3
10^2
10
Lateral Support Deflection, mils
0 20 40 60 80 100 120 140
Excitation Frequency, cycles/sec

FIGURE 5 14 Lateral Support Deflection Versus Frequency

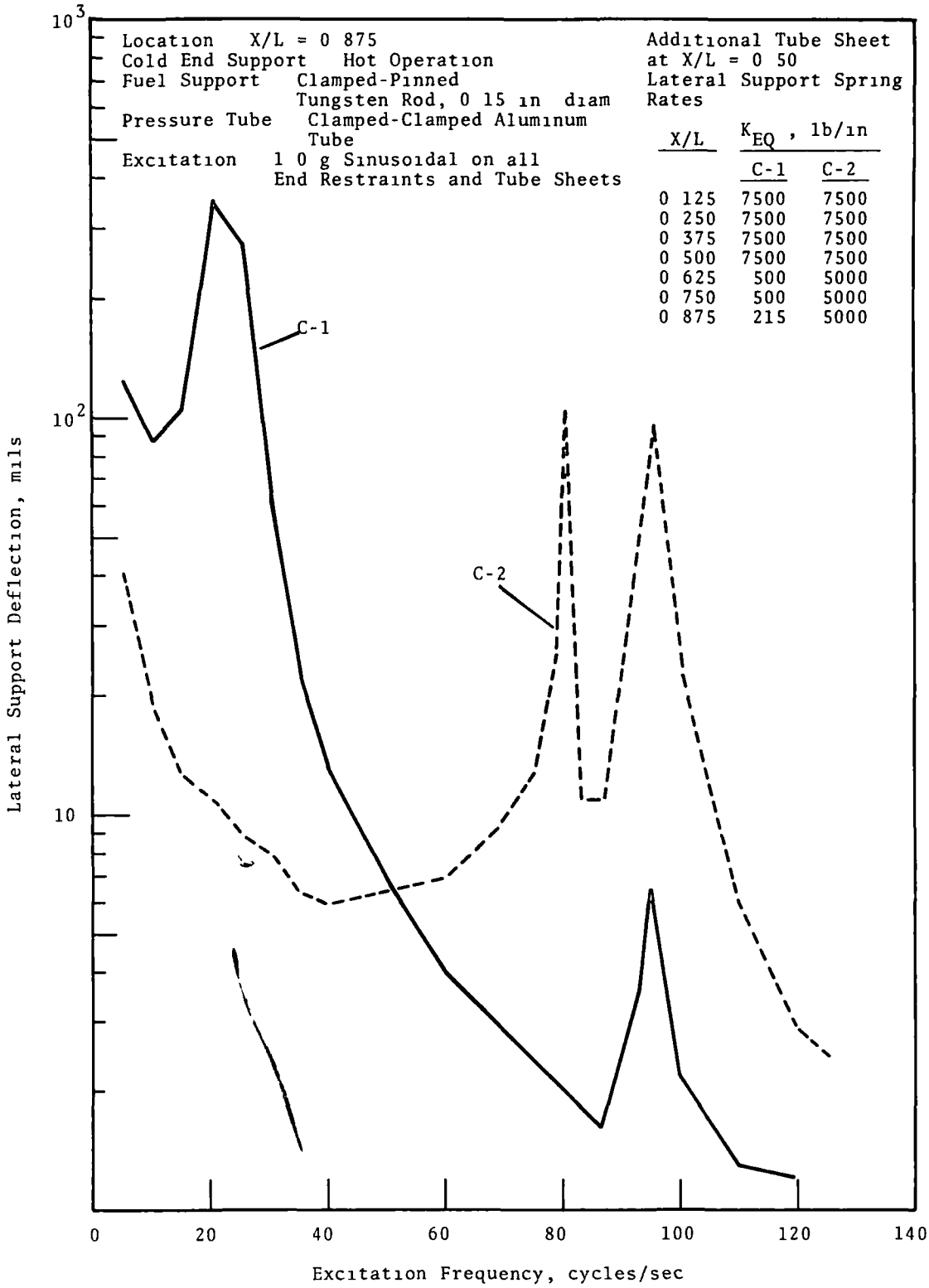

FIGURE 5 15 Lateral Support Deflection Versus Frequency

CONFIDENTIAL

not evident at the clamp of the fuel support member Lateral support deflections at the hot end are prohibitive at 20 and 30 cycles/sec The deviation made in attempting to cause the fundamental of the system to occur at a frequency lower than the anticipated excitation is considerable Additional modifications to the tie rod concept that would result in significant response attenuation are not immediately evident, therefore, this concept was considered impracticable

Bending stresses and lateral support deflections of all conservative models considered were excessive and prohibitive Attempts to force the tubes to oscillate in phase and of equal amplitude were not successful The attempt to lower the fundamental frequency and bending stresses did not achieve the desired degree of attenuation The remaining means of reducing the dynamic parameters is by providing sufficient energy dissipation in the lateral supports

Damping in the lateral supports would be principally due to frictional forces or coulomb damping This is, by definition, proportional to the difference in relative deflection between two members and opposing the velocity change The simulation of coulomb damping in the equivalent lateral supports would require more analog components than were available Therefore, viscous damping was considered, which would provide information regarding the magnitude of damping required to result in reasonable stress levels Parametrically, fractions of critical damping of 20 and 50% based on support tube-fuel mass were considered with the original cold end support model

The bending stresses at resonance are shown in Figure 5 16 to decrease exponentially with fraction of critical damping These data indicate that the system must be nearly critically

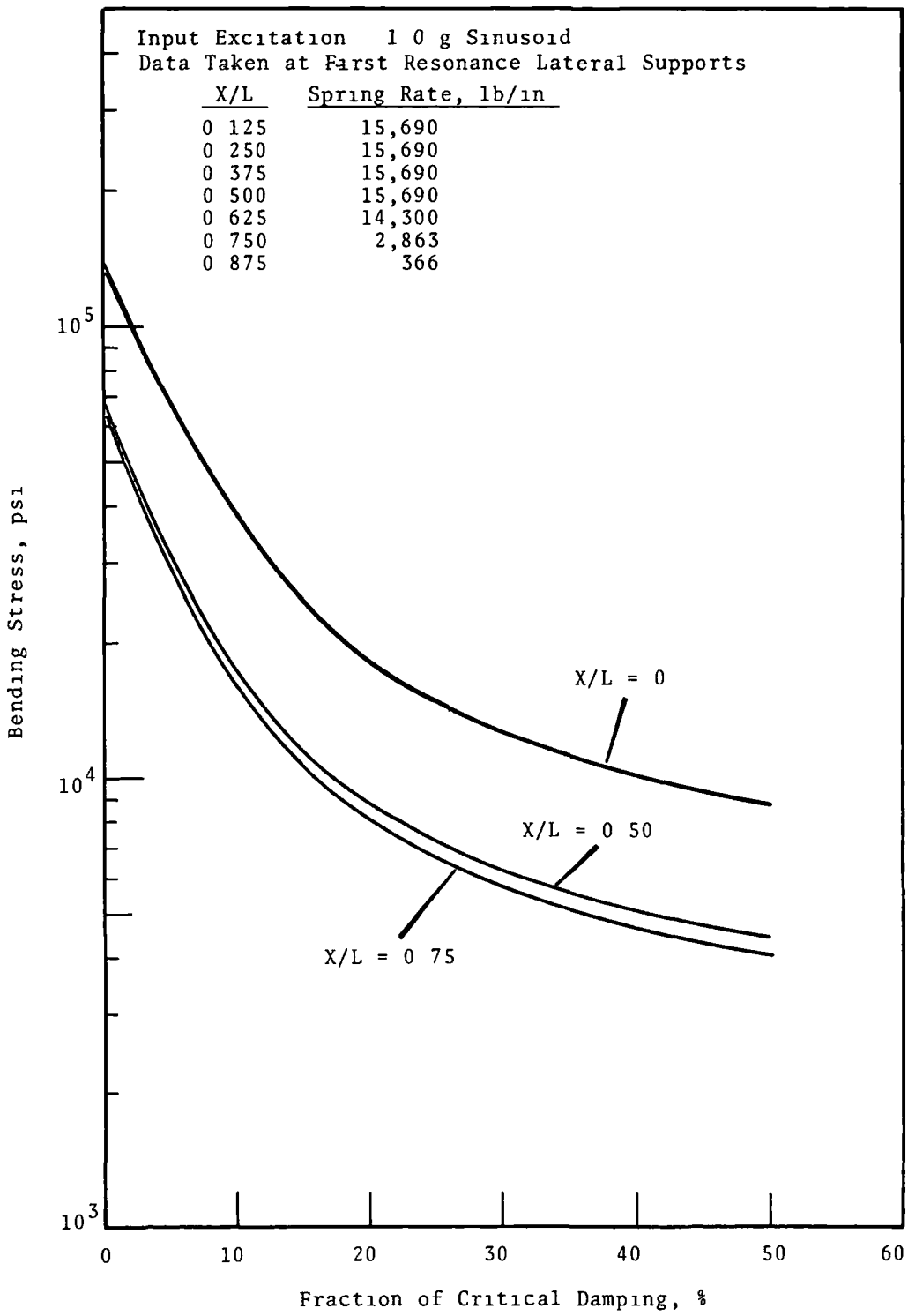

FIGURE 5 16 Effect of Lateral Support Damping (Inlet End Support Model with Clamped-Pinned Boundary Conditions)

damped to result in acceptable bending stresses Minimum lateral support deflections at resonance of 5 25 mils and 4 mils at $(X/L)_V$ of 0 75 and $(X/L)_V$ of 0 875, respectively, as shown in Figure 5 17 are still excessive for the exit end

Analysis of the cold end support model under simulated cold or launch conditions was completed This run assumed the same physical lateral supports as in the last hot model study Spring rates for the cold model increased as Young's modulus increased The spring rate was, however, limited to 50,000 lb/in by initial amplitude scaling The analog simulation was not rescaled as 1) decreasing model voltages would degrade the simulation, 2) converting to high gain equipment with external 1 0% components would degrade the model As the resonant bending stress plotted versus lateral support spring rate is nearly zero for a constant spring rate of 10,000 lb/in , the error introduced was believed to be negligible Lateral support damping of 10% of critical was assumed

Resonance was calculated to be 57 cycles/sec and the resonant data extrapolated from that obtained at 55 and 59 cycles/sec Data were obtained to 150 cycles/sec which is beyond the first major resonance Support tube resonant bending stress at the clamp was indicated to be $4\ 5 \times 10^4$ psi while that an $(X/L)_V$ of 0 50 was $2\ 4 \times 10^4$ psi

Comparison of response characteristics for simulated hot and cold operating conditions (nodal data summarized in Table 5 3) indicate that the combined increased stiffness of the support tube and lateral supports reduces bending stresses and lateral support deflections to tolerable magnitudes Resonant bending stress at the cold end clamp was reduced from $1\ 35 \times 10^5$ to $4\ 5 \times 10^4$ psi for the hot and cold case respectively as shown in Figure 5 18

NASA-CR-72031

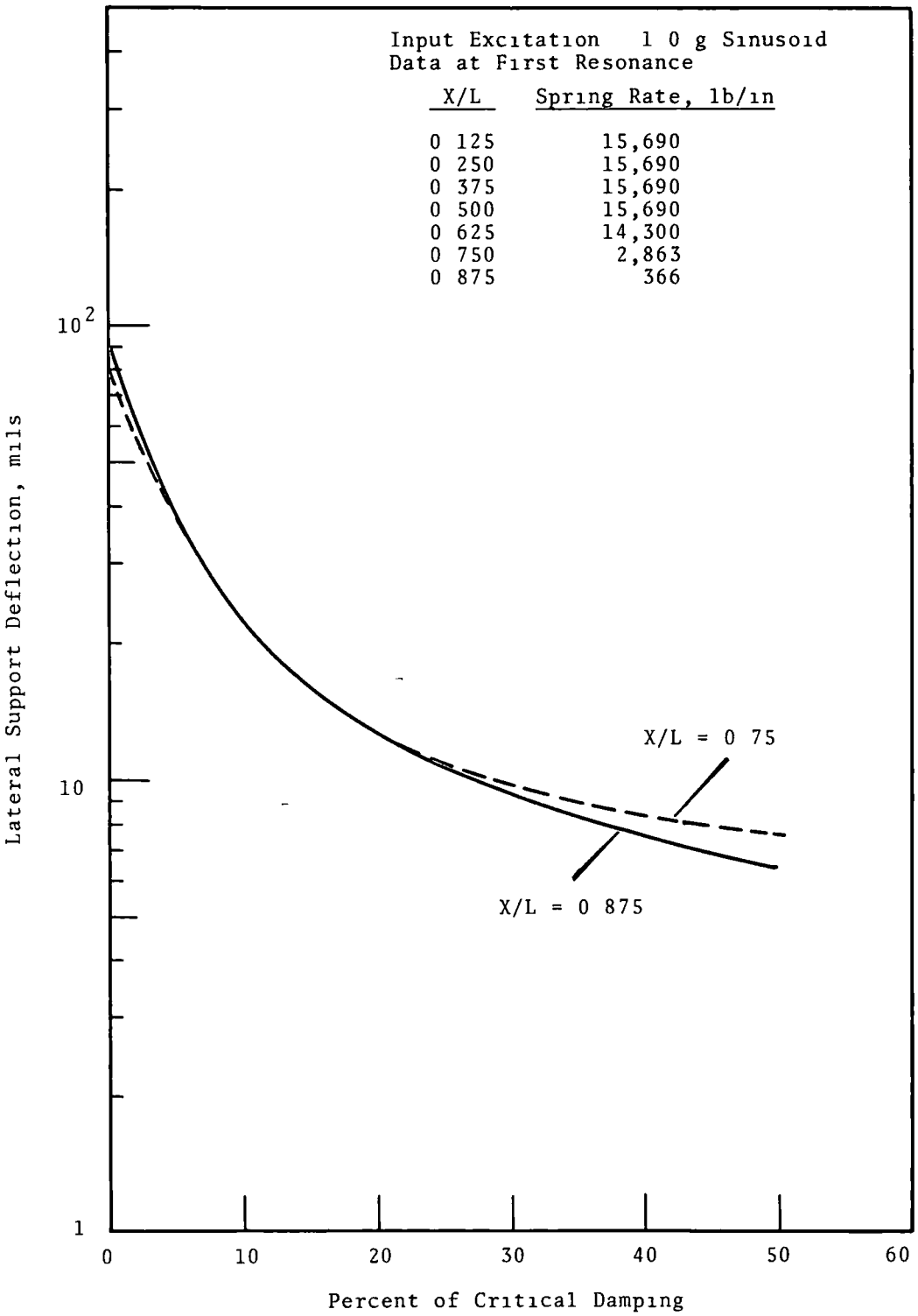

FIGURE 5 17 Effect of Lateral Support Damping (Cold End Support Model with Clamped-Pinned Boundary Conditions)

CONFIDENTIAL

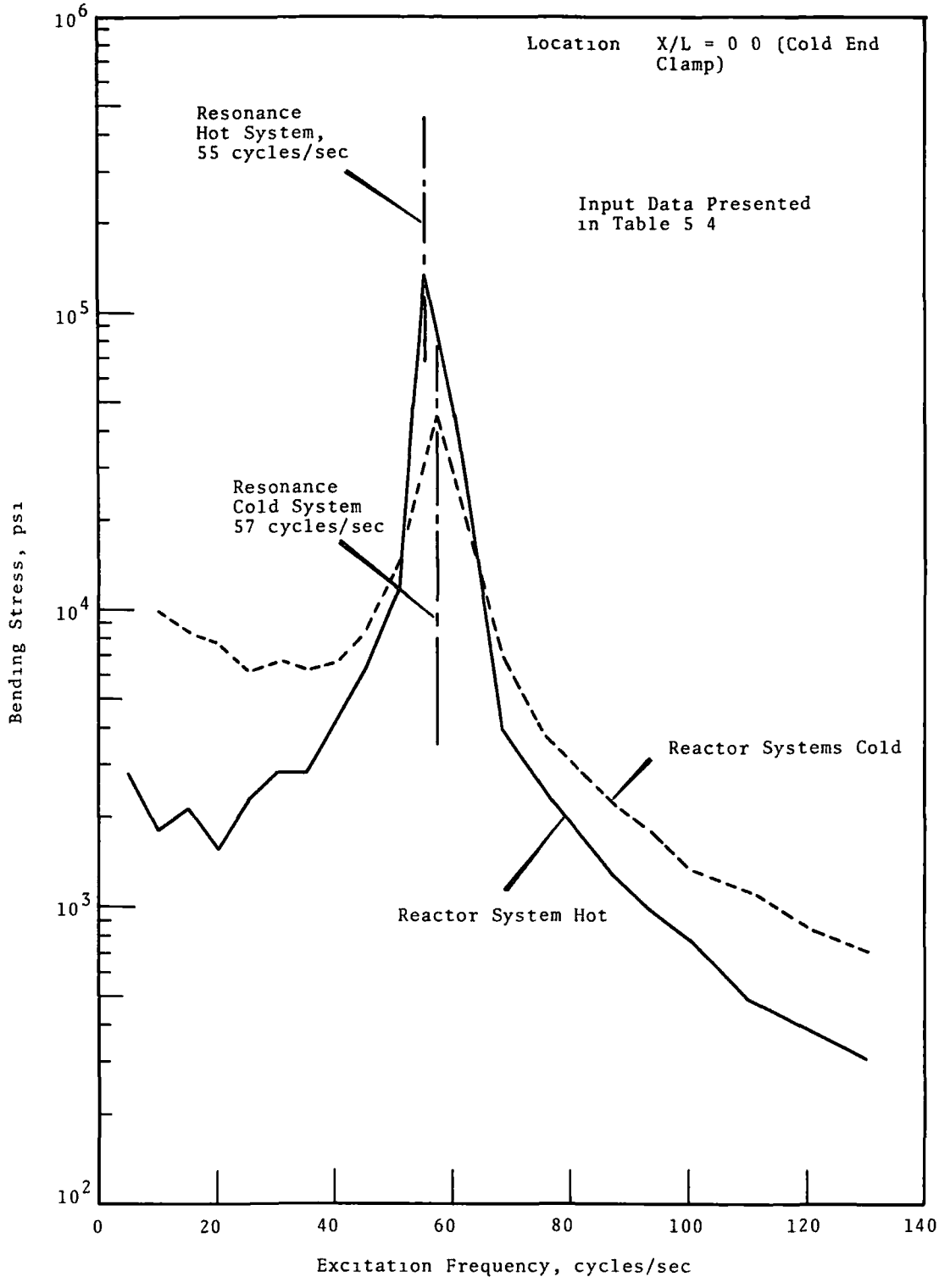

FIGURE 5 18 Support Tube Bending Stress Comparison of Hot and Cold Operation

Bending stresses at $(X/L)_V$ = 0 50 of 5 6 x 10^4 and 2 5 x 10^4 psi were recorded for the hot and cold cases respectively as shown in Figure 5 19 Lateral support deflections at $(X/L)_V$ of 0 75 were reduced from 105 to 24 mils for the hot and cold case respectively (Figure 5 20) while that at $(X/L)_V$ of 0 875 was reduced from 101 to 26 mils as shown in Figure 5 21

The apparent resonance factor, Q, for the hot case is observed to be greater than that for the cold case As the fraction of critical damping was identical for both runs this effect must result from decreased stiffness or increased nodal resistance to spring rate relationships This effect is predictable from a simple nonconservative two degrees of freedom forced model which indicates that the lateral support deflection will be larger at frequencies less than and greater than the fundamental resonance with an increase in stiffness Lateral support deflection of the simple model at resonance when considered as a plot versus stiffness is not as clearly defined, however, preliminary analyses indicate that the deflection should be smaller with increased stiffness

Bending stresses and lateral support deflections of the cold end support system appear acceptable for cold operation The design, however, does not permit system excitation of 1 0 g when subjected to design thermal operating conditions

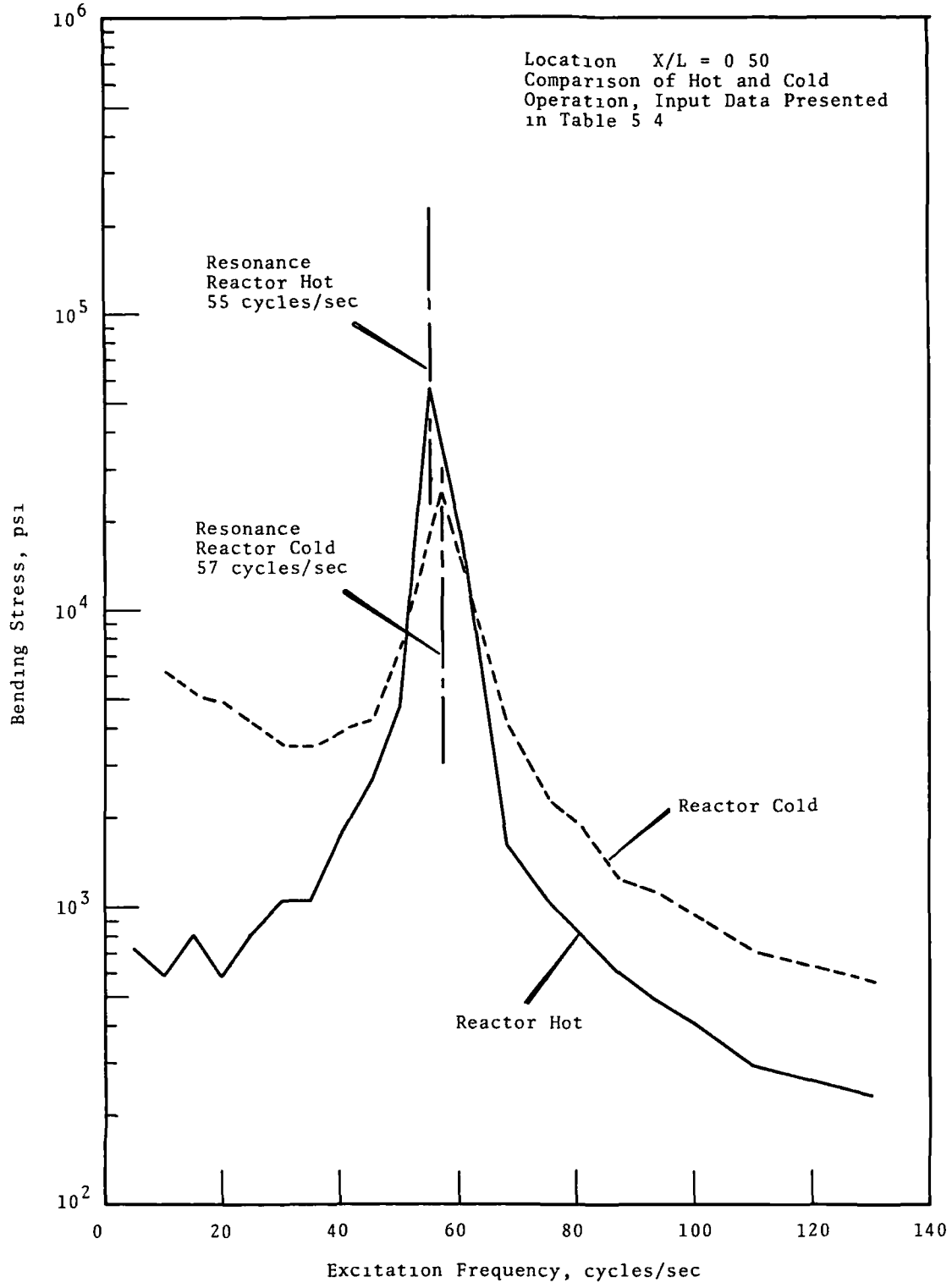

FIGURE 5 19 *Support Tube Bending Stress*

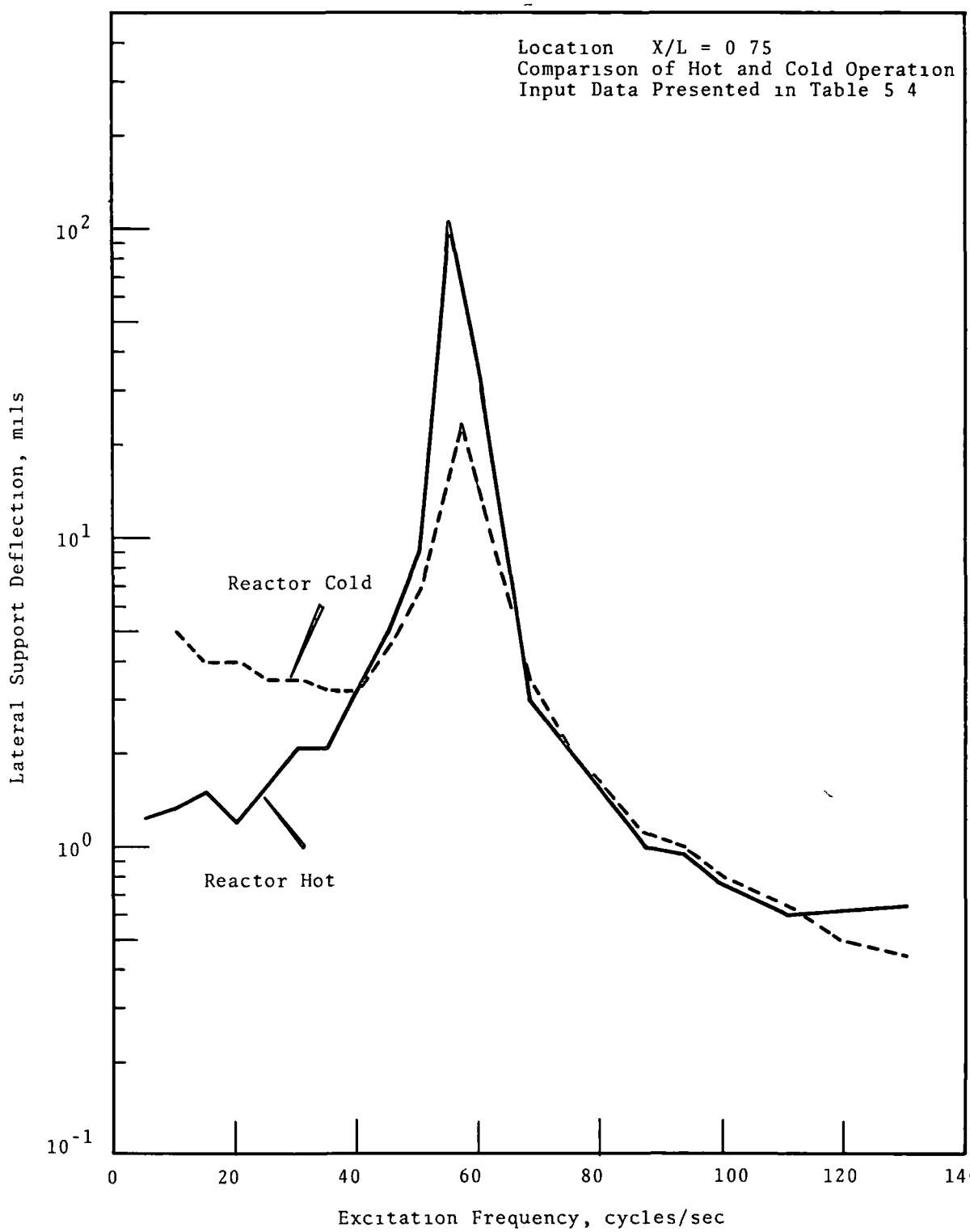

FIGURE 5 20 Lateral Support Deflection

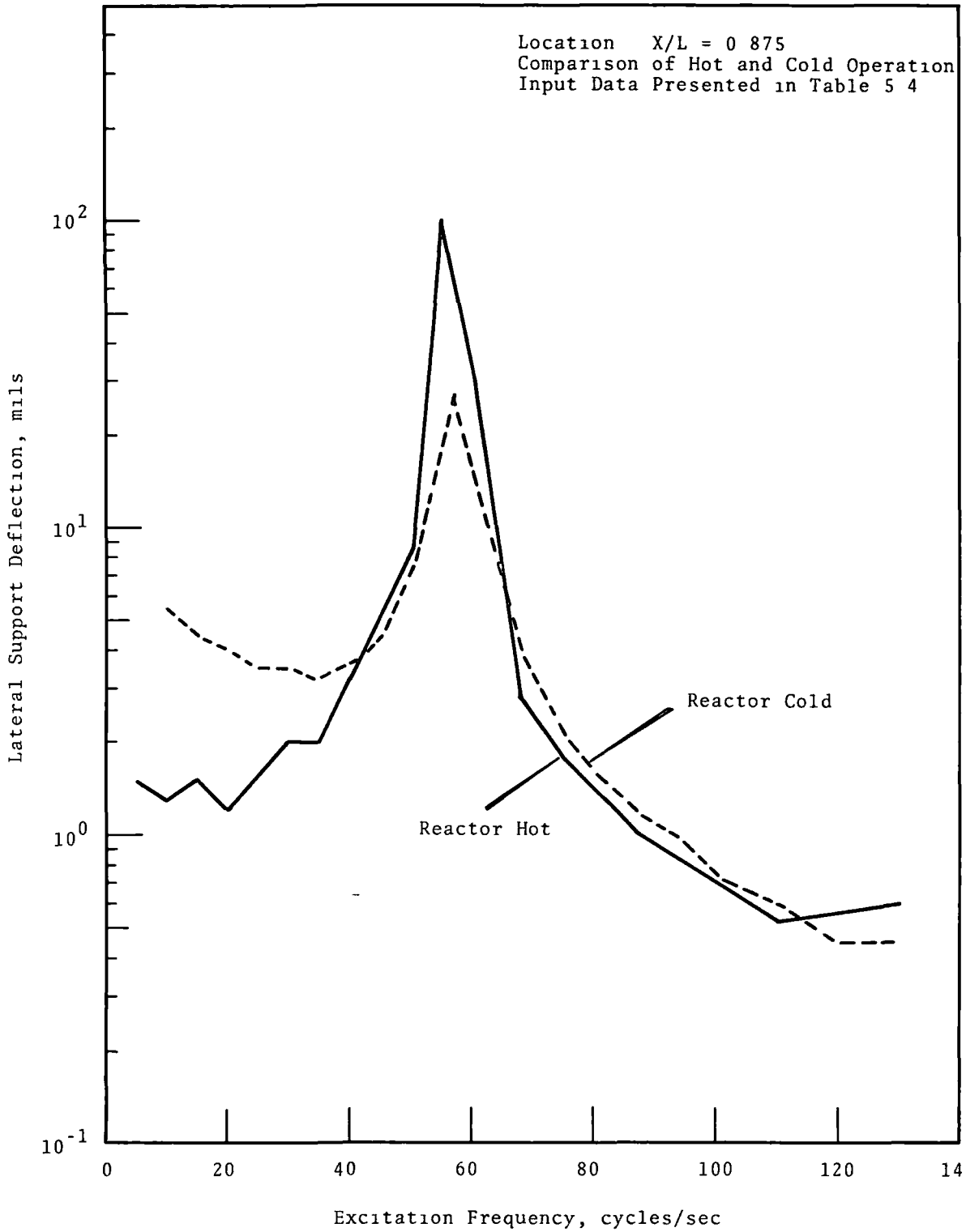

FIGURE 5 21 Lateral Support Deflection

TABLE 5 4 ANALOG SIMULATION PARAMETERS

				Operating Condition							
				Hot				Cold			
						Damping lb sec/in				Damping, lb-sec/in	
$(X/L)_V$	Node	Nodal Mass lb sec/in ^{2}	Moment of Inertia in ^{4}	E lb/in x 10^6	Spring Rate, K lb/in	C_C	C	E lb/in	Spring Rate, K lb/in	C_C	C
1 000	1	8 0773(10^4)	3 488(10^1)	10 0	NA	NA	NA	10 0	NA	NA	NA
0 875	2				1,016	1 811	0 1811		1,923	2 49	0 249
0 750	3				1,058	1 85	0 1850		1,923	2 49	0 249
0 625	4				8 766	5 32	0 532		14 290	6 79	0 679
0 500	5				42 319	11 68	1 168		50 000	12 69	1 269
0 375	6				44,792	12 05	1 205		50,000	12 70	1 270
0 250	7				50 000	12 70	1 270		50,000	12 70	1 270
0 125	8				50 000	13 81	1 381		50,000	12 70	1 270
0	9	8 0773(10	3 488(10^1)	10 0	NA	NA	NA	10 0	NA	NA	NA
1 000	10	0 01443	9 02(10^2)	36 8				58 4			
0 875	11			38 7							
0 750	12			42 1							
0 625	13			45 6							
0 500	14			48 6							
0 375	15			51 4							
0 250	16	0 01443		53 7							
0 125	17	0 003048		56 1							
0	18	0 002402	9 02(10^2)	58 7				58 4			

CONFIDENTIAL

CONFIDENTIAL

5 42

NASA-CR-72031

5 3 References

1 A F Lietzke "Description of Reference Nuclear Rocket Reactor Concept," NASA Lewis Research Center, 1965

2 R D Mindlin, F W Stubner, and H L Cooper "Response of Damped Elastic Systems to Transient Distrubances," Proc Soc for Experimental Stress Analysis, vol V, no II pp 69-87 edited by C Lipson and W M Murray Addison-Wesley Press Inc , Cambridge, Mass , 1948

3 A L Kimball "Vibration Problems, Part V," Applied Mechanics Design Data and Methods, ASME, N Y 1953 p 160

4 K Sewaza "On the Decay of Waves in Visco-Elastic Solid Bodies," Bulletin of the Earthquake Research Institute, Tokyo Imperial University, vol III, p 50 September 1927

5 W F Stokey "Vibration of Systems Having Distributed Mass and Elasticity," Shock and Vibration Handbook, vol 1, chapter 7, edited by C M Harris and C E Crede, McGraw-Hill Book Company, Inc , N Y , 1961

6 K M Entwhistle "The Damping Capacity of Metals," The Physical Examination of Metals, p 500, edited by B Chalmers and A G Quarrell, Arnold (Publishers) Limited, London 1960

6 0 HOT END SUPPORT DESIGN

The tungsten support tube may be eliminated by supporting the fuel stages with a structure located at the hot end of the fuel column However, the severe temperatures at this location introduce problems in developing a satisfactory method of attaching the structure to the aluminum components which must be maintained at relatively low temperatures

The function of the support device is to transmit the axial fuel column loads to the aluminum pressure tube The thermal analysis was directed toward development of a support structure which would not produce excessive pressure tube and tube sheet temperatures.

6 1 METHOD OF THERMAL ANALYSIS

Thermal analysis of the hot end support models was conducted in essentially the same manner used to analyze a lateral support device A model geometry approximating an actual device was defined, appropriate boundary conditions were established and necessary material properties were specified The model was divided into an adequate number of heat conduction and radiation nodes for application of the computerized numerical technique All models considered the water temperature in the plenum to be 250 °F with propellant at 4040 °F The hydrogen gas between the radiation shield and pressure tube or tube sheet was assumed stagnant Material thermal properties were the same as those used in the lateral support analysis except for the addition of the necessary stainless steel properties listed below

$$K = 12 \text{ Btu/(hr)(ft}^2\text{)(°F)}$$

$$E = 0\ 53$$

A gamma heating value, appropriate to an axial position, X/L = 1 0, was assumed This value may be slightly high for some portions of the hardware as a result of gamma attenuation by other

parts of the structure The gamma heat rate for ceramic insulation and stainless steel was estimated from a material density ratio and application of Figure 3 1

6 2 PRELIMINARY SUPPORT MODELS

Figure 6 1 illustrates the first support model analyzed Contact coefficients between conducting surfaces were 35,000 Btu/(hr)(ft^2)(°F) and the estimated coolant film coefficient and the plenum film coefficient were 2200 and 5600 Btu/(hr)(ft^2)(°F), respectively The film coefficient used for the moderator is the same as used in the lateral support analysis and is probably significantly overestimated except near the exit of the flow splitter

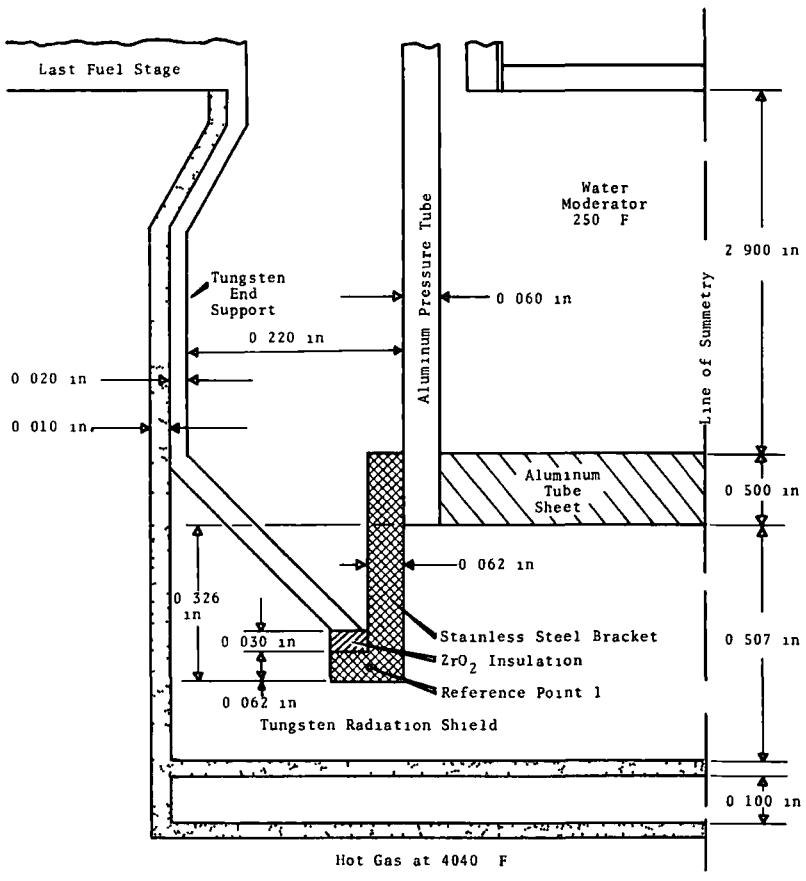

FIGURE 6 1 Heat Transfer Model for Hot End Support Analysis

CONFIDENTIAL

Computer calculations showed that the temperatures in the support structure hardware and aluminum tube sheet were severe, being on the order of 2100 °F at Reference Point 1 (Figure 6 1) and about 700 °F in the tube sheet

These results indicated that the general position of the stainless steel bracket was unacceptable A substantial improvement could be made by locating the bracket at a location where the film coefficient is not severely degraded A location near the upper portion of the plenum would be well-suited since at that point the film coefficient would be quite high and if need be, the flow splitter could be extended to maintain the moderator film coefficient

6 2 1 Hanger Support

Incorporation of the improvements indicated by the above investigation led to the hanger model shown in Figure 6 2 The primary functions of this model were to explore a different placement of the support hardware and to study the effect of an extended contact area between the support hardware and the pressure tube A 30-mil stainless steel liner locates the support structure axially, and is insulated from the hanger with 10 mils of ZrO_2 Both tungsten and stainless steel hanger materials were employed in the analysis, the insulating pad between the support leg and hanger was assumed to be a 50 mil thickness of ZrO_2

For heat transfer calculations, the model shown in Figure 6 2 was broken in two parts 1) the support device and adjacent structure, and 2) the bottom tube sheet and radiation shield Figure 6 3 shows the support hardware model which is considered to be thermally isolated from the bottom tube sheet Subsequent calculations showed this assumption to be reasonable since the axial temperature distribution an inch toward the reactor exit from the hanger hardware was essentially flat, indicating insignificant thermal communication between the two

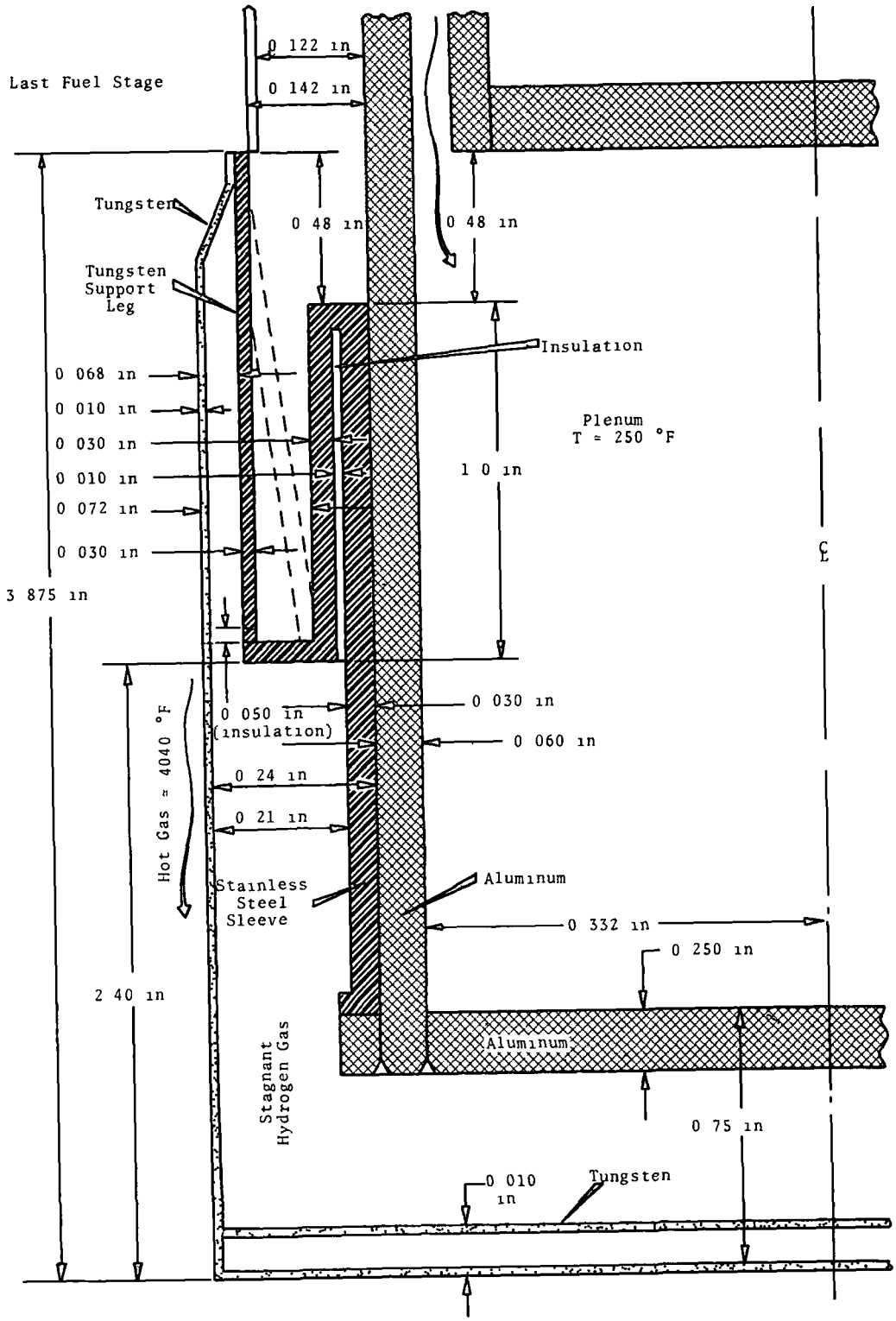

FIGURE 6 2 Hot End Support Model

The same general model configuration was used in all study cases investigated A minor model variation was an extension of the hanger as indicated by the dashed lines shown in Figure 6 3 Computations considered variations in the tungsten support leg thickness, hanger length, hanger material, and contact coefficients, h_2, h_3, and h_4 Table 6 1 summarizes the results which indicate that maximum temperatures in a stainless steel hanger will be somewhat higher than those obtained with a tungsten hanger The maximum temperature in the pressure tube will be slightly lower if a stainless steel hanger is used Higher contact coefficients between the structural members and a thicker support leg will cause higher pressure tube temperature The hanger length, L, has little effect on the maximum pressure tube temperature, at least over the range 0 7 in $\leq$ L $\leq$ 1 3 in Comparison of cases B-2 and E-3 (Table 6 1), Reference Point No 2 verifies this conclusion

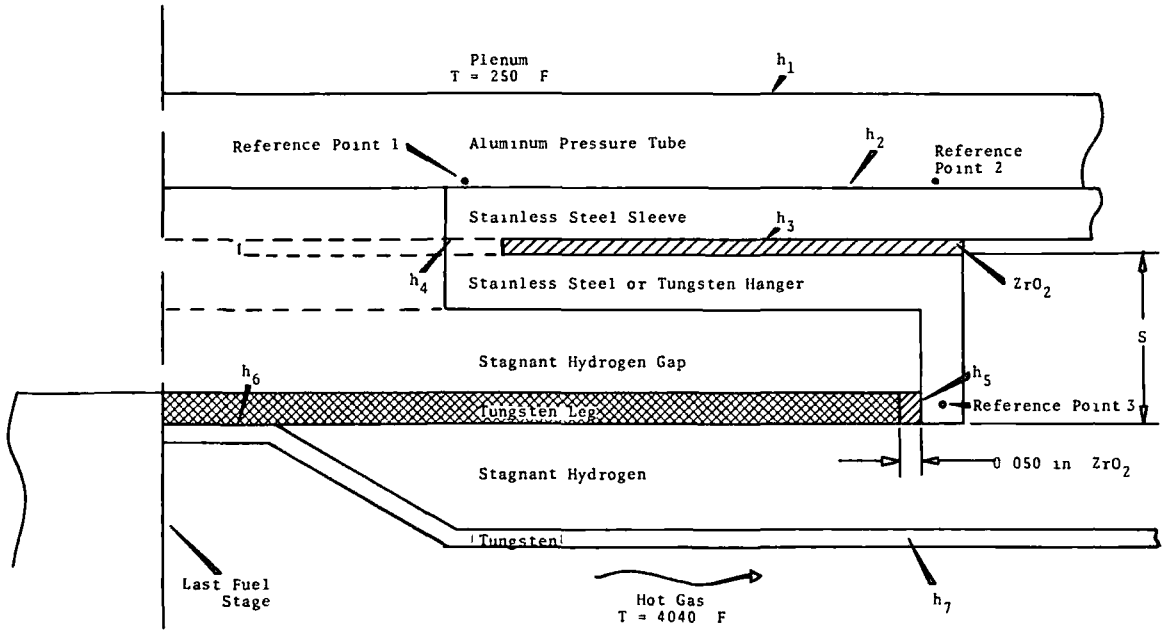

h_1 = 5600 and 2300 Btu/(hr)(ft2)(F)
$h_2 = h_3 = h_4 = h_5$ = 5000 and 35 000 Btu/(hr)(ft^2)(F)
h_6 = 4000 Btu/(hr)(ft^2)(F)
h_7 = 2200 Btu/(hr)(ft^2)(F)

FIGURE 6 3 Heat Transfer Model for Exit End Support

TABLE 6 1 SUMMARY OF HOT END SUPPORT HEAT TRANSFER CALCULATIONS--HANGER SUPPORT

Case No	L, in	t, in	Hanger Material	h_2, h_3, h_4, Btu/(hr)(ft^2)(°F)	Temperature, °F Reference Point No 1	Reference Point No 2	Reference Point No 3
A-1	1 0	0 040	W	5,000	330	345	1325
A-2	1 0	0 040	W	35,000	331	348	1320
A-3	1 0	0 040	SST	5,000	315	335	1845
A-4	1 0	0 040	SST	35,000	320	340	1730
B-1	1 0	0 030	W	5,000	310	335	1200
B-2	1 0	0 030	SST	5,000	314	331	1653
C-1	1 3	0 040	W	5,000	330	345	1320
C-2	1 3	0 040	W	35,000	326	346	1318
C-3	1 3	0 040	SST	5,000	317	335	1835
C-4	1 3	0 040	SST	35,000	318	341	1720
D-1	0 7	0 040	W	5,000	330	348	1325
D-2	0 7	0 040	W	35,000	335	350	1320
D-3	0 7	0 040	SST	5,000	315	340	1850
D-4	0 7	0 040	SST	35,000	320	345	1940
E-1*	1 0	0 030	W	5,000	332	345	1220
E-2*	1 0	0 030	W	35,000	350	348	1195
E-3*	1 0	0 030	SST	5,000	300	330	1660
E-4*	1 0	0 030	SST	35,000	302	335	1665
F-1+	1 0	0 030	SST	5,000	380	412	1740

* *Extended Hanger (Dotted lines in Figure 11)*

\+ h_1 = *2300 Btu/(hr)(ft^2)(°F)*

Comparison of cases B-1 and F-1, Table 6 1, illustrates the importance of a good plenum film coefficient A film coefficient, h_1, of 5600 Btu/(hr)(ft^2)(°F) could be obtained near the pressure tube--support device contact location by simply extending the flow splitter

The hanger type support design seems satisfactory from a thermal standpoint, but fabrication of this device will present a problem

6 2 2 Bracket Support

The third general configuration of hot end support structure is illustrated in Figure 6 4 This structure is called a

bracket support to distinguish it from the hanger support The bracket support transmits the load to the stainless steel sleeve through a cylindrical bracket loaded in compression. The bracket is insulated from the stainless steel sleeve by 10 mils of ZrO_2 and insulated from the tungsten support leg by a ZrO_2 pad

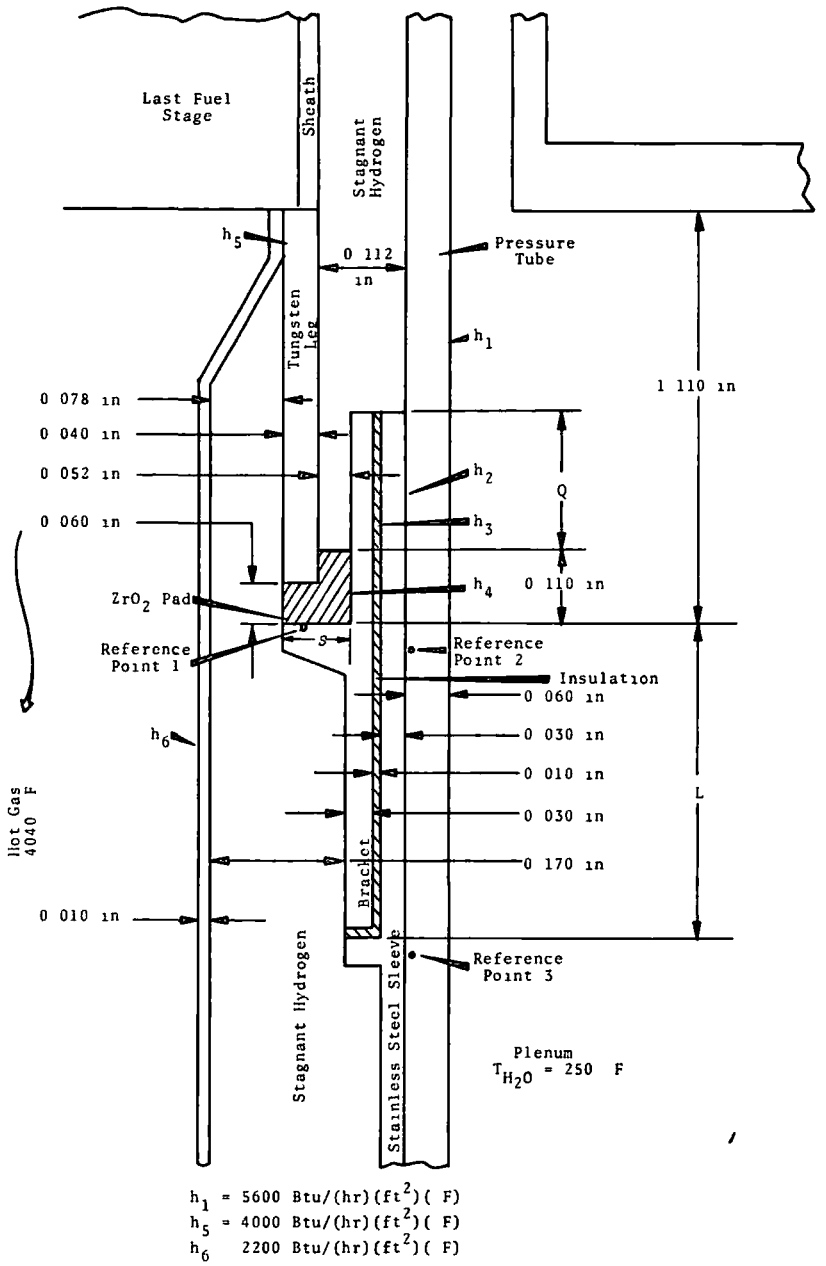

FIGURE 6 4 Bottom Support Heat Transfer Model

Three different geometric variations of this model were analyzed Two of the variations involved changing the length L in Figure 6 4 Lengths of 1 12 and 2 12 in were investigated The third variation eliminated part of the bracket extending above the ZrO_2 insulating pad This portion of the bracket is designated dimension "Q" on Figure 6 4 Results were obtained for two different values of the contact coefficients, h_2, h_3, and h_4, and for two different bracket materials, stainless steel and tungsten A summary of the results which show the temperatures at Reference Points 1, 2, and 3 (on Figure 6 4) is given in Table 6 2

TABLE 6 2 SUMMARY OF HOT END SUPPORT HEAT TRANSFER COMPUTATION (BRACKET SUPPORT)

Case No	L, in	Q, in	Bracket Material	h_2, h_3, h_4, h_5, Btu/(hr)(ft^2)(°F)	Reference Point No 1	Reference Point No 2	Reference Point No 3
A-1	1 12	0 50	SST	5,000	1340	342	325
A-2	1 12	0 50	SST	35,000	1195	347	335
A-3	1 12	0 50	W	5,000	1100	350	335
A-4	1 12	0 50	W	35,000	925	360	335
B-1	1 12	--	SST	5,000	1350	340	335
B-2	1 12	--	SST	35,000	1190	347	335
B-3	1 12	--	W	5,000	1100	350	335
B-4	1 12	--	W	35,000	925	358	338
C-1	2 12	--	SST	5,000	1340	340	335
C-2	2 12	--	SST	35,000	1190	347	335
C-3	2 12	--	W	5,000	1105	350	335
C-4	2 12	--	W	35,000	925	360	335
D-1	2 12	0 50	SST	5,000	1345	340	335
D-2	2 12	0 50	SST	35,000	1190	345	335
D-3	2 12	0 50	W	5,000	1105	350	335
D-4	2 12	0 50	W	35,000	925	355	335

The temperatures shown in Table 6 2 indicate that extending the length of the bracket from 1 12 to 2 12 in and/or eliminating structure above the insulating pad have only a minor effect

on the temperature at the three designated reference points The use of a tungsten bracket will cause lower temperatures at Reference Point 1 and higher temperatures at Reference Points 2 and 3 than obtained with a similar stainless steel bracket A similar effect is noted as the contact coefficients, h_2, h_3, and h_4, are increased from 5000 to 35,000 Btu/(hr)(ft^2)(°F)

To indicate the temperature distribution in the support hardware, Figures 6 5 through 6 8 illustrate results for cases A-1, A-3, B-1, and C-1 These results are typical of all the cases investigated and indicate the effect of varying the dimensions L and Q and the effect of using different bracket materials

6 3 MODEL COMPARISONS

Both the hanger and bracket models result in reasonable average temperature and temperature distributions in the aluminum pressure tube Fabrication problems may, however, show the hanger model less attractive than the bracket model The problem with the bracket model of Figure 6 4 is the questionable mechanical integrity of the insulating pad between the bracket and support leg

If the actual design of a hot end support is similar to the bracket or hanger heat transfer models, a material other than ZrO_2 may be used for insulating the bracket from the sleeve In all cases evaluated the maximum temperature of this insulation is less than 800 to 900 °F A broad selection of insulations are available that would be suitable both from a thermal and mechanical design standpoint

The temperature drop across the insulation pad between the tungsten support leg and the bracket may be as great as 1800 °F Temperatures are 2800 to 3000 °F maximum, and few insulating materials will remain mechanically sound under the required normal operating conditions The extreme temperature gradients

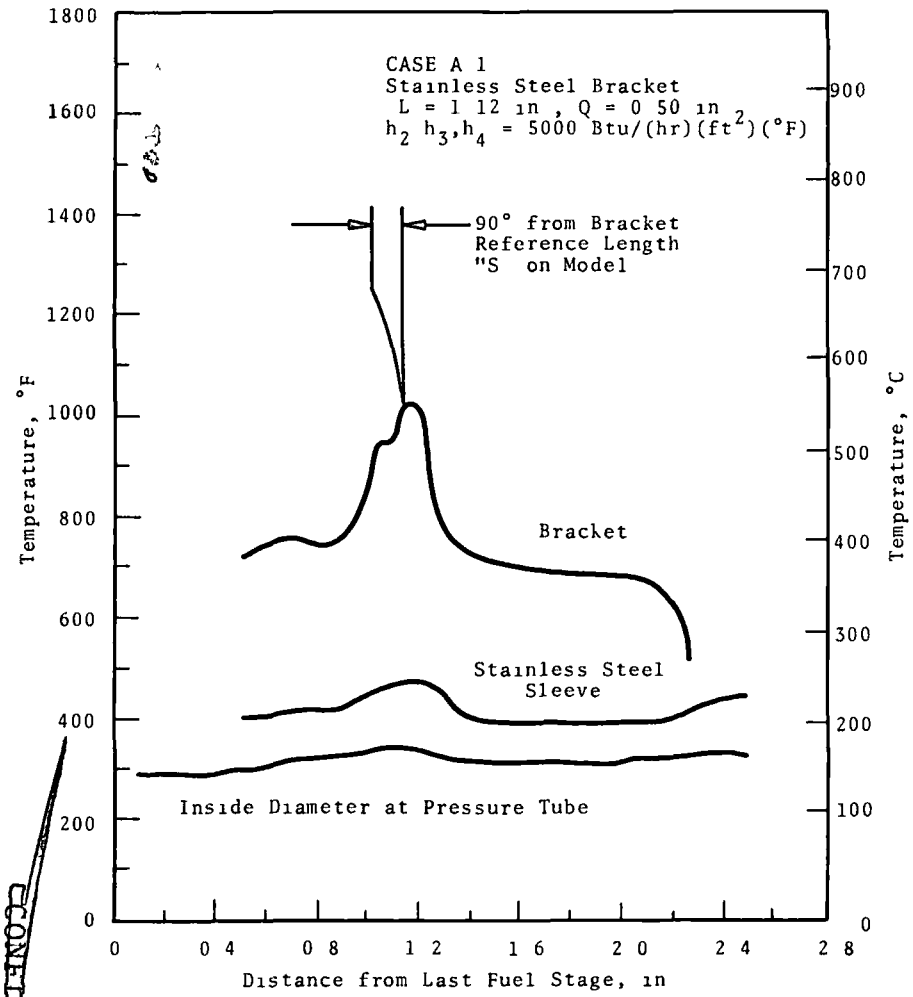

FIGURE 6 5 Temperature Distributions (Hot End Support Components) Versus Distance from Last Fuel Stage

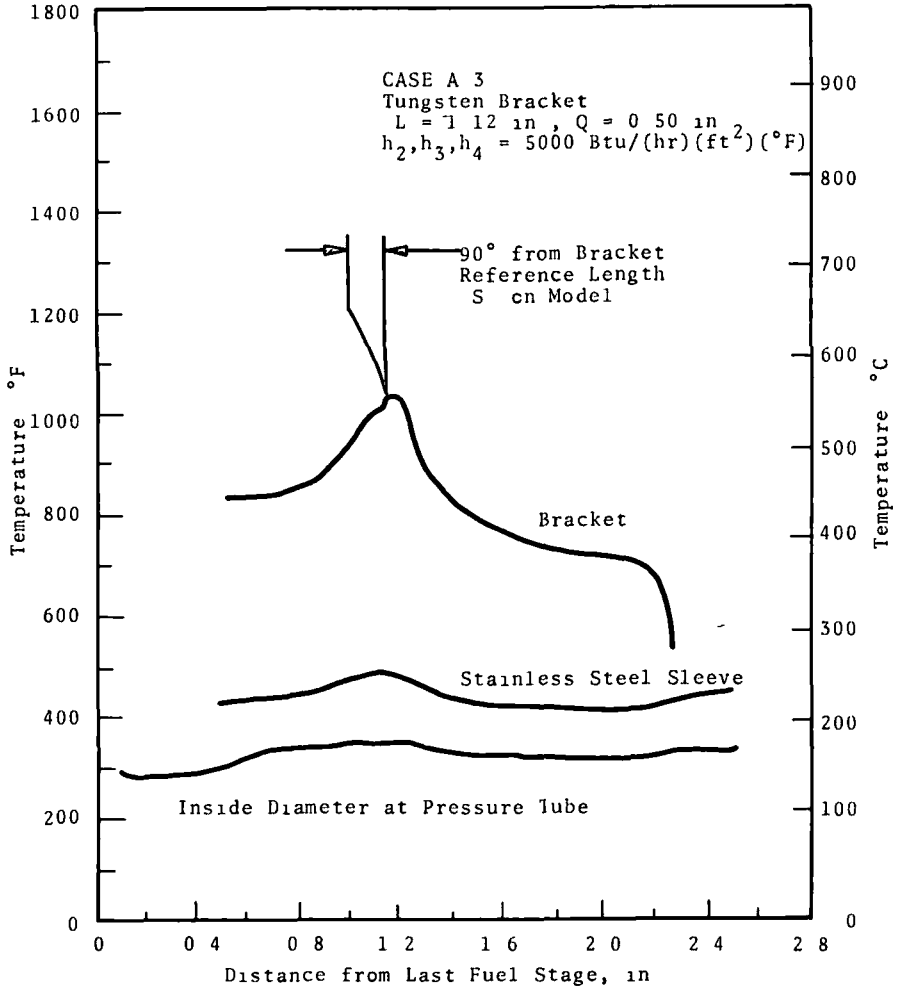

FIGURE 6 6 Temperature Distributions (Hot End Support Components) Versus Distance from Last Fuel Stage

CONFIDENTIAL

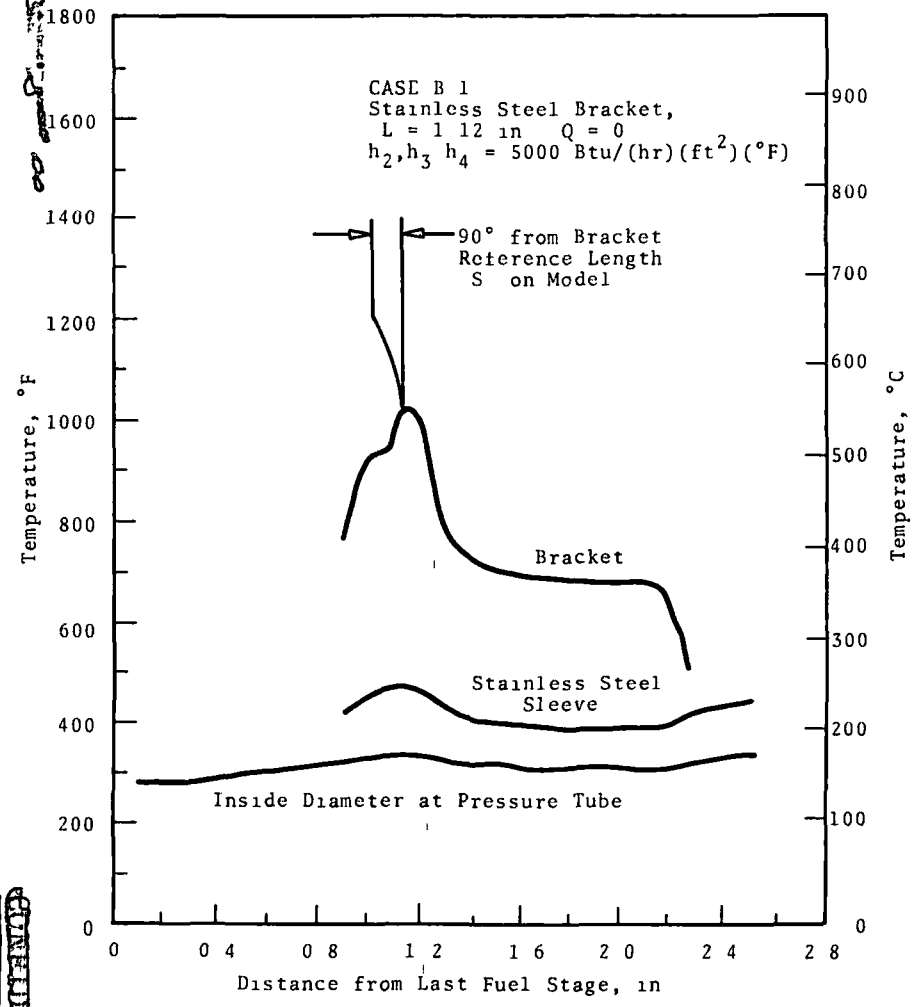

FIGURE 6 7 Temperature Distributions (Hot End Support Components) Versus Distance from Last Fuel Stage

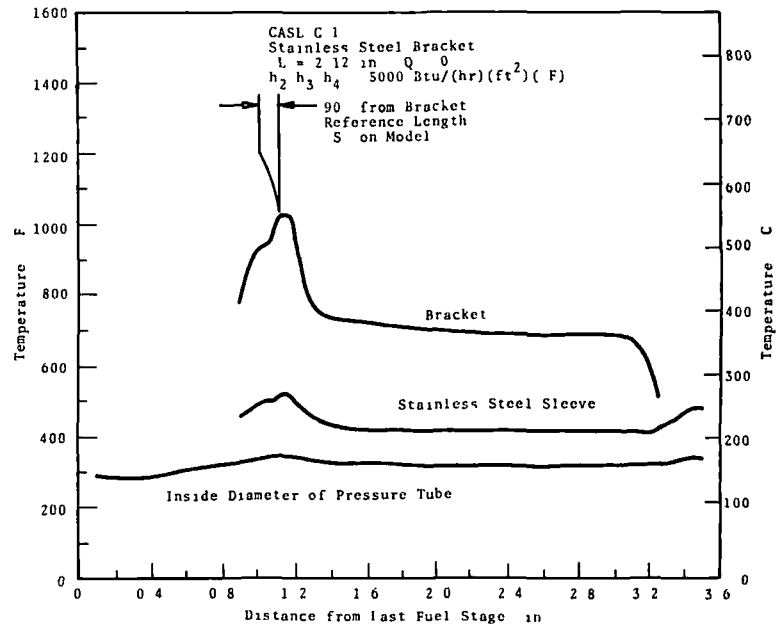

FIGURE 6 8 Temperature Distributions (Hot End Support Components) Versus Distance from Last Fuel Stage

through the pad would probably induce a mechanical failure through thermal stress if the pad were a solid piece One alternative might be use of a laminated pad The problem of a pressure seal between the fuel column-pressure tube annulus and reactor exit is also apparent with the solid pad, and would be worse with a laminated insulating pad

These difficulties prompted elimination of the insulating pad. The bracket and support leg were considered one solid piece and the 10 mils of insulation between the bracket and sleeve was increased to 30 mils This change caused a maximum pressure tube temperature increase to about 360 °F Refinements or detailed investigation of this configuration were not pursued, only the design feasibility is suggested

Elimination of the insulating pad between the tungsten leg and the support bracket does not alleviate problems concerning mechanical integrity of the insulation between the bracket and the stainless steel sleeve Few choices of materials are available because of temperatures on the order of 2000 °F A design concept illustrated in Figure 6 9 shows the insulating material enclosed in a thin metallic membrane If the material crumples or fractures, and the membrane remains intact, a thermal failure of the insulation would not be expected Thermal evaluation of this concept was not performed A fiber-reinforced ceramic material would also be a candidate here

6 4 TUNGSTEN SUPPORT LEG STRESSES

An initial estimate of required tungsten support leg wall thickness was obtained by considering pressure stresses and axial stress due to aerodynamic and fuel loads acting on the structure

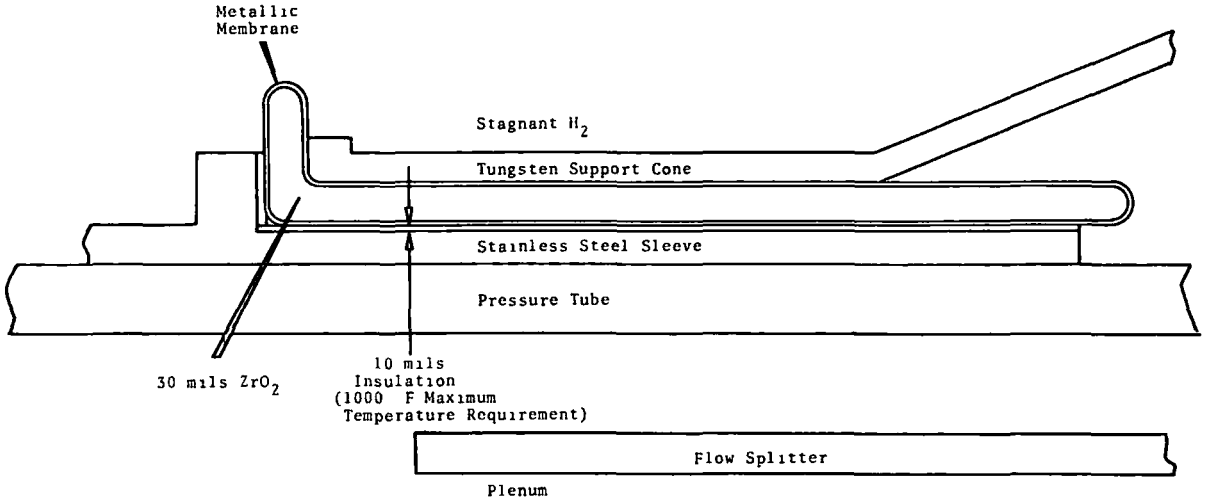

FIGURE 6 9 Design Concept Showing Insulating Material Enclosed in Thin Metallic Membrane

Axial fuel loads were assumed to be applied suddenly, and on this basis an impact factor of 2 was used A maximum aerodynamic loading of 358 lb was based on 103 psi ΔP across the fuel column with tungsten leg dimensions corresponding to 0 125 in hydrogen gap study cases Axial loads were not critical in determining the support leg wall thickness

Primary membrane stresses were evaluated Selection of an allowable membrane stress based on 80% of recrystallized tungsten yield strength, with support leg temperatures greater than 3200 °F, gave an estimated minimum wall thickness requirement of about 0 036 in (Figure 6 10)

An estimate of critical buckling pressure, as a function of average support leg temperatures in the 3400 to 4000 °F range, was obtained by considering the tungsten leg as a thin ring uniformly loaded by external pressure This calculation, which neglected the stiffening effect of ring edge constraints, gave conservatively thick estimates of the tube wall requirements between 0 032 and 0 040 in (Figure 6 10) When the length of the tungsten leg is not large compared with its

diameter, the ring end conditions should not be neglected in the critical buckling pressure calculation A short shell buckling analysis, taking into account the ring boundary conditions would predict higher critical pressures and therefore thinner required support wall dimensions

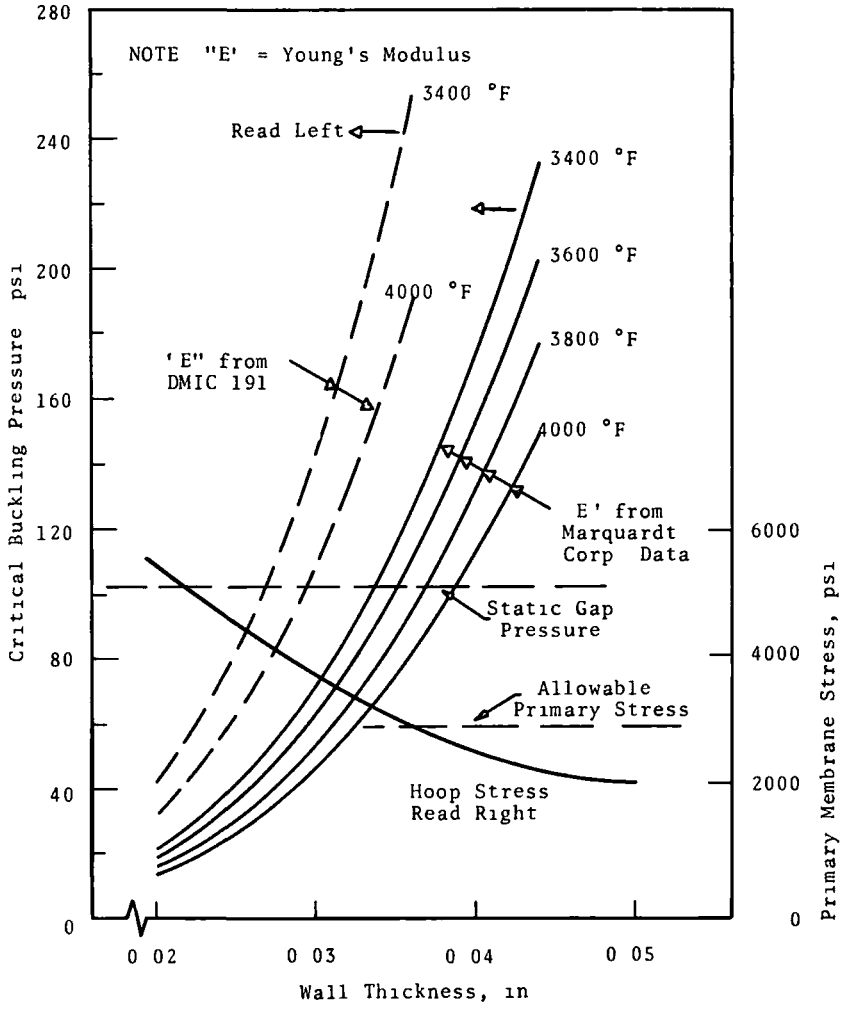

FIGURE 6 10 Hot End Support Tungsten Support Leg Critical Buckling Pressure and Primary Membrane Stress

The selection of a 0 040 in support tube wall thickness, based on a calculated hoop stress of 2700 psi and an allowable stress of 3000 psi, assured adequate strength to resist both

pressure and buckling loads Other hot end support materials and dimensions were parametrically studied in the heat transfer analysis

Figure 6 10 also indicates the effect of discrepancies in Young's Modulus data on calculated buckling pressures

7 0 REENTRANT-FLOW-COOLED LATERAL SUPPORT DESIGN

7 1 Introduction

During the early stages of the design of a fuel support for the TWMR, some concern was expressed about being able to fabricate the tungsten support tube used in the reference design However, before a more fabricable material could be considered, some cooling had to be provided to lower the operating temperature of the support tube With the large supply of low-temperature hydrogen available in the vicinity of the support tube, it seemed desirable to bleed some of this into the annulus between the support tube and pressure tube for cooling the fuel support structures

Since the bleed flow had to remain at relatively low temperature to be an effective structural coolant, discharging any significant amount of it into the main reactor exhaust stream would degrade the rocket performance Since the estimated bleed flow required to cool the support tube down to a temperature allowing stainless steel to be used was high (10 to 20% of the main coolant flow), the degradation of rocket performance by discharging this much low temperature coolant (1000 to 1500 °F) directly to the reactor exhaust was felt to be excessive For this reason the bleed flow circuit investigated was the reentrant type so the coolant was exhausted to the main coolant stream near the inlet end of the reactor

Several ways of incorporating the lateral fuel supports in the reentrant flow design were given at least a qualitative evaluation Since the corrugated strip was being investigated in detail in other phases of this study, it was decided to use a modified version of this for the preliminary reentrant flow design Rather than use strips, however, a corrugated cylinder running the full length of the fuel column was proposed This acts not only as the lateral support but also provides a flow divider in the annulus to provide downflow and upflow passages

If the concept of a support tube for supporting the axial fuel loads at the cold end of the reactor should be abandoned in favor of a hot end support concept, bleed flow cooling may be necessary for cooling the bottom support structure This, however, was not studied in any detail in this analysis By redefining the model in the computer code used, this case could be looked at

The analysis reported here estimates the structural material temperatures and bleed flow parameters well enough to establish the feasibility of the concept and allow the selection of some initial values for starting a detailed design No stress analysis was performed on the structural members, however, in general, the trends developed in the other parts of this program will also apply to the reentrant-flow-cooled design

7 2 Thermal Hydraulic Analysis

7 2 1 Model Development

The thermal-hydraulic model analyzed in this study had to meet two major criteria First of all the model had to be a reasonable representation of the actual fuel subassembly as far as thermal paths and resistances and hydraulic paths and resistances were concerned The model also had to be simple enough to allow many calculations to be performed with a variety of dimensional and flow parameters in a reasonable time

With these criteria in mind, the simpliefied model shown in Figure 7 1 was used To adequately predict the material temperatures of interest, the mathematical description of this model had to involve three dimensional heat conduction in the structural material portions of the fuel column as well as the necessary hydraulic characteristics of the bleed flow paths

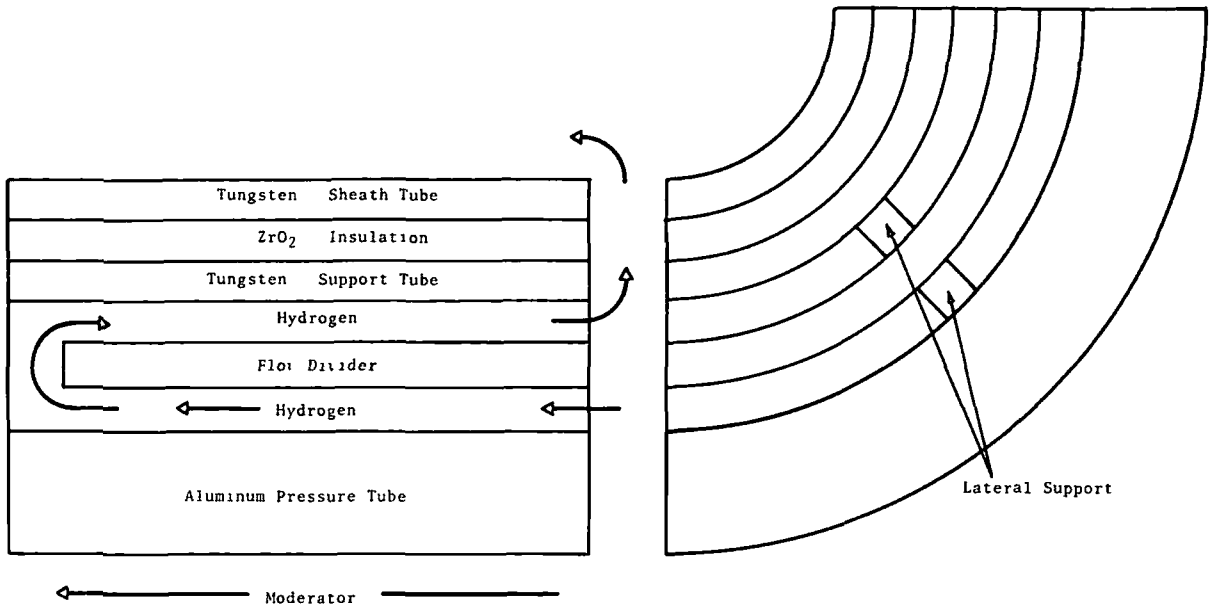

Model for Evaluation of Reentrant Bleed Flow Cooling of Lateral Support

FIGURE 7 1 Model for Evaluation of Reentrant Bleed Flow Cooling of Lateral Supports

The gamma heating in the structural material was assumed the same as for the static hydrogen annulus study This has been discussed in Section 3 2 of this report The assumed boundary conditions on the inside of the sheath tube and the outside of the pressure tube are also discussed in that section The assumed moderator axial temperature profile, which is the boundary condition on the outside of the pressure tube, is not very accurate for this case because there is much less heat lost from the fuel subassembly with reentrant flow in the annulus However, varying this had negligible effect on the structural material temperatures of interest so no corrections were made for this particular study

Using a quadrant of the subassembly as shown was felt to be adequate for determining the information necessary to establish feasibility The edges of this segment are lines of symmetry and the model is exact for a real case having four lateral supports around the circumference of the subassembly

Unless a very large number of lateral supports (i e >20) were considered, this assumption should not significantly affect the results of the feasibility study

Radiation of heat across the flow annulus was neglected in the reentrant flow design because the temperature gradients between the support and pressure tubes are much lower with the flowing hydrogen in the annulus and because the flow divider also acts as a radiation shield

The turn-around space provided at the hot end of the subassembly is simply an effective flow cross section which need not be rigorously defined for this study

During the flow stability part of the analysis, metering channels were added to the inlet of the bleed flow circuit to vary the overall pressure drop This is discussed in more detail in Section 7 2 3

7 2 2 Structural Material Temperatures

Predicting the structural material temperatures required a three-dimension heat conduction analysis of the model in Figure 7 1 along with the hydraulic's calculations performed on the bleed flow coolant Preliminary analysis indicated that hand calculations could not adequately determine feasibility in a reasonable length of time

A brief survey was made to find a digital computer code which would perform both the reentrant bleed flow hydraulics calculations and the three-dimensional heat conduction calculations There are several codes that have been written which perform compressible flow and three-dimensional heat conduction calculations They are not, however, readily adaptable to the reentrant flow geometry This is primarily due to the uncertainty in how to handle the region between the entrant-flow and exhaust-flow passages

To use these codes would involve unfolding the model in Figure 7 1 so it resembled a once-through bleed flow circuit The boundary conditions on the outside of the exhaust-flow passage and the inside of the entrant-flow passage would then have to be modified as the calculations progressed Accomplishing this with the codes available would have required a considerable amount of time It appeared to be more expedient to add the compressible flow analysis to the STHTP computer code, used in calculations on the static hydrogen gap lateral support evaluation, discussed in Section 3 0 of this report

To obtain the temperatures of interest with the STHTP Code, the model in Figure 7 1 was divided into four major axial segments and one thin axial segment at the hot end of the reactor for more detail in this critical area The model was also split into three circumferential segments and each material region was divided into three radial segments This degree of segmentation yields enough information to establish axial, circumferential, and radial temperature profiles in the regions of interest The axial segmentation selected divides the bleed flow path into nine nodes, which were adequate for purposes of this analysis

In performing the calculations, the modified STHTP Code assumes an initial temperature distribution in the bleed flow circuit It makes each fluid node a constant temperature sink and performs a heat balance on all the materials' nodes to obtain an estimate of the structural materials' temperatures and the heat transferred to the fluid nodes at their assumed temperature It then modifies the bleed flow temperature profile and repeats the heat balance This procedure is repeated until the heat transferred to the fluid nodes for two successive heat balances is within some acceptable error limit

As it is currently dimensioned, the modified STHTP Code will handle a total of twenty fluid nodes including the boundary conditions on the inside and outside of the region of interest This is somewhat limiting but can be increased, if need be, in the future The Code will handle up to two hundred structural material nodes One hundred fifty-three were used in this analysis

One other factor that should be discussed here is the materials' properties used in this analysis Although STHTP allows variation of thermal conductivity with temperature to be used, it adds considerably to the solution time for a complex problem For this particular study it would not affect the results enough to justify the additional machine time The following constant values of thermal conductivity were used throughout the reentrant flow study

Stainless Steel	K = 10 0 Btu/(hr)(ft^2)(°F)
Tungsten	K = 60 0 Btu/(hr)(ft^2)(°F)
Aluminum	K = 100 0 Btu/(hr)(ft^2)(°F)
Zirconium Oxide	K = 1 16 Btu/(hr)(ft^2)(°F)(100% TD)

The relative gamma heating in the various materials has been discussed in Section 3 2 of this report and the same values were used in this analysis

7 2 3 Bleed Flow Hydraulics

The bleed flow circuit was divided into nine nodes, as mentioned in the previous section, for performing calculations on the IBM 7090 computer For this particular study, the bleed flow rate (lb/sec) and the channel dimensions were independent parameters For a given iteration in the overall solution of the problem, the following quantities were calculated for each fluid node The term fluid node as will be discussed here pertains only to the bleed flow circuit and does not include the main

hydrogen flow stream or the moderator flow which are fixed boundary conditions

ΔT_n = temperature rise along the node

ΔP_n = pressure drop along the node including momentun losses due to density change, entrances, exits, and change in direction of flow, where applicable as well as the friction loss along the channel

h_n = average heat transfer coefficient on the walls of the bleed flow passage based on local physical properties and velocity

If a value for the heat flowing into a node, n, is known from the heat balance performed on the model, a new temperature rise for the fluid in the node is given by

$$\Delta T_n = Q_n / WCp_n \qquad (7\ 1)$$

where

Q_n = The assumed heat flow into the node (Btu/hr)

W = Bleed flow rate (lb/hr)

Cp_n = Specific heat of hydrogen evaluated at the mean temperature of the node

The mean temperature and outlet temperature of the bleed flow hydrogen in each node are then given by

$$\overline{T}_n = (T_{in})_n + \frac{\Delta T_n}{2} \qquad (7\ 2)$$

$$(T_{out})_n = (T_{in})_n + \Delta T_n \qquad (7\ 3)$$

These calculations are repeated for each node along the bleed flow circuit The new mean node temperatures then become the sink temperatures when the next heat balance is performed

The pressure loss along each node for a heated compressible fluid was approximated by

$$\Delta P_n = \frac{G_n^2}{g_c \bar{\rho}_n} \left\{ \frac{2fL_n}{D_h} + \frac{(T_{out})_n - (T_{in})_n}{\bar{T}_n} \right\} \qquad (7\ 4)$$

A derivation of Equation (7 4) beginning with the momentum equation is contained in Appendix E of this report In Equation (7 4)

$\bar{T}_n$ = bulk average coolant temperature in the node
G_n = mass velocity in the node (lb/sec-ft^2)
g_c = gravity constant (ft/sec^2)
$\bar{\rho}_n$ = average hydrogen density in the node
$\bar{\rho}_n = \bar{P}/R\bar{T}$ (lb/ft^3)
$f \approx 0\ 046/Re^{0\ 2}$
Re = local Reynold's No $= \dfrac{G\ D_h}{\bar{\mu}_n}$

D_h = hydraulic diameter of the coolant passage
= 4 (free-flow cross section)/the wetted perimeter of the passage (ft)
$\bar{\mu}_n$ = mean viscosity of the hydrogen in the node (lb/sec-ft)
$\bar{P}_n$ = average pressure in the node
L_n = length of the node

For the cases having a metered flow to reduce the sensitivity of the bleed flow rate to pressure fluctuations in the main coolant stream, several metering channels around the circumference of the subassembly were used as a control device Comparing metering channels with metering orifices, the channels have the advantages of being less subject to wear, requiring fewer of a given diameter to accomplish the control necessary and a larger degree of flexibility in shape to make matching the annular region, which must

be fed, easier The pressure drop through these channels was estimated with a relationship similar to Equation (7 4), but without the temperature change term

$$\Delta P_{ent} = \frac{G_c^2}{2\bar{\rho}_n g_c}\left\{\frac{2fL_c}{D_c} + 1\ 5\right\} \qquad (7\ 5)$$

where

G_c = mass velocity in the metering channels (lb/sec-ft)
L_c = length of the metering channels
D_c = hydraulic diameter of the metering channels

The 1 5 factor is the combined entrance and exit coefficient for the metering channels

From momentum considerations the static pressure loss due to turning the bleed flow 180° at the hot end of the sub-assembly was estimated at two velocity heads Hence, for the fluid node in which the flow was turned around, Equation (7 4) became

$$\Delta P_{turn} = \frac{G_n^2}{2\bar{\rho}_n g_c}\left\{\frac{2fL_n}{D_h} + \frac{(T_{out})_n - (T_{in})_n}{\bar{T}_n} + 2\ 0\right\} \qquad (7\ 6)$$

where the symbols are the same as in Equation (7 4)

For these calculations the heat transfer coefficient on the sides of each node were estimated using the following form of the Dittus-Boelter equation

$$h_n = 0\ 021\ \frac{K_b}{D_h}\ (Re)_b^{0\ 8}\ (Pr)_b^{0\ 4} \qquad (7\ 7)$$

where

K_b = thermal conductivity of the hydrogen (Btu/(hr)(ft^2)(°F)

$$\text{Re} = \text{local Reynold's No} = \frac{G_n D_h}{\bar{\mu}_n}$$

$$\text{Pr} = \text{local Prandtl No} = \frac{C_{p_n} \mu_n}{K_n}$$

The subscript, b, indicates all physical properties were evaluated at the average bulk temperature of the hydrogen in the node

The hydrogen properties used in Equations (7 4), (7 5), (7 6), and (7 7) were taken intact from the NASA-Lewis aerodynamics code used to perform calculations on the concentric ring-fueled subassembly for the TWMR These properties were in the temperature and pressure range of interest

7 2 4 Reentrant Flow Computer Code

The Reentrant Flow computer code, as mentioned previously, is a version of the Steady State Heat Transfer Program (STHTP) [1] This code is written in Fortran II for the IBM 7090 computer

The purpose of this discussion is not to generate a user's manual for the Reentrant Flow Code, but rather to clarify the calculational procedure it contains since this is important in judging the overall validity of the results The best explanation is obtained by following through the schematic diagram in Figure 7 2, and pointing out the modifications made This diagram does not show all the components of the program, only the ones which aid in understanding the procedures were included

The preliminary input information, read in to the main program, is only two cards long These two cards contain such information as

- Case number
- Number of nodes in the problem
- Number of materials tables used

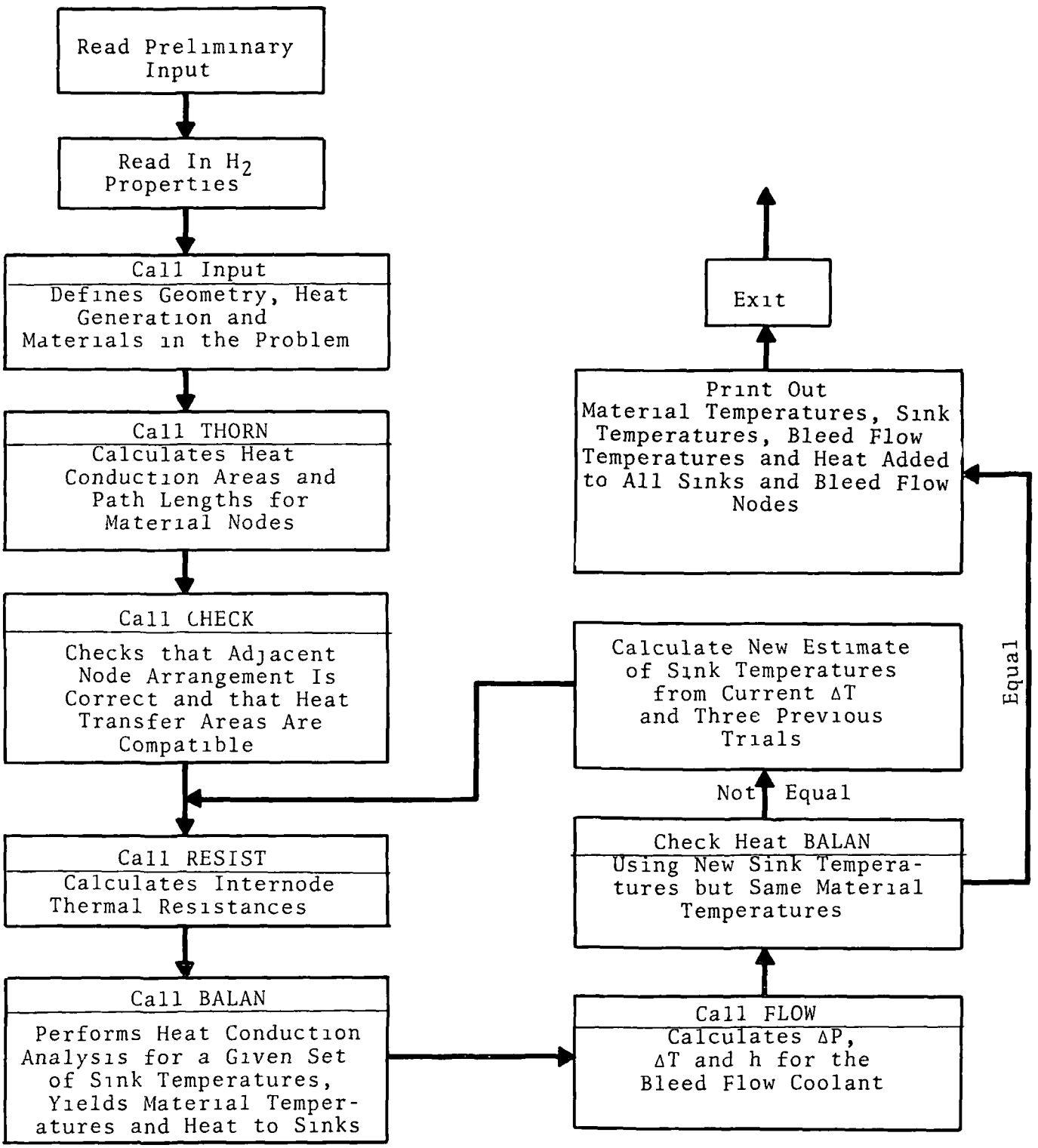
Read Preliminary Input
Read In H_2 Properties
Call Input
Defines Geometry, Heat Generation and Materials in the Problem
Call THORN
Calculates Heat Conduction Areas and Path Lengths for Material Nodes
Call CHECK
Checks that Adjacent Node Arrangement Is Correct and that Heat Transfer Areas Are Compatible
Call RESIST
Calculates Internode Thermal Resistances
Call BALAN
Performs Heat Conduction Analysis for a Given Set of Sink Temperatures, Yields Material Temperatures and Heat to Sinks
Call FLOW
Calculates ΔP, ΔT and h for the Bleed Flow Coolant
Check Heat BALAN
Using New Sink Temperatures but Same Material Temperatures
Not Equal
Calculate New Estimate of Sink Temperatures from Current ΔT and Three Previous Trials
Equal
Print Out Material Temperatures, Sink Temperatures, Bleed Flow Temperatures and Heat Added to All Sinks and Bleed Flow Nodes
Exit

Schematic Diagram of Reentrant Flow Code, Main Program

FIGURE 7 2 Schematic Diagram of Reentrant Flow Code--Main Program

- Number of constant temperature sinks
- Three different output options
- Whether or not it is the first case in a series of cases
- An acceleration factor for changing the rate of convergence of the solution
- An extrapolation factor for estimating new temperatures between heat balances
- The allowable errors for all iterative procedures
- The total number of iterations allowed before a nonconvergent solution is assumed

If the case being run is the first of a series, the hydrogen properties are then read in, if not the main program calls subroutine INPUT

This subroutine defines the geometry and critical properties of the problem to be solved, i e , the node connections, the material properties of each region, the heat generation rate in each region, the physical dimensions of each region, what surfaces have contact coefficients associated with them and the value of the coefficients, the temperatures of the heat sinks and an initial guess for all node temperatures This subroutine is the same as used in STHTP except the heat conduction areas and path lengths associated with each node face are calculated internally, only the radii of the regions in Figure 7 1 are put in along with the circumferential segment size, i e , quarter cylinder, the thickness of the lateral support rib, length of each axial segment and the bleed flow rate

The subroutine THORN takes the dimensions read in and calculates the heat conduction areas and path length for each face of each materials node In STHTP this information is fed in as input Since the radial thickness of each region was an independent parameter in this study, it was advantageous to incorporate these calculations in the code rather than generating this information for each set of dimensions by hand calculation

Subroutine CHECKK is unchanged from the original STHTP code Trying to run a heat balance on a problem in which duplicate node numbering or improper interconnection of nodes was specified would take a great deal of computer time This subroutine checks for these conditions, terminates the calculations if they exist and indicates the nodes where the discrepancy was located

Subroutine RESIST calculates the internode resistances using the geometric information generated by THORN and the materials properties, contact and convective heat transfer coefficients from the input data

Subroutine BALAN then performs a heat balance on the materials nodes in the model, assuming the current estimate of bulk coolant node temperature as the first nine constant temperature sinks, to find the materials temperatures and heat rejected to all the sinks This is the main subroutine in the STHTP code and no attempt will be made here to explain the relaxation techniques used and their refinements Instead, the reader is referred to the "User's Manual"[1] for this information

Subroutine FLOWW contains the equations outlined in Section 7 2 2 for calculating the bulk bleed flow temperature rise, pressure drop and new convective heat transfer coefficients using the bleed flow rate from the input and the heat rejected to each node as calculated in Subroutine BALAN The hydrogen properties as a function of temperature are contained in a Function Subprogram, which is called by simply indicating the properties, such as viscosity, specific heat and thermal conductivity, which are functions of temperature directly in the equation they are used For example Equation (7 1) in Section 7 2 3 is written in the computer as

$$\Delta T_n = Qn/W\ Cp_n\ (\bar{T}n) \qquad (7\ 1a)$$

This automatically evaluates the specific heat CP at the average bulk coolant temperature of the node Simple iterative loops were used for both the temperature rise and pressure drop equations since the hydrogen properties were allowed to vary during the calculations Simple linear extrapolations gave rapid convergence in all cases for both of these loops

As soon as control returns to the main program, indicating FLOWW has a new set of sink temperatures, these are used to calculate the heat flow to each bleed flow node assuming the materials temperatures are the same as recently calculated by Subroutine BALAN If the heat flowing to each node of the bleed flow coolant under these conditions is within 0 1% of the heat flow recently calculated by BALAN, the solution is assumed to have converged Symbolically, the solution has converged if

$$\frac{Q_n(I) - Q_n'(I)}{Q_n(I)} \leq 0\ 001 \qquad (7\ 8)$$

where

$Q_n(I)$ = Heat transferred to node, n, as calculated by the, I^{th}, pass through Subroutine BALAN

$Q_n'(I)$ = Heat transferred to node, n, using bleed flow temperatures calculated by the, I^{th}, pass through Subroutine FLOWW, but material temperatures from the I^{th} pass through Subroutine BALAN

If this convergence criteria is not met, the main program estimates a new set of bleed flow temperatures using

$$T_n = (T_{in})n + \left\{\frac{\Delta T_n(I) + \Delta T_n(I-1) + \Delta T_n(I-2) + \Delta T_n(I-3)}{8}\right\} \qquad (7\ 9)$$

It was found that averaging the three previous predicted bleed flow temperature rises gave a more rapid convergence to the final, $\overline{T}_n$ Doing this reduced large fluctuations in

estimated, $\bar{T}_n$, when the initial guess temperatures were considerably off from the final value

Using the $\bar{T}_n$'s from Equation (7 9) as new sink temperatures, the main program returned for the $(I + 1)^{st}$ pass through Subroutines RESIST, BALAN AND FLOWW This is repeated until Equation (7 8) is satisfied

On the average, I = 40 was necessary to complete each case with a corresponding 7090 running time of about 5 min

7 3 Parameter Studies

7 3 1 Flow Channel Sizing

It was assumed, in sizing the flow channels, that the gap between the support tube and pressure tube would remain at approximately 1/8 in The only variation in channel dimensions was then the relative size of the entrant-flow and exhaust-flow passages During the initial checkout of the code this relative sizing was set so the pressure drop in the exhaust-flow passage was only slightly higher than that in the entrant-flow passage and so the heat transfer coefficients in both passages were reasonably close together

For a typical case the values in Table 7 1 were obtained

TABLE 7 1 FLOW CHANNEL SIZING PARAMETERS

	Entrant Passage	Exhaust Passage
Passage Dimensions, in	0 050	0 070
Pressure Drop, psi	9 66	11 18
Average Heat Transfer Coefficient (Btu/(hr)(ft^2)(°F)	2670	2140
Bleed Flow Rate (lb/sec)	0 25	0 25

The passage dimensions of 0 050 and 0 070 in were used for the results that are presented in this report

7 2 3 Insulation Thickness

The primary function of the insulation in the reentrant bleed-flow design is to sustain the bulk of the large temperature gradient that will exist between the fueled region of the subassembly and the exhaust bleed-flow passage at the hot end of the reactor This gradient, taken in the sheath and support tube, would cause excessively large thermal stresses Since the insulation is not a primary structural member, there is more freedom in such things as laminated design and containing the insulation such that even if it breaks apart its function of sustaining the necessary thermal gradient is not completely eliminated

The heat rejected to the bleed-flow coolant with the existing thermal graidents is also much more reasonable when these gradients are sustained by a ceramic material This is illustrated in Figure 7 3 if bleed-flow outlet temperature is taken as a measure of the heat flowing to the reentrant cooling stream Figure 7 3 depicts the average The comparison is more severe if made at a local spot near the hot end of the reactor

Perhaps the most determining factor in selection of an insulation thickness is its effect on the support tube maximum temperature This is shown in Figure 7 4 By increasing the bleed-flow rate the maximum support tube temperature can be lowered to where stainless steel can be used The only exception studied here was the case with no insulation Even with all the hydrogen flow making a pass through the bleed-flow passages, the maximum support tube temperature was above 1900 °F

For the final studies made here an insulation thickness of 0 020 in was used This gave support tube temperatures in a range which allowed stainless steel to be considered, while

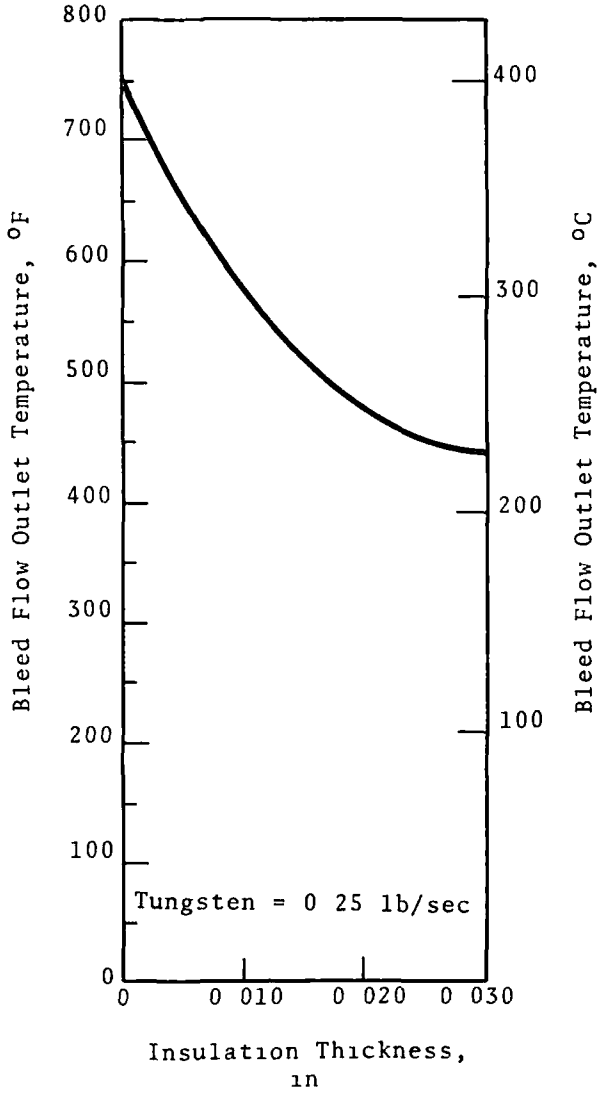

FIGURE 7 3 Bulk Bleed Flow Outlet Temperature Versus Insulation Thickness

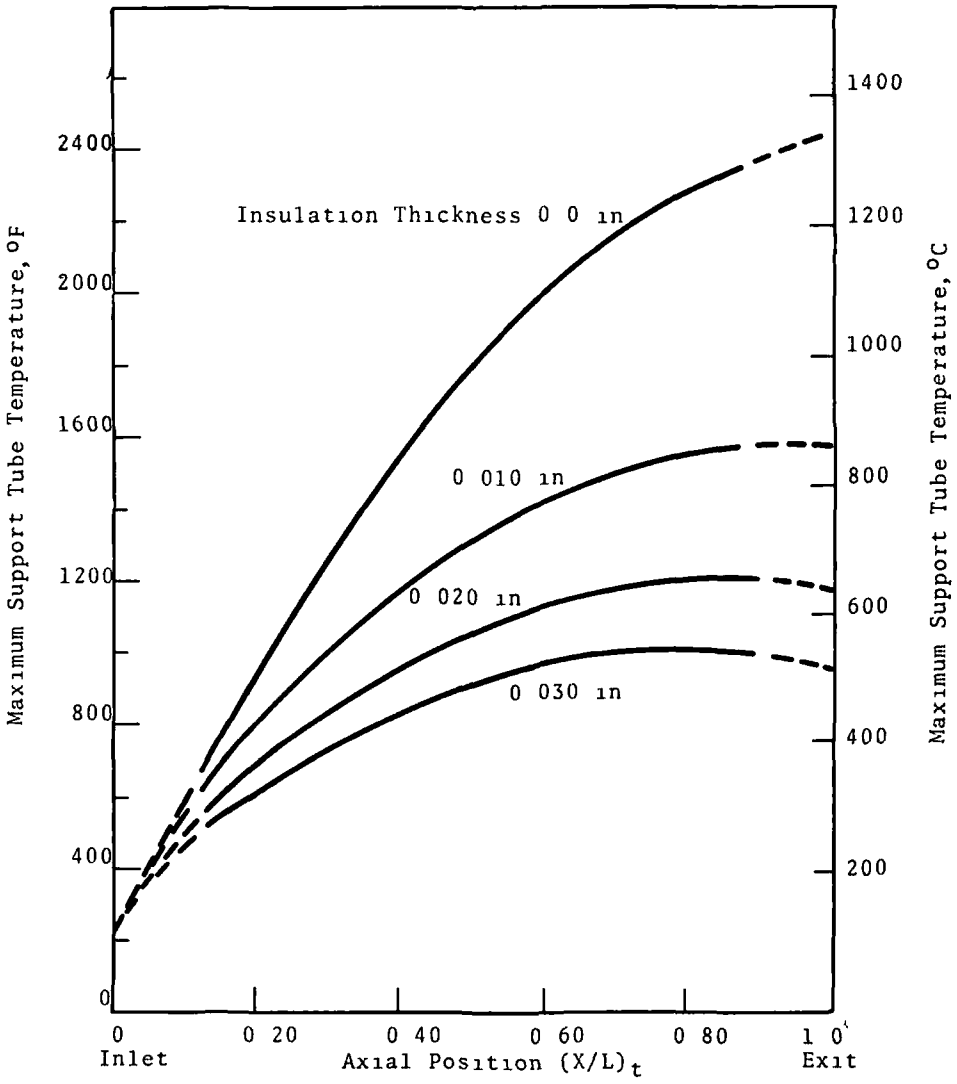

FIGURE 7 4 Maximum Support Tube Temperature Versus Axial Position for Various Insulation Thicknesses

requiring a bleed-flow rate low enough so excessive pressure losses were not incurred but were high enough to insure some stability of the flow

7 3 3 Support Tube Material

Two facts were felt worthy of comment when comparing stainless steel and tungsten as support tube materials These are illustrated in Figure 7 5

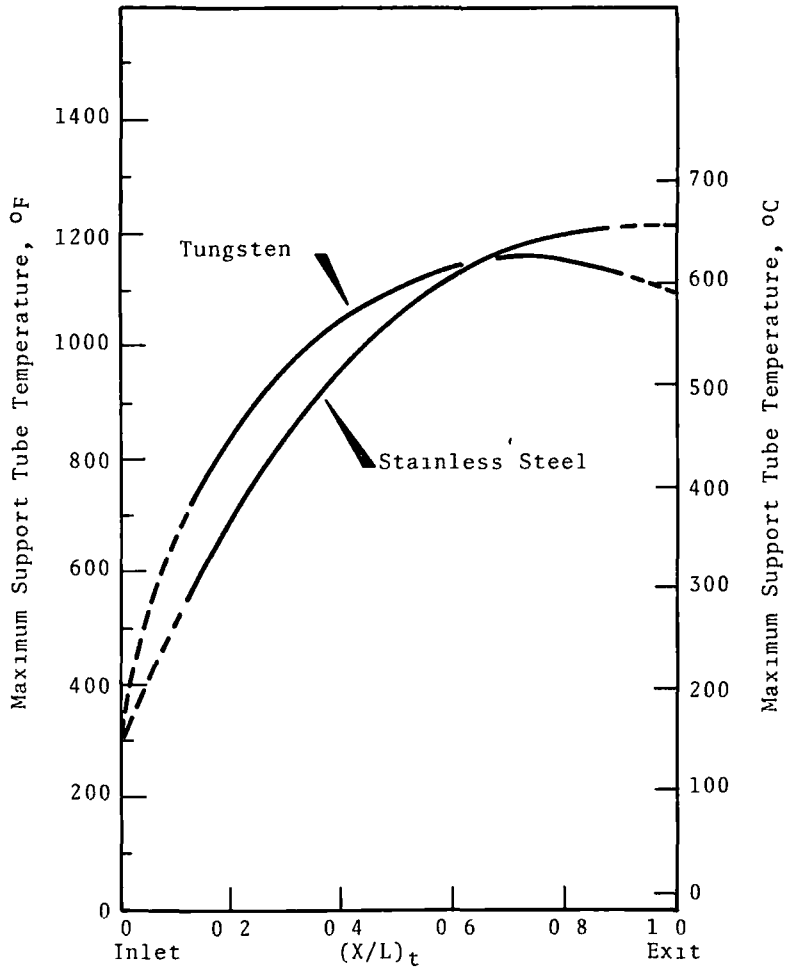

FIGURE 7 5 Comparison of Support Tube Temperatures for Stainless Steel and Tungsten Support Tube Materials (W = 0 25 lb/sec, Insulation Thickness = 0 020 in)

The lower thermal conductivity of the stainless steel compared to tungsten [10 0 Btu(hr)(ft^2)(°F) compared to 60 0] is reflected in the peak temperatures near the hot end of the subassembly Stainless steel peak temperatures are more dependent on the boundary temperatures assumed and, hence, maximizes where the main coolant temperatures are the highest

The different γ heating rates are reflected in the fact that the tungsten, having a considerably higher γ heating rate, has a maximum peak temperature much nearer the axial location where the γ heating is a maximum (Reference Figure 3 3 for γ heating axial distribution)

We see also that for the same dimensional and flow parameters, the stainless steel maximum peak temperature will be slightly higher

7 3 4 Outlet Pressure Fluctuations

Fluxuations of the main coolant stream pressure near the point where the bleed-flow coolant discharges could have a severe affect on the bleed-flow rate This was especially true when the flow rate in the bleed-flow circuit was about 0 1 lb/sec Under these flow conditions, the pressure drop was only 5 psi At the same time the materials temperatures are very sensitive to flow rate The low pressure drop and high sensitivity made it possible to get large variations in materials temperatures

The purpose of introducing orificing into the bleed flow circuit was to control the flow a little better by introducing more pressure drop into the bleed-flow path The ideal control situation would be to maintain a critical pressure ratio across the orifices This, of course, is not practical at the pressure levels found in the TWMR but an increase to 50 psi entrance loss would not degrade the rocket performance significantly

Figure 7 6 shows the sensitivity of the maximum support tube temperature to pressure fluctuations at a reference bleed-flow rate of 0 25 lb/sec

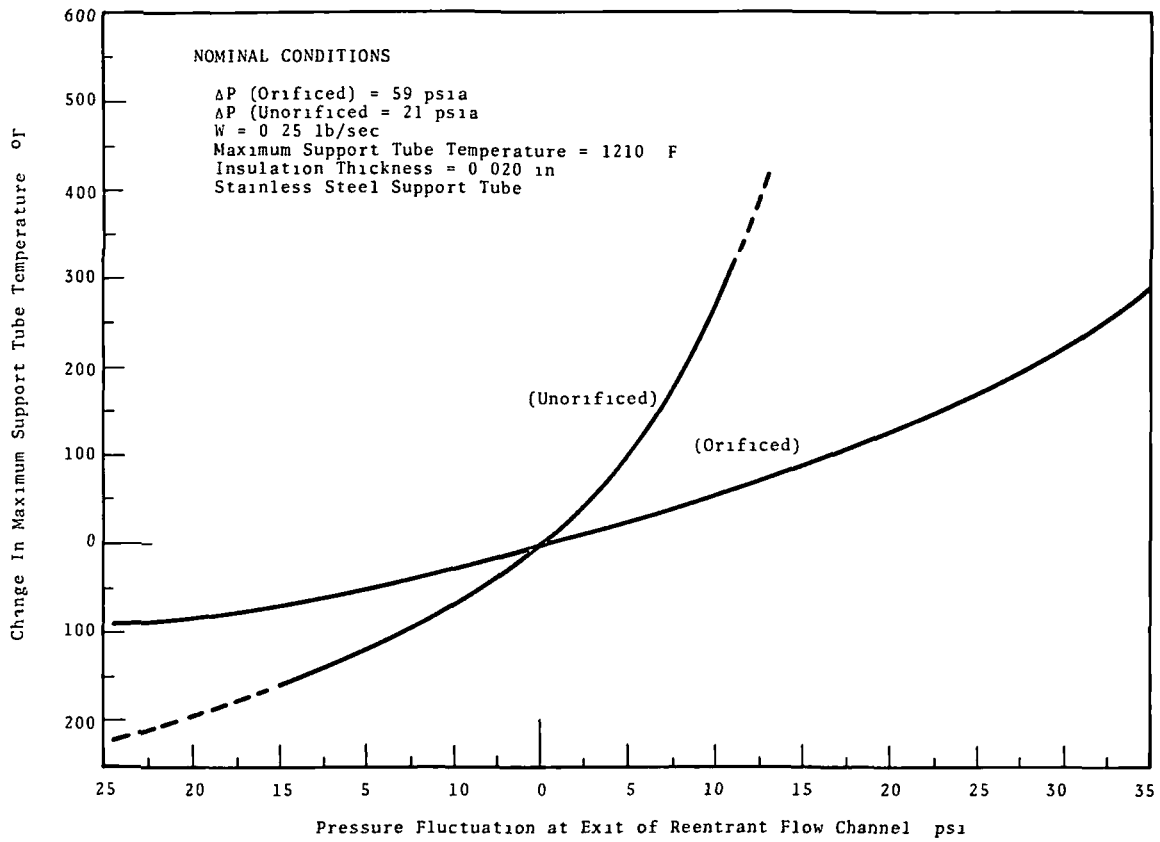

FIGURE 7 6 Deviation of Maximum Support Tube Temperature Versus Fluctuation of Main Coolant Pressure

It is felt that orificing may not be necessary in the TWMR because reasonable support tube temperatures could probably be insured by slightly increasing the flow rate thus lowering both the nominal support tube temperatures and the sensitivity to pressure fluctuations It still remains, however, an item to check in a final design analysis

7 4 Conclusions and Recommendations

7 4 1 Reference Flow and Dimensional Parameters

Table 7 2 summarizes a set of reference parameters which give a reentrant flow cooled fuel support design which meets the criteria established for this study, i e , support tube temperatures which allow stainless steel to be used, a seemingly stable flow, a reasonable pressure drop and exhaust temperatures which allow mixing with the main coolant stream near the reactor inlet

TABLE 7 2 REENTRANT BLEED FLOW REFERENCE PARAMETERS

Bleed-Flow Rate, lb/sec	0 25
Sheath Tube Thickness, in	0 020
Insulation Thickness, in	0 020
Support Tube Thickness, in	0 020
Entrant Flow Passage Thickness, in	0 050
Exhaust Flow Passage Thickness, in	0 070
Flow Divider Thickness, in	0 010
Pressure Tube Thickness, in	0 060
Gap Height for Flow Turn Around, in	0 050
Lateral Support Thickness, in	0 006

Figure 7 7 shows the bulk bleed-flow temperature rise for the reference case as well as for several flow rates around the reference value

Figures 7 8 and 7 9 show the maximum support tube and pressure tube temperatures, respectively, for flow rates near the reference flow

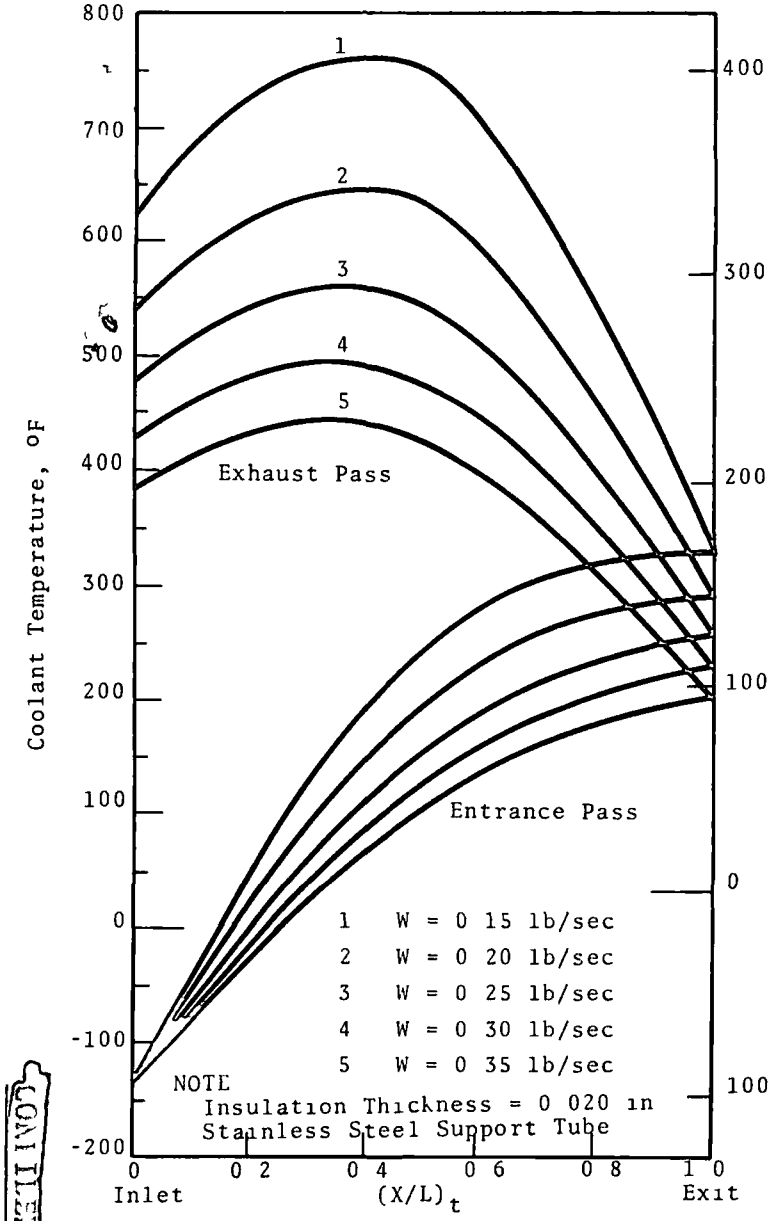

FIGURE 7 7 Bleed Flow Temperature Rise

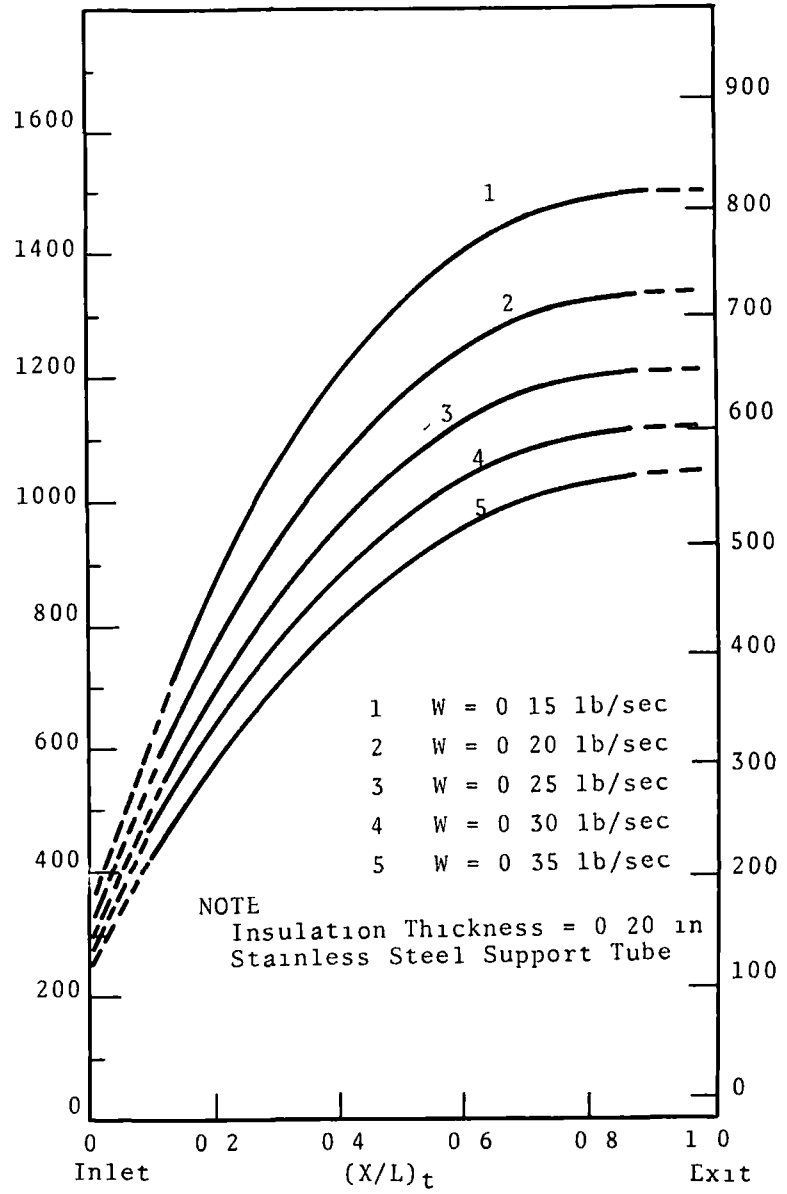

FIGURE 7 8 Maximum Stainless Steel Support Tube Temperature Versus Axial Location

NASA-CR-72051

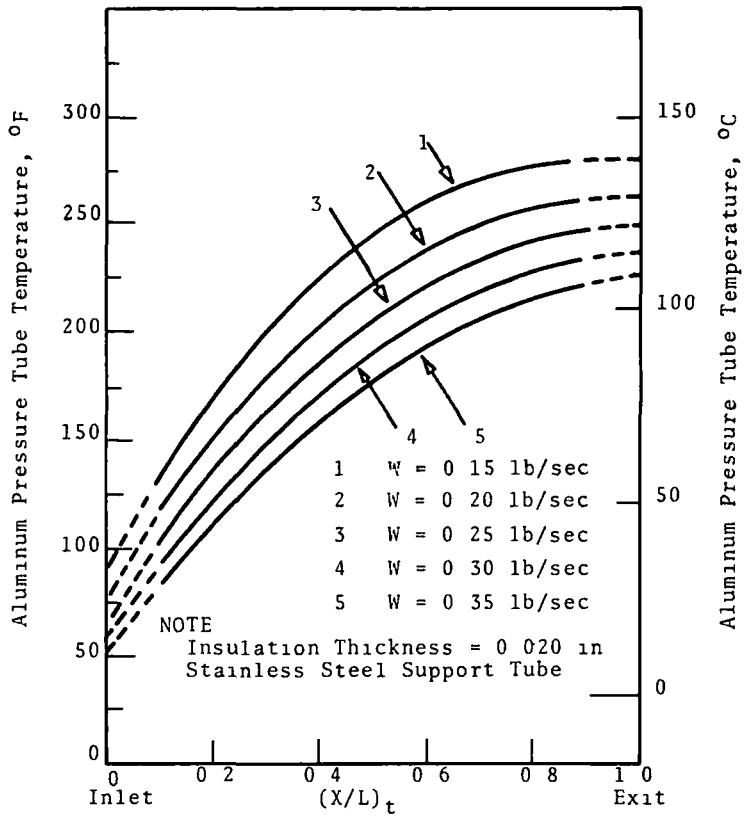

FIGURE 7 9 Maximum Aluminum Pressure Tube Temperature Versus Axial Location

7 4 2 Recommendations

In a detail design of a reentrant flow cooled support system for the TWMR there are some things which should be defined more rigorously

For example, the boundary conditions chosen for this study were based on the inside of the sheath tube being exposed primarily to the main coolant stream These conditions results from the "Egg Crate" fuel design, considered in other parts of this study, which actually has a small fraction of the sheath tube in contact with the fuel itself In the case of honeycomb fuels considered also for the TWMR, this assumed boundary

condition will most likely be reversed such that a fuel temperature would make a more realistic boundary condition

The assumed boundary conditions on the outside of the pressure tube, the moderator temperature distribution, are a little high for a bleed flow cooled design because the net heat flux was from the moderator to the bleed flow coolant These should be reevaluated for bleed-flow conditions in a final design

The information generated in the lateral support design should also be included in the detail design of a reentrant flow cooled support system The scope of this study did not allow the incorporation of these details, they are, however, applicable if corrections are made for materials properties at the temperatures found in detailed analysis of reentrant-flow conditions

Reentrant flow cooling should also be considered for the hot end support design Its function here would be to cool the bottom support structure The ceramic sleeve shown in Figure 6 9 may cause design problems when long-term integrity is considered If this sleeve must be eliminated, the support structure must be cooled primarily to keep the aluminum pressure tube temperatures down to acceptable levels

7 5 References

1 *F J Mollerus, Jr* *User's Manual for STHTP - A Steady State Heat Transfer Program for the IBM 7090 Computer*, *HW-73668, General Electric Company, Richland, Washington May 21, 1962*

8 0 FLAT PLATE STOCK W-UO_2 TWMR FUEL DESIGN

This section presents the results of studies conducted at Battelle-Northwest on the design of fuel elements for the Tungsten Water-Moderated Reactor concept being evaluated at the NASA Lewis Research Center The objective of the program was to conduct a design, fabrication, and evaluation investigation which would lead to the construction of W-UO_2 fuel elements from flat plate stock

The reference reactor design called for fuel elements 42 in in length consisting of 28 fuel stages A flow area between 1 and 2 5 in ^{2} with a hydraulic diameter of 0 08 to 0 14 in , were specified Fuel elements were to be constructed of 0 015 to 0 030 in W-UO_2 plate stock containing an average of 20% UO_2 In the fuel section the ratio of total tungsten to fueled tungsten had to be less than 1 1/2 1 The propellent gas was to be hydrogen with an inlet temperature of 360 °R, an exit temperature of 4500 °R and a flow rate of 0 3 to 0 45 lb/sec/in ^{2}

The fuel element design was to include provision for supporting the fuel within an aluminum pressure tube with the intervening annulus a minimum consistent with insulation and structural requirements

Fabrication feasibility was to be demonstrated using "state-of-the-art" techniques This requirement had reference to joining techniques primarily and precluded the use of designs that would require any significant development work in welding or bonding in order to accommodate a given design concept

Design philosophy was based on the circumstance that the fuel structure had to remain stable under a dynamic head of 12 psi or greater, with material properties similar to those of lead

at room temperature In order of importance the objectives in designing were therefore

1 Structural strength
2 Fabricability
3 Fuel grading

It was apparent from ANP and LRC flow test data[1,2] that the most stable fuel geometries involved very short unsupported spans in the fueled plates The optimum geometry for this is a fully bonded hexagonal grid or honeycomb, but since this exact structure is not practical to fabricate from sheet, a design was sought which should approach the honeycomb geometry, and which could also be assembled from sheet stock These considerations lead to the adoption of a rectangular grid assembled with interlocking strips in the fashion of eggcrate construction The machining requirements for the assembly of such a grid from plate stock did not appear unreasonable, and the basic assembly did not require joining of the tungsten by fusion welding or other bonding techniques, therefore, this design was adapted for contruction of test models Numerous plate configurations were considered in the evolution of the "eggcrate" fuel design Representative geometries which were examined in the process are described along with their limitations in Figures 8 1, 8 2, and 8 3

The rectangular grid concept has a definite shortcoming in regard to radial grading of the fuel, particularly if fine variations in fuel content are important A rough division into two or three zones quite possibly could be achieved by longitudinally partitioning the U^{235} loading in the fuel plates when they are laid up before compacting In the fabrication of cermet plates it is necessary to keep the ceramic content uniform across the plate, therefore, grading would depend on the use of UO_2 in a uniform quantity but with various U^{235} enrichments

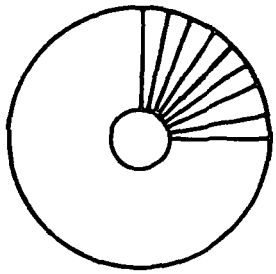

With plates as straight radial fins, it is not possible to get sufficient fuel into the cross section

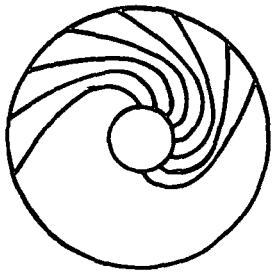

Curved plates permit more fuel in the section, but radical curvature in the plates is necessary to obtain the required equivalent diameter

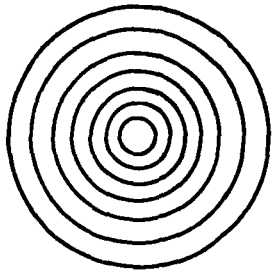

Increased curvature of the plates leads to concentric cylinders. These, however, have such a long unsupported span that stability under the dynamic load may be lacking

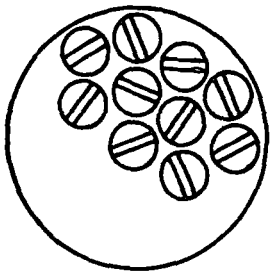

Twisted ribbons, which are attractive from the stand point of graded fuel loading possibilities, defy attempts to arrange into a stable structure

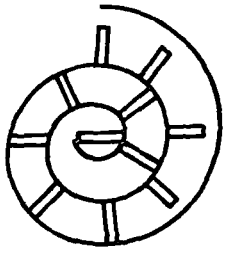

Spiral winding with spasms is considered to be possible to fabricate but is complex and impractical

FIGURE 8 1 Geometries Considered in Grid Design Studies

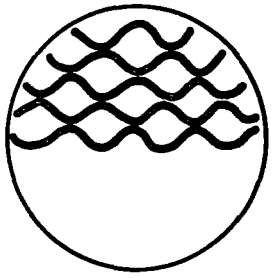

Corrugated plates contacting on each other would be subject to hot spot difficulties

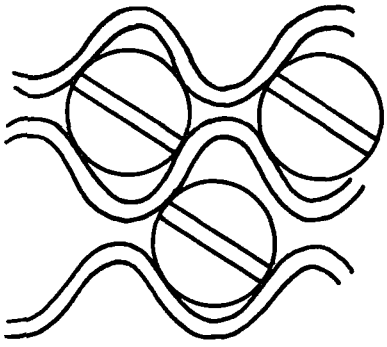

Corrugated plates separated with twisted ribbons obviates the hot spot problem, but it is not possible to get sufficient fuel into the section

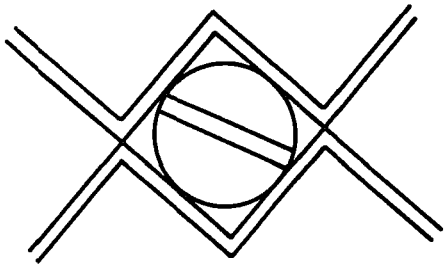

It is possible to obtain the required equivalent diameter with rectangular corrugations, but in order to assemble into a stable array would call for reliable welds

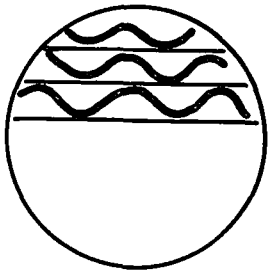

With fueled straight plates hot spots would result at contact points With unfueled straight plates insufficient fuel is in the section

FIGURE 8 2 Geometries Considered in Grid Design Studies

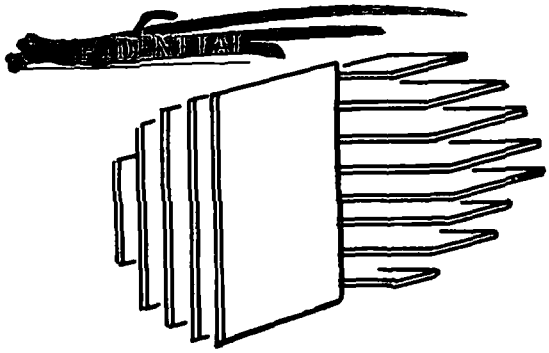

An array of crossed plates which support each other with common notches possibly would unstable but would block flow if the required number of fuel plates were used There also is a possible hot spot at plate juncture

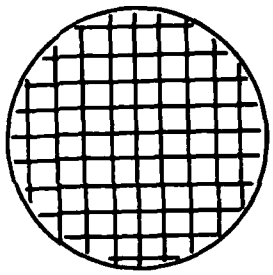

The continuous egg crate concept provides adequate fuel in the section and leaves short unsupported spans in fuel plates

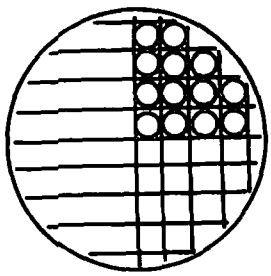

Egg crate loaded with twisted ribbons provides for some fuel grading, gives support for flaps between notches, and reduces the number of notches necessary

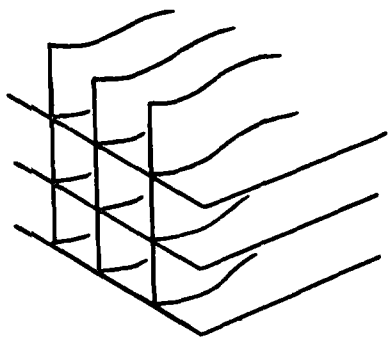

A concept employing longitudinal waves in spaces between flat plates offered advantages of stability and some full grading but involved too many assembly difficulties

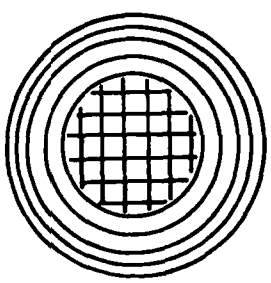

Combination of concentric rings and egg crate concepts were considered for most efficient fuel loading

FIGURE 8 3 Geometries Considered in Grid Design Studies

Another approach for achieving some degree of fuel grading would be in the use of twisted strips inside each cell, as shown in Figure 8 2 This would reduce the number of cells, provide structural support and allow for some fuel grading by variations in fuel content within individual strips This construction would require bonding or welding for attachment of the strips, therefore could not be considered as a primary design candidate

A possible structural weakness in the eggcrate concept may arise from the presence of the panels between the slots which have essentially cantilever support and which might become vibrating reeds in the gas stream This consideration led to the dimensioning of the strips, shown in Figure 8,4, wherein the length of the "reed" is no greater than the width As a possible means of positive support for this portion of the structure, bonding by tunsten vapor deposition was examined briefly One grid model was submitted to the San Fernando Laboratories, Pacoima, California, for processing by the hydrogen-tungsten hexafluoride decomposition process The type of coating which can be obtained by this process is shown in Figure 8 5 It can be seen that the process effectively fills interstices Some experimentation would be required to adjust the processing variables to assure a uniform coating throughout the length of a fuel grid, but the vendor was confident that this could be achieved

Models such as those shown in Figures 8 6 and 8 7 were fabricated from unfueled tungsten for flow testing and for the purpose of evaluating the fabricability of the design Typical detail and the tolerances which were met in the fabrication of these models is shown in Figure 8 4 Shop procedure was nominally as follows the 1/2 and 1/4 in strips were roughed out by hot shearing This consisted of torch heating to a dull red heat before conventional shearing The strips were ground to the final width dimensions

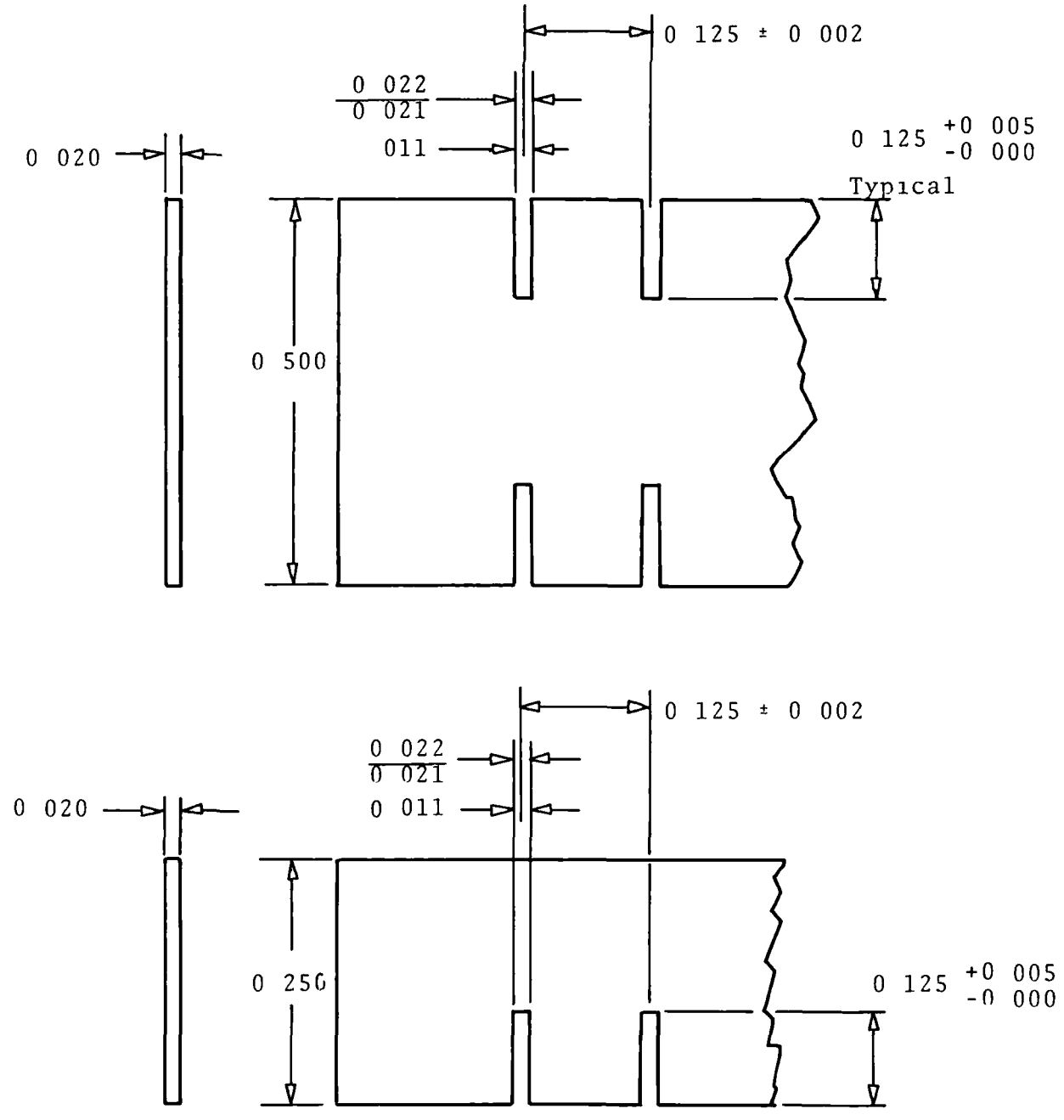

FIGURE 8 4 Typical Detail - Slotted Strips

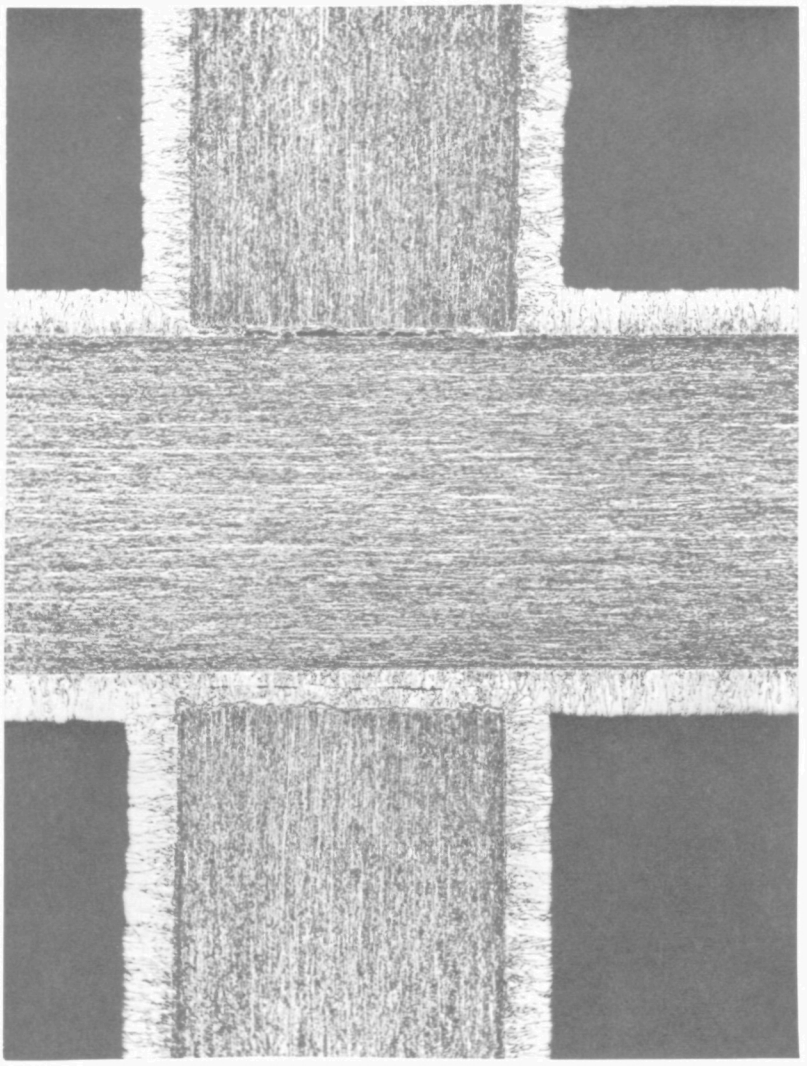

75X

FIGURE 8.5. Transverse Section Through the Grid Coated by the Hydrogen-Tungsten Hexafluoride Decomposition Process

Neg. 5Z5087B

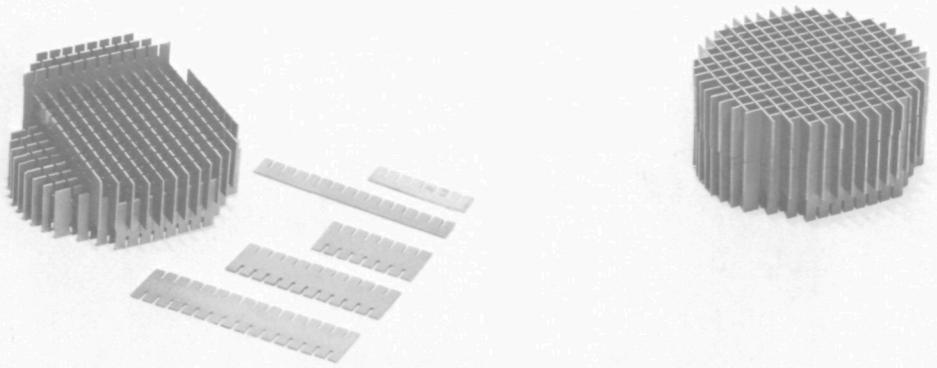

FIGURE 8.6. Model Number One of the Plate Stock Fuel Grid Assembly. Component Parts are Shown at Left. This Model was Built with 0.25 in. Unfueled Tungsten Sheet and was Used in Vapor Deposition Studies

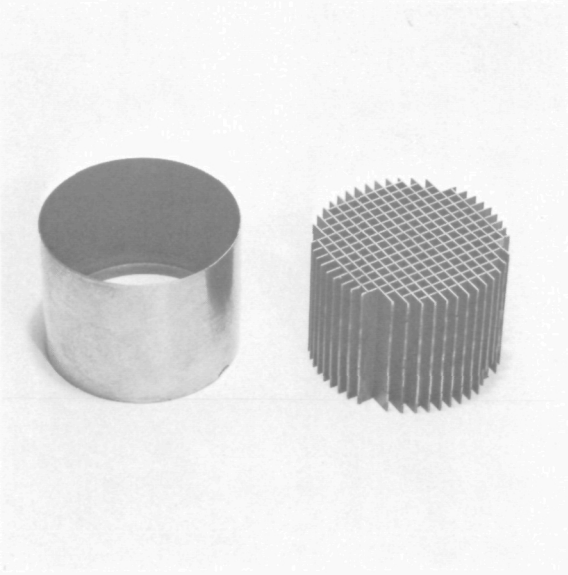

FIGURE 8.7. Model Number Two of the Plate Stock Fuel Grid Built with 0.020 in. Unfueled Tungsten Sheets. This was One of Two Models Delivered for Flow Test Purposes.

The slots were formed by electric discharge machining using a rotating electrode consisting of silver-tungsten discs spaced at the 0 125 in slot intervals Approximately ten strips were stacked and slotted in a single operation The grid was assembled and trimmed to fit the sheath tube ID using EDM with a rotating, cylindrical, brass electrode

The sheath tube which held the fuel grid was a 0 020 in wall tungsten tube with a 0 035 in internal flange to support the grid The length of the sheath tube exceeded the fuel length by 0 125 in to provide for hydrogen mixing between stages

The first sheath tube model was fabricated without difficulty by the EDM process, but subsequent attempts to machine the part were not successful because of crack formation Spinning proved to be the best fabrication method for this tube One such tube was made by the Super Metal Corporation of Santa Fe Springs, California to the dimensions shown in Figure 8 8 The part was formed at elevated temperature starting with a disc of 0 060 in sheet This was spun into a cup, the bottom was partially removed leaving the internal flange, and the OD was then ground to meet the wall thickness tolerance

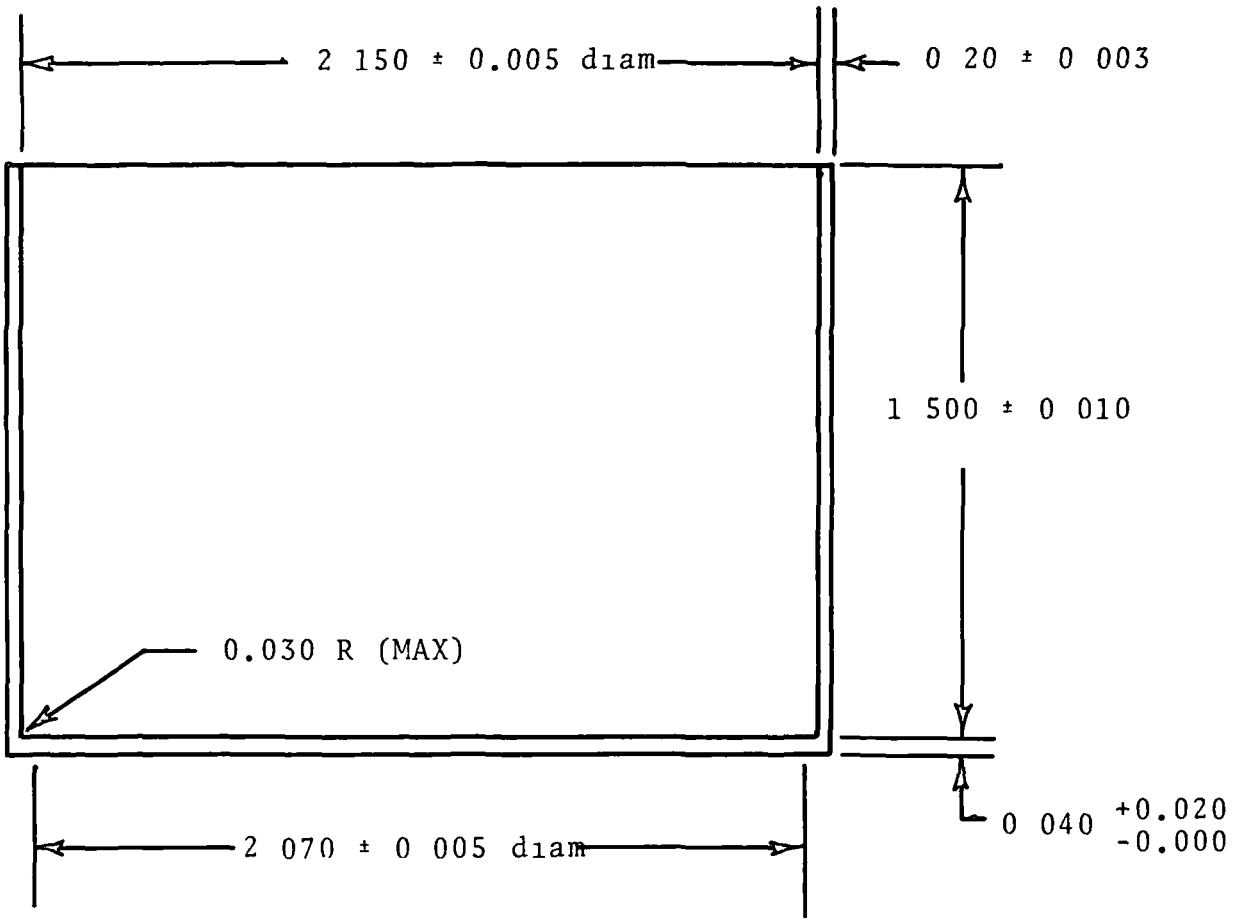

FIGURE 8 8 Detail of Tungsten Sheath Tube Spun from 0 060 in Gage Sheet

8 1 References

1 *R G Cook, M B Goldstein, C W Moon, and W Z Prickett* *Gas-Cooled High Temperature Nuclear Reactor Design Technology*, *APEX-800, Part B, General Electric, Cincinnatti June 30, 1962*

2 *R L Smith* *Cold Flow Tests on Simulated Fuel Elements*, *NASA-MEMO-2811, NASA Lewis Research Center January 14, 1964*

APPENDIX A

TUNGSTEN SUPPORT TUBE
AND ALUMINUM PRESSURE TUBE

SELECTED
STRESS COMPONENT CURVES
FOR
STUDY CASES 4 THROUGH 9

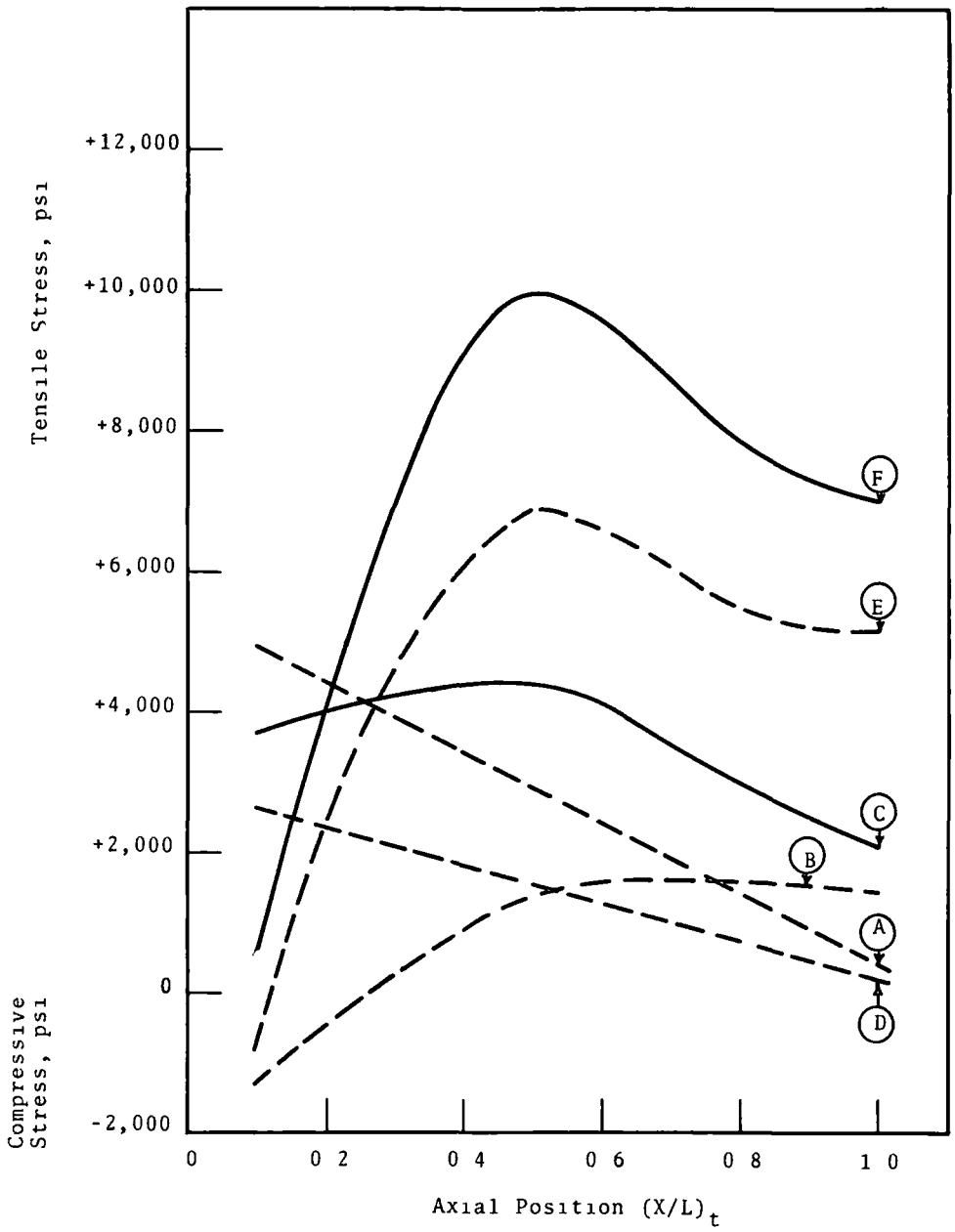

A Hoop Stress
B Stress Due to Radial Gradient
C Total Tangential Stress = A + B
D Aerodynamic + Fuel Weight Stress
E Stress Due to Circumferential Temperature Gradient
F Axial Stress = B + D + E

FIGURE A 1 Cold End Support, Maximum Tungsten Support Stress at Outer Tube Radius - Case 4

CONFIDENTIAL

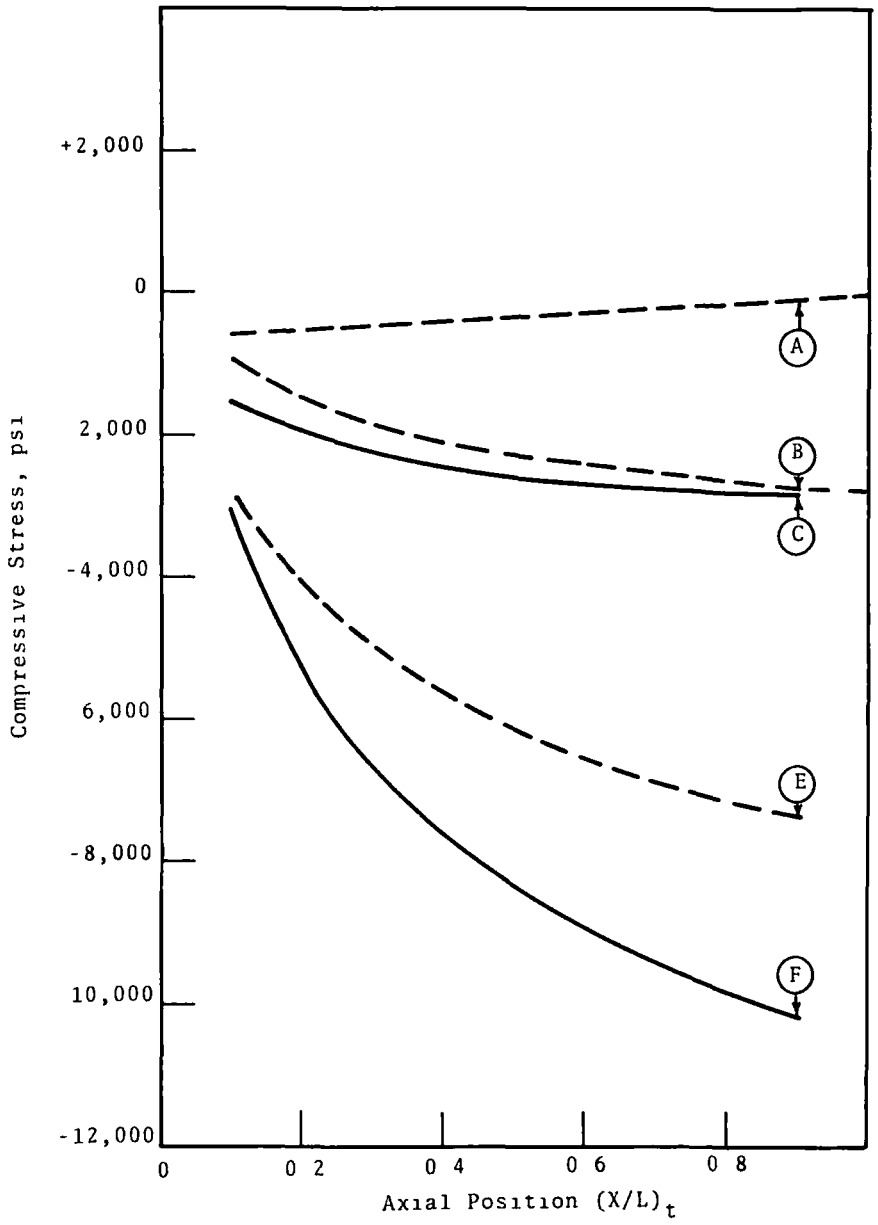

A Hoop Stress
B Stress Due to Radial Temperature Gradient
C Tangential Stress = A + B
E Stress Due to Circumferential Temperature Gradient
F Axial Stress = B + E

FIGURE A 2 Cold End Support, Maximum Aluminum Tube Stress at Inside Tube Radius - Case 4

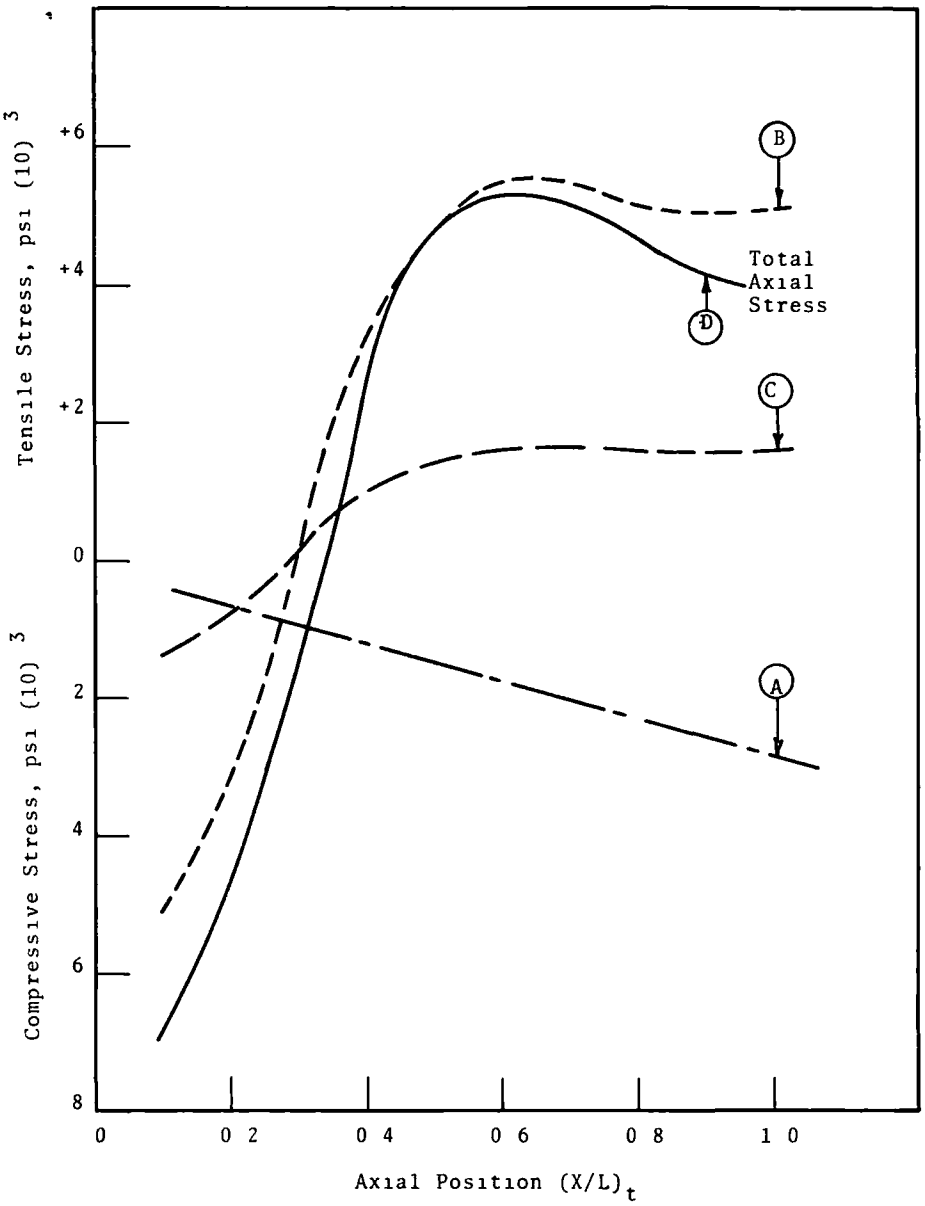

A Aerodynamic + Fuel Weight
B Stress Due to Circumferential Temperature Gradient
C Stress Due to Radial Temperature Gradient
D A + B + C

FIGURE A 3 Hot End Support, Tungsten Sheath Tube Axial Stress at Outside Tube Radius - Case 7

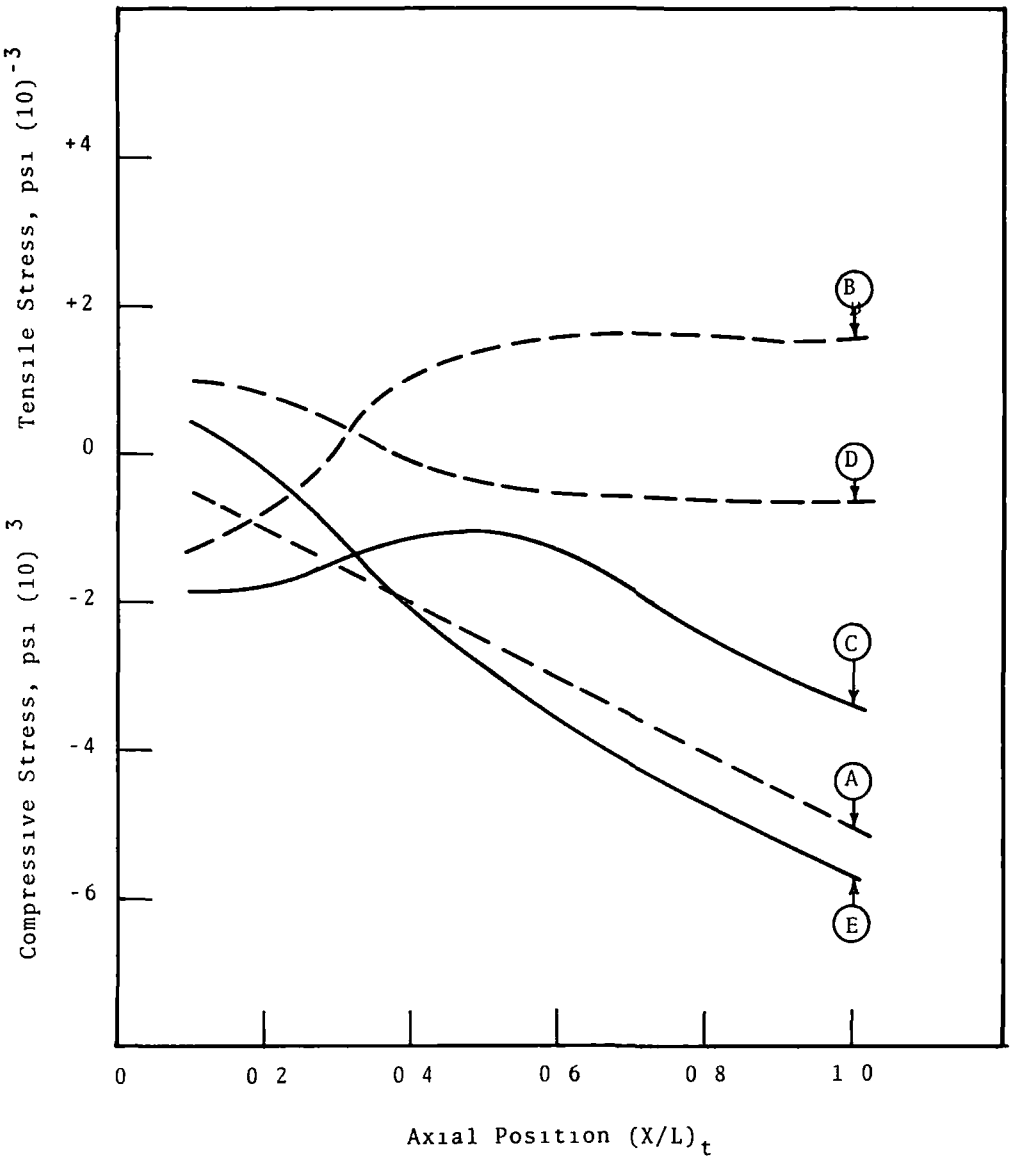

A Hoop Stress
B Stress at Outside Tube Radius Due to Radial Temperature Gradient
C A + B = Tangential Stress at Outside Tube Radius
D Stress at Inside Tube Radius Due to Radial Temperature Gradient
E A + D = Tangential Stress at Inside Tube Radius

FIGURE A 4 Hot End Support, Maximum Tungsten Sheath Tube Tangential Stress Versus Axial Position - Case 7

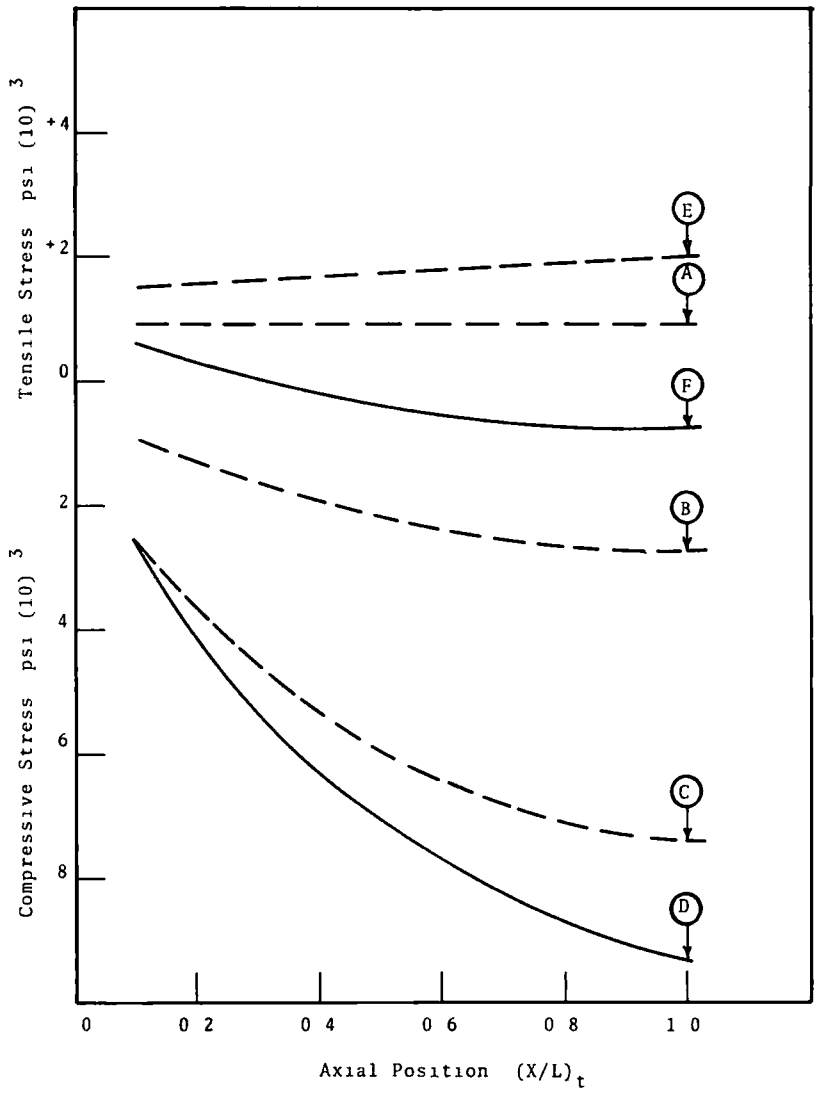

A Axial Aerodynamic + Fuel Weight Stress
B Axial and Tangential Stress Due to Radial Gradient
C Axial Stress Due to Circumferential Gradient
D Total Axial Stress = A + B + C
E Hoop Stress
F Total Tangential Stress = B + E

FIGURE A 5 Hot End Support, Maximum Aluminum Tube, Stress at Tube Inner Radius and Support Contact Case 7

~~CONFIDENTIAL~~

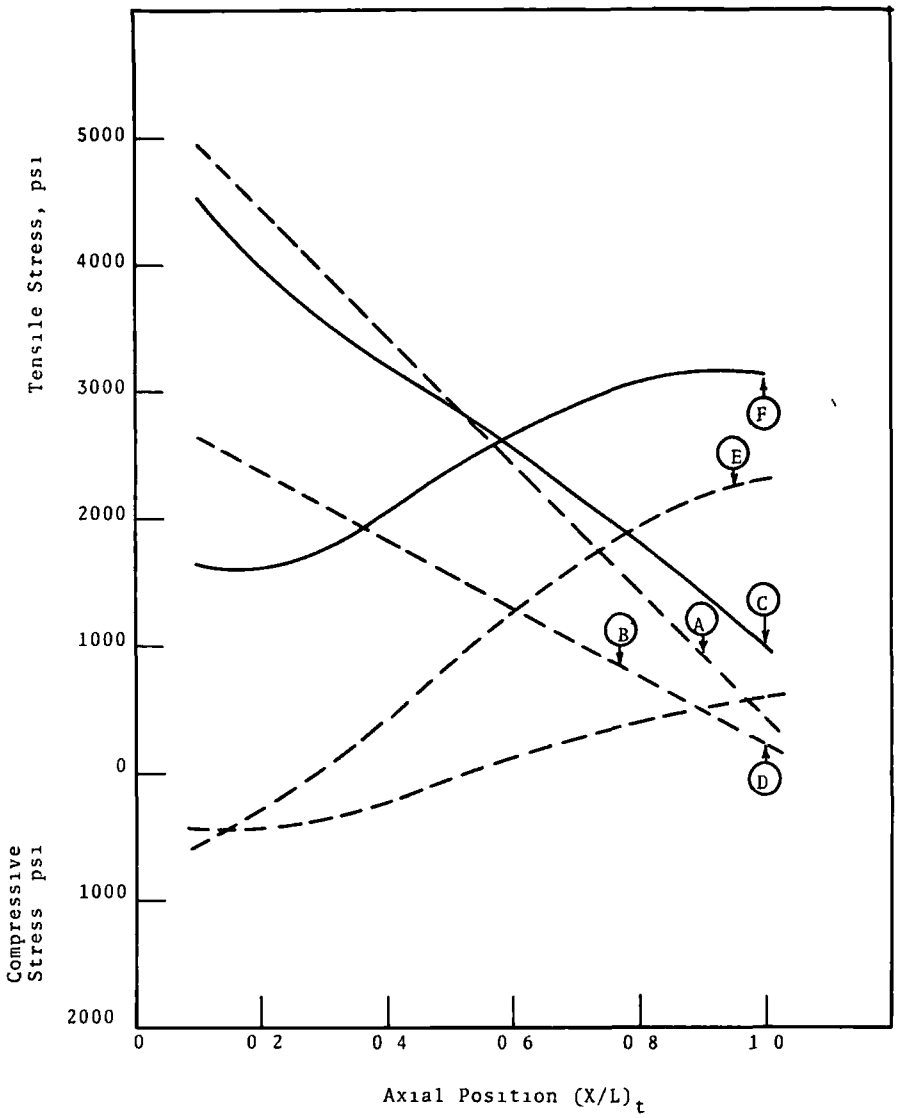

A Hoop Stress
B Stress from Radial Temperature Gradient
C Tangential Stress = A + B
D Aerodynamic + Fuel Weight Stress
E Stress from Circumferential Temperature Gradient
F Axial Stress = B + D + E

FIGURE A 6 Cold End Support, Maximum Tungsten Support Tube Stress at Outer Tube Radius - Case 8

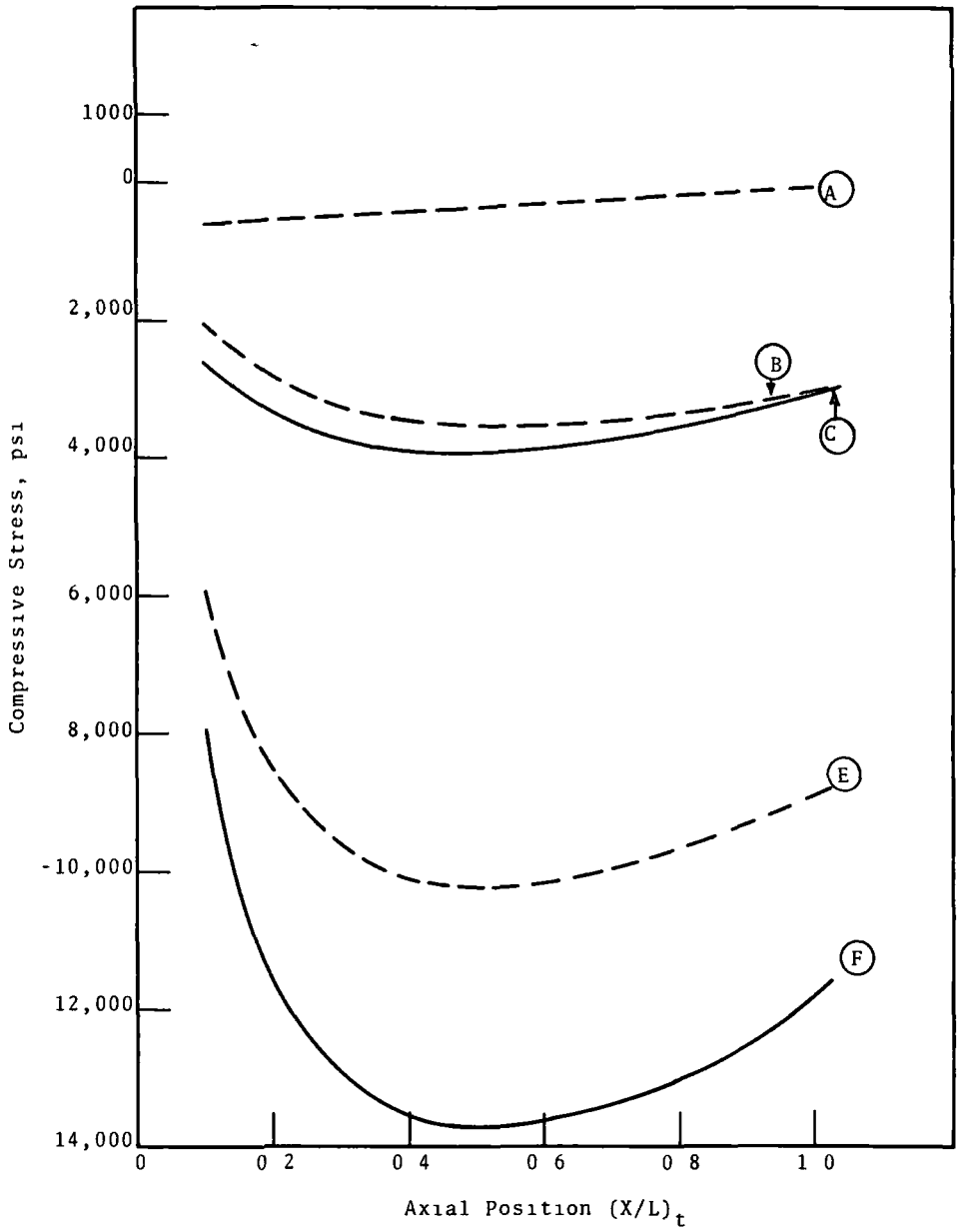

A Hoop Stress
B Stress Due to Radial Temperature Gradient
C Tangential Stress = A + B
E Stress Due to Circumferential Temperature Gradient
F Axial Stress = B + E

FIGURE A 7 Cold End Support, Maximum Aluminum Tube Stress at Inside Tube Radius - Case 8

CONFIDENTIAL

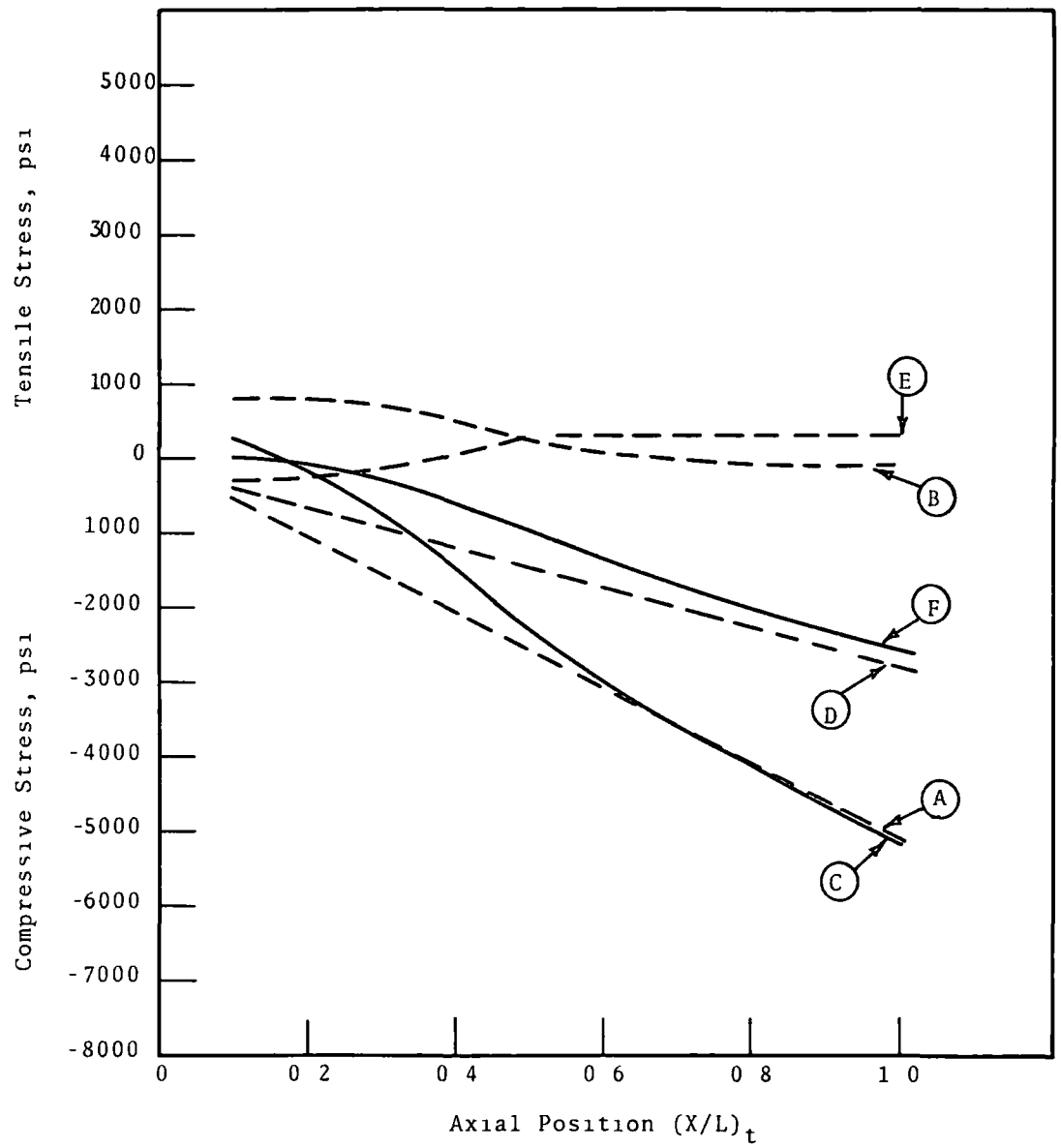

A Hoop Stress
B Stress Due to Radial Temperature Gradient
C Total Tangential Stress
D Aerodynamic + Fuel Weight Stress
E Stress Due to Circumferential Thermal Gradient
F Total Axial Stress

FIGURE A 8 Hot End Support, Tungsten Sheath Tube, Maximum Stress at Inside Tube Radius - Case 9

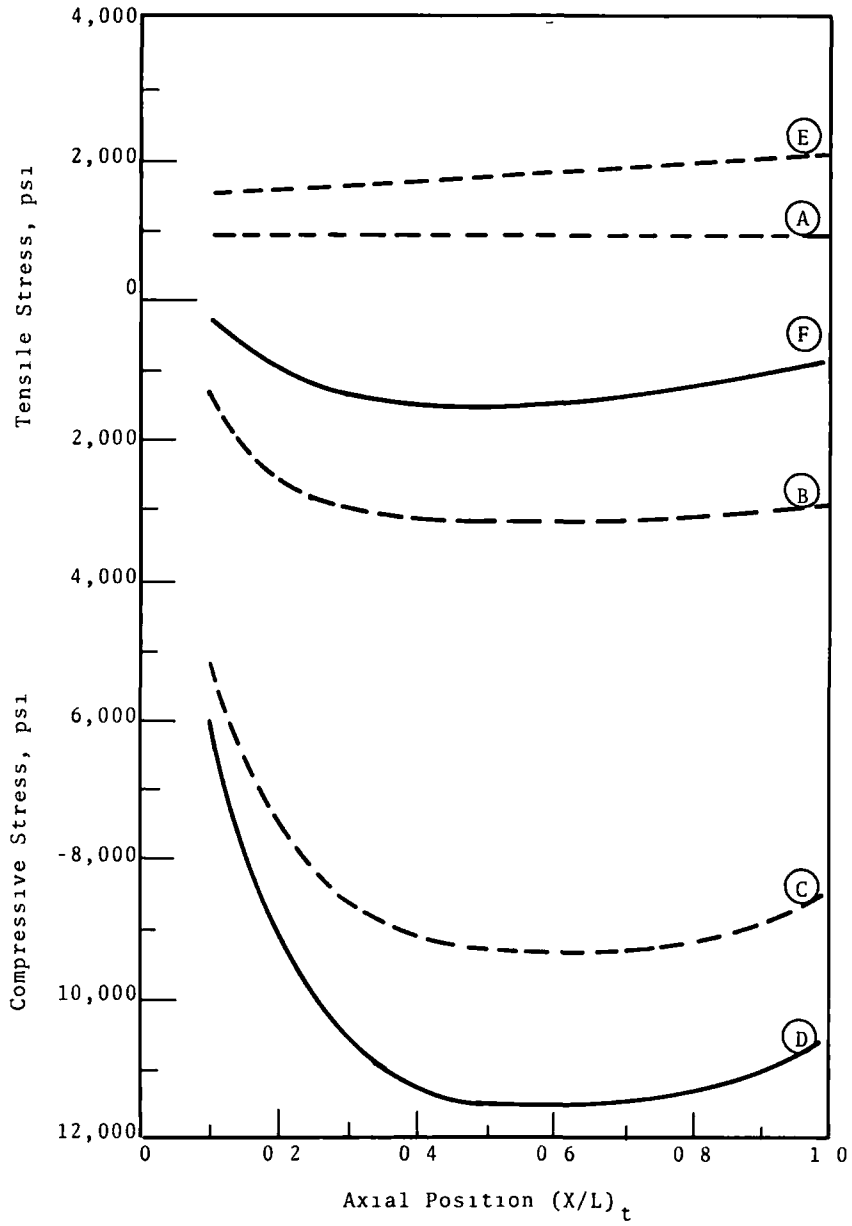

A Axial Aerodynamic + Fuel Weight Stress
B Axial and Tangential Stress Due to Radial Temperature Gradient
C Axial Stress Due to Circumferential Temperature Gradient
D Total Axial Stress = A + B + C
E Hoop Stress
F Total Tangential Stress = B + E

FIGURE A 9 Hot End Support, Maximum Aluminum Tube Stress at Tube Inner Radius and Support Contact, Case 9

APPENDIX B

NOMENCLATURE
and
DERIVATION OF EXPRESSIONS FOR THE CORRUGATED STRIPS LOAD FUNCTIONS AND ELASTIC CONSTANTS

APPENDIX B

NOMENCLATURE

x, y, z	Coordinate system
A, B, C, D	Frame joint locations
m	Bending moment distribution
E	Young's Modulus
I	Moment of inertia
ε	Total angular deformation of the frame from joint A to joint D
ds	Incremental length of frame
a, b, L, s, p	Frame dimensions defined by Figure B 1
$\bar{X}$, $\bar{Z}$	Define the centroid of the frame M/EI diagram
θ, θ_a	Angular deformation (subscript refers to joint location)
α	Angular deformation at joint A due to unit bending moment at A
β	Angular deformation at joint D due to unit bending moment at joint A
w	Frame load per unit length
Δ_Q	Linear deformation of joint A due to frame load
Δ^m	Linear deformation of joint A due to unit bending moment at joint A
Δ_n	Net linear (circumferential) displacement of lateral support segment
N	Number of segments in the corrugated strip lateral support

DERIVATION OF EXPRESSIONS FOR THE CORRUGATED STRIPS LOAD FUNCTIONS AND ELASTIC CONSTANTS

Load Functions

The load functions θ and Δ_o in Figure B 1, i e , angular and linear deformations due to the applied load on the frame, can be determined from the following general Equations[1] (1) through (6)

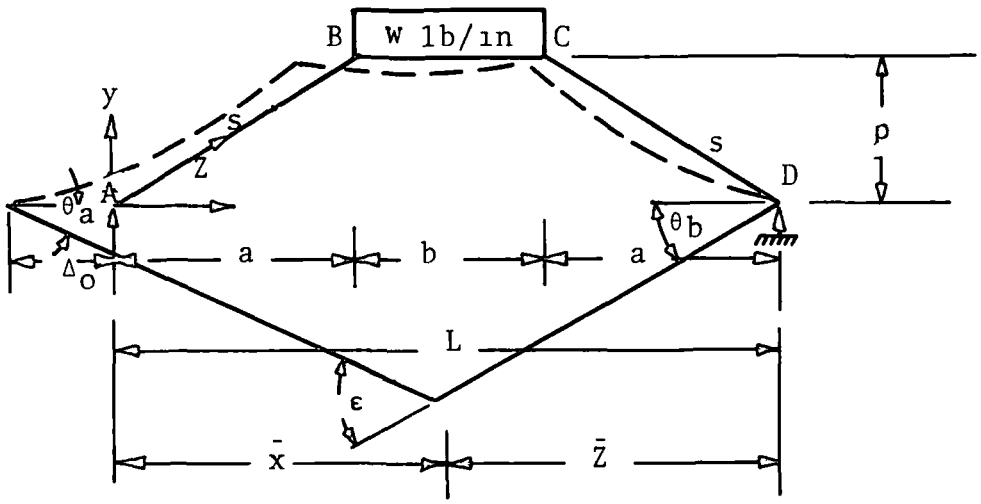

FIGURE B 1 Lateral Support Segment Elastic Constants Model

$$\varepsilon = \int_A^D \frac{m\,ds}{EI} \tag{1}$$

$$\bar{x} = \frac{1}{\varepsilon} \int_A^D \frac{m x\,ds}{EI} \tag{2}$$

$$\bar{z} = L - \bar{x} \tag{3}$$

$$\theta_a = \frac{\varepsilon\,\bar{z}}{L} \tag{4}$$

$$\theta_b = \frac{\varepsilon \bar{x}}{L} \tag{5}$$

$$\Delta_o = \int_A^D \frac{myds}{EI} \tag{6}$$

Figure B 1 and the table of nomenclature define the individual terms in the above equations

Considering EI constant, Equation (1) can be expresses

$$EI\varepsilon = \int_o^s M_{AB}\, dz + \int_a^{a+b} M_{BC}\, dx + \int_o^s M_{CD}\, dz$$

Substituting the appropriate bending moments gives

$$EI\varepsilon = \frac{wab}{2s}\int_o^s z dz + \frac{w}{2}\int_a^{a+b}\left[bx - (x-a)^2\right] dx$$

$$+ \frac{wab}{2}\int_o^s \left[1 - \frac{z}{s}\right] dz$$

and, after integrating

$$EI\varepsilon = \frac{wabs}{2} + \frac{w}{2}\left[\frac{L^3}{6} - 2a^2 L + \frac{8a^3}{3}\right]$$

Since the frame loading is symmetric

$$\bar{x} = z = \frac{L}{2}$$

and $EI\theta_a = EI\theta_b = EI\theta$

$$EI\theta = \frac{wabs}{4} + \frac{w}{2}\left[\frac{L^3}{12} - a^2L + \frac{4a^3}{3}\right] \tag{7}$$

Considering EI constant, Equation (6) can be expressed

$$EI\Delta_o = \int_A^B M_{AB}\, y_{AB}\, ds + \int_B^C M_{BC}\, y_{BC}\, dx + \int_C^D M_{CD}\, y_{CD}\, ds$$

where

$$y_{AB} = \frac{p_z}{s},\ y_{BC} = p,\ y_{CD} = p\left(1 - \frac{z}{s}\right)$$

Substituting the appropriate bending moments and integrating gives

$$EI\Delta_o = \frac{wabp}{2s^2}\int_o^s z^2\, dz + \frac{w}{2}\int_a^{a+b}\left[bx - (x-a)^2\right] dx$$

$$+ \frac{wabp}{2}\int_o^s \left[1 - \frac{z}{s}\right]^2 dz$$

$$EI\Delta_o = \frac{wabps}{3} + wp\left[\frac{L^3}{12} - a^2L + \frac{4a^3}{3}\right] \tag{8}$$

Elastic Constants

The elastic constants α, β, and Δ^m due to unit moment at joint A depend on the geometrical shape of the frame (Figure B 2) These constants may also be determined from the general Equations (1) through (6) In this case, however,

$$\alpha = \frac{\varepsilon\, \bar{z}}{L} \tag{9}$$

$$\beta = \frac{\varepsilon\, \bar{x}}{L} \tag{10}$$

$$\Delta_{\theta_o}^m = \int_A^D \frac{myds}{EI} \tag{11}$$

CONFIDENTIAL

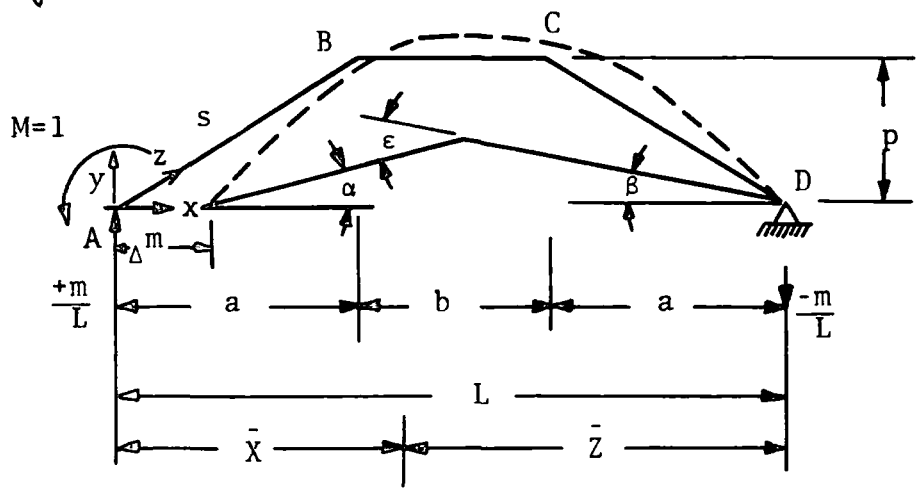

FIGURE B 2 Lateral Support Segment Elastic Constants Model

Considering unit moment at joint A and a frame segment with constant EI, Equation (1) can be written

$$EI\varepsilon = \int_A^B M_{AB}\, dz + \int_a^{a+b} M_{BC}\, dx + \int_o^x M_{CD}\, dz$$

or

$$EI\varepsilon = \int_o^s \left[1 - \frac{az}{Ls}\right] dz + \int_a^{a+b} \left[1 - \frac{x}{L}\right] dx$$

$$+ \int_o^s \left[1 - \frac{a}{L} - \frac{b}{L} - \frac{az}{Ls}\right] dz$$

which yields

$$EI\varepsilon = \left(s + \frac{b}{2}\right) \qquad (12)$$

From Equation (2)

$$\bar{x} = \frac{1}{EI\varepsilon}\left\{\int_o^s M_{AB}\, x_{AB}\, dz \int_a^{a+b} M_{BC}\, x_{BC}\, dx + \int_o^s M_{CD}\, x_{CD}\, dz\right\}$$

where

$$x_{AB} = \frac{az}{s}\ ,\ x_{BC} = x \qquad x_{CD} = \frac{az}{s} + a+b$$

$$\bar{x} = \frac{1}{\left(s + \frac{b}{2}\right)}\left\{\frac{a}{s}\int_o^s \left[1 - \frac{az}{Ls}\right] z dz + \int_a^{a+b} \left[1 - \frac{x}{L}\right] x dx + \int_o^s \left[1 - \frac{a}{L} - \frac{b}{L} - \frac{az}{Ls}\right]\left[\frac{az}{s} + a + b\right] dz\right\}$$

and

$$\bar{x} = \frac{2as\ (3L - 2a) + L^3 - 6a^2L + 4a^3}{3L\ (2s + b)} \tag{13}$$

Solving for $\bar{z}$ from Equation (3) gives

$$\bar{z} = L - \left[\frac{2as\ (3L - 2a) + L^3 - 6a^2L + 4a^3}{3L\ (2s + b)}\right] \tag{14}$$

The elastic constants α and β can now be determined from the equations

$$EI\alpha = \left(s + \frac{b}{2}\right)\ \frac{\bar{z}}{L} \tag{15}$$

and

$$EI\beta = \left(s + \frac{b}{2}\right) \frac{\bar{x}}{L} \tag{16}$$

where $\bar{z}$ and $\bar{x}$ are defined by Equations (14) and (13)

The linear deformation of joint A due to unit moment can be determined from Equation (11) as follows

$$EI\Delta^m = \int_0^s \left[1 - \frac{az}{Ls}\right] y_{AB}\, dz + \int_a^{a+b} \left[1 - \frac{x}{L}\right] y_{BC}\, dx$$

$$+ \int_0^s \left[1 - \frac{a}{L} - \frac{b}{L}\frac{az}{Ls}\right] y_{CD} dz$$

where

$$y_{AB} = p\,\frac{z}{s}\ ,\ y_{BC} = p,\ y_{CD} = p\,(1 - \frac{z}{s})$$

Substituting these values of y into the equation for $EI\Delta^m$ and integrating gives

$$EI\Delta^m = \frac{P}{2}\,(s + b) \tag{17}$$

The lateral support configurations of interest have segment dimensions shown in Table B 1

TABLE B 1 LATERAL SUPPORT SEGMENT DIMENSIONS

Number of Segments/360° N	a, in	b, in	p, in	s, in	L, in
4 *	0 693	0 132	0 429	0 814	1 518
8	0 345	0 132	0 196	0 397	0 822
12	0 212	0 132	0 151	0 260	0 556
16	0 143	0 132	0 136	0 197	0 418

The load functions and elastic constants for each lateral support configuration are indicated in Table B 2

TABLE B 2 LOAD FUNCTIONS AND ELASTIC CONSTANTS

Number of Segments/360° N	Load Functions		Elastic Constants		
	$EI\theta/w$, in ^{3}	$EI\Delta_o/w$, in ^{4}	$EI\alpha$, in	$EI\beta$, in	$EI\Delta m$, in ^{2}
4 *	$2\ 11(10)^{-2}$	$1\ 28(10)^{-2}$	0 590	0 292	$2\ 03(10)^{-1}$
8	$6\ 12(10)^{-3}$	$1\ 81(10)^{-3}$	0 310	0 153	$5\ 18(10)^{-2}$
12	$2\ 82(10)^{-3}$	$6\ 68(10)^{-4}$	0 219	0 106	$2\ 96(10)^{-2}$
16	$1\ 64(10)^{-3}$	$3\ 62(10)^{-4}$	--	--	$2\ 24(10)^{-2}$

* *Four-segment lateral supports with dimensions indicated in Table B 1 cannot be placed in the 1/8-in static gas gap This configuration was of interest only in estimating the maximum moment to load ratio for the 16-segment support configuration (See Figure B 4)*

Lateral Support Bending Moment at Tungsten Tube

The statically indeterminate lateral support bending moments at tungsten tube reaction points can now be determined in terms of the applied lateral support segment loads An eight segment lateral support is selected to illustrate the procedure Figure B 3 indicates a symmetrical portion of the eight-segment lateral support configuration with reaction moments and applied loads referenced to the pinned end condition

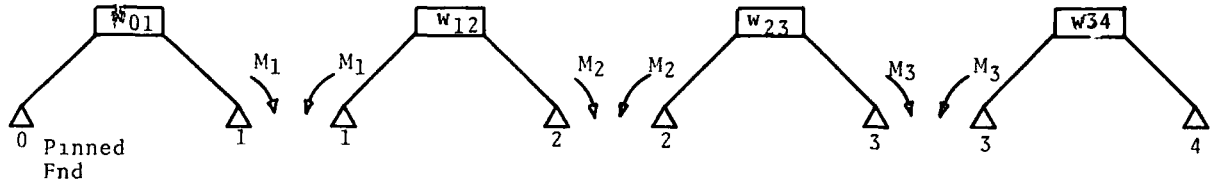

FIGURE B 3 Reaction Moments on Symmetrical Portion of Eight Segment Lateral Support

The selected sign convention considers the angular deformation at a reaction to be positive when the moment or load produces clockwise rotation The angular deformation at reaction 1, produced by the load on segment 0-1 is -EIθ or $-6\ 12(10)^{-3}\ w_{01}$ The angular deformation at reaction 1, due to bending moment M_1, is M_1 times the angular deformation caused by unit moment at reaction 1 The angular deformation at reaction 1 is therefore

$$-6\ 12(10)^{-3}\ w_{0,1} + 0\ 31\ M_1$$

Considering the angular deformation at reaction 1 due to the load and moments applied to segment 1-2 gives

$$6\ 12(10)^{-3}\ w_{1,2} - 0\ 31\ M_1 - 0\ 153\ M_2$$

Equating the angular deformations at reaction 1 gives

$$0\ 62\ M_1 + 0\ 153\ M_2 = 6\ 12(10)^{-3}\ (w_{0,1} + w_{1,2}) \qquad (18)$$

Similar equations expressing the bending moments in terms of the applied segment loads can be written at each reaction location

At reaction 2,

$$0\ 153\ M_1 + 0\ 62\ M_2 + 0\ 153\ M_3 = 6\ 12(10)^{-3}\ (w_{1,2} + w_{2,3}) \tag{19}$$

and at reaction 3,

$$0\ 153\ M_2 + 0\ 62\ M_3 = 6\ 12(10)^{-3}\ (w_{2,3} + w_{3,4}) \tag{20}$$

Simultaneous solution of Equations (18), (19), and (20) gives the three lateral support bending moments at tungsten reaction points The general moment equation to be applied at each reaction point can be expressed

$$\beta M_{J-1} + 2\alpha M_J + \beta M_{J+1} = \theta\ (w_{J-1,J} + w_{J,J+1}) \tag{21}$$

In the case of radially symmetric loads

$$w_{J-1,J} = w_{J,J+1}$$

The desired bending moments in terms of lateral support segment loads are indicated in Table B 3 for various numbers of segments

TABLE B 3 LATERAL SUPPORT BENDING MOMENTS AT TUNGSTEN TUBE CONTACT LOCATIONS

Number of Segments/360° N	M_1/w, in ^{2}	M_2/w, in ^{2}	M_3/w, in ^{3}	M_4/w, in ^{2}	M_5/w, in ^{2}
4	$3\ 58(10)^{-2}$	--	--	--	--
8	$1\ 70(10)^{-2}$	$1\ 14(10)^{-2}$	$1\ 70(10)^{-2}$	--	--
12	$1\ 09(10)^{-2}$	$8\ 06(10)^{-3}$	$9\ 0\ (10)^{-3}$	$8\ 06(10)^{-3}$	$1\ 09(10)^{-2}$
16	$0\ 79(10)^{-2}$*	--	--	--	--

* *Estimated maximum moment - see Figure B 4*

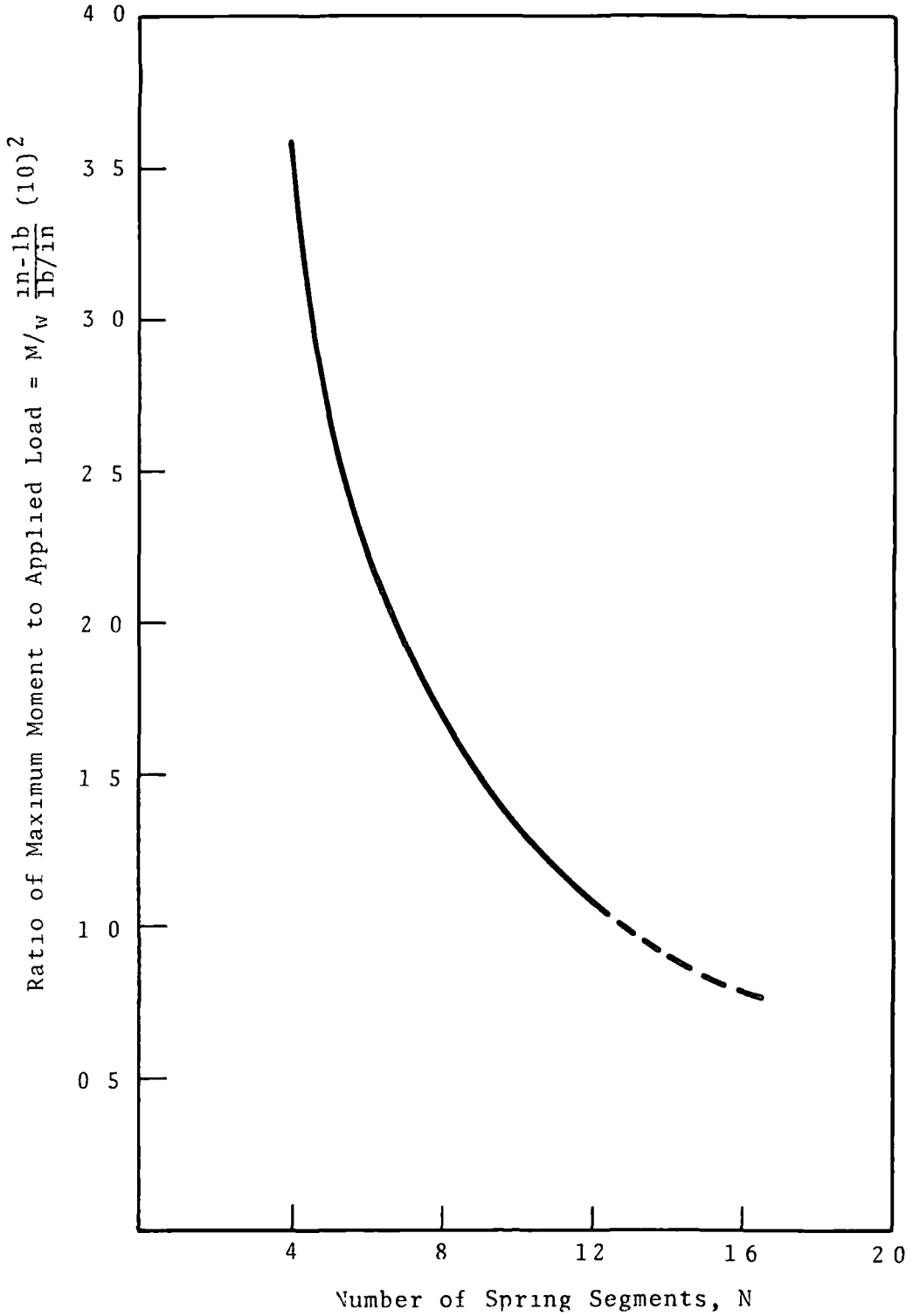

FIGURE B 4 Moment/Load Ratio Versus Number of Spring Segments

Allowable Segment Load

Having determined the value and tungsten tube contact location at which maximum lateral support bending moment occurs, the allowable segment loads can be calculated from the well-known flexure formula Assuming unit depth of lateral support segment

$$\sigma_b = \frac{6M}{h^2}$$

σ_b = allowable bending stress

M = maximum bending moment

h = lateral support segment thickness

The hot condition allowable loads are calculated for the eight-segment lateral support with temperature distributions of study Case 10 (See Table 3 3, Section 3 for Case 10 description) Allowable bending stress and maximum lateral support segment temperatures for Case 10 are indicated by Figure B 5

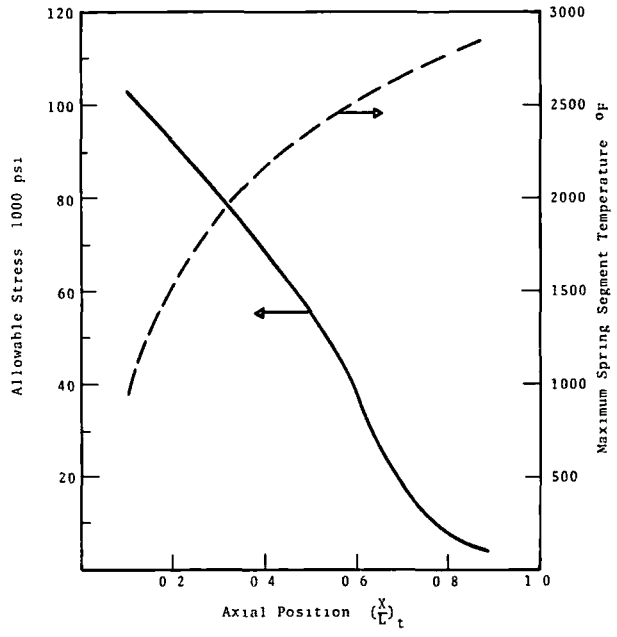

FIGURE B 5 Maximum Strip Temperature and Allowable Bending Stress Versus Axial Position

CONFIDENTIAL

$$\sigma_b = \frac{6\ (1\ 70)(10)^{-2}\ w}{h^2}$$

or

$$\frac{W}{h^2} = 1\ 293\ \sigma_b \qquad (22)$$

where

$$W = bw = 0\ 132\ w$$

Table B 4 shows the total allowable lateral support segment load at axial positions between 0 1 and 0 9, with three assumed segment thicknesses

TABLE B 4 ALLOWABLE LATERAL SUPPORT SEGMENT LOADS FOR 0 003, 0 006 AND 0 010 in THICK SEGMENTS (8 Segment Model)

Axial Position, $(X/L)_t$	W/h^2, lb/in^2	Segment Thickness h, in	Allowable Load W, lb
0 1	$1\ 33(10)^5$	$3\ 0(10)^{-3}$	1 20
		$6\ 0(10)^{-3}$	4 78
		$1\ 0(10)^{-2}$	13 30
0 3	$1\ 035(10)^5$	$3\ 0(10)^{-3}$	0 93
		$6\ 0(10)^{-3}$	3 73
		$1\ 0(10)^{-2}$	10 35
05	$7\ 37(10)^4$	$3\ 0(10)^{-3}$	0 66
		$6\ 0(10)^{-3}$	2 65
		$1\ 0(10)^{-2}$	7 37
0 7	$2\ 33(10)^4$	$3\ 0(10)^{-3}$	0 21
		$6\ 0(10)^{-3}$	0 84
		$1\ 0(10)^{-2}$	2 33
0 9	$4\ 33(10)^3$	$3\ 0(10)^{-3}$	0 039
		$6\ 0(10)^{-3}$	0 156
		$1\ 0(10)^{-2}$	0 433

Lateral Support Segment Deflection

The net circumferential displacement of the lateral support segment 0-1 can be estimated by substracting the displacements caused by the bending moment at reaction location 1 from the displacement due to the applied load on segment 0-1

$$EI\Delta_n = EI\Delta_o - EI\Delta^m (M) \qquad (23)$$

Table B 5 shows the deflections due to applied load and reaction moment The total lateral segment load is also indicated in terms of the net circumferential deflection for various numbers of segments

TABLE B 5 CIRCUMFERENTIAL DISPLACEMENTS OF LATERAL SUPPORT SEGMENT

Number of Segments N	$\frac{EI\Delta_o}{w}$, in^4	$EI\Delta^m$, in^2	$\frac{M_1}{w}$, in^2	$\frac{EI\Delta^m M_1}{w}$, in^4	$\frac{EI\Delta_n}{w}$, in^4	W, lb
4	$1\ 28(10)^{-2}$	$2\ 03(10)^{-1}$	$3\ 58(10)^{-2}$	$7\ 27(10)^{3}$	$5\ 53(10)^{-3}$	$23\ 9\ EI\Delta_n$
8	$1\ 81(10)^{3}$	$5\ 18(10)^{-2}$	$1\ 70(10)^{-2}$	$8\ 81(10)^{4}$	$9\ 29(10)^{4}$	$142\ EI\Delta_n$
12	$6\ 68(10)^{-4}$	$2\ 96(10)^{-2}$	$1\ 09(10)^{-2}$	$3\ 23(10)^{4}$	$3\ 45(10)^{-4}$	$392\ EI\Delta_n$
16	$3\ 62(10)^{4}$	$2\ 24(10)^{-2}$	$7\ 90(10)^{-3}$	$1\ 77(10)^{-4}$	$1\ 85(10)^{-4}$	$714\ EI\Delta_n$

In the calculation of support segment load-deflection characteristics values of Young's Modulus for tungsten[2] are taken at the average segment temperature

Consider reactor operating conditions with lateral support segment temperatures associated with study Case 10 and an eight-segment corrugated strip The average lateral support temperatures, at various axial positions along the fuel column are indicated in Table B 6 These temperatures are based on an assumed 0 010-in corrugated strip thickness

TABLE B 6 AVERAGE SEGMENT TEMPERATURE, STATIC YOUNG'S MODULUS AND TOTAL SEGMENT LOAD VERSUS AXIAL POSITION ALONG FUEL COLUMN (Case 10, with 8 Segment Support Model)

Axial Position, $(X/L)_t$	Average Segment Temperature, °F	Static Youngs's Modulus, E $(10)^6$ lb/in	Total Segment Load $W = 142\ EI\Delta_n$
0 1	805	45 8	$6\ 51(10)^9\ I\Delta_n$
0 3	1710	39 6	$5\ 62(10)^9\ I\Delta_n$
0 5	2032	37 2	$5\ 28(10)^9\ I\Delta_n$
0 7	2251	35 3	$5\ 01(10)^9\ I\Delta_n$
0 9	2383	34 0	$4\ 83(10)^9\ I\Delta_n$

The use of average support temperatures based on 0 010 in thick segments gives somewhat conservative deflections for the 0 003 and 0 006 in thick segments since the latter will operate at slightly lower temperatures

Substitution of the appropriate moment of inertia values corresponding to 0 003, 0 006, and 0 010 in thick segments into the total segment load expressions of Table B 6 gives the load (in terms of circumferential deflection) as a function of axial position

TABLE B 7 SEGMENT LOAD AS A FUNCTION OF AXIAL POSITION, SEGMENT THICKNESS AND CIRCUMFERENTIAL DISPLACEMENT

Segment Thickness h, in	I in ^{4}	$(X/L)_t = 0\ 1$ $W = 6\ 5(10)^9$ $I\Delta_n$	$(X/L)_t = 0\ 3$ $W = 5\ 62(10)^9$ $I\Delta_n$	$(X/L)_t = 0\ 5$ $W = 5\ 28(10)^9$ $I\Delta_n$	$(X/L)_t = 0\ 7$ $W = 5\ 01(10)^9$ $I\Delta_n$	$(X/L)_t = 0\ 9$ $W = 4\ 83(10)^9$ $I\Delta_n$
0 003	$2\ 25(10)^{-9}$	$14\ 65\ \Delta_n$	$12\ 65\ \Delta_n$	$11\ 9\ \Delta_n$	$11\ 25\ \Delta_n$	$10\ 85\ \Delta_n$
0 006	$1\ 80(10)^{-8}$	$11\ 70\ \Delta_n$	$101\ 0\ \Delta_n$	$95\ 0\ \Delta_n$	$90\ 0\ \Delta_n$	$86\ 9\ \Delta_n$
0 010	$8\ 33(10)^{-8}$	$542\ \Delta_n$	$468\ \Delta_n$	$440\ \Delta_n$	$417\ \Delta_n$	$402\ \Delta_n$

Neglecting the change in frame length due to bending, an approximate relationship between the lateral displacement λ and the net circumferential displacement Δ_n can be determined from the frame geometry

From Figure B 6

$$(a + e)^2 + (p-\lambda)^2 = (a - e + \Delta)^2 + (p - \lambda)^2$$

or

$$e = \frac{\Delta}{2}$$

Also

$$\left(a + \frac{\Delta}{2}\right)^2 + (p - \lambda)^2 = a^2 + p^2$$

from which

$$\lambda = p - \left[p^2 - a\Delta - \frac{\Delta}{4}^2\right]^{1/2} \qquad (24)$$

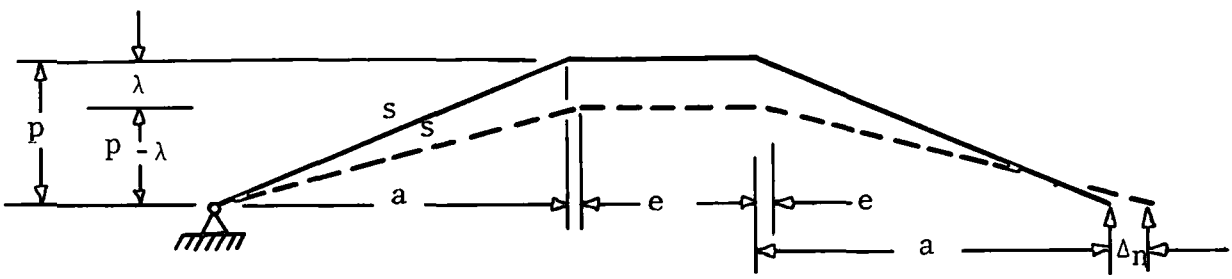

FIGURE B 6 Lateral Support Frame Geometry

Figure B 7 shows the relationship between the circumferential and lateral segment displacements

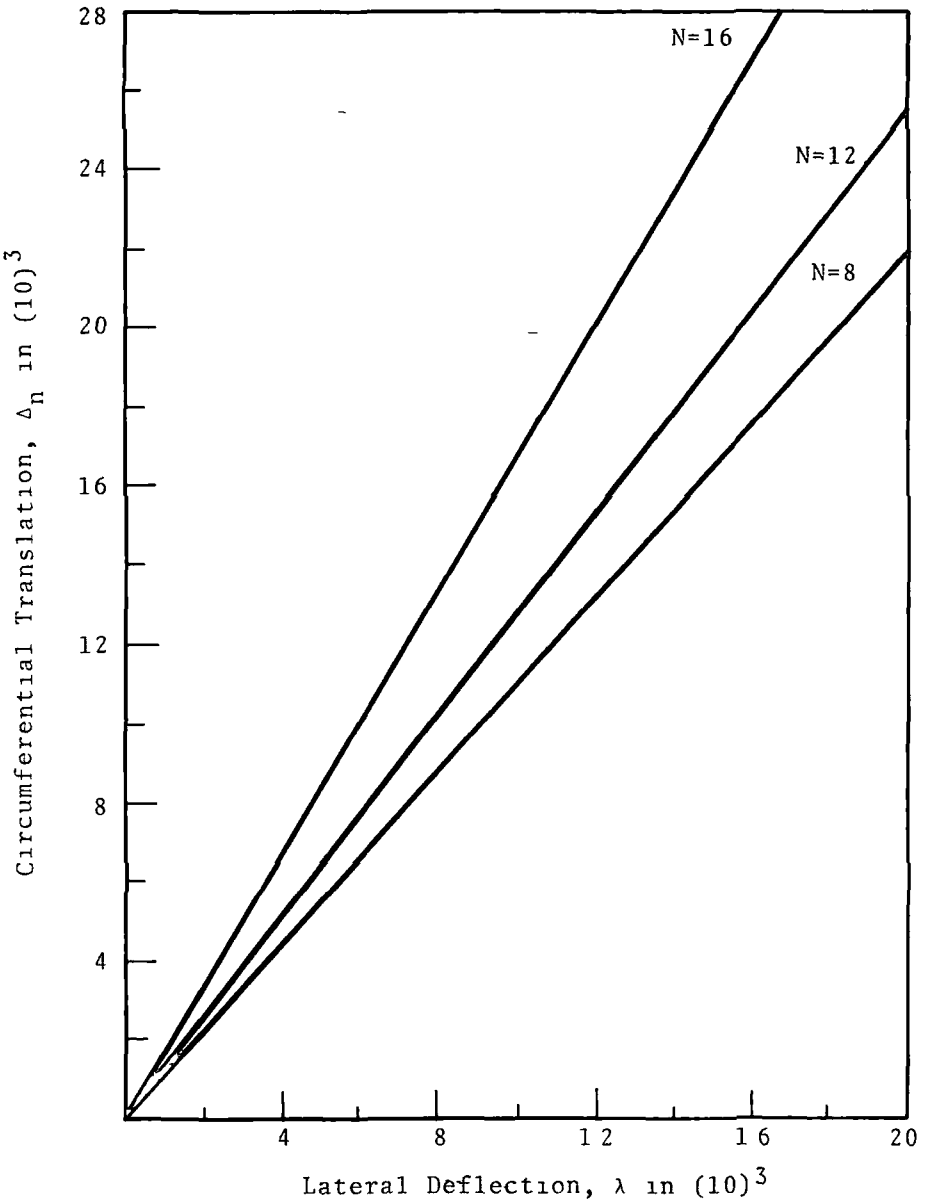

FIGURE 7 Circumferential Translation Δ_n Versus Support Lateral Deflection

The eight-segment support lateral load-deflection characteristics can now be determined as a function of axial location along the fuel column Selection of a lateral deflection λ, and substitution of the appropriate value of circumferential displacement Δ_n (from Figure B 7) into the tabulated loads in

Table B 7 gıve the desıred result A cross-plot of allowable support segment loads at each axıal posıtıon $\frac{X}{L}$ provıdes an ındıcatıon of the lımıtıng lateral deflectıon of the segment along the fuel column (See Fıgure 4 4)

A sımılar procedure yıelds the cold condıtıon load-deflectıon characterıstıcs of the lateral support segment (Fıgure 4 7)

B 1 References

1 *M Smolıra "Analysıs of Structures," Concrete Publıcatıons Ltd , London, 1955 pp 44*

2 *F F Schmıdt and H R Ogden The Engıneerıng Propertıes of Tungsten and Tungsten Alloys, DMIC-191, Fıgure A-15 September 27, 1963*

APPENDIX C

SOLUTION OF A HOMOGENEOUS CLAMPED-PINNED TUBE WITH MATERIAL DAMPING AND WITH END RESTRAINT EXCITATION

APPENDIX C

SOLUTION OF A HOMOGENEOUS CLAMPED-PINNED TUBE WITH MATERIAL DAMPING AND WITH END RESTRAINT EXCITATION

For small elastic deformations, the classical flexural formula states

$$E^1 I = \frac{\partial^2 y}{\partial x^2} = M \tag{1}$$

where E^1 = Young's modulus
I = moment of inertia
y = beam deflection
x = axial distance from boundary
M = bending moment

In the absence of externally applied moments

$$\frac{\partial M}{\partial x} = V \tag{2}$$

where V = vertical shear

and

$$\frac{\partial V}{\partial x} = f_y \tag{3}$$

where f_y = applied force distribution in the Y plane

From Newton's second law

$$-\rho A \frac{\partial^2 y}{\partial t^2} = \frac{\partial V}{\partial x} = \frac{\partial^2}{\partial x^2}\left(E^1 I \frac{\partial^2 y}{\partial x^2}\right) \tag{4}$$

results which defines the motion of a conservative system Equation (4) may be written as

$$m\frac{\partial^2 y}{\partial t^2} + \frac{\partial^2}{\partial x^2}\left(E^1 I \frac{\partial^2 y}{\partial x^2}\right) = \rho \tag{5}$$

where m = mass per unit length of the tube

Material or structural damping of the system is required to afford a better model of the tungsten support tube Sewaza[1] recommends a Stokes viscosity coefficient This would, however, simulate the damping by a frequency dependent term Recent investigations[2] indicate that material damping is independent of frequency which has resulted in the suggestion that structural damping be modeled by replacing the Young's modulus, E^1, in the conservative system defined by Equation (5) by

$$E^1 = E + \frac{E}{Q\omega}\left(\frac{\partial}{\partial t}\right) \tag{6}$$

where E = dynamic Young's modulus in nonconservative system
Q = Q of system
ω = circular frequency
$\frac{\partial}{\partial t}$ = operator

Making this substitution results in

$$\frac{\partial^2}{\partial x^2}\left(EI\frac{\partial^2 y}{\partial x^2} + \frac{EI}{Q\omega}\frac{\partial^3 y}{\partial x^2 \partial t}\right) + m\frac{\partial^2 y}{\partial t^2} = 0 \tag{7}$$

or

$$\frac{\partial^4 y}{\partial x^4} + \frac{1}{Q\omega}\frac{\partial^5 y}{\partial x^4 \partial t} + \frac{M}{EI}\frac{\partial^2 y}{\partial t^2} = 0 \tag{8}$$

Assuming a product solution of the form

$$y(x,t) = X(x)T(t)$$

results in

$$TX^{IV} + \frac{1}{Q}T^1 X^{IV} + \frac{M}{EI}XT^{11} = 0 \tag{9}$$

which may be separated by dividing by $X^{IV}T^{11}$

Solution of the separated equations

$$\frac{M}{EI}X = \lambda X^{IV}$$

and $$\lambda T^{II} + \frac{T^{I}}{A\omega} + T = 0$$

may be written as

$$X = A_1 \cos \phi x + B_1 \sin \phi x + C_1 \cosh \phi x + D_1 \sinh \phi x \qquad (10)$$

and $$T = C_1' e^{Zt} + C_2' e^{-Zt} \qquad (11)$$

where A_1, B_1, C_1, D_1 are constants defined in material which follows

$$\phi^4 = a_2/\lambda$$

$$a_2 = M/EI$$

$$a_3 = 2\beta/\omega\lambda$$

$$a_4 = 1/\lambda$$

$$Z = \frac{\sqrt{4a_4 - a_3^2}}{2}$$

when the initial condition

$$Y_0 = 0 \quad \text{(independent of axial location x)}$$

is considered The separation constant, λ, will, of course, be resolved upon application of the boundary conditions

The boundary conditions applicable to the forced clamped-pinned beam are defined below

1 $\left.\frac{dX}{dx}\right|_{x = 0} = 0$ (zero slope at the clamp)

2 $\left.\frac{d^2X}{dx^2}\right|_{x = 1} = 0$ (zero moment at the pin)

3 $Y_{0,t}\big|_{max} = a/\omega^2$

4 $Y_{1,t}\big|_{max} = a/\omega^2$

Substitution of the boundary conditions into Equations (10) and (11) and limiting to steady state response gives

$$A_1 = \frac{\gamma_3 D_1 - \gamma_2 B_1}{\gamma_1}$$

$$B_1 = \frac{\frac{a}{\omega^2}\left[1 - \left(\gamma_3 + \gamma_3 \frac{\gamma_4}{\gamma_1}\right)\right]}{\gamma_2 \left(1 - \frac{\gamma_4}{\gamma_1}\right) - \gamma_3 \left(1 + \frac{\gamma_4}{\gamma_1}\right)}$$

$$C_1 = -A_1$$

$$D_1 = \frac{a}{\omega^2} - B_1$$

The separation constant, λ, becomes

$$\lambda = \frac{1}{2\omega^2}\left[1 + \sqrt{1 - 4\beta^2}\right]$$

and the term, ϕ^4, becomes

$$\phi^4 = \frac{2M\omega^2}{EI\left(1 + \sqrt{1 - 4\beta^2}\right)}$$

$$Z = \sqrt{\frac{\omega^2\lambda - \beta^2}{\omega^2\lambda^2}}$$

CONFIDENTIAL

$$a_3 = \frac{4\omega}{1 + \sqrt{1 - 4\omega^2}}$$

and

$$Z = \sqrt{\frac{\omega^2\lambda - \beta^2}{\omega^2\lambda^2}}$$

The complete equation defining the steady state dynamic motion of the forced nonconservative clamped-pinned tube is then given by

$$Y_{x,t} = (A \sin \phi x + B \cos \phi x + C \sinh \phi x + C \cosh \phi x) \sin Zt$$

where the following terms are presented for convenience

$$A_1 = \frac{\gamma_3 D_1 - \gamma_2 B_1}{\gamma_1}$$

$$B_1 = \frac{\frac{a}{\omega^2}\left[1 - \gamma_3\left(1 + \frac{\gamma_4}{\gamma_1}\right)\right]}{\gamma_2\left(1 - \frac{\gamma_2}{\gamma_1}\right) - \gamma_3\left(1 + \frac{\gamma_4}{\gamma_1}\right)}$$

$$C_1 = -A_1$$

$$D_1 = \frac{a}{\omega^2} - B_1$$

$$\gamma_1 = \sin \phi\ell + \sinh \phi\ell$$

$$\gamma_2 = \cos \phi\ell$$

$$\gamma_3 = \cosh \phi\ell$$

$$\gamma_4 = \sin \phi\ell - \sinh \phi\ell$$

$$\phi^4 = \frac{2m\omega^2}{EI\left(1 + \sqrt{1 - 4\beta^2}\right)}$$

$$Z = \frac{\omega\left\{2\left[\left(1 + \sqrt{1 - 4\beta^2}\right) - 2\beta^2\right]\right\}^{1/2}}{\left(1 + \sqrt{1 - 4\beta^2}\right)}$$

$$a_3 = \frac{4\beta\omega}{\left(1 + \sqrt{1 - 4\beta^2}\right)}$$

C 1 REFERENCES

1 *K Sewaza "On the Decay of Waves in Visco-elastic Solid Bodies," Bulletin of the Earthquake Research Institute, Tokyo Imperial University, vol III, p 50, September 1927*

2 *R D Mindlin, F W Stubner, and H L Cooper "Response of Damped Elastic Systems to Transient Disturbances," Proceedings of the Society for Experimental Stress Analysis, vol V, no II, pp 69-87, edited by C Lipson and W M Murray Addison-Wesley Press Inc , Cambridge, Mass , 1948*

APPENDIX D

FIGURES
NASA FUEL SUPPORTS
FOR TUNGSTEN-WATER MODERATED REACTORS

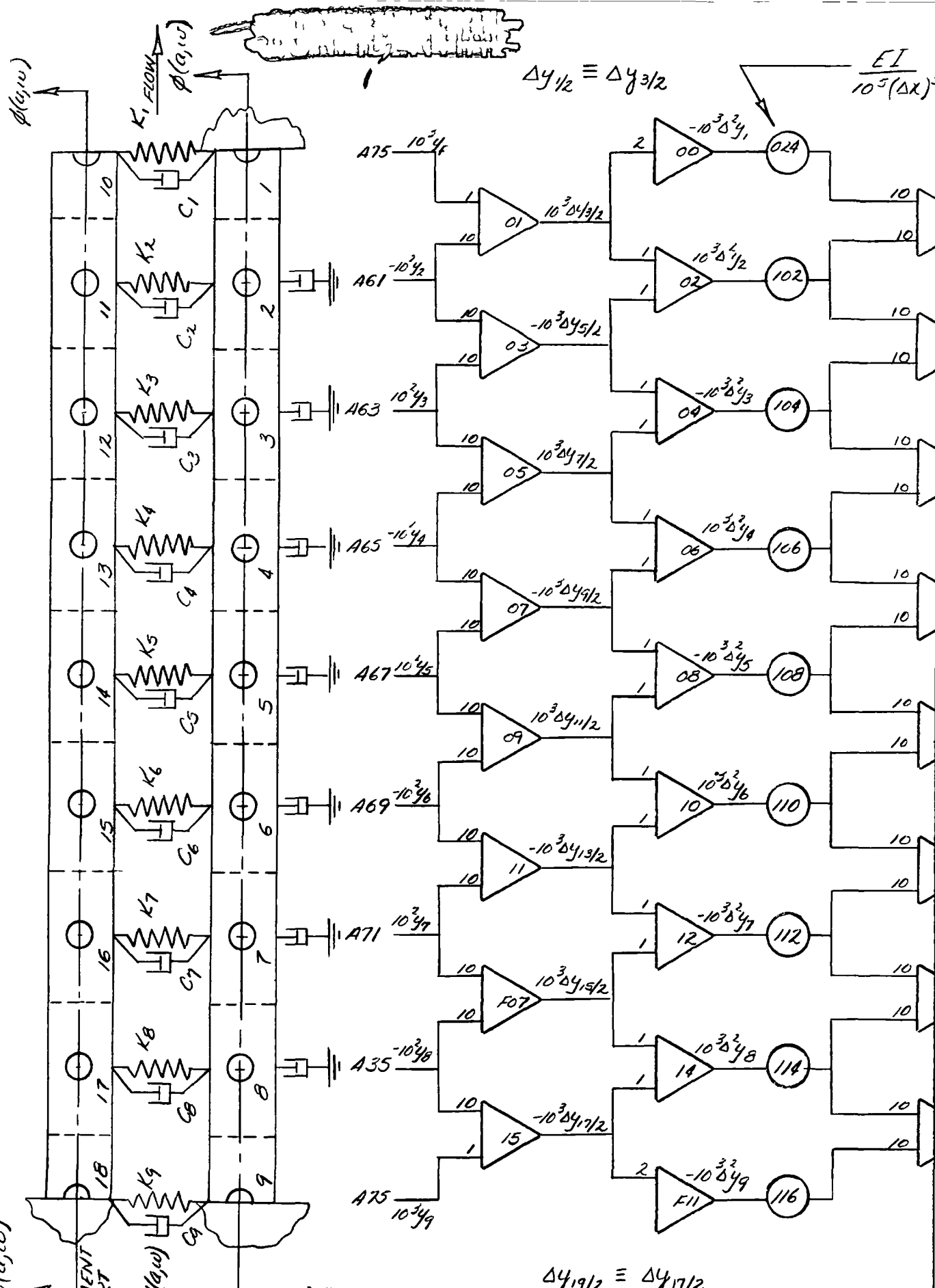

Figure D 1 NASA Fuel Support, (Cold End Support Model Pres

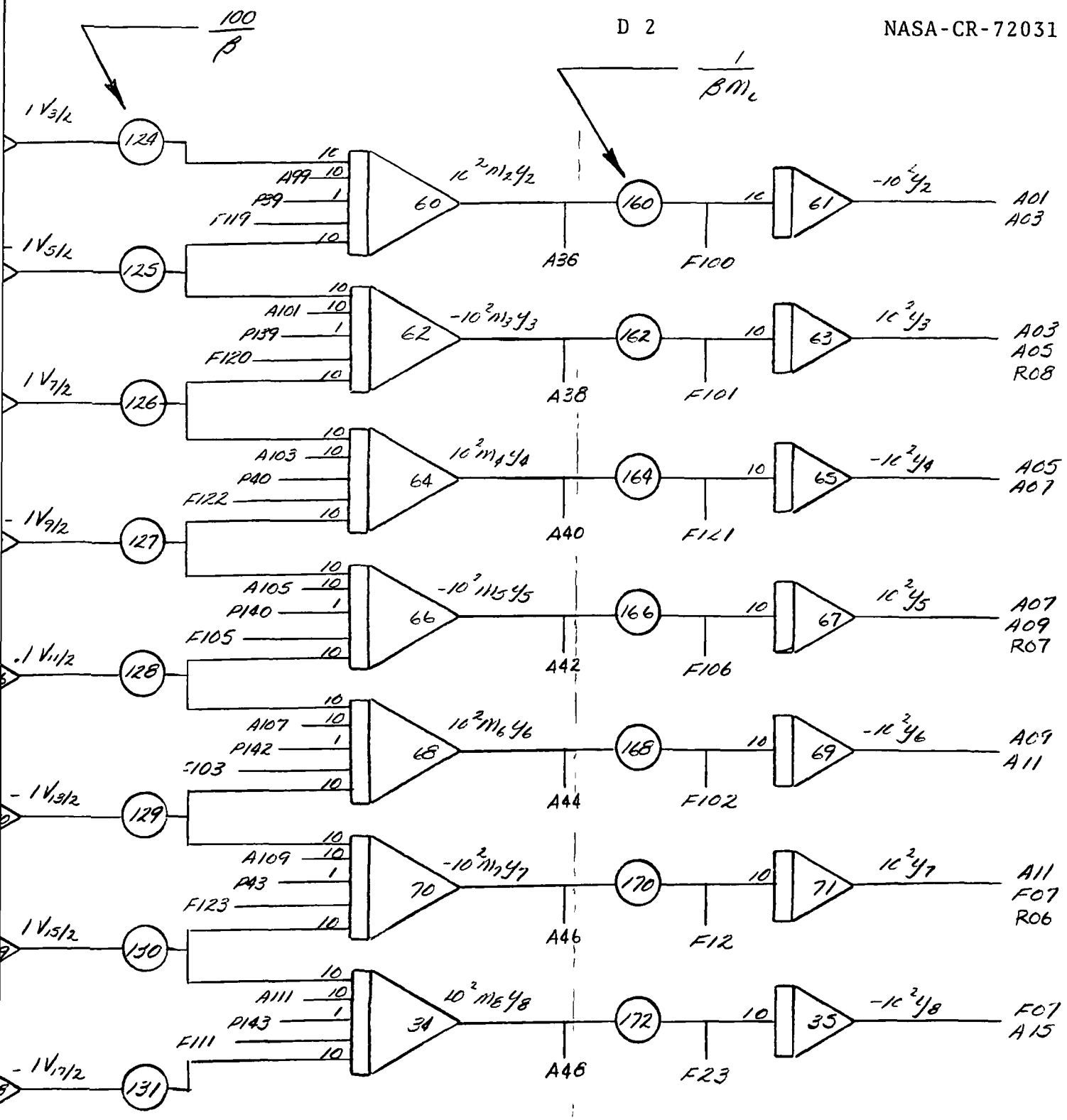

Tungsten-Water Moderated Reactor
ure Tube Simulation)

CONFIDENTIAL

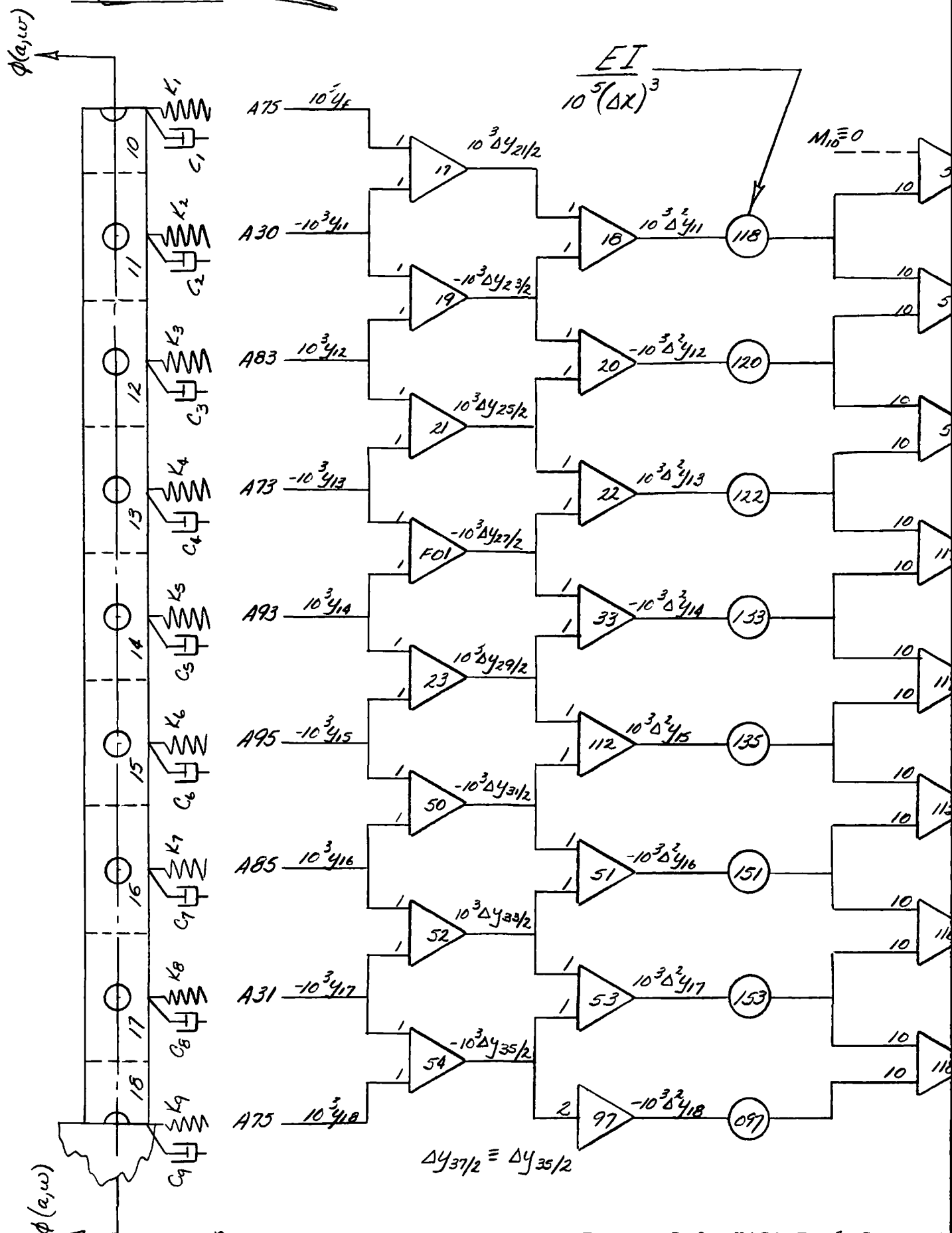

Figure D 2 NASA Fuel Support
(Cold End Support Model Fue

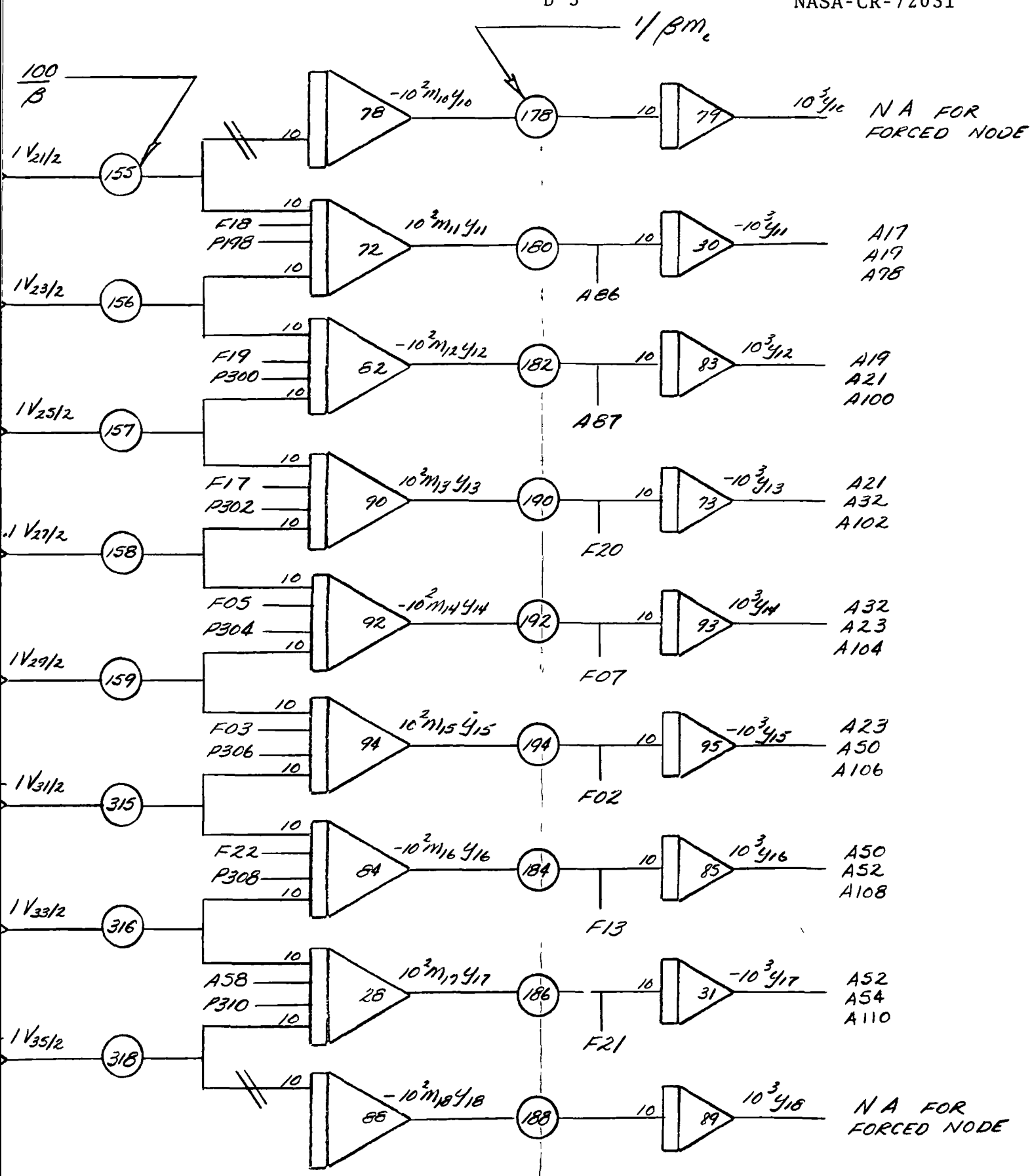

Tungsten-Water Moderated Reactor and Fuel Support Simulation)

CONFIDENTIAL

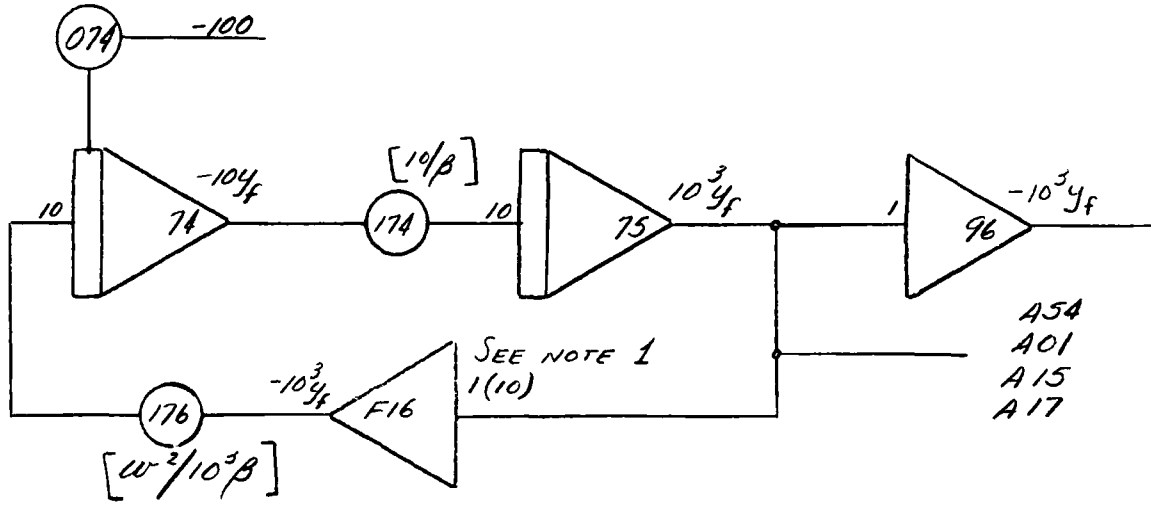

SINE WAVE EXCITATION GENERATOR

NOTE 1 GAIN 10 USED FOR FREQUENCIES ABO

POT 176 REDEFINED AS $\left(\omega^2/10^4\beta\right)$ WH

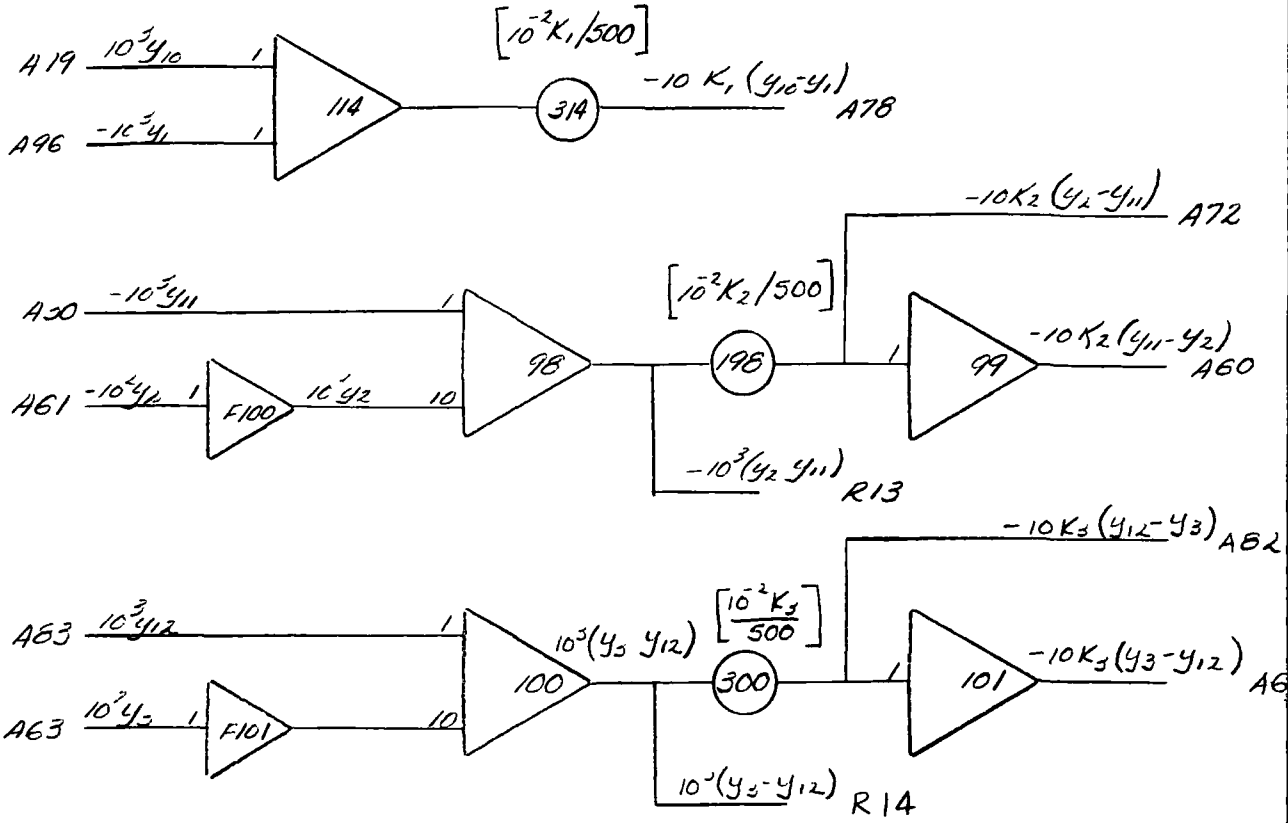

Figure D 3 NASA Fuel Support
(Excitation Oscillator and La

A114
A113
R01
R09

E 100 CPS

N GAIN 10 USED

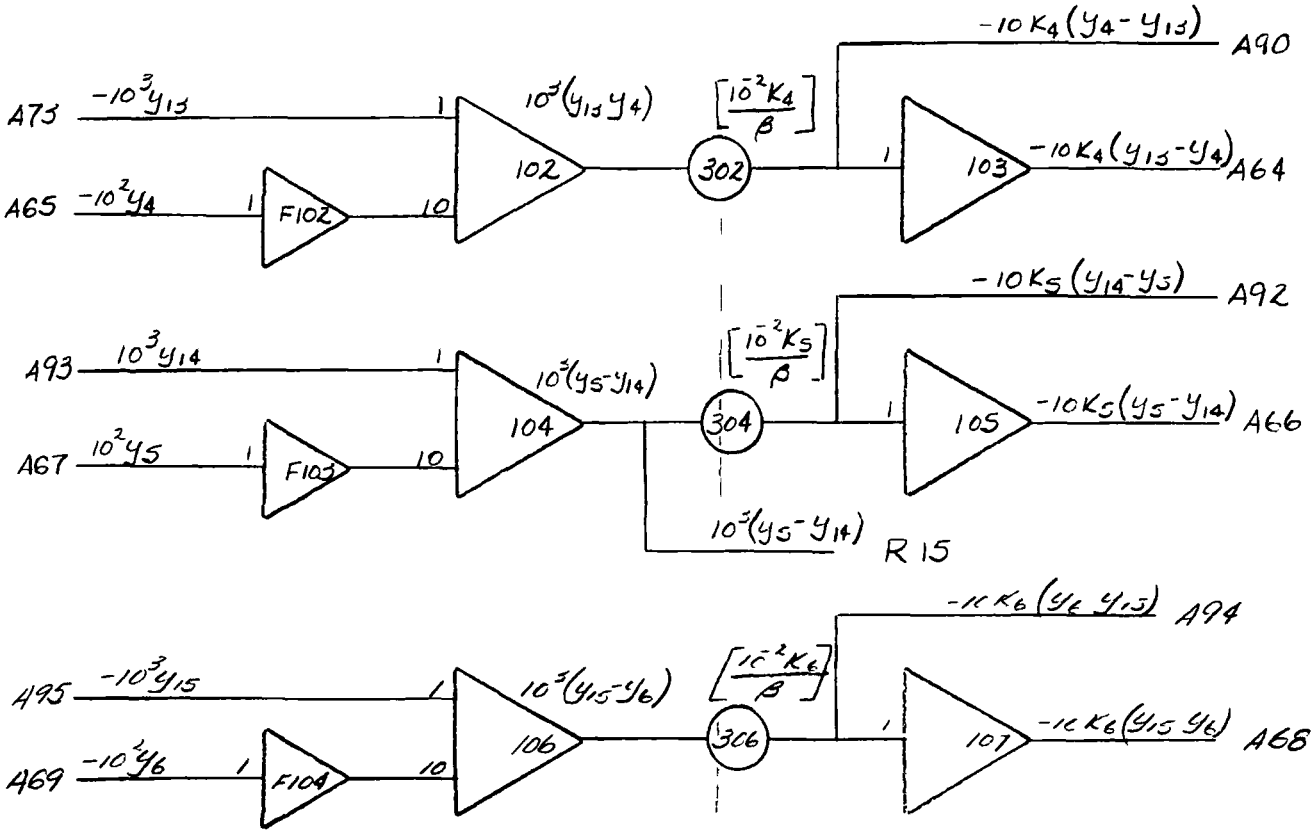

Tungsten-Water Moderated Reactor
eral Support Coupling)

CONFIDENTIAL

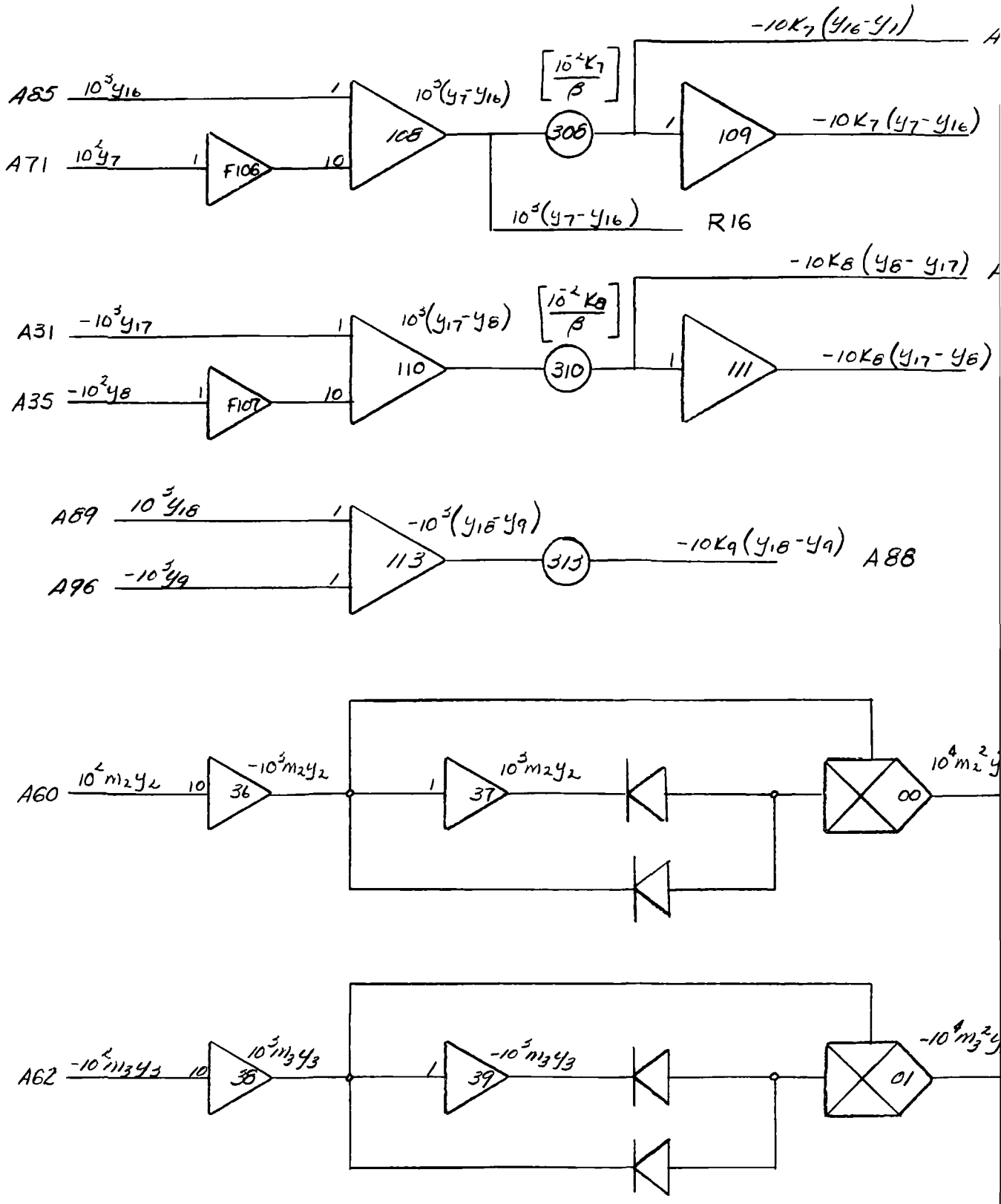

Figure D 4 NASA Fuel Support
(Lateral Support Coupling and

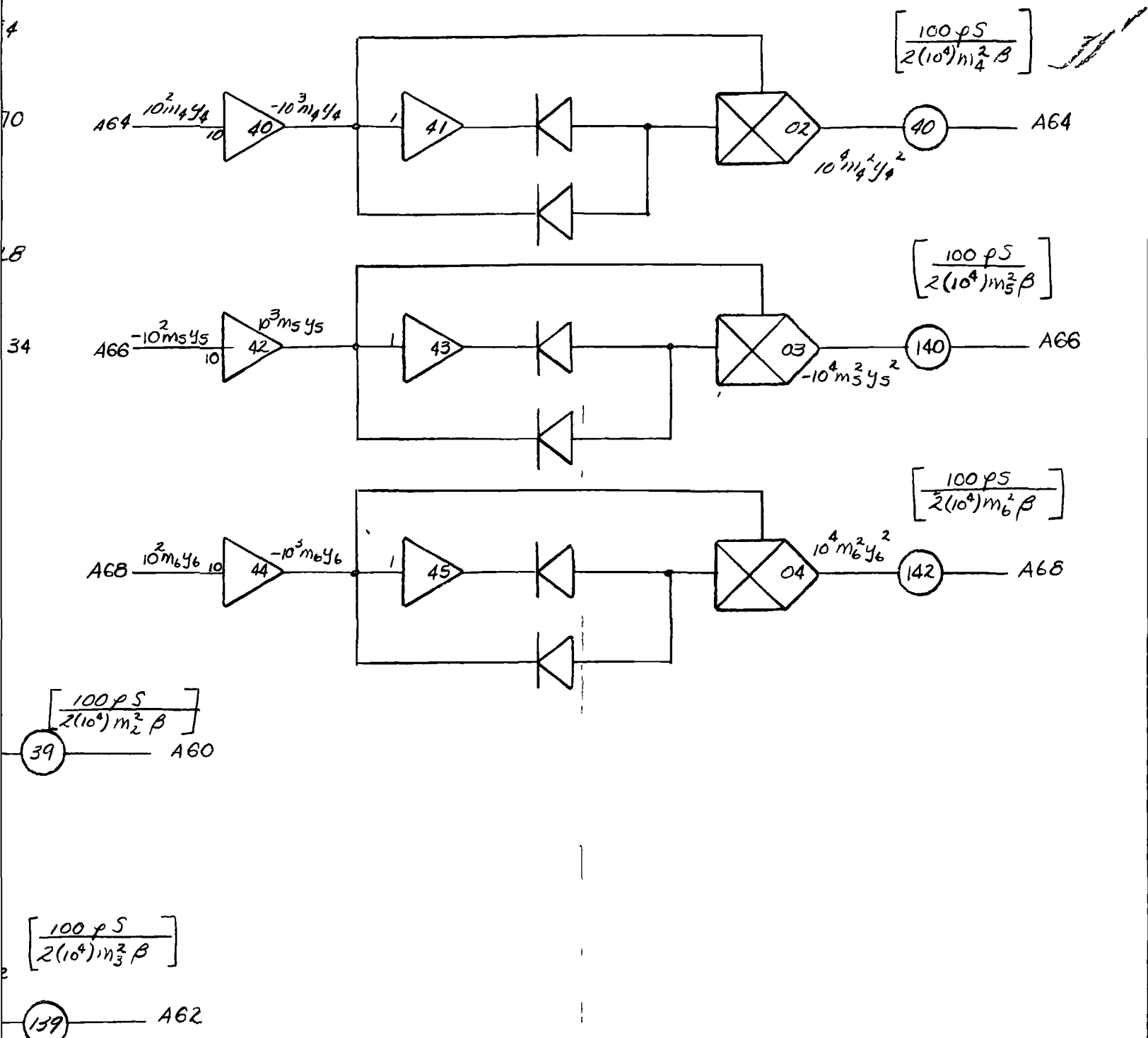

Tungsten-Water Moderated Reactor
(oderator Damping)

CONFIDENTIAL

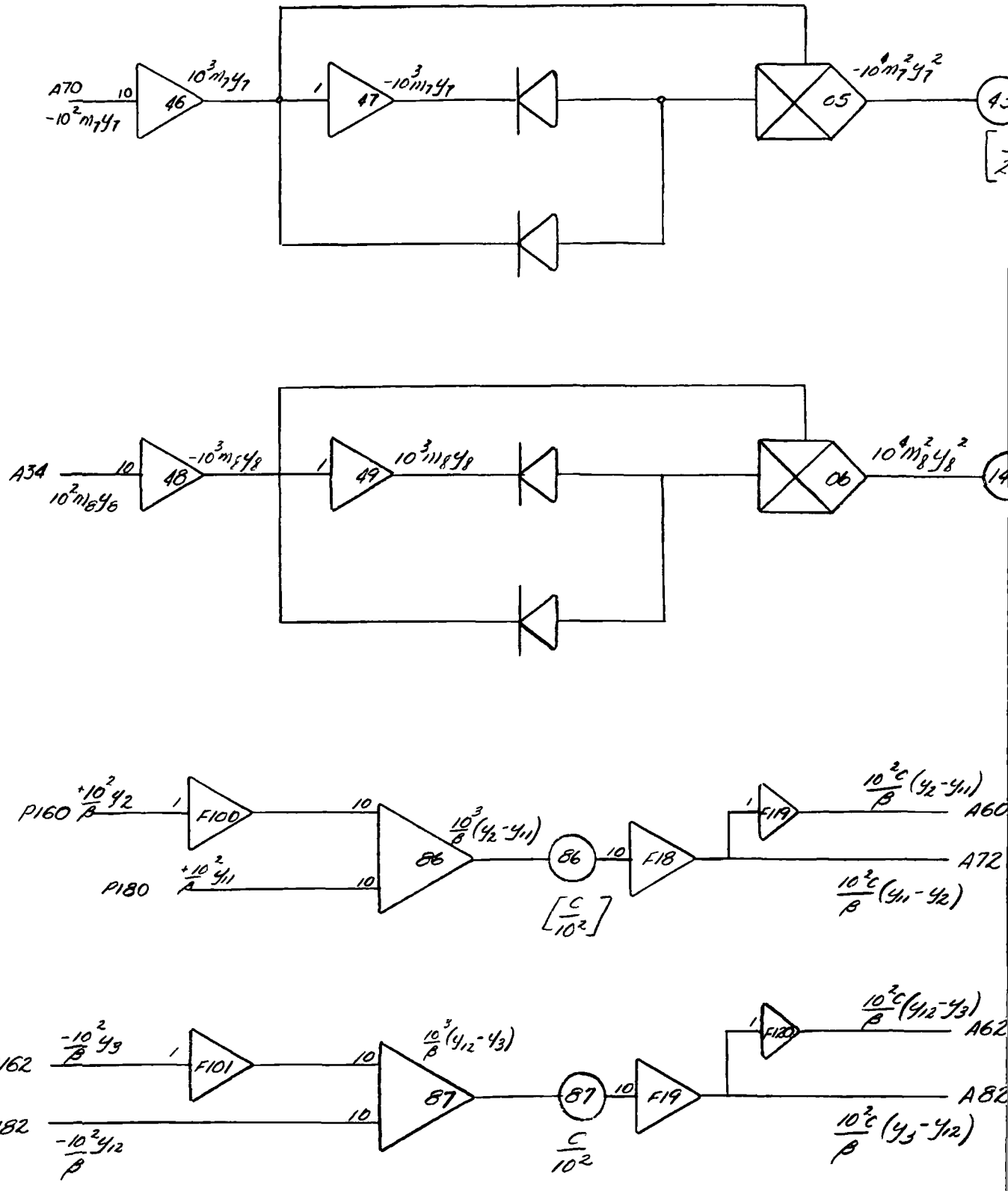

Figure D 5 NASA Fuel Support, (Moderator and Lateral Support

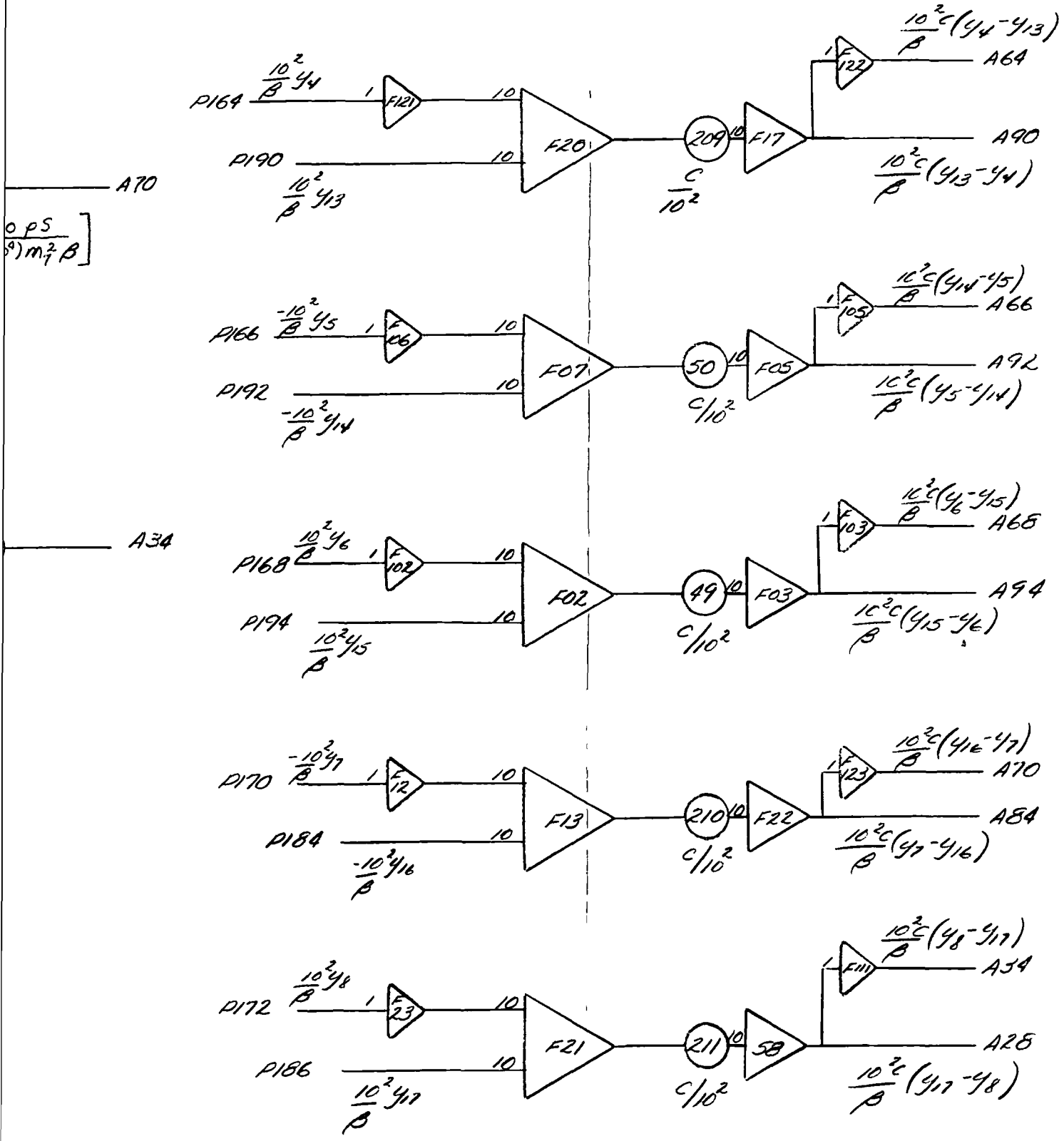

Tungsten-Water Moderated Reactor
Damping)

CONFIDENTIAL

D. 6-2

DISTRIBUTION

Number of Copies	
1	ACF Industries, Inc
1	AEC Patent Office
2	Aerojet-General Corporation (NASA)
1	Aerojet-General Corporation, Sacramento
2	Aeronautical Systems Division
1	Aerospace Corporation
1	Air Force Foreign Technology Division
1	Air Force Headquarters
1	Air Force Research and Technology Division
1	Air Force Rocket Propulsion Laboratory
2	Air Force Weapons Laboratory
1	Air University Library
1	Airesearch Manufacturing Company, Phoenix
2	Albuquerque Operations Office
1	Allison Division—GMC
1	Argonne National Laboratory
3	Argonne National Laboratory J Marchaterre R A Noland J Schumar
1	Army Director of Transportation
1	Army Materials Research Agency
1	Army Missile Command
1	Army Nuclear Defense Laboratory
1	Army Picatinny Arsenal
1	Aro, Inc
1	AEC-NASA Space Nuclear Propulsion Office, Nevada
10	Atomic Energy Commission, Washington
4	Atomic Energy Commission, Washington AEC/NASA Space Nuclear Propulsion Office Division of Reactor Development H B Finger J M Morrissey F C Schwenk W Yingling
1	Atomics International
1	Battelle Memorial Institute
3	Battelle-Northwest
1	Brookhaven National Laboratory
2	Bureau of Naval Weapons
1	Central Intelligence Agency

Number of Copies	
1	Chicago Patent Group
1	Defense Atomic Support Agency, Sandia
1	Director of Defense Research and Engineering
1	duPont Company, Aiken
1	EG&G, Inc , Goleta
1	EG&G, Inc , Las Vegas
1	General Atomic Division
1	General Dynamics/Fort Worth
1	General Electric Company, Cincinnati
1	General Electric Company (FPD)
1	Institute for Defense Analyses
1	Jet Propulsion Laboratory
1	Johns Hopkins University (APL)
1	Lockheed-Georgia Company
1	Lockheed Missiles and Space Company (NASA)
2	Los Alamos Scientific Laboratory
1	NASA Ames Research Center
2	NASA Goddard Space Flight Center
1	NASA Langley Research Center
6	NASA Lewis Research Center
8	NASA Lewis Research Center Report Control Office Patent Council Office Office of Reliability and Control Assurance L V Humble S J Kaufmann M H. Krasner A F Lietzke S Weiss
1	NASA Manned Spacecraft Center
5	NASA Marshall Space Flight Center
3	NASA Scientific and Technical Information Facility
6	NASA Scientific and Technical Information Facility NASA Representatives
4	National Reactor Testing Station (PPCO)
1	Naval Air System Command
1	Naval Missile Center
1	Naval Radiological Defense Laboratory
1	Naval Ships System Command
1	Nevada Operations Office
1	Oak Ridge Operations Office
1	Office of the Chief of Naval Operations
2	Office of the Chief of Naval Operations (OP-03EG)

Number
of Copies

1 Pratt and Whitney Aircraft Division (NASA)
1 Rand Corporation
1 Rocketdyne
2 Sandia Corporation
1 Strategic Air Command
1 TRW Systems
1 Union Carbide Corporation
5 Union Carbide Corporation (ORNL)
1 Union Carbide Corporation (Paducah Plant)
2 University of California, Livermore
1 Westinghouse Electric Corporation (NASA)
2 White Sands Missile Range
10 Division of Technical Information Extension

3 Division of Technical Information Extension
for retransmittal to

NASA Flight Research Center
P O Box 273
Edwards, California 93523

Library (1)

NASA Western Operations (1)
150 Pico Boulevard
Santa Monica, California 90406

National Aeronautics and Space Administration, Wash

Library (1)

59 Battelle-Northwest

D T Aase (7)
F W Albaugh
H J Anderson
R J Baker, Jr
J L Bates
J M Batch
R V Bowersock
D W Brite
J E Brown
R L Brown, Jr
J J Cadwell/O J Wick
D L Condotta/R E Peterson
G J Crandall
D R de Halas
K Drumheller

Number of Copies

P L Farnsworth
L M Finch
J F Fletcher
J C Fox
C L Frederick
J R Hague
W L Hampson, Jr
H Harty
R A Harvey
R M Hiatt
G R Horn
D L Hovorka
C N Jackson
M T Jakub
F J Kempf
W C Kinsel
G A Last
C E Leach
J E Minor
D P O'Keefe
L T Pedersen
F B Quinlan
W E Roake
R K Robinson
D S Rowe
C H Shaw
E A Snajdr
J C Spanner
K R Sump
W C Townsend
D S Trent
R G Wheeler
D C Worlton
Technical Information Files (5)

3 Richland Operations Office

L R Lucas
R K Sharp (2)

APPENDIX E

APPROXIMATE PRESSURE LOSSES FOR HEATED COMPRESSIBLE FLUID

APPENDIX E

APPROXIMATE PRESSURE LOSSES FOR HEATED COMPRESSIBLE FLUID

1 Momentum balance

$$\frac{VdV}{gc} + vdP + \frac{4fV^2dL}{2g_cD} = 0$$

2 $V = Gv$, $dV = Gdv$

3 $$\frac{G^2vdv}{v^2} + \frac{vdP}{v^2} + \frac{4fG^2dL}{2g_cD} = 0$$

4 $$\frac{G^2dv}{v} + \frac{dP}{v} + \frac{4fG^2dL}{2g_cD} = 0$$

5 Gas law

$$v = \frac{RT}{P} = \frac{1}{\rho}$$

6 $$\frac{G^2}{g_c} \ln\frac{v_2}{v_1} + \int_1^2 \frac{PdP}{RT} + \frac{4fG^2L}{2gD} = 0$$

7 $$\frac{G^2}{g_c} \ln\frac{v_2}{v_1} + \frac{P_2 - P_1}{RT_{avg}} \left(\frac{P_1 + P_2}{2}\right) + \frac{4fG^2L}{2g_cD} = 0$$

R = constant, using T_{avg} as an approximation

8 $$\frac{G^2}{g_c} \ln\left(\frac{T_2}{T_1} \quad \frac{P_1}{P_2}\right) + \frac{P_2 - P_1}{RT_{avg}} \left(\frac{P_1 + P_2}{2}\right) + \frac{4fG^2L}{2g_cD} = 0$$

9 $$P_1 - P_2 = \Delta P = \left(\frac{4fG^2L}{2g_cD} + \frac{G^2}{g_c} \ln\frac{T_2}{T_1} \quad \frac{P_1}{P_2}\right) \frac{RT_{avg}}{P_{avg}}$$

10 $$\Delta P = \frac{G^2}{g_c \rho_{avg}} \left(\frac{4fL}{2D} + \ln \frac{T_2}{T_1} + \ln \frac{P_1}{P_2} \right)$$

$$= \frac{G^2}{g_c \rho_{avg}} \left(\frac{2fL}{D} + \frac{T_2 - T_1}{T_{avg}} + \frac{P_1 - P_2}{P_{avg}} \right)$$

Approximation for ln terms

CONFIDENTIAL

CONFIDENTIAL